PATTERN ADAPTATION AND ITS INTEROCULAR TRANSFER IN THE PRIMARY VISUAL CORTEX

Thesis submitted to the University of Wales Cardiff by Christopher Howarth
In candidature for a degree of Philosophiae Doctor

Supervised by Professor Frank Sengpiel

Department of Biosciences

ProQuest LLC
789 East Eisenhower Parkway
P.O. Box 1346
Ann Arbor, MI 48106-1346

DECLARATION

This work has not previously been accepted in substance for any degree and is not concurrently submitted in candidature for any degree.

Signed .....(candidate) Date..21/05/08...

STATEMENT 1

This thesis is being submitted in partial fulfilment of the requirements for the degree of PhD.

Signed .....(candidate) Date..21/05/08.....

STATEMENT 2

This thesis is the result of my own investigations, except where otherwise stated. Other sources are acknowledged by giving explicit references, with an appended bibliography.

Signed .....(candidate) Date..21/05/08...

STATEMENT 3

I hereby give consent for my thesis, if accepted, to be available for photocopying and for inter-library loan, and for the title and summary to be made available to outside organisations.

Signed .....(candidate) Date..21/05/08....

ACKNOWLEDGEMENTS

I would like to give my eternal gratitude towards my supervisor Frank Sengpiel for providing much needed guidance at a moments notice and critical, yet diplomatic appraisal of my work. Without his neverending patience and belief in my ability to finish this thesis would never have been realised. There isn't room here to mention all the myriad ways Vasily Vorobyov has helped over the course of this thesis, so instead I'll just say thanks for all the tea. Many thanks to Dr Stuart Faulkner for moral support, surefire advice and laboratory assistance. My most heartfelt love and appreciation goes towards my family, for being the bedrock foundation from which all of this has been possible. A million and one thanks to all my friends both near and far, who have provided me with amusement, distractions galore and enough interesting experiences to fill a novel or two.

ABSTRACT

Adaptation to a high contrast grating temporarily reduces the contrast sensitivity of neurons in the primary visual cortex (V1). If this adaptation is induced in one eye and the contrast tested with the other a partial transfer of the after-effect is produced, known as interocular transfer (IOT). Intrinsic hyperpolarisation of a cells membrane explains most of this effect, but not the orientation selective nature of adaptation.

Optical imaging of intrinsic signals in anaesthetised cats and tree shrews was used to visualise orientation selective responses in V1 before and after brief and chronic adaptation. Short term adaptation was achieved with drifting gratings of 12.5 or 50% contrast and fixed orientation (θ). Three 1-sec flashes of a 100% contrast grating were used as test stimuli. 8 orientation domains were created according to orientation preference, determined on the basis of pre-adaptation orientation maps. 8 oriented test stimulus responses for each domain were obtained from the absorption signal time course averaged over all pixels. Orientation tuning curves comparable to those in single-cell experiments were produced for the orientation selective pixel populations. A region specific reduction in response was seen in the tuning curves such that responses to θ were reduced most strongly in regions responding best to θ. An additional stimulus specific reduction was observed in responses to θ, even if θ wasn't the optimal orientation for a domain. Chronic adaptation was induced with 1 hour of drifting sinusoidal grating in tree shrews. In contrast to a similar experiment in the cat, no alteration in the functional layout of the orientation map was observed.

Extracellular recording of IOT in the cat primary visual cortex was performed to elucidate its physiological substrate. Orientation tuning curves were recorded before and after left or right eye adaptation with a 25% or 50% contrast drifting grating with the cells preferred orientation and spatial frequency. Cells were *a priori* categorised according to the binocularity of their control responses. Surprisingly, significant levels of IOT were observed in virtually all monocular cells. Only a weak link was found between ocular dominance and IOT in the full cell population. However, a moderate link between OD and IOT was seen in simple cells. An increase in the response to orthogonal stimuli was also seen in both monocular and binocular cells after adaptation with the non-dominant eye. A subset of complex cells did not display any IOT when adapting with the non-dominant eye and testing with the dominant eye.

CONTENTS

Chapter 4 - Inter Ocular Transfer Experiments

CHAPTER ONE

INTRODUCTION TO THE VISUAL PROCESSING SYSTEM

There is an enormous amount of information in the visual scene bombarding our retina on a moment by moment basis. The capacity of our visual system to extract the relevant details from such an array of possibilities is quite phenomenal. After conversion of photons into nerve impulses in the retina, information is processed via parallel pathways. Impulses pass along the optic nerve, via the optic chiasm to the Lateral Geniculate Nucleus (LGN) in the thalamus which is segregated into layers. Each layer responds to either the left or right eye and contains neurones that preferentially respond to movement, fine detail or colour. This information is then propagated along afferents from the LGN to the occipital lobe and the primary visual cortex (V1) as shown in the pathway in figure 1.1.

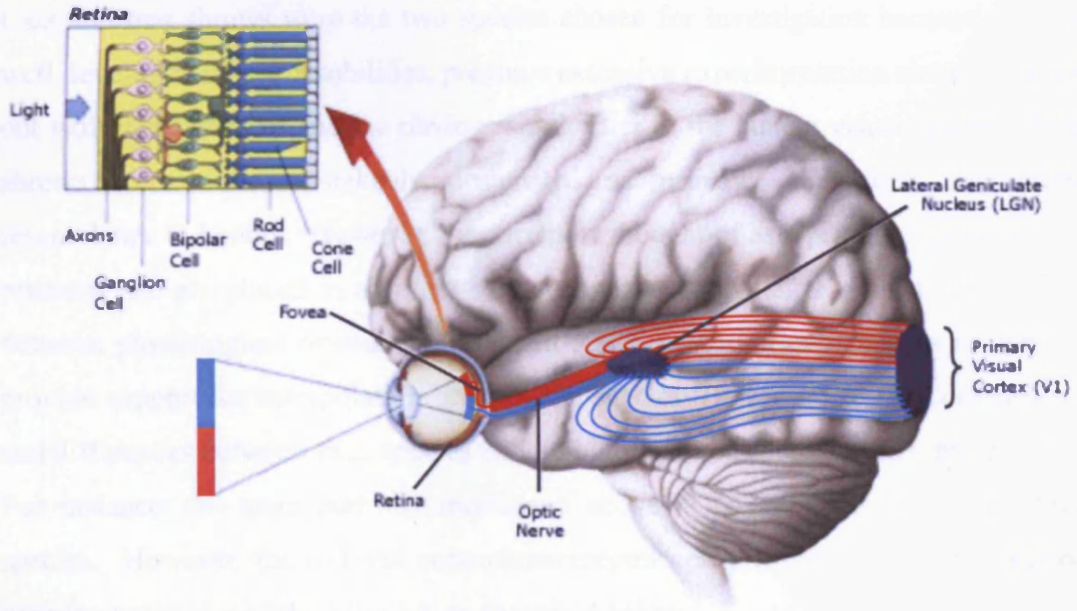

Figure 1.1 - Shows the main pathway of visual information flow in humans, from the eye to the primary visual cortex. Surprisingly, light rays must penetrate through layers of neurons in the retina before reaching the photoreceptors (rods and cones) at the back. Following phototransduction, electrical signals generated by the photoreceptors pass via bipolar cells to retinal ganglion cells, and the resulting nerve impulses travel along the optic nerve to the LGN and are then relayed to the primary visual cortex via the optic radiation. The red and blue bar produces an inverted image on the retinal surface, and a point-to-point topographic representation is preserved in both the LGN & V1 (Pathway drawing adapted from 'Images of Mind' Posner & Raichle, 1994; retinal cells drawing adapted from 'Eye, Brain and Vision' David H. Hubel, 1998).

Processing of the different aspects of the visual scene results in individual neurones in the primary visual cortex that respond quite specifically to orientation, motion, colour, contrast, and monocular or binocular information. This allows the visual system to respond to individual parameters in a specific and precise manner using the relatively narrow digital range of impulses produced by single neurones. As the environment changes around us, the information presented to the eyes can be vastly altered from one moment to the next outside one neurones limited range. Yet, the visual system possesses the ability to function effectively in an incredible number of different conditions. To ensure that the visual system can respond in an appropriate manner it has to adapt to the changing circumstances. The mechanism of the adaptive process occurring in the primary visual cortex and what this reveals about its function and the underlying network is the main focus of this thesis.

Cats and tree shrews were the two species chosen for investigation because of their well developed visual capabilities, previous extensive experimentation already carried out with these animals and the obvious similarities to the human visual system. Tree shrews were once mistakenly designated as primates due their anatomical resemblance to lemurs. However, they are now thought of as a primitive prototype of primates and are placed in an order of their own, Scandentia. Relevant correlations between physiological recordings in the cat and behavioural experiments in humans provide support for extrapolation between the species (Berkley, 1990). Comparisons and differences between each species will be highlighted throughout this introduction. For instance, the main pathway mentioned above is preserved between the three species. However, the rod and cone photoreceptor cell proportions and distribution over the retina is slightly different, as described below.

1. Retinal Photoreceptors

There are two main types of retinal photoreceptor, namely cone and rod cells. Cone cells provide information connected with colour and fine detail. Rod cells are 100 times more sensitive to light but insensitive to colour and therefore respond better in lower light level environments. There are three types of cone cells in humans, each of which contain colour sensitive pigments that respond optimally to different wavelengths of light; red-558nm, green-531nm and blue-419nm (Dartnall *et al*,

1983). The rod and cone retinal distribution is very similar for both cats and humans, with the majority of cones located in a central region called the area centralis or fovea respectively, and a high density ring of rod cells surrounding this (Steinberg, Reid, & Lacy, 1973). The nocturnal nature of cats has produced a primarily rod dominated retina and reflective *tapetum lucidum* (Ollivier *et al* 2004) which provide excellent low light vision. With only two different cone types making up a relatively small proportion of the photoreceptors cats have relatively poor, de-saturated colour vision as compared to primates (Wienrich & Zrenner 1984, Ringo & Wolbarsht 1986, Loop *et al* 1987). Tree shrews are also dichromats with two cone varieties that dominate the retina and have peak wavelength sensitivities of 555nm and 428nm, corresponding well with those found in primates, but less than 5% of the total photoreceptors are rods (Petry & Harosi, 1990; Jacobs & Neitz, 1986). Most likely due to their semi-arboreal nature and diet of insects and small fruits, the receptors are arranged in concentric ellipsoid iso-density bands rather than the more precise circular central regions required for locating and tracking fast moving prey founds in cats & primates (Muller & Peichl 1989).

2. Ganglion Cell Receptive Fields

The size, shape and response properties of cells and their receptive field in the visual system varies considerably, depending on which level in the visual hierarchy they occur and where their afferent input originates. Retinal ganglion cells receive their afferent input from circular arrays of rod and cones, via bipolar cells. The attributes of the receptive field depend on the catchment area of the cells' direct inputs and the inhibitory and excitatory effects of the surrounding network. A relatively simple circuit involving bipolar, amacrine and horizontal cells produces concentric circular receptive fields with either an ON-centre and OFF-surround or vice versa (see figure 1.2). Note that a reduction in activity occurs when using a stimulus that is opposed to the optimal, i.e. illuminating the surround part of an ON-centre ganglion receptive field.

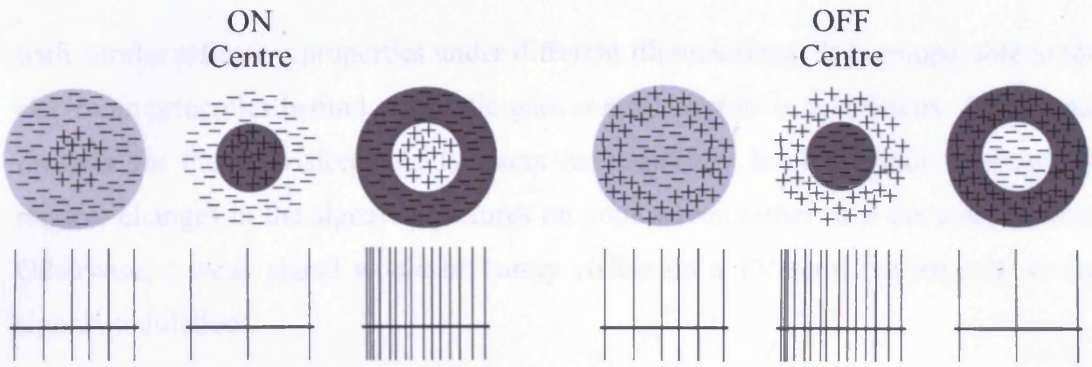

Figure 1.2 – Shows the difference between the on-centre and off-centre ganglion cell responses in three different stimulation scenarios. From left to right is shown an equiluminant stimulus (light grey circle), light hitting the surround only (small dark grey circle) and a centrally lit stimulus (dark grey ring). Directly below each stimulus scenario is the associated firing rate of the two ganglion cell types, with each vertical line representing an individual spiking event. The on-centre ganglion cells are activated by photons bombarding its central region, whereas off-centre cells are stimulated by light in the surround. The greatest activity occurs when there is a large difference between the illumination levels hitting the different parts of the receptive field, regardless of overall illumination level. (Diagram adapted from 'The Human Brain' John Nolte, 1999)

3. Light Adaptation in the Retina

Such circular receptive fields are concerned with the brightness (luminance) difference or contrast and allow the detection of edges, regardless of orientation. The contrast of a stimulus can be calculated using the Michelson formula as shown below:

$$\text{Contrast} = \frac{L_{max} - L_{min}}{L_{max} + L_{min}}$$

Where L_{max} is the maximum luminance and L_{min} is the minimum luminance, producing a contrast value that is independent of the total luminance.

In essence, this means that the retina provides information about the different contrasts of the natural scene regardless of the ambient lighting level. But how is this stable level of activity maintained? The answer lies in light adaptation, the ability of the retinal receptor cells to change their responsive state and provide a steady flow of activity as the incident level of illumination changes. This is largely a property of the rod and cone photoreceptors themselves and allows the retina to function effectively over a huge range of light intensities. This is very useful for perception of objects

with similar reflective properties under different illuminations. It is comparable to the electronic principles behind automatic gain control circuits in televisions: The signal receiver for the television quickly alters its sensitivity level in order to show the relative changes in the signal as pictures on your screen rather than the overall level. Otherwise, a weak signal would be barely visible on a TV sensitive for only strong signal modulations.

Part of the mechanism that underlies this light adaptation comes from the fact that in high level light conditions the photopigments in rods are bleached. This bleaching renders the rods ineffective at responding to stimuli and they can no longer contribute to the visual signal from the retina. If a gradual increase in the ambient luminance from dark to light occurs then the proportion of bleached rods gradually increases and the cone system takes over in order to maintain effective vision. This system can be disrupted by an abrupt, intense illumination of a portion of the retina. This bleaches a large number of rods instantaneously and results in an afterimage once the illumination is removed. In other words, this intense stimulation has a direct effect on subsequent perception. The study of such alterations in perception can yield clues as to the functioning of underlying system. This approach has been undertaken to elucidate different types of adaptation mechanisms that occur at higher levels of the visual hierarchy.

Light adaptation is a well-known and widely experienced aspect of vision but does not explain other adaptive responses of the visual system. It is only one form of many which can be thought of as different solutions to a similar problem. Although similar in some aspects, its physiological substrate and any underlying mechanisms are distinct from the adaptation that occurs later on in the visual system that is the focus of the work in this thesis.

The resulting output of a retinal ganglion can be described mathematically as a difference of two gaussians and this has been utilised in numerous computational models investigating the visual system (Rodieck 1965, Cai *et al* 1997).

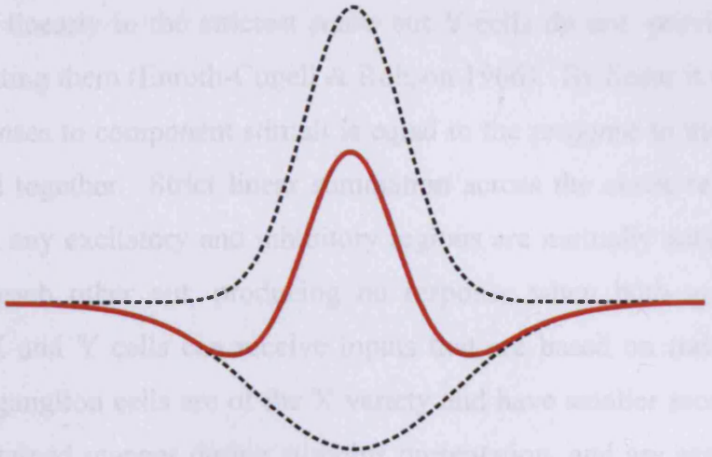

Figure 1.3 - The red line shows the resulting difference of gaussians for an ON-centre ganglion cell. The upper dotted line shows the ON-centre & lower the OFF-surround, each possessing the same total response, but with the ON-centre concentrated in a smaller region. Obviously, this is only one 2-D slice, and after rotation through 360° the full circular 3-D receptive field would be represented. The same shape holds true for both rod and cone based fields, with the former generally being much wider than the latter.

The spatial discrimination of stimuli is largely dependent on the amount of convergence of rod or cones onto an individual ganglion cell. Greater convergence is found with rod cells rather than cones and with larger eccentricities in the retina. Tree shrews possess a relatively low ratio of convergence, which produces the basis for good spatial acuity (Muller & Peichl 1989, Petry *et al* 1984).

4. Ganglion Cell Classification

There are parallel processing pathways for visual information, concerning form, motion & colour. This distinction between the different types of information is preserved throughout the visual system, until binding of all image characteristics into a cohesive complete perception, although where and precisely how this occurs has not been elucidated. The retinal ganglion cells can be placed into groups according to anatomical and physiological properties, associated with each of the processing streams.

The two main types of ganglion cell in the cat are termed X and Y cells, each of which has clearly distinguishing characteristics. X-cells summate spatial and

temporal stimuli linearly in the strictest sense but Y-cells do not, providing a good method of separating them (Enroth-Cugell & Robson 1966). By linear it is meant that the sum of responses to component stimuli is equal to the response to the component stimuli presented together. Strict linear summation across the entire receptive field would mean that any excitatory and inhibitory regions are mutually antagonistic and as such cancel each other out, producing no response when both are stimulated equally. Both X and Y cells can receive inputs that are based on rods and cones. Over half of all ganglion cells are of the X variety and have smaller receptive fields, respond in a sustained manner during stimulus presentation, and are associated with fine detailed vision. Only 5-10% of ganglion cells are of the Y type, which have much larger receptive fields and faster conduction velocities than X-cells and respond in a transient fashion to the onset and offset of stimulus presentation. These properties make them likely candidates as the providers of input to motion sensitive cells in the primary visual cortex. There is also a group called W-cells, but this group is not as clearly defined, especially when considering the differing properties of LGN cells innervated by them. W-cells have a weak sustained response that diminishes when a spot of low contrast moves across its field, have relatively large receptive fields and display non-linearity of response (Rodieck 1965, Saito 1983). They also have poor contrast sensitivity, responsiveness and spatial resolution (Sur & Sherman 1982). Tree shrews have corresponding groups of cells to the X & Y categories found in the cat, i.e. sustained responses and small receptive fields for former, and transient larger receptive fields for the latter (van Dongen *et al* 1976). The Y-cells tended to have larger field with greater eccentricity whereas the X-cell field size remains constant throughout the retina (Sherman *et al*, 1975). Direction sensitive cells, although very rare in the cat have been found in significant numbers in the tree shrew (van Dongen *et al* 1976).

After leaving the retina the ganglion afferents decussate into left and right field pathways at the optic chiasm as shown in figure 1.4. Tree shrew eyes are placed much more laterally on the cranium and point in such a direction that a line drawn perpendicularly from the centre of the retina will subtend a 56° angle from the midline (Conway & Schiller 1983). As such, the temporal region of the retina and binocular area of the visual field is much smaller and the vast majority of retinal output crosses over to the contralateral hemisphere.

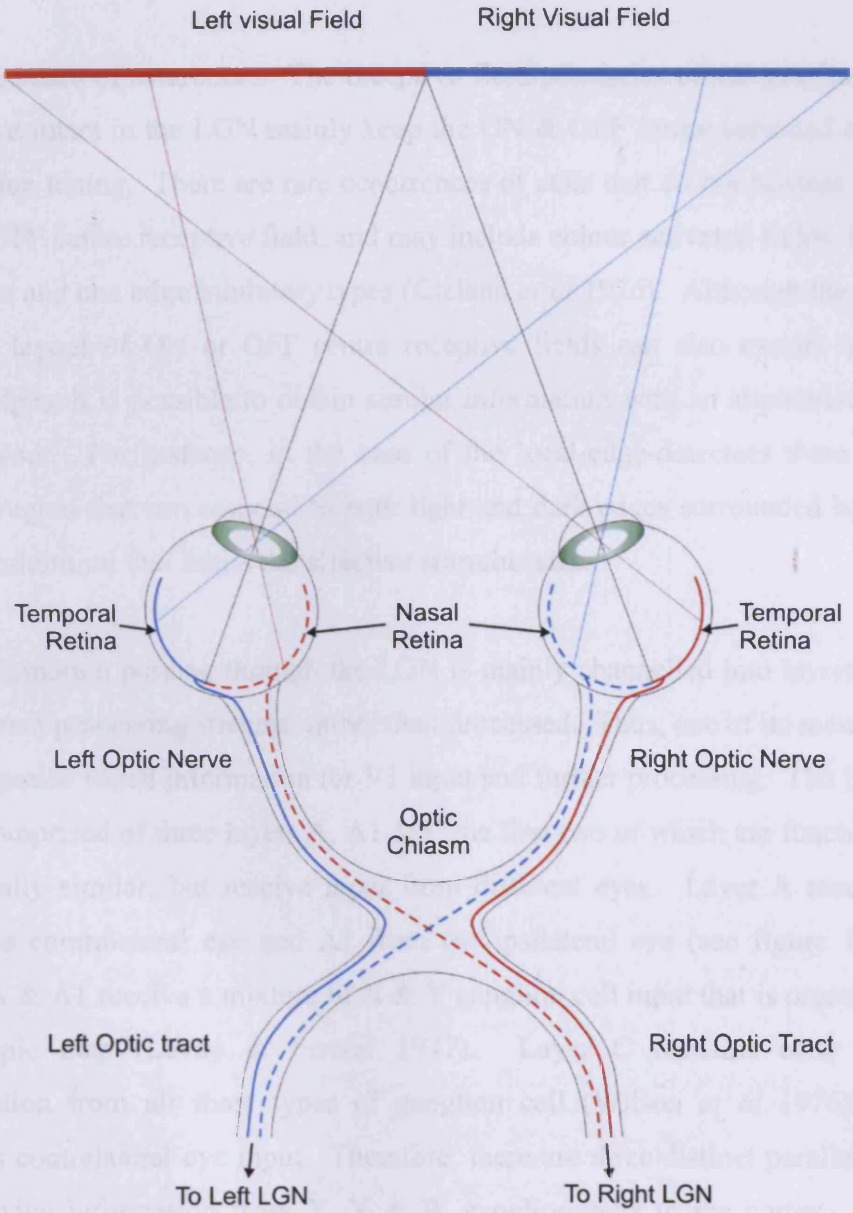

Figure 1.4 - Ganglion cell afferent segregation in the Cat - Clearly shows how right and left visual field information is separated with signals from the nasal portions of the retina crossing over to the contralateral hemisphere and afferents from the temporal retina remaining on the ipsilateral hemisphere.

5. The Lateral Geniculate Nucleus (LGN)

The LGN is located in the dorsal and as its name suggests, lateral portion of the thalamus and acts as a relay centre for information between the eye and the neocortex. The translation of thalamus means antechamber, which is a fitting name for one of its functions, as a gateway for deciding the admittance of information to the main throne room, or neocortex. In this way, it is involved in control of the different waking and

sleeping states of awareness. The receptive field properties of the ganglion cells are preserved intact in the LGN mainly keep the ON & OFF centre surround and lack of orientation tuning. There are rare occurrences of cells that do not possess the typical ON or OFF centre receptive field, and may include colour activated fields, local-edge-detectors and one edge inhibitory types (Cleland *et al* 1976). Although the concentric circular layout of ON or OFF centre receptive fields can also extract information about edges, it is possible to obtain similar information with an alternative receptive field layout. For instance, in the case of the local-edge-detectors there is a large central region that can respond to both light and dark edges surrounded by a narrow ring of inhibition that limits the effective stimulus size.

The information passing through the LGN is mainly channelled into layers dedicated to different processing streams, rather than processed. Thus, one of its main functions is to organise visual information for V1 input and further processing. The LGN in the cat is comprised of three layers A, A1 & C the first two of which are functionally and structurally similar, but receive input from different eyes. Layer A receives input from the contralateral eye and A1 from the ipsilateral eye (see figure 1.5). Both layers A & A1 receive a mixture of X & Y ganglion cell input that is organised into a retinotopic map (Levay & Ferster 1977). Layer C contains cells that relay information from all three types of ganglion cell (Wilson *et al* 1976), but only receives contralateral eye input. Therefore, there are three distinct parallel pathways for relaying information from X, Y & W ganglion cells to the cortex. The only difference between Y-cells in lamina A or C is that those in C have greater spatial and temporal contrast sensitivity (Frascella & Lehmkuhle 1984).

Interestingly, the relative proportions of LGN input are not as expected, with the majority consisting of cortico-thalamic projections. There are three types of clearly identifiable synaptic contacts made within the whole of lamina A, retinal, cortical and inhibitory interneuronal. These take up respectively a fifth, half and a third of the total synapses found in the whole of lamina A (Erisir *et al* 1998, Montero 1991). There is however, a difference in the ratio of each type depending on whether interneurones or relay cells are considered. It appears that interneurones receive greater input from the retina, whereas relay cells are mainly innervated by cortico-thalamic projections. Thus, the influence of cortical activity on thalamic response and

receptive field structure is likely to be significant (Sillito *et al* 1994, Murphy *et al* 1999).

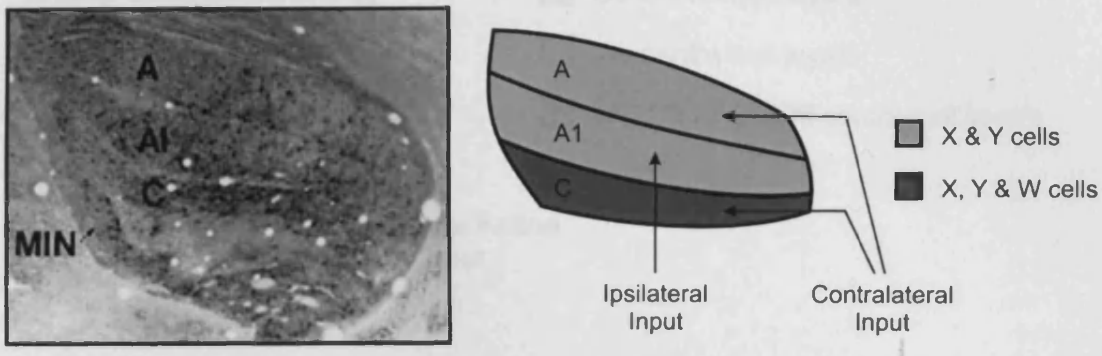

Figure 1.5 - The histological picture on the left shows SMI-32 staining of Y-cell bodies in the cat LGN, clearly showing their presence in all three laminar A, A1 & C and the medial interlaminar nucleus - MIN (picture taken from Bickford *et al* 1998). The diagrammatic representation of the important features of the cat LGN is shown on the right, indicating eye preference and cell characteristics of cells within each lamina.

The tree shrew LGN is separated both histologically and functionally into six distinct laminae and a single group of inter-laminar zones (ILZ). Each layer has a full retinotopic map of the visual field. If layer one is taken as the most medial and layer six as the closest to the optic tract then each layer can be distinguished as follows. Contralateral input dominates the LGN providing input to layers 2, 3, 4 & 6 leaving only 20% of cells receiving ipsilateral input in layers 1 & 5 (Conway & Schiller 1983). The six layers can be split into three pairs, depending on whether the cells receptive fields are ON-centre, OFF-centre cells or a mixture of both. Layers 1 & 2 are predominated by ON-centre cells, whereas layers 4 & 5 are innervated by OFF-centre ganglion cells as shown in figure 1.6 (Conway & Schiller 1983, Holdefer & Norton 1995). Layer 3 contains both ON-centre and OFF-centre cells, layer 6 contains ON-OFF centre cells and the ILZ zones cells resemble those found in 3 & 6 (Holdefer & Norton 1995). Layer 3, 6 & the ILZ are thought to relay information from the W ganglion cell category to the cortex. It appears that layers 2, 4 & 5 are connected with X-cell activity, although this is far from conclusive (Conway & Schiller 1983).

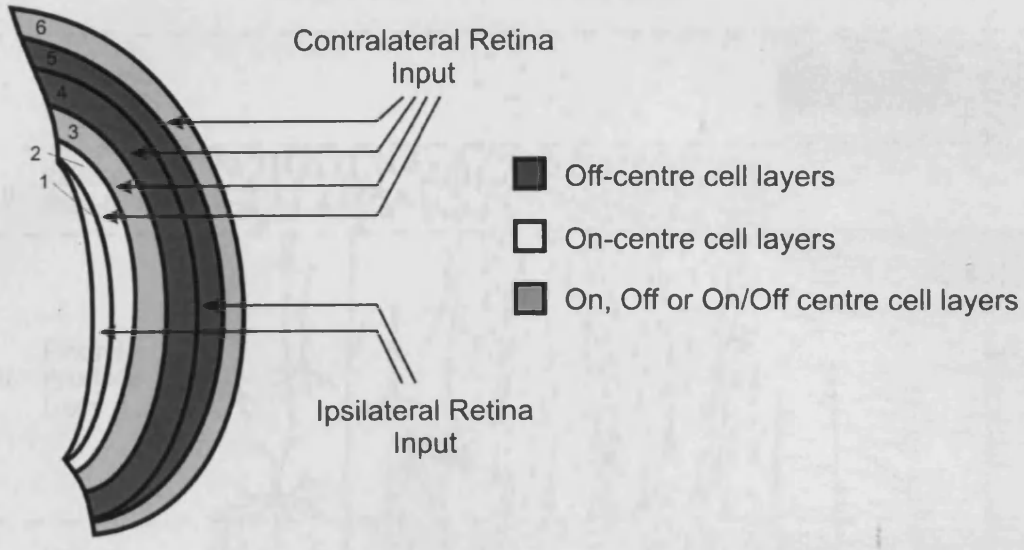

Figure 1.6 - Diagrammatic representation of the tree shrew lateral geniculate nucleus. Numbering of the layers is started on the left, from the smallest most medial layer. Full explanation is provided in the text (Diagram adapted from Conway & Schiller 1983).

It is also worth noting that the connections of ganglion cells in the LGN are less precise in the cat with ganglion afferents innervating more than one lamina such as contralateral Y-cells that send projections to laminae A, C & the MIN (Bowling and Michael 1984). In the tree shrew however, individual cells project to single laminae (Condo *et al* 1986) and this segregation is maintained in the initial input to the cortex.

6. The Primary Visual Cortex

The primary visual cortex (V1) is located in the occipital lobe of the cerebrum and is the first cortical stage in the visual hierarchy where major processing of the image occurs. A stripe of myelinated fibres can be seen throughout V1 in primates, running in a line parallel to the surface midway between the pia and white matter and this is what gives it the name striate cortex. It has been described as the granular cortex, due to the relatively large number of small stellate cells and the fact that most output is to adjacent cortical areas and as such only small pyramidal cells with short axons are required. In the cat it is usually termed area 17 after the name given as part of the numbering system originally created by Brodman.

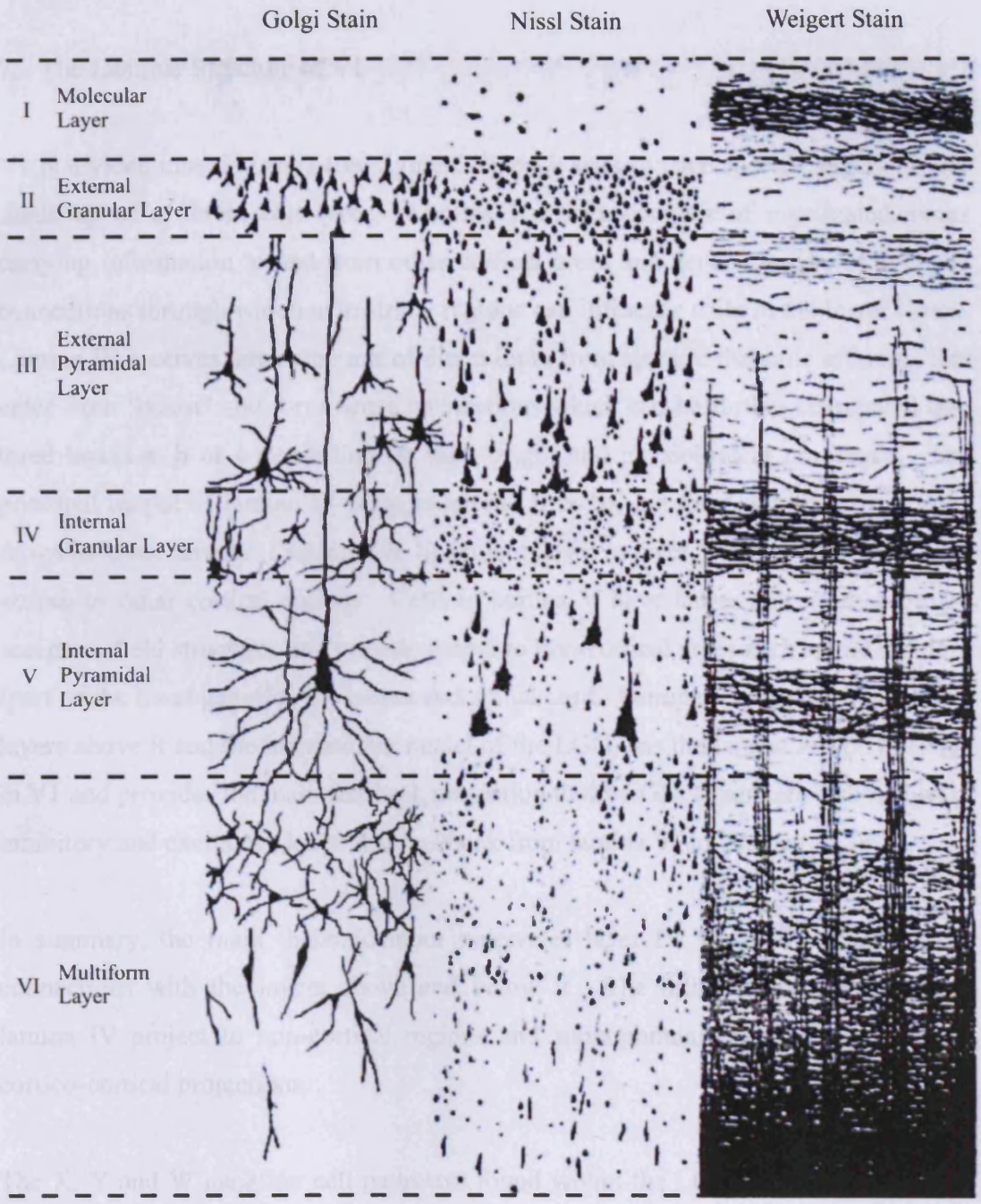

Figure 1.7 - Shows the laminar structure of the neocortex, after three different staining techniques. Golgi staining completely stains a small number of cells, clearly showing the distinctive pyramidal neurones. Layer III & V have the largest of these cells, whose axons innervate extrastriate and sub cortical regions respectively. Nissl staining only targets the cells bodies, clearly delineating the laminar boundaries and from which the granular appearance gives layer II & IV their name. Weigert staining highlights myelin, revealing vertically oriented afferents and efferents of the cortical cells. The two thick horizontal strips of axons in layer IV & V are called the outer & inner bands of Baillarger. They were at first thought to be axonal collaterals from thalamocortico projections, but ablation of cortical afferents revealed that they actually belonged to interneurones. (Picture adapted from Brodman K, VergleichendeLokalisation lehre der Grossirnrinde in ihren Prinzipien dargestellt auf Grund des Zellenbaues, 1909).

7. The Laminar Structure of V1

V1 is divided into six layers (see figure 1.7), each with its own specific functions and made up of different cell types. Lamina I mainly consists of myelinated axons carrying information to and from other cortical areas and dense clusters of synaptic connections through which extrastriate regions can influence cells in the lower layers. Lamina IV receives large amounts of direct input from specific thalamic afferents that enter from 'below' and form dense connections which can be further segregated into three layers a, b or c depending on their origin and physiological properties. The principal output of lamina IV is up to lamina II & III, but there are also projections down to lower layers. Lamina II & III project down to layer V and produce the main output to other cortical regions. Cells in lamina V have larger and more complex receptive field structures and provide output to non-cortical areas such as the striatum (part of the basal ganglia), brainstem and spinal cord. Lamina VI receives input from layers above it and the interlaminar nuclei of the LGN, has the largest receptive fields in V1 and provides the main feedback projection to the LGN. There are also recurrent inhibitory and excitatory loops that feedback from lamina VI to IV.

In summary, the main thalamic input innervates layer IV which forms excitatory connections with the layers above and below it. The infragranular layers below lamina IV project to non-cortical regions and supragranular layers above produce cortico-cortical projections.

The X, Y and W ganglion cell pathways found within the LGN are preserved in V1 and each projects to specific sub-laminae. X-cells only project to area 17 whereas Y-cells mainly project to area 17 with some very large cells projecting to area 18 (Levay & Ferster 1977). Y-cells project to lamina IV a & b, X-cells project to lamina IVc and both produce more minor X & Y-cell projections to lamina VI (Leventhal 1979, Levay & Gilbert 1976). Cytochrome Oxidase (CO) histology stains areas of the cortex that have high metabolic activity and reveals CO blobs that extend throughout the supragranular layers (lamina II & III) and the upper portion of layer IV in the cat (Murphy *et al* 1995, Boyd & Matsubara 1996). These blobs are evenly spaced with interblob regions between them, and show a tendency to remain within regions devoted to the left or right eye in primates (Hendrickson *et al* 1981), but this is not so

prevalent in cats (Murphy *et al* 1995). It has been shown that layer C LGN inputs to V1 (Boyd & Matsubara 1996) and low spatial, but high temporal frequency domains (Shoham *et al* 1997) are aligned with CO blobs. These observations indicate that layer C, Y-cells project to lamina IVa, CO blob regions and W-cells project to layer III blobs.

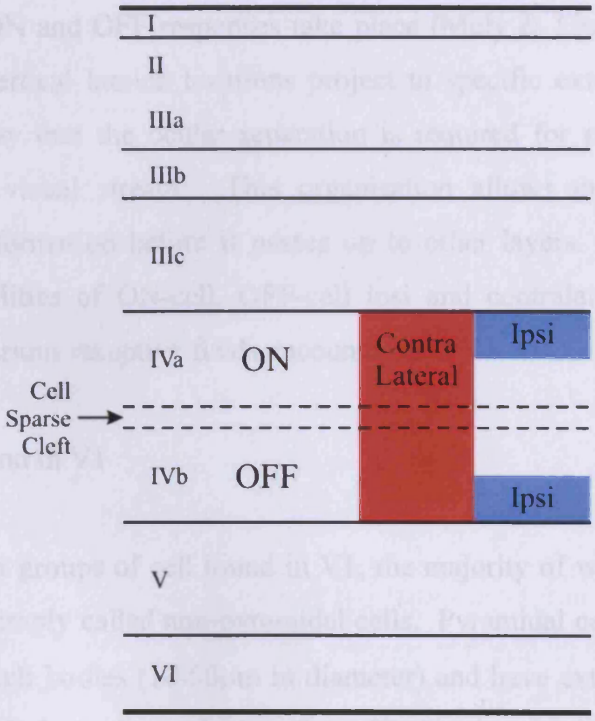

Figure 1.8 - Shows a diagrammatic representation of the tree shrew cortex, with almost half of the area taken up by lamina III, which can be split three ways into lamina a, b & c by cell density. The LGN projections to lamina IV are highlighted, with the contralateral eye projecting to the entire of the layer and the ipsilateral eye only to the upper and lower regions. Layer IV is also split into two halves by a cell sparse cleft, which matches functionally with the ON & OFF central geniculate terminations (Diagram adapted from Muly & Fitzpatrick 1992).

The functions of the tree shrew laminae are very similar to the cat, even if there are slight anatomical differences in their size and subdivisions, although the way left and right eye cells are organised is completely different. The LGN projects solely to the primary visual cortex in the tree shrew and not to other cortical areas (Conley *et al* 1984). As in the cat, the main thalamic input is directly into layer IV, which is functionally split depending on the nature of the thalamo-cortical projections (see figure 1.8). Contralateral eye input innervates the entirety of layer IV, whereas

ipsilateral eye input only innervates the very upper and lower portions (Harting *et al* 1973, Conley *et al* 1984). Layer IV is also split histologically into two halves by a cell sparse cleft, making the upper ON-cell subdivision IVa and lower OFF-cell subdivision IVb (Harting *et al* 1973). This ensures that any point in visual space is represented by both eyes and ON & OFF cell types. The ocularity of connections made in layer IV is maintained in the stratified projections up to lamina II & III where a combination of ON and OFF responses take place (Muly & Fitzpatrick 1992). As cells at different vertical lamina locations project to specific extrastriate regions, it raises the possibility that the ocular separation is required for particular processes further down the visual stream. This organisation allows the segregation and restructuring of information before it passes on to other layers. Thus, the various convergent possibilities of ON-cell, OFF-cell ipsi and contralateral characteristics contribute to the various receptive fields encountered in V1.

8. Cell Types Found in V1

There are two main groups of cell found in V1, the majority of which are pyramidal cells and the rest, simply called non-pyramidal cells. Pyramidal cells are named after the shape of their cell bodies (10-50μm in diameter) and have extensive arborisation oriented perpendicularly to the cortical surface. Their spiny dendrites are made up of an apical extension that reaches up from the cell body towards the cortical surface, forming a cluster of synapses at its tip and a basal tree that extends horizontally out from the bottom of the cell. Their axons can remain within the cortex or travel large distances to other extrastriate regions where excitatory glutamatergic synapses are forged, making them the output cells of V1. Non-pyramidal cells come in many different shapes and sizes, although most of them are either stellate or granular and have much smaller cell bodies (<10μm). Their axon collaterals rarely leave V1 making them the main interneurones. The stellate cells are excitatory and spiny like the pyramidal cells, with shorter axons that relay information from lamina IV to II/III (Feldemeyer *et al* 2002, Thomson *et al* 2002). There are also the star pyramidal cells (see figure 1.9F), named by Lorente de no (1949) whose cell bodies are located in layer IV and which possess similarities to both stellate and pyramidal cells. The radiating dendritic field, dense spine distribution and axonal reach are reminiscent of

stellate cells whereas the apical dendrites mimic those of pyramidal cells, although shorter and less complex (Jones 1975, Smith & Populin 2001). The remaining cells are smooth inhibitory cells that form GABAergic synapses and can be split into many types when described morphologically (see figure 1.9).

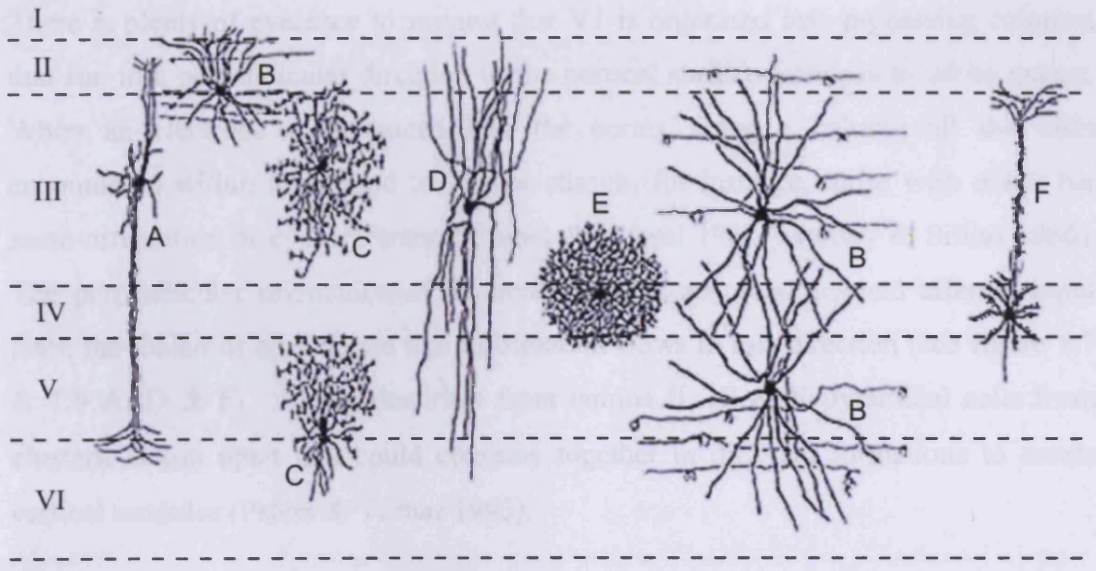

Figure 1.9 - Shows the main types of non-pyramidal cells encountered in the primary visual cortex. The six cortical laminae are delineated with dotted lines and numbered on the left. (A-E) are all smooth inhibitory GABAergic interneurones; (A) Double bouquet cell, (B) Basket cells are the main inhibitory neurone of V1 and come in various sizes, (C) Chandelier cells target the axons of pyramidal neurones, (D) Bitufted cells, (E) Neuroglial cells. Unlike the other interneurones star pyramidal cells (F) are glutamatergic excitatory cells that receive direct thalamic input and relay this information onto lamina II/III (Diagram adapted from Hendry & Jones 1991).

The main inhibitory cells in V1 are the basket cells, which take their name from the basket type shape created when many cells make convergent synapses around the pyramidal cell somata and proximal dendrites (Wang *et al* 2002). These connections allow basket cells to control the gain of the integrated response. There are also a large number of Martinotti cells found throughout laminae II-V whose axons ascend to lamina I and bifurcate extensively. They inhibit the apical dendritic tufts of pyramidal cells and thus play a role in feedback recurrent inhibition of cells in lower layers (Wang *et al* 2004). Chandelier cells are axon targeting cells that branch in such a way that vertical sections resembling candlesticks are formed. As can be seen from the brief descriptions above, inhibitory inter-neurones can also be divided depending on

the specific location of their axonal targets. Double bouquet cells, bitufted cells and neuroglial cells all target the dendrites of pyramidal cells (Markram *et al* 2004).

9. The Vertical & Horizontal Layout of V1

There is plenty of evidence to suggest that V1 is organised into processing columns that run in a perpendicular direction to the cortical surface from pia to white matter. When an electrode is advanced into the cortex along a column all the cells encountered within it respond to similar stimuli, for instance, those with either the same orientation or eye preference (Hubel & Wiesel 1962, Murphy & Sillito 1986). The perpendicular orientation of pyramidal cell axons, dendrites and afferent input from the thalamus all indicate that information flows in this direction (see figure 1.7 & 1.9 A, D & F). Apical dendrites from lamina II, III & V pyramidal cells form clusters, 56μm apart that could combine together in different formations to create vertical modules (Peters & Yilmaz 1993).

The size and influence of a column depends on the linking physiological property and the extent of horizontal connections that are made by the cells within it. When an electrode is advanced into the cortex tangentially to the surface the eye preference (or Ocular Dominance (OD)) changes at regular intervals (Hubel & Wiesel 1962). The layout of these OD regions has been mapped out with various histological techniques to produce a striped pattern in the macaque and patchy appearance in the cat (Hubel & Wiesel 1969, Levay *et al* 1978).

A much more complex picture is revealed when trying to produce similar maps based upon orientation preference (Hubel *et al* 1978). The mixture of gradual and abrupt changes in preference found in single tangential electrode tracks are difficult to reconstruct into a complete map. To account for these findings and to ensure that each both OD and orientation are given full representation at each retinal location an ice cube model was suggested (see figure 1.10 below).

Experiments involving optical imaging of the intrinsic signal allowed large areas of cortical response to be recorded, finally solving the riddle of the orientation map

layout. They revealed iso-oriented bands much like in the ice cube model and areas of rapid orientation change, either along fracture lines or around a single point, forming singularities called pinwheels. It has since been shown that the OD and orientation maps are intimately linked, with pinwheels tending to be located in the centre of OD patches (Hubener *et al* 1997)

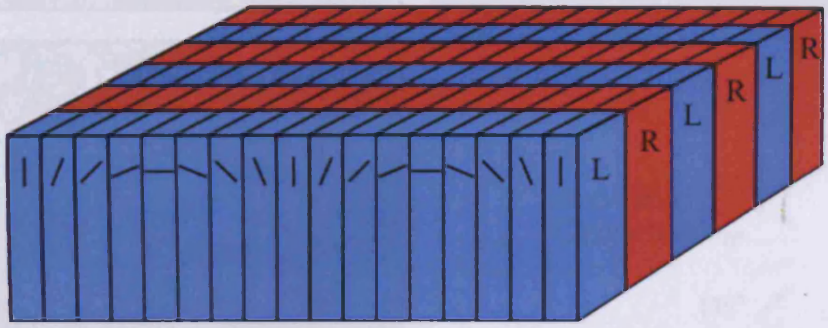

Figure 1.10 - Ice cube model that accounts for both OD and orientation layout indicated by single cell recording experiments. Ocular dominance slabs for left and right eye are shown in blue and red respectively, with much smaller orientation stripes cutting across the borders. Each ocular stripe has a full representation of all orientations, bearing in mind that this is an unrealistically regular diagrammatic representation (Diagram adapted from Hubel & Wiesel 1978).

There are horizontal connections made primarily by the pyramidal cells, that extend parallel to the cortical surface in layers II/III. Histological studies of the axonal arborisations emanating from these pyramidal cells reveal periodic patches of clustered connections over relatively large distances of around 2-5mm (Gilbert & Wiesel 1983, Rockland & Lund 1982). The cells within these patches tend to have similar receptive field properties, such as sharing the same orientation preference (Gilbert & Wiesel 1989). There are usually reciprocal connections between these patches, which could form the basis of an excitatory recurrent network (Kysvardy & Eysel 1992). In the tree shrew cortex the full range of these horizontal connection terminals covers a large elongated, anisotropic area. The axis of this elongated region is aligned with the preferred orientation of a cell when mapped out in visual space (Bosking et al 1997, Fitzpatrick 1996). However, the more local connections that are made within 500μm of the soma do not show this axial geometry, and connect cells that possess a broader orientation preference.

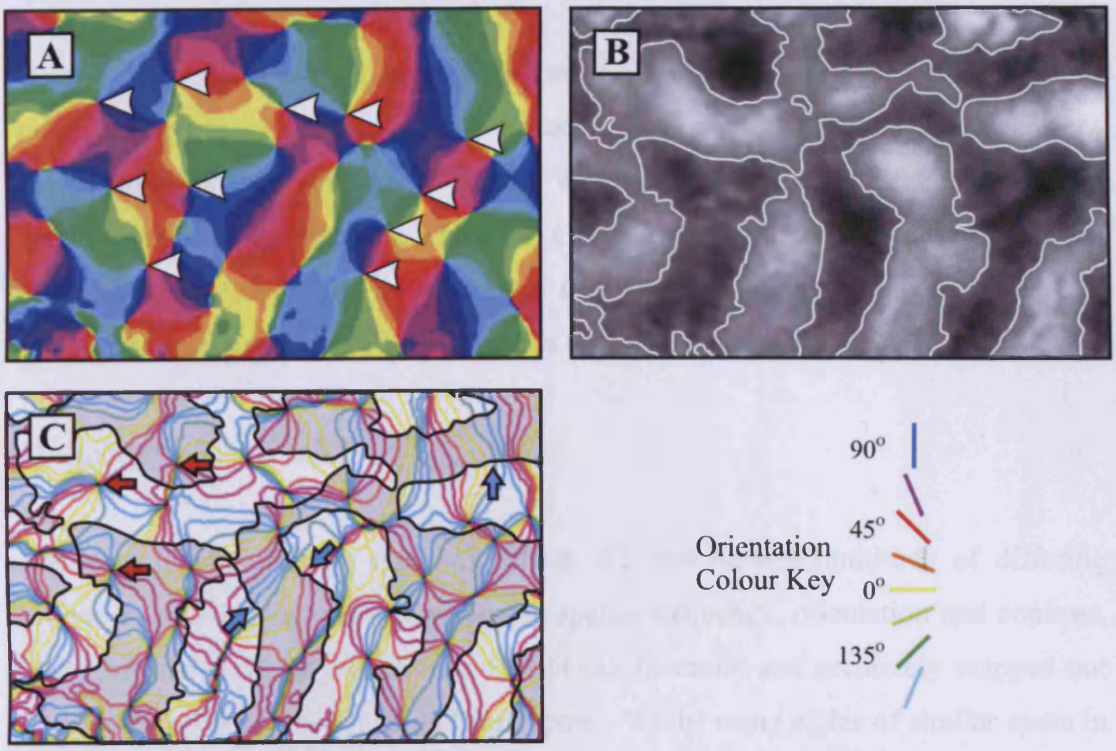

Fig 1.11 - Shows the different map layouts as recorded with optical imaging taken from experiment on 24/10/02. A - Shows a typical angle map, with each pixel coloured depending on its preferred orientation according to the key shown. The arrowheads pick out some of the most obvious pinwheel centres, and iso-orientation stripes are clearly seen throughout the image. B - Shows the ocular dominance map recorded from same animal, with the shading indicating dark left eye pixels and light right eye regions. The white contour delineates the boundary midway between OD extremes. C - Shows the link between orientation and OD maps by taking contour plots of each. The black contours are the same as the white ones in B and the three red arrows pick out the same three pinwheel centres in the top left corner of image A. As can be clearly seen, the pinwheel centres tend to be located in the centre of OD columns. Iso-orientation stripes run perpendicularly to OD column boundaries, as highlighted with the light blue arrows. This creates regions which are essentially the same as that proposed by the ice-cube model.

10. Retinotopic Representation in V1

Visual space is represented retinotopically in the primary visual cortex in both the tree shrew and the cat (Tusa *et al* 1978, Fitzpatrick 1996), in that stimulating two adjacent points in the visual field will evoke a response in neighbouring regions of V1. Due to the much greater convergence occurring in the periphery of the retina, there is less ganglion cell output from these areas. It follows that different retinal areas are not given equal representation, with the largest expanse of V1 devoted to processing information from the area centralis where visual acuity is greatest and convergence

least. This distorted representation can be mathematically described with a magnification factor (mm of cortical surface / degrees of visual field) that decreases exponentially with eccentricity (Daniel & Witteridge 1961). More local changes have been observed in the macaque where the OD and orientation maps cause distortions (Blasdel & Campbell 2001). Neither of these distortions is so marked in the tree shrew, although there is still a bias towards central region processing.

11. Receptive Fields in V1

There are many different types of cell in V1 that have a multitude of differing properties and display tuned responses to spatial frequency, orientation and contrast. The receptive fields of the retina and LGN can be easily and accurately mapped out with correctly positioned light and dark spots. Whilst using slides of similar spots in V1 Hubel & Wiesel noticed that oriented edges were far superior stimuli. This almost accidental observation occurred when changing stimuli, as the edge of the slide produced a vertical shadow which moved across the cells receptive field like a dark, oriented line. Out of these many possibilities it is surprising that only two categories, either simple or complex are needed to classify most of the cells in V1, depending on their receptive field shape and response properties (Hubel & Wiesel 1962). Simple cells have distinct excitatory and inhibitory regions and increase or decrease activity when a correctly oriented stimulus moves across each respective area. Such cells undergo linear spatial summation within regions, which means the underlying mechanism is linear and therefore possesses the property of additivity. This is best explained by example. If a first light spot (L1) is shone within an excitatory sub region of a simple cell receptive field it will produce a response (R1). A second light spot (L2) shone on an adjacent area within the same sub region will evoke a second response (R2). Additivity means that when shining L1 and L2 together the response will be equal to R1 + R2. In other words, as the spatial size of the stimuli increases or decreases there is a process of linear summation across the sub region that results in a corresponding change in the cell response. These sub regions are also mutually antagonistic, as displayed by their lack of response to illuminating stimuli covering the whole receptive field. They are thought to receive their initial feedforward input from aligned projections of ON-centre and OFF-centre LGN cells.

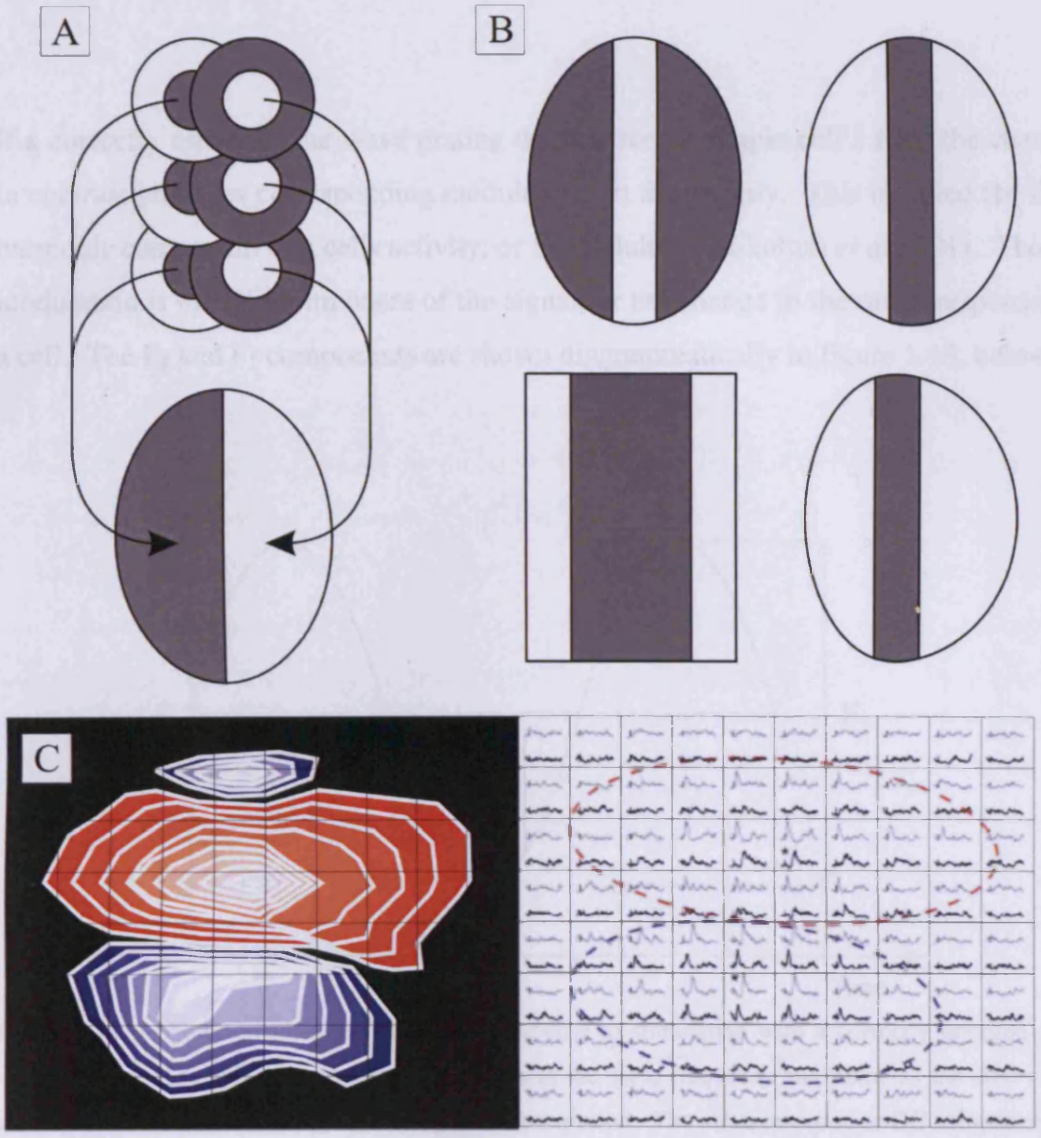

Figure1.12 - In all receptive field diagrams grey and blue areas denote off-subregions and white and red areas on-subregions. A - Shows a model of thalamo-cortical connections first proposed by Hubel and Wiesel, with a number of aligned LGN ganglion cells contributing input to a single simple cell. This convergence of the circular fields provides the initial excitatory input required to form the elongated, oriented receptive fields found in V1. The LGN ON-cells, shown with white centre/grey surround provide input to ON subregions and the OFF-cells to corresponding OFF subregions (diagram adapted from Hirsch 2003) B - Diagrammatic representations of four types of simple cell receptive fields, all with distinctive ON & OFF subregions. (adapted from Hubel & Wiesel 1962) C - Shows a linear kernel of a simple cells receptive field mapped out with grey and black flashing squares. Pairs of averaged responses to each grid position are displayed on the right, with the top grey traces corresponding to light flashes and the bottom traces to dark flashes. The dotted lines show approximate shapes & size of ON & OFF subregions. The flashes are shown pseudo-randomly, and a cross correlation with location and response is used to calculate responses. The left-hand panel shows a contour plot of the final smoothed field calculated by subtracting dark from bright responses. Linear fields mapped out in this manner are much broader than those recorded with oriented gratings and show that some form of non-linear processing is required to produce the resultant sharp orientation tuning (figure adapted from Hirsch *et al* 2003).

If a correctly oriented sine wave grating drifts across a simple cell's field the change in contrast produces corresponding modulations in the activity. This is called the first harmonic component of a cells activity, or F_1 modulation (Skottun *et al* 1991). The F_0 modulation is the DC component of the signal, or the change in the mean response of a cell. The F_0 and F_1 components are shown diagrammatically in figure 1.13, below.

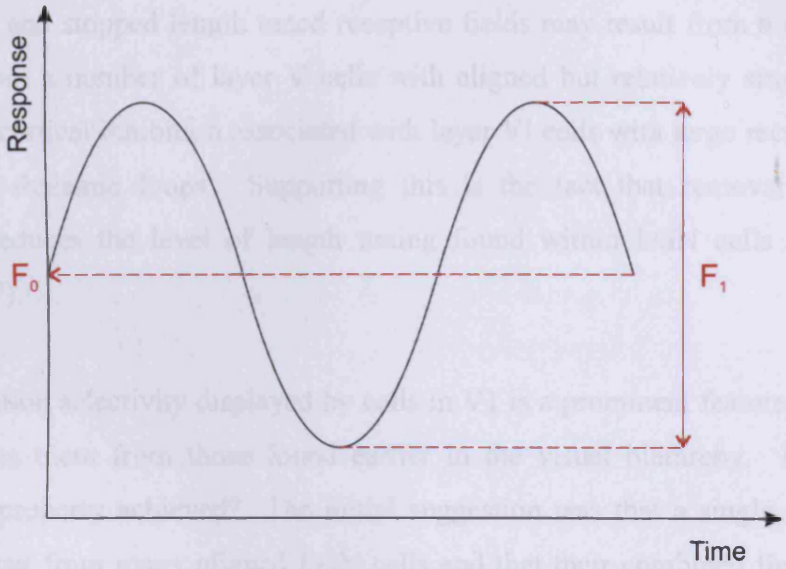

Figure 1.13 – Shows an idealised simple cell response to stimulation with a correctly oriented sine wave grating. The spike rate response modulates at the same frequency and phase as the sine wave stimulus, which is indicative of underlying linear integration. The mean response or DC component of the signal is designated F_0 and the first harmonic modulation is designated F_1. A cell can be accurately classified as simple if the F_1: F_0 ratio is greater than 1. In this idealised case all the responses are clearly separable from any spontaneous activity and the full modulation is visible. However, when recording actual responses a certain amount of half wave rectification occurs sometimes because it is not possible to have a negative firing rate. This would cause a flattening of the trough in the above curve, although changes can still occur in the cell on a sub-threshold level.

Complex cells also show a strong preference for oriented lines or edges, but their receptive fields do not show the distinct sub-regions, spatial summation or mutual antagonism as observed in simple cells. A drifting sine wave invokes a mostly sustained discharge for the period it passes over the receptive field or in other words little or no change in the F_1 modulation, which also provides a good way to easily classify cells experimentally.

Simple cells are mainly found in lamina IV and the upper portion of lamina VI, which are also the regions that receive direct thalamic input. There is a recurrent loop

between the simple cells found within these two layers (Hirsch *et al* 1998). Complex cells are found throughout laminae II, III, V & VI. Complex cells in lamina VI project up and connect with complex cells in laminae II, III and V (Hirsch *et al* 1998).

There also appear to be endstopped cells, which can be simple or complex, found mainly in layer VI and that respond to corners and specific lengths of oriented stimuli. Such large, end stopped length tuned receptive fields may result from a combination of input from a number of layer V cells with aligned but relatively small receptive fields, intracortical inhibition associated with layer VI cells with large receptive fields and cortico-thalamic loops. Supporting this is the fact that removal of cortical influence reduces the level of length tuning found within LGN cells (Murphy & Sillito 1987).

The orientation selectivity displayed by cells in V1 is a prominent feature that clearly distinguishes them from those found earlier in the visual hierarchy. How is this distinctive property achieved? The initial suggestion was that a single cortical cell receives input from many aligned LGN cells and that their combined fields produce the oriented response (Hubel & Wiesel 1962) and has since received support experimentally (Reid & Alonso 1995). This certainly appears to be the case, but the sharpness of tuning is still much greater than the linear summation of many gaussian inputs (see figure 1.12c). The influence of the cortical network connections, both inhibitory and excitatory is required.

Even though orientation selectivity is not shown strongly in the LGN how much does it contribute to the affect? Some cells in the tree shrew LGN display directional bias (van Dongen *et al* 1976) but this is rare in the cat. The receptive field of LGN cells occasionally has a slightly ellipsoid shape, some cells show direction selectivity in the tree shrew but this is much too small to account for orientation tuning of cells found in V1. Dense corticofugal axonal arborisation has been shown to correspond to the preferred orientation of the originating cell in visual space, when mapped out in the LGN visual field (Murphy *et al* 1999). The extent of the projection field is larger than a single LGN receptive field, and thus the feedback from a cortical cell influences the very same thalamic cells that provide its input. These cortico-thalamic projections, although not producing orientation selectivity in individual neurones of the LGN,

could influence response on a temporal scale, inducing synchronisation of many cells that are responding to a single elongate stimulus inducing a more prominent oriented response (Sillito *et al* 1994). Thus the quality of information relayed to the cortex for more efficient processing is improved, without changing the inherent spatial aspect of the thalamic cells.

12. Adaptation

In a similar way to light adaptation in the retina, cells in the visual cortex have to adapt to the changing environment to process visual information accurately and efficiently. The location and mechanism that produces this adaptive process is completely separate to that found in the retina. It was first noticed due to the alterations in perception that occur during the period immediately following certain visual stimuli. For example, the waterfall illusion is an optical effect that has been known since the time of Aristotle. After focusing on a waterfall for at least 30s and then looking away, the objects in front of you will then appear to move upwards in the opposing direction to that of the flowing water. This was extensively investigated by Wohlegemuth (1911) and is known in scientific circles as the motion aftereffect (MAE).

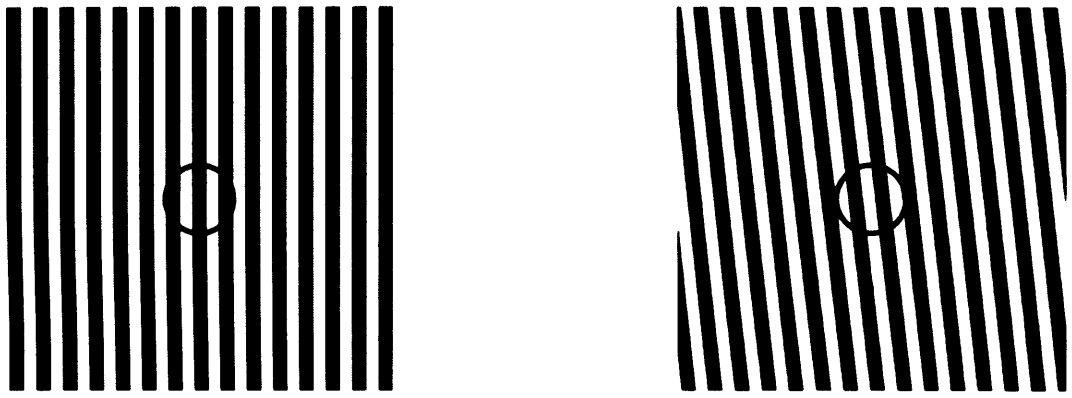

Figure 1.14 - A demonstration of the tilt aftereffect (TAE), a type of pattern adaptation. Fixating the gaze in and around the circle in the centre of the right diagram causes adaptation to that grating. The after effect caused by this adaptation means that the left vertical grating appears slanted in the opposite direction.

The perception of colour, position, contrast, orientation and spatial frequency can also be altered in a similar manner. The tilt aftereffect occurs after presentation of an obliquely oriented grating for thirty seconds or so. It causes a following vertical grating to appear tilted in the opposite direction to the original (see figure 1.14). This occurs because the perception of orientation is based upon the integration of information from large numbers of neurones. During the post adaptation period when the adaptive effect is strongest, those neurones that respond preferentially to the oblique adapting grating are suppressed. This causes a bias in perception towards those neurones which prefer an orientation orthogonal to the adapting stimulus, resulting in the observed effect. After looking at a high contrast pattern consisting of black and white bars subsequent similar patterns of lower contrast become harder to perceive (Georgeson, 1980). In other terms, the contrast threshold of observed square wave gratings is raised after adaptation to a high contrast stimulus. This contrast threshold elevation is very useful experimentally, as it relies less on the subjective estimation of test subjects.

In fact, virtually any strong steady visual stimulus will produce an aftereffect through adaptation mechanisms. These two effects, involving the perception of orientation and contrast are known as pattern adaptation and will be utilised in this thesis to elucidate the mechanisms of the primary visual cortex.

13. Physiological Correlates of Adaptation

Where does this reduction in neuronal responsiveness occur in the visual system? The first neural correlate of adaptation was seen in directionally sensitive cells in the rabbit retina. Barlow and Hill (1963) found that the spontaneous activity recorded from single cells was reduced after prolonged stimulation in the preferred direction. Unfortunately, the marked differences between the visual system organization in rabbits, cats and tree shrews make direct comparisons between the species impossible. This initiated the use of single cell recordings in providing physiological explanations of adaptation. The initial attempts sought to compare results with earlier psychophysical studies. The discharge rate of directionally sensitive cells in V1 declines after lengthy activation with a moving grating (Vautin and Berkley 1976). A similar reduction in firing caused by spatial contrast adaptation follows the same time-

course of adaptation and recovery as the perceptual aftereffects, providing a good causative link (Albrecht *et al* 1984). V1 is the first stage in the visual hierarchy that binocular and orientation selective neurones are present. Thus, the orientation selectivity and inter-ocular transfer of adaptation give further weight to its cortical origin. These aspects are considered in much greater detail in chapters 2 & 3.

Extensive studies by Ohzawa *et al* (1982, 1985) delineated the single cell properties of adaptation. A comparison between responses in the LGN and V1 in the cat discovered little adaptation in the LGN, providing conclusive evidence for the cortical origin of this phenomenon (Ohzawa *et al* 1985). No adequate correlate for adaptation has been found in subcortical structures and it appears that they are largely unaffected by the process (Movshon & Lennie 1979).

14. Adaptation as a Contrast Gain Control System

In a similar way to the luminance gain control found in the retina, adaptation can be described as a contrast gain control system (Ohzawa *et al* 1985). Plotting the response of cells on a log-contrast scale produces a sigmoidal function with characteristics that are dependent on the context in which it is recorded (see figure 1.15). The sharp gradient of this contrast response function (CRF) indicates a large differential of response and high sensitivity over a small range of contrasts. After adaptation to a high contrast grating the threshold of the cell is raised and the function undergoes a rightward shift along the log-contrast scale (Ross & Speed 1996). A lateral shift has also been observed after adaptation to low contrast gratings, indicating that increases in activity are also possible (Sclar *et al* 1985). The result of such adaptation is to centre the steep linear portion of the CRF on the adapting contrast. In other words, the contrast needed to produce a half-maximal response is equivalent to the adapting contrast. Gain is defined in electronic terms as an increase in signal power by an amplifier expressed as the ratio of output to input. An adaptation induced rightward shift of the CRF along the log-contrast axis indicates a reduction in the output:input ratio, or in other words there has been a decrease in gain. Thus, adaptation can be thought of as a contrast gain control mechanism that changes a cells response properties depending on the ambient level of contrast. It is worth highlighting that there is no fixed CRF for an individual cell and that contrast

processing is a dynamic process, reflecting the continually changing environment. Thus, any contrast response can only capture the functional state of the neurone in that moment. The function of such a mechanism is to allow neurones with a precise, but limited response range to provide accurate and sensitive information over a large range of contrasts.

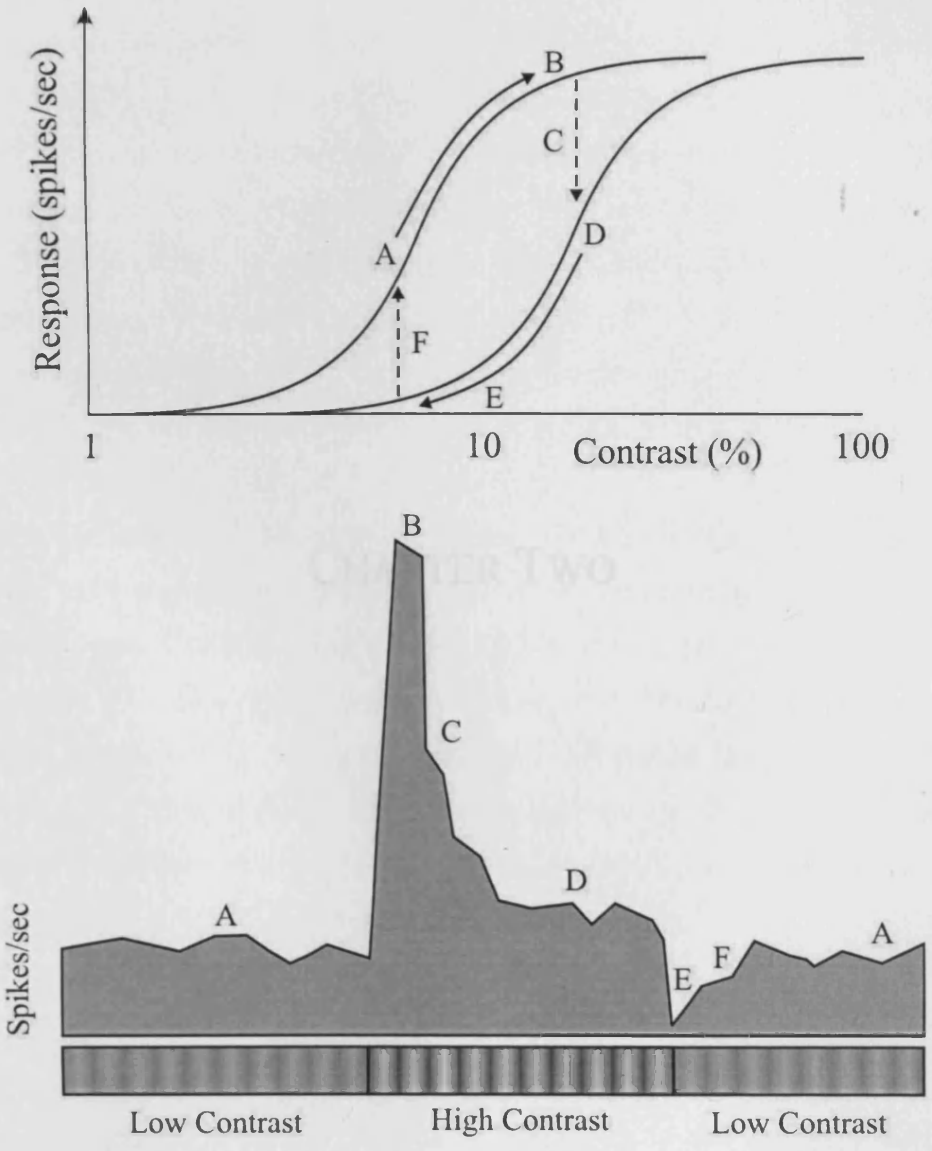

Figure 1.15 - Shows what happens in the ideal cortical gain loop transferring from one adapted state to another and back again. The lower diagram shows the spiking response of a typical simple cell in V1 before, during and after adaptation. The actual adaptation itself occurs at point C and results in a reduced response at point D and post-adaptation suppression at point E (Responses adapted from Albrecht *et al* 1984).

CHAPTER TWO

INTRODUCTION TO OPTICAL IMAGING

1. Functional Brain Mapping Techniques

There are many different methods for investigating the functional activity of the visual cortex, from the most invasive procedures like extracellular recording with multiple electrodes to more external methods such as functional magnetic resonance imaging (f-MRI). Each one has its benefits and disadvantages, and a full range of techniques is required to appreciate the workings of the visual cortex at different levels. Those techniques which rely on haemodynamic or metabolic parameters and have a direct relevance to optical imaging (OI) of intrinsic signals will be briefly discussed below. Positron emission topography (PET), f-MRI, near infrared spectroscopy (NIRS) and OI all rely on changes in the vascular response associated with neuronal activity to produce functional maps of the primary visual cortex.

One of the first methods to reveal the functional layout of the visual cortex utilises the connection between metabolic activity and neuronal responses by using a radioactive glucose analogue, 2-deoxyglucose (2-DG). After administration, visual stimulation causes uptake of 2-DG by metabolically active cells. Removal of the brain and histological preparation of the tissue is required to visualise the pattern of activity, whether that be OD or even orientation columns (Hubel *et al* 1977). Although the high spatial resolution is a distinct advantage, the timescale involved in this process is too long for study of the relatively short effects of adaptation.

2. Positron Emission Tomography

Positron emission tomography (PET) was first discovered in the seventies and can be used to observe cerebral blood flow (CBF), oxygen & glucose metabolism and receptor concentrations of the brain *in vivo*. Attaching positron emitting molecules such as 11C, 13N, 15O or 18F can create a variety of mildly radioactive isotopes of biologically active molecules. Depending on the intended use different tracers can be administered, the most common of which include radioactive water ($H_2{}^{15}O$) and glucose (fluoro-2-deoxyglucose or FDG) for measuring CBF and metabolic rate

respectively (examples of use in cats; Hassoun *et al* 2002, Schaller *et al* 2004). Once in the bloodstream, these tracers are transported to the brain, where the emitted positrons collide with free electrons to produce pairs of gamma rays. Increased blood flow or metabolism in active regions means a greater number of radioactive molecules and collisions occur in that location, producing a larger signal. Coincidental recording of gamma ray pairs allows the collision location to be pinpointed in space, the data from which is then recreated into computerised 2-D or 3-D images. More recently developed compounds have allowed the concentration of neurotransmitter receptors and psychoactive drugs in both humans and cats to be visualised (Shimada *et al* 2000, Hassoun *et al* 2002, Ginovart *et al* 2003). Unfortunately, there are numerous limitations with this technique, in that the half-life of the isotopes requires long imaging sessions, their radioactive nature limits repeated use and the spatial resolution is low, reaching 5-10mm at best.

3. Functional Magnetic Resonance Imaging

Functional magnetic resonance imaging (f-MRI) is a more recent non-invasive technique that can record blood oxygen-level-dependent (BOLD) changes that are related to oxygen utilisation and cerebral blood flow. A coherent spin in atomic nuclei (mainly protons) that is aligned with a homogenous magnetic field can be induced with radio frequency electromagnetic pulses. The radio wave signal produced by this paramagnetic field decays quicker in those molecules that are more susceptible to magnetism (Cohen & Bookheimer 1994). Deoxy-haemoglobin (HbR) is an endogenous paramagnetic agent that has a greater susceptibility than oxyhaemoglobin (HbO_2), and this provides the basis for the contrast between areas with different HbR-HbO_2 ratios (Ogawa *et al* 1992). Cortical activity causes an increase in regional cerebral blood flow and the influx of oxygenated blood reduces the HbR-HbO_2 ratio (see figure 2.2), which in turn lengthens the decay time and increases the signal in that area. This positive BOLD signal has a relatively low spatio-temporal resolution of a few millimetres recorded over a period of seconds, that is far too coarse to discern cortical columns, but is very useful for use in clinical applications and experiments in humans. This technique has been used to show distinct V1 activation during visual stimulation in humans (Kwong *et* al 1992) and changes in the BOLD signal have also been monitored in cats after respiratory

challenge (Turner *et al* 1991). More recently, Kim *et al* (2000) have achieved a greater spatio-temporal resolution in cat V1 by utilising the 'initial dip' in the BOLD signal (explained in greater detail below). They recorded maps of orientation columns in the primary visual cortex of cats, although the link between the BOLD signal and underlying cortical function at this scale is still uncertain.

4. Voltage Sensitive Dye Imaging

A much more direct method of visualising V1 activity involves voltage-sensitive dyes (VSD), which as their name suggests, change their fluorescence depending on the potential across the membrane to which they bind. The spatio-temporal resolution of this technique is its main advantage, allowing visualisation of changes in activity occurring in cortical columns, over millisecond time periods (Shoham *et al* 1999). The membrane potential alterations occurring in the relatively large surface area of dendritic trees contribute as much as evoked neuronal activity to the voltage changes measured with this technique (Grinvald *et al* 2003). This means that the subthreshold neuronal activity can be clearly discerned, providing a way to see such things such as the dynamic regional cortical responses underlying spontaneous spiking activity (Arieli *et al* 1995, Tsodyks *et* al 1999, Kenet *et al* 2003). It can also be utilised to monitor the spread of activity across the cortex and investigate dynamic changes in orientation tuning curves. Refinement of the technique has resulted in successful long-term studies of functional cortical maps in primates (Slovin *et al* 2003), contrary to earlier attempts in which bleaching and photodynamic damage occurred (Orbach *et al* 1985). There are pharmacological implications of using dyes which cause slowed responses and reduced signal to noise ratios which place limits on intensive recording sessions and dye concentrations (Slovin *et al* 2003). A complementary combination of VSD and optical imaging of intrinsic signals was used in pioneering experiments investigating the possibility of using intrinsic parameters alone for imaging (Grinvald *et al* 1986). VSD imaging was also used to first reveal the functional layout of orientation columns in the monkey striate cortex (Blasdel & Salama 1986)

5. Optical Imaging of Intrinsic Signals

Any change that occurs in the optical properties of cortical tissue due to electrical or metabolic activity is known as the intrinsic signal. Optical imaging of intrinsic signals (OI) uses digital cameras to observe these changes in order to ascertain the function and properties of underlying cortical activity. It is a recently developed technique that was first discovered and investigated by Grinvald and co-workers in the mid eighties and early nineties (Grinvald *et al* 1986, Frostig *et al* 1990, Bonhoeffer and Grinvald 1996). The fact that large areas of the cortex can be imaged at the same time, coupled with relatively good spatial and temporal resolution makes this method ideal for revealing the architecture underlying functional maps of the neocortex (Chen-Bee *et al* 1996 & 2000). It is not as invasive as electrophysiology and does not need any potentially damaging pharmacological applications, which makes it ideal for chronic studies of cortical development with repeated imaging sessions of the same animal in vivo.

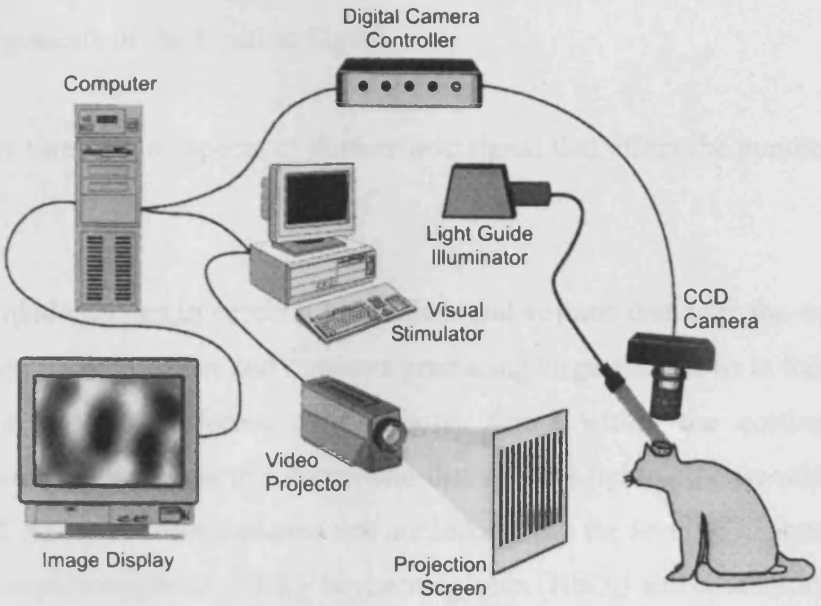

Figure 2.1 - Typical imaging setup required to perform optical imaging of intrinsic signals in cats to produce activity maps (Bonhoeffer & Grinvald 1996).

Optical imaging has contributed greatly to our understanding of how the visual cortex is organised and solved many riddles that were virtually impossible with alternative techniques. This technique utilises the close link between cortical activity and

changes in haemoglobin between its different oxygenated states (Chance *et al* 1962) and alterations in the amount of light scattering due to cell swelling. Transmittance measurements of near-infrared radiation to monitor the amount of oxygenation of particular metabolites showed that these changes could be determined optically (Jobsis *et al* 1977). The initial attempts at OI were performed with a combination VSDs and electrical recordings, to verify that the intrinsic signal is closely correlated with neuronal activity (Grinvald *et al* 1986).

A more refined setup than that used in those first experiments for OI in the cat can be seen in figure 2.1 (Bonhoeffer and Grinvald 1996). A projection screen is used to show grating stimuli that activate cells in the visual cortex. Red light is directed onto the exposed cortical surface and any reflected photons are recorded by a digital camera. This information is passed onto a computer where analysis produces greyscale images in which the dark areas represent areas of high neuronal activity (see below).

6. Components of the Intrinsic Signal

There are three main aspects of the intrinsic signal that affect the number of reflected photons:

i. Global changes in cerebral blood flow and volume that alter the overall level of haemoglobin, water and nutrients producing large alterations in the signal.
ii. The ratio of different chromophores found within the cortical tissue. A chromophore refers to a compound that absorbs light at the wavelength used for OI. Relevant chromophores that are linked with the level of oxygenation include deoxyhaemoglobin (HbR), oxyhaemoglobin (HbO_2) and cytochrome oxidase.
iii. Scattering of light originating from chaotic refraction from the various organelles, ions, cell membrane and difference in refractive indices found between intra and extracellular fluid. This last aspect is even present in cortical slices, which have no blood flow (Lipton 1973). Activation of neurones and the accompanying ion and water exchanges, capillary expansion and neurotransmitter release cause highly localised increases in the level of light scattering.

The part of the signal related to the oxygen level is very small, with the change in reflectance affecting only 1 part in 1000. These different components can be recorded by using a whole spectrum of light wavelengths combined with spectroscopy. The wavelength of light chosen for these OI experiments is sensitive to changes in the chromophores and levels of light scattering.

7. The Importance of Light Wavelength

The wavelength of light used determines how deep the photons penetrate into the cortex, how much absorption occurs and how many are reflected back out for recording. Longer wavelengths penetrate deeper and reflect less photons than shorter wavelengths. For the purposes of OI of the intrinsic signal the relative extinction coefficients of the different oxygenated states of haemoglobin are vitally important (see figure 2.2).

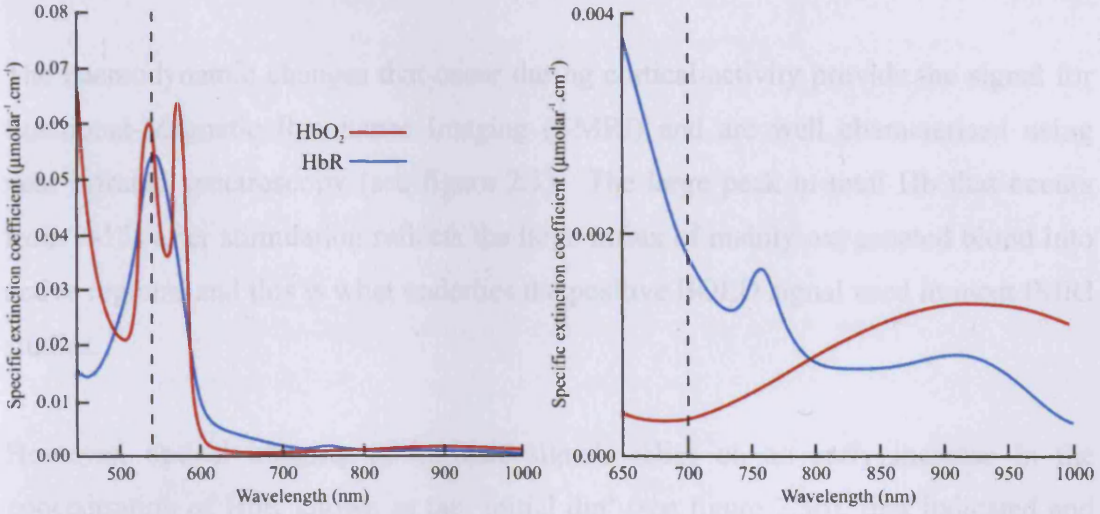

Figure 2.2 - Shows the absorption spectra of HbR and HbO_2 for different wavelengths of light in the visible and near infrared regions. The graph on the right is a zoomed in portion of that on the left to show the relative difference in spectra at 700nm more clearly. The greater absorption by HbR at higher wavelengths explains its slightly blue appearance compared to the well known bright red of oxygenated blood. The dotted lines indicate the two wavelengths used in our experiments for visualising blood vessel patterns and intrinsic signal imaging at 540nm and 700nm respectively (more explanation in text). Wavelengths of around 680nm and 830nm are used in near infrared spectroscopy to separate the responses to both HbR and HbO_2 during simultaneous recording. (Diagram adapted from Horecker, 1943)

Below 600nm a greater proportion of the signal contains information about vascular events rather than neuronal activity due to the relatively large absorption by both types of Hb (McLoughlin & Blasdel 1998). A shorter wavelength range of 500-550nm (green light) only penetrates a short distance before being absorbed by haemoglobin in the blood vessels or bounced back by the surface layers. This reveals the blood vessel pattern as clear dark lines, contrasted against the lighter surrounding neural tissue. OI can be performed with light of wavelengths between 650-720nm (red light), in which range a compromise between deeper penetration beyond the surface blood vessels and a greater loss of photons is reached. The intensity of light is adjusted to the maximum level possible without saturating the CCD chip wells in the camera. Even after such compensation it is very difficult to obtain a reliable signal below lamina IV, with most images recorded from lamina II-III. The important factor is that HbR absorbs a greater proportion of light than HbO_2 that shows up as dark patches of locally activated regions.

8. The Link Between the Intrinsic Signal and Neuronal Activity

The haemodynamic changes that occur during cortical activity provide the signal for functional-Magnetic Resonance Imaging (f-MRI) and are well characterised using near infrared spectroscopy (see figure 2.3). The large peak in total Hb that occurs from 2-15s after stimulation reflects the large influx of mainly oxygenated blood into active regions, and this is what underlies the positive BOLD signal used in most fMRI studies.

However, optical imaging of intrinsic signals relies on an early increase in the concentration of HbR known as the 'initial dip' (see figure 2.3b), first indicated and verified using imaging spectroscopy (Grinvald *et al* 1986, Frostig *et al* 1990). OI of the 'initial dip' has been performed in the visual cortex of cats and both awake and anaesthetised primates (Malonek *et al* 1997, Shtoyerman *et al* 2000). It also produces a negative BOLD signal that has been used in f-MRI studies of cats and primates to obtain a greater spatial resolution, capable of imaging cortical columns (Logothetis *et al* 1999, Kim *et al* 2000, Duong *et al* 2001). The link between the 'initial dip' and functional columns was confirmed in a study by Thompson *et al* (2003) in which

simultaneous recording of tissue oxygenation and single cell neuronal activity was performed in the primary visual cortex of cats.

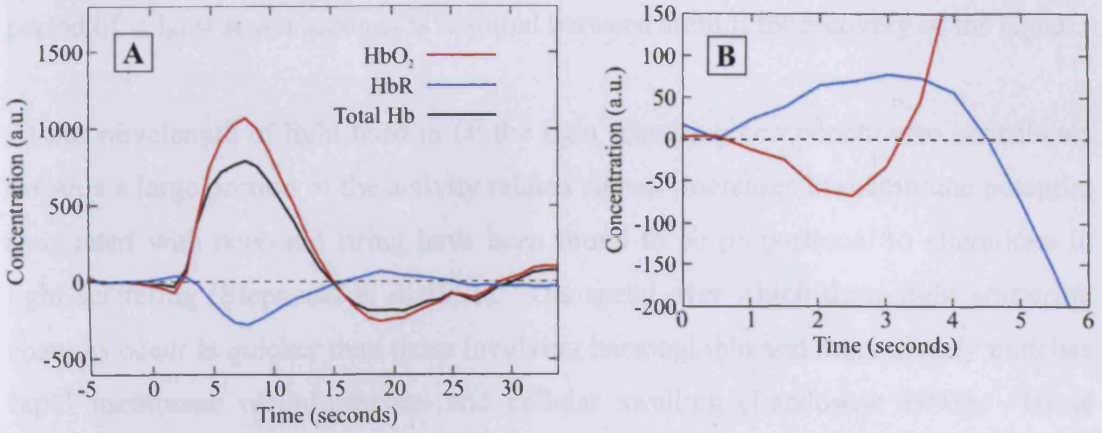

Figure 2.3 - A Shows the results of a near infrared spectroscopy (NIRS) study of the primary and secondary visual cortex in humans after intense stimulation with a flashing counter phase checkerboard. By using two different wavelengths of 682 & 830nm light the simultaneous change in both HbR and HbO_2 can be seen with this technique. The large increase in HbO_2 & Total Hb at 3s and decrease in HbR at 4s is clearly visible, due to the influx of fresh blood to the activated region.
B - Shows the 'initial dip' in HbO_2 and rise in HbR occurring between 1-4s that is thought to be the result of local increases in metabolic consumption of O_2 that are closely coupled to neuronal firing (see text for details). These two curves are not merely a close up of those in A as the differential path length is not the same in each case (Diagrams adapted from Jasdzewski et al 2003).

The most likely explanation is that neuronal activity in the cortex produces a localised increase in the metabolic consumption of oxygen, which occurs 1-2s after stimulus presentation, before an increase in cerebral blood flow. This idea is supported by combining phosphorescence quenching and OI which confirmed a drop in blood oxygenation levels that precedes any change in blood volume (Vanzetta *et al* 2002). Thus, ratio of HbR:HbO_2 is increased, which in turn raises the level of absorption, producing the dark regions of activity in an image. This tight coupling of chromophore alteration and cortical activity allows a good spatial resolution of 100μm to be reached, providing information on individual cortical columns. This figure is limited by the size of the microvasculature and the point spread of the signal. The point spread is due to the fact that oxygen consumption is related to both synaptic and action potentials, so the resolution of the signal is less than that for an individual

firing event. Having said that, the intrinsic signal is still closely linked with the spiking rate of a cell. This is because action potential propagation places the greatest energy demand on the cortex (Attwell & Laughlin 2001) and thus oxygen consumption and energy usage is largely governed by the action potential rate. A period of at least seven seconds is required between stimuli for recovery of the signal.

At the wavelength of light used in OI the light scattering component also contributes towards a large portion of the activity related signal. Increases in membrane potential associated with neuronal firing have been found to be proportional to alterations in light scattering (Stepnoski *et al* 1991). The speed over which these light scattering changes occur is quicker than those involving haemoglobin and more closely matches rapid membrane reconformation and cellular swelling (Landowne 1993). These factors contribute to the tight spatial and temporal coupling between the light scattering component of the signal and physiological activity (Rector *et al* 1993).

9. Functional Maps of the Primary Visual Cortex

The part of the signal that corresponds to changes in neuronal activity is a tiny fraction of the whole (about 1 part in 1000) and has to be carefully extracted through data analysis. There are various factors that have to be considered, and methods have been created to ensure that activity maps are based on the neuronal response.

Sinusoidal moving gratings are the most commonly used stimuli to obtain functional maps of visual parameters such as orientation, ocular dominance and spatial frequency. This relies on an event-related design in experiments, where the change in reflectance to a stimulus is averaged over many repeated presentations. Global stimulation of the visual cortex that occurs with such stimulus protocols that is not directly coupled to the spiking rate has to be removed. For example, in the case of orientation maps a set of oriented stimuli is used to cover the full 180° range. Addition of all the images captured whilst viewing each orientation and taking an average gives a 'cocktail blank' image. This represents that portion of the signal that is constant throughout stimulation with each orientation. Subtracting this cocktail blank from the image recorded with a single grating creates an orientation activity map as shown in figure 2.4 a&b.

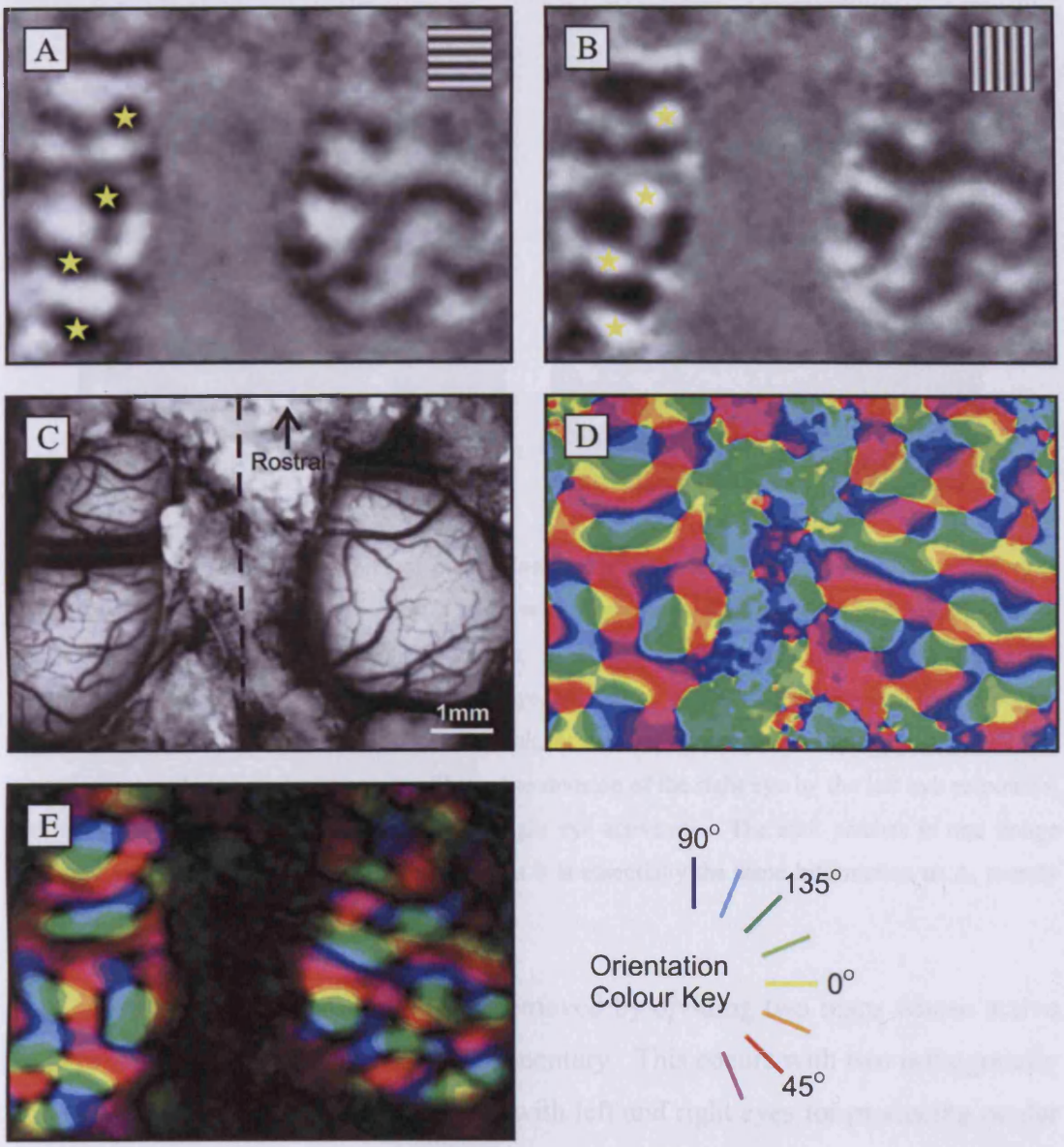

Figure 2.4 - Shows typical examples of blood vessel and activity maps recorded using optical imaging from the primary visual cortex in cat 171201. A – The orientation activity map recorded after stimulation with a drifting sine wave grating of 0° orientation (stimulus shown in top right corner). The dark patches indicate activated regions, with yellow stars indicating four strongly responding areas in the left hemisphere. B - Shows the orientation activity map after stimulating with an orthogonally oriented 90° sine wave grating. The yellow stars are in precisely the same location as in A, which allows a direct comparison between the two figures. This highlights the way the maps compliment each other such that the active regions of the 0° map match the light inactive areas of the 90° maps. C – Shows the blood vessel map for this imaging session recorded using green light with a wavelength of 540nm. The dashed line down the centre of the image indicates the intact cranium along midline, which separates the two revealed regions of cortex from each respective hemisphere. D - Shows the angle map produced after vectorial addition of the orientation maps. The colour of each pixel indicates its preferred orientation, as designated by the adjacent orientation colour key. E – Shows a polar map in which the brightness of each pixel gives an indication of the signal strength. The strongest responding regions match the areas of the cortex revealed in figure C that are most clearly in focus and free from large blood vessels. (An explanation of angle and polar map creation is found within the main text).

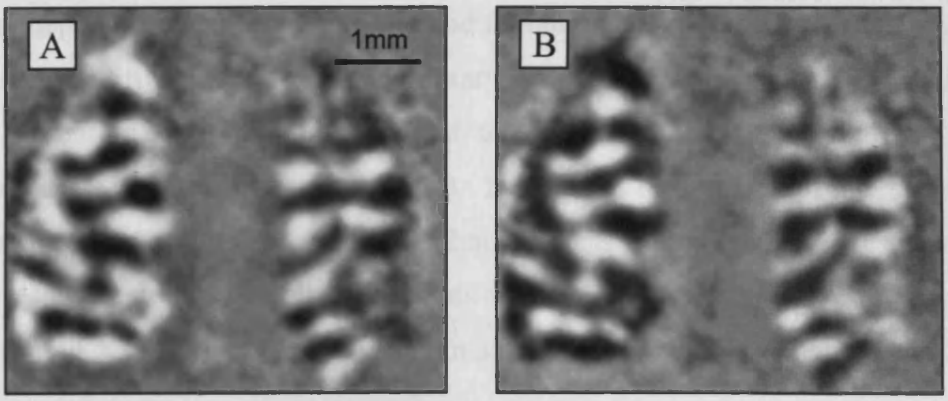

Figure 2.5 - Shows typical examples of ocular dominance maps recorded in cat 170303. The grey featureless regions of the maps are areas of bone, with a central band splitting the two hemispheres in which there are clear ocular dominance columns. A – This activity map is created by adding the responses to all the orientations shown to the left eye, by the sum of all those for the right eye. There is no need to divide the images with a cocktail blank, as any constant signal between the two maps is cancelled out within the calculation. B - Shows the division of the right eye by the left eye responses, with the dark patches in this case representing right eye activation. The dark patches in one image match the light ones in the other and vice versa as it is essentially the same information as A, merely presented with a reversed greyscale.

This constant global signal can also be removed by dividing two maps whose active regions are spatially opposite and complementary. This occurs with two orthogonally oriented stimuli (as in figure 2.4 a&b) or with left and right eyes for producing ocular dominance maps (see figure 2.5). Various features of the visual scene including ocularity, spatial frequency and temporal frequency can be used to produce activity maps (Issa et al, 2000) which have provided us with a better understanding of the functional architecture and the representation of key visual parameters across the cortical surface.

An angle map can be created via vectorial addition of activity maps for four or eight orientations (0, 22.5, 45, 67.5, 90, 112.5, 135 & 157.5). The response of a pixel to each individual orientation is first converted into a vector, the angle of which is determined by the respective stimulus. After vectorial addition a single vector is produced for each pixel, the angle of which provides the orientation preference by which a colour can be assigned according to the scale in figure 2.4. The first pioneers who used this technique solved the major puzzle of cortical organization of orientation columns with this method (Bonhoeffer & Grinvald 1991). An example of

such a map can be seen in figure 2.4e and it contains many distinct features that are found across different species in the primary visual cortex. A polar map contains an extra dimension of information, in that the length of the vector for each pixel determines its brightness (see figure 2.4d). This allows the strength of the response to be visualised across the imaged area although it has limitations. For instance, if a pixel responds strongly to all orientations their vectors will cancel each other out, appearing like a weakly responding area in a polar map when this is not the case.

10. Optical Imaging in Different Species

OI of the intrinsic signal has also been used to compare and contrast functional maps between different species. The angle maps in both cats and tree shrews are very similar, with recognisable features such as pinwheels, fracture lines and iso-oriented regions presents in both. The area of the primary visual cortex available for imaging is much greater in the tree shrew however, as can be seen in figure 2.6. This means that the combined receptive fields of those neurones within this imaging region cover a large area of the total visual field seen by the tree shrew. There is relatively little retinotopic distortion, as can be seen from the rather uniform width of striped zones of activity outlined in figure 2.6C. This is in direct contrast to the cat or primates, where a greater area of the cortex is devoted to neurones whose receptive fields correspond to the central area of the visual field as compared to more peripheral areas.

Large areas of cortex have to lie in the same parallel plain as the CCD chip in the optical imaging camera in order to obtain an accurate focus and strong signal. The smaller size of the tree shrew and the lack of gyri or sulci on its cortical surface both aid in this particular issue. Unfortunately, a large part of V1 in cats is unavailable for imaging due to its physically unreachable location along the calcarine fissure and between the hemispheres. However, the combined receptive fields of the neurones in the region that is available for accurate imaging cover the central area of the visual field.

Attempts at obtaining an OD map similar to that in primates and cats in the tree shrew have proved impossible, confirming earlier histological and single cell recording findings. This is due to the organisation of inputs from the two eyes being arranged in

laminae that run parallel to the cortical surface (see figure 1.8 in main introduction) and are thereby inseparable when viewed from above.

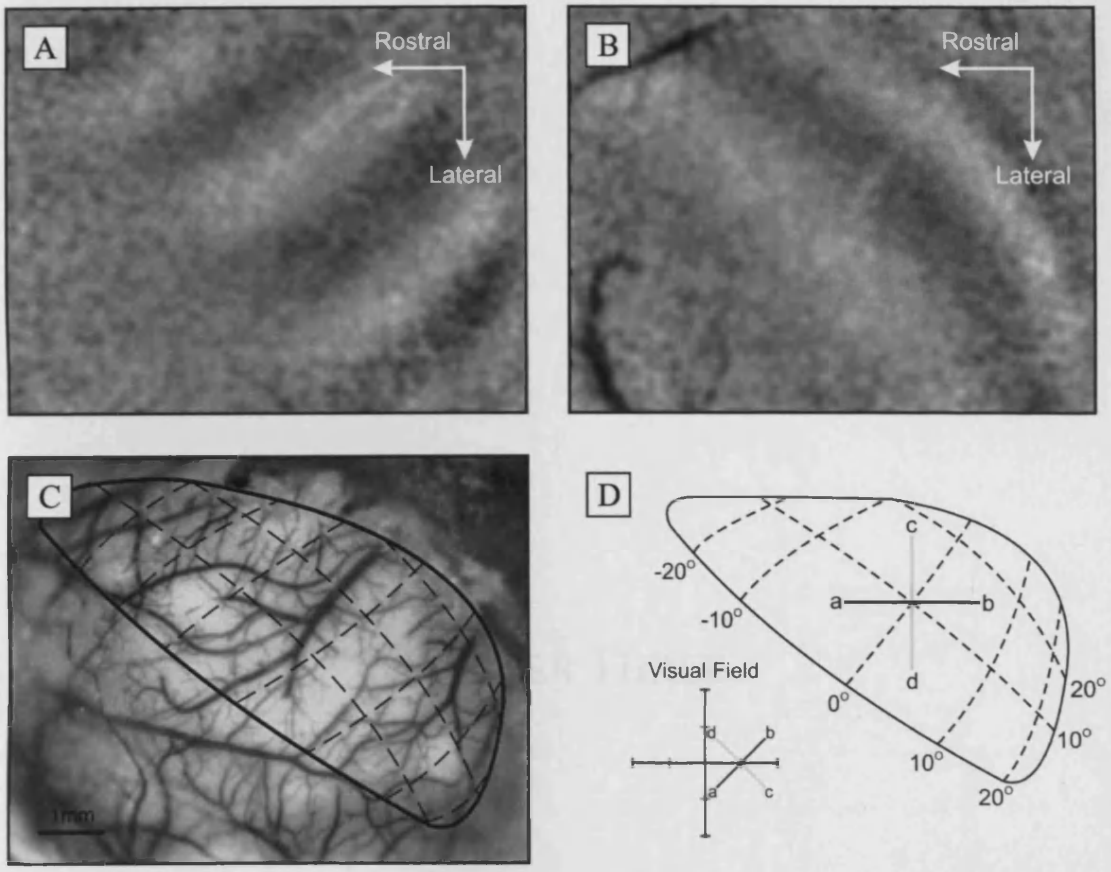

Figure 2.6 - The two images in A and B are taken from tree shrew 011101 and emphasise the large area of visual space that is available for imaging in this species. Alternating stripes of uniform grey and flashing black and white checkerboard each 5.1° wide covering the whole screen were used to stimulate the cortex. Dividing images recorded with stimuli of opposing and complimentary areas of visual space produces images without the need to use cocktail blanks. A – Shows an activated region covering 35-40° of visual space when using horizontal stripes. The central two stripes are slightly wider indicating a greater amount of cortical space devoted to processing information from the central visual area. B - The activated region of the cortex covers 15°- 20° of visual space when using vertical stripes. C – The dashed lines indicate the approximate boundaries of the stripes taken from the above images, overlaid onto the blood vessel map. D – Shows a diagrammatic representation of the left visual cortex and right visual field with two lines overlaid as they would appear in each (Adapted from Bosking *et al* 1997). Due to the nature of the stimuli used in the above protocol it is not possible to accurately assign degrees to the dashed lines in figure C, although the similarities between figures C and D allow approximate comparisons to be made.

CHAPTER THREE

INTRODUCTION TO ADAPTATION

1. Psychophysics: After Effects Caused by Adaptation

Many psychophysical studies have attempted to work out the mechanisms behind the striking visual effects caused by adaptation. The strength, velocity and luminance thresholds of the motion after-effect (MAE) have been investigated by numerous people over the years and were important for defining its extent and nature (Goldstein 1957, Sekuler and Ganz, 1963, Sekuler and Pantle 1966). To explain this phenomenon, Sutherland (1961) proposed that perceived motion is an attribute of the changing ratio between the activities of cells responding to different directions. In the case of the waterfall, this would mean that those cells responding to the downward motion adapt and their activity is reduced. This adaptation of cells for one particular direction tips the balance in favour of its opposite when a stationary object is then observed. More commonly used methods of achieving this effect in the laboratory are inward or outward moving spirals, moving unidirectional gratings and the like.

The early work mentioned above involving pattern adaptation was used to try and understand the primary visual cortex, about which little was known at the time. The threshold at which patterns and gratings can be seen is an important measure for quantification of these effects and understanding the underlying processes. The contrast threshold is the lowest contrast at which a pattern can be perceived. If contours uniformly moving in one direction are observed for a few seconds then the contrast threshold for these movements will be raised when compared to the threshold for contours moving in the opposite direction (Sekuler and Ganz 1963). This is known as the contrast threshold elevation (CTE) adaptation aftereffect. Similar increases in threshold are observed with respect to other attributes of the visual scene. The CTE effect observed when adapting to high contrast gratings is greatest when the adapting and test orientations are the same (Blakemore and Campbell 1969a). These are the first hints of the highly specific nature of effects of adaptation, dependent on which stimuli are used to adapt and test, which are supported by later investigations (Movshon and Lennie 1979, Snowden &

Hammett 1996). The raising of the contrast threshold occurs in both eyes even if only one eye is adapted to the stimulus. This transfer of the effect from one eye to the other is termed interocular transfer (IOT) and is the subject of chapter 4. Both these discoveries suggest that adaptation occurs at the cortical level, as this is the first occurrence of oriented cells and binocular combination of visual information.

The specificity of the adaptive effect is an important feature and has been clearly demonstrated in many studies looking at orientation and spatial frequency (Blakemore and Nachmias 1971, Blakemore *et al* 1973). The perceived contrast of a striped pattern is greatly reduced if preceded by a pattern of greater overall contrast but similar orientation and spatial frequency. If the orientation of the testing pattern is incrementally altered away from that of the preceding pattern the relative effect of the adaptation is reduced (Gilinsky 1968). Here, the idea of highly selective channels that process precise parts of the image comes into play. The spatial frequency is the width of the light and dark bands of a grating and is commonly measured in cycles per degree. Adaptation with a grating of one spatial frequency only affects those channels that respond best to that frequency. This causes an increase in contrast threshold over a limited range of frequencies which appears as a trough on a contrast sensitivity function curve (Blakemore and Campbell 1969b).

It appears that all the attributes of the visual scene that are represented in the visual cortex are affected by adaptation, which can produce similar striking illusions and after effects. Fortunately, outside of the laboratory, such steady unchanging circumstances rarely happen and the process is almost entirely beneficial towards accurate perception. The benefits come from the ability of the visual system to adapt to the changing environment. This process ensures that the system can discriminate changes in the visual scene effectively and encodes information efficiently. Thus, observations from psychophysics experiments explain a great deal of the properties of adaptation, but still leave doubt as to the underlying neural mechanism. The following experiments attempting to identify the physiological substrate of adaptation cast some light on this matter.

2. Adaptation Merely as Fatigue of Neuronal Response

For bi-directional cells, a decline in response to a continuously drifting grating is seen in either direction and is greater for the preferred rather than null direction (Hammond *et al* 1985) . The amount of response change appears to be dependent upon and proportional to the response elicited. This direct link between the magnitude of response elicited by the stimulus and the size of the adaptive effect suggests a non-specific reduction, or fatigue of the cell. This fatigue could be due to a number of factors, possibly involving the temporary reduction of metabolites and energy required for a cell to fire rapidly or a running down of ion gradients. If the period between discharges is too short, the cell does not have time to recover sufficiently. This means that every subsequent discharge is affected to a limited degree by the one preceding it, causing a decline in the discharge rate. The intrinsic factors involved in this theory predict that the greater the firing rate of a cell to a particular stimulus the larger and quicker the downward change in response.

3. Adaptation through Inhibition

The aforementioned spatially specific aspect of adaptation has also been correlated with single cell activity in the cat. Adaptation can be measured as an increase in contrast response threshold, the lowest contrast that produces a significant response (Movshon and Lennie 1979). The increase in threshold depends upon what spatial frequency is used to adapt and to test the response afterwards. For example, if an adapting spatial frequency of 0.8c/deg is used, the reduction in response will be much greater if the test stimulus is 0.8c/deg in comparison to 1.6c/deg, even if the response elicited by a 1.6c/deg test stimulus is greater. This agrees with the psychophysics but casts doubt on the fatigue explanation. However, an adaptive effect is still seen when using any test stimuli including stimuli which are different from the adaptor. In fact, stimuli that do no elicit any kind of spiking response can nevertheless produce an adaptation effect, suggesting that a combination of fatigue and some other mechanism underlie adaptation.

The most popular alternative explanation emerging from early studies revolves around the idea of inhibition between different channels. The specific nature of adaptation seen in perceptual studies showed stimuli that elicit a response also cause adaptation. However, the bandwidth of stimuli causing adaptation is greater than that eliciting suprathreshold activity. The contrast threshold of a channel can be increased using an adapting stimulus with a spatial frequency in its subthreshold range (Dealy and Tolhurst 1974, Toth *et al* 1996). This suggests that parallel inhibition between different channels occurs, possibly carried out by inhibitory interneurones in the cortex. Direct influence of LGN cells on inhibitory neurones, or recurrent inhibition more dependent on the cell's response have been suggested in a similar vein. Unfortunately, most of these theories have been put to rest after experiments showing that γ-aminobutyric acid (GABA), the most prevalent inhibitory neurotransmitter in the cerebral cortex is not involved in contrast adaptation (DeBruyn and Bonds 1986, Vidyasagar 1990, Mclean and Palmer 1996). Iontophoretic application of N-methyl bicuculline (NMB), a potent GABA-A antagonist, to the primary visual cortex can be used to prevent GABAergic inhibition. This raises the overall response from cells but has no effect on the magnitude of adaptation (DeBruyn and Bonds 1986). This shows that inhibition is unlikely to be involved in adaptation. Because of the fact that the fatigue hypothesis relies upon discharge rates and adaptation being intimately linked, the disconnection of the two under NMB contends with this idea and leads the investigation elsewhere. Inhibition although apparently not involved in adaptation has been shown to play a vital role in sharpening the tuning of cells to specific stimulus parameters (Bonds 1989, Crook 1998) and producing a sparser more efficient response to visual information.

4. Modification via Excitatory Transmission and Synapses

If fatigue or inhibition does not explain adaptation then an alternative, such as a reduction in excitatory transmission through a decrease in synaptic efficacy, could provide the answer. Mclean and Palmer (1996) therefore investigated the various different receptors associated with glutamate, the main excitatory neurotransmitter in the neocortex . Single cell recording and two adaptation paradigms similar to those used by Albrecht *et al*

(1984) produced adaptive effects with which to compare and contrast. Application of a large range of agonists and antagonists for different receptors, including N-Methyl-D-Aspartic acid (NMDA), α-amino-3-hydroxy-5-methyl-4-isoxazolepropionic acid (AMPA) and second messenger metabotropic glutamate receptors (mGluR) allowed the identification of those receptors involved in adaptation. The only chemicals found to significantly change the adaptive effect were the mGluR antagonist's α-methyl-4-carboxyphenylglycine (MCPG) and 2-amino-2-methyl-4-phosphonobutanoic acid (MAPV4). Both act at presynaptic glutamate autoreceptors which when activated are known to mediate a depression of glutamate receptors at various locations in the brain. This feedback inhibition provides explanations for the awkward aspects of gain control that other theories lack. The time scale of this process fits as mGluRs act via G-proteins and second messengers, the cascade of which is relatively slow and builds up over a few seconds. This mechanism is similar to long-term depression over a short period of time. The highly specific nature of adaptation may result from the excitatory connections between neurones after alteration of synaptic strength. This effect is further amplified by its effect on recurrent excitation (Douglas *et al* 1995). Such synaptic modulation can occur at subthreshold levels of neuronal activity.

5. The Intrinsic Adaptation Mechanism

Studies in the past few years have shown that although fatigue itself does not appear to be involved in adaptation other factors intrinsic to individual cells (in addition to synaptic or network effects) could be. Intracellular recordings of the membrane potential to sine wave gratings can be described by three different aspects:

- each cycle of the moving grating (the F1 component) causes a modulation in the spike rate
- each cycle causes the F1 modulation of membrane potential
- the change in mean membrane potential around which the modulation occurs (the DC component)

As the contrast of the grating is increased, so is the magnitude of all three components. After adaptation, as we have seen earlier, the spike rate function undergoes a rightward shift along a log-contrast axis. However, the DC component significantly changes, undergoing hyperpolarisation, whereas the F1 modulation of the membrane potential does not. This indicates that tonic hyperpolarisation is what causes the change in firing and sensitivity (Carandini and Ferster 1997, Sanchez-Vives *et al* 2000 a,b). Also, the timescale of the DC component and its subsequent recovery fits that seen in psychophysics. Simulation of adaptation protocols can be achieved by mimicking high and low contrast stimulation with current injections into individual cells. This allows recording without the network influence interfering with or reinforcing the effects. Many characteristics of actual adaptation including reduction in neuronal response during high intensity stimulation and lack of responsiveness post stimulus have been replicated in such artificial protocols. This supports the idea that intrinsic mechanisms to single cells without synaptic modifications can result in adaptation. *In vitro* intracellular recordings have provided an explanation for this slow hyperpolarisation. The large number of discharges evoked by a high contrast stimuli results in the increase of the intracellular concentration of sodium (Na^+) and calcium (Ca^{2+}). This causes activation of Na^+ and Ca^{2+} dependent potassium currents out of the cell and hyperpolarisation. Thus, adaptation appears to stem from a combination of network interaction via excitatory synapse modification and intrinsic cellular mechanisms.

6. Aims and Objectives

The main aim is to show that using optical imaging techniques to investigate adaptation is possible, with the hope of elucidating more clearly the network based portion of any effects. Adaptation produces a lateral shift in the contrast response function (CRF) recorded extracellularly from individual neurons in the primary visual cortex of the cat (Ohzawa *et al* 1985). An event related optical imaging technique can be used to obtain CRF's and orientation tuning curves from individual pixels in functional maps of cat V1 (Swindale *et al* 2003, Carandini and Sengpiel 2004). Is it possible to use optical imaging of intrinsic signals to show adaptation related changes in the CRF and orientation

responses? A shift in the contrast response function after adaptation, comparable to that observed in single cell recording studies (Ohzawa *et al* 1985, Sclar *et al* 1985) would provide evidence to show the validity of this approach. The activity of a large number of neurones within the imaged cortical area contributes to intrinsic signals recorded with this technique. This allows the simultaneous recording of a population of neurones that cover the full range of orientation preferences. Comparing the control and adapted responses of different orientation domains should reveal both region specific and test stimulus orientation specific adaptation effects.

A study by Dragoi *et al* (2000) showed that presenting an adaptation stimulus for 1 hour can induce significant alterations in the functional layout of the primary visual cortex of adult cats. They reported shifts in the preferred orientation of pixels extracted from angle maps away from the adapting orientation, which indirectly causes the location of pinwheel centres to change. However, the stability of cortical map organisation in developing kittens has been demonstrated over long periods from hours up to many weeks (Kim and Bonhoeffer 1994, Godecke and Bonhoeffer 1996). Even longer periods of consistency in orientation maps have been recorded in primates over the course of a whole year (Slovin *et al* 2002). Considered in the light of such evidence, the observations in the Dragoi paper seem unusual, so a similar chronic adaptation procedure will be carried out in tree shrews. The larger cortical area available for imaging results in a greater number of pixels over which comparisons can be made than that found in the cat, providing a more robust verification of this result. I hypothesise that even long periods of adaptation will not produce significant alterations in the functional layout of the primary visual cortex in adult tree shrews.

METHODS

1. Animal Preparation

All procedures were carried out on laboratory-bred animals, with the approval of the Home Office inspectorate and in accordance with the Animals (Scientific Procedures) Act of 1986.

Seven cats and seven tree shrews were used in these experiments. Anaesthesia was induced with an intra-muscular (i.m.) injection of ketamine (25mg/kg) and xylazine (Rompun 4mg/kg). A subcutaneous (s.c.) injection of anti-inflammatory dexamethasone (200μg/kg) to reduce swelling and stop cortical oedema and i.m. injection of atropine (90μg/kg) to inhibit salivary secretions were administered. These effects were upheld with an intravenous (i.v) infusion of atropine, dexamethasone and 4% glucose saline solution at 3ml/kg/hr. Artificial respiration through a tracheal cannula with halothane (1-2%), or isoflurane (2-2.5%) in a 60/40 mixture of nitric oxide and oxygen was used to maintain anaesthetic depth during surgery and reduced for recording (0.7-1% halothane, 1-1.5% isoflurane). The animal was placed in a stereotaxic frame and its core body temperature kept at 37.5 with a homoeothermic-heated mat. Electrocardiogram, encephalogram, respiration rate and end tidal CO_2 (kept between 3.5 & 4%) were closely monitored throughout experiments. In order to dilate the pupils and retract the nictitating membrane, atropine hydrochloride and phenylephrine eye drops were applied when inserting the gas permeable contact lenses. After insertion, an ophthalmoscope was used to focus on the blood vessels in the retina at three dioptres, this being the strength of lenses needed to focus the eyes on a monitor screen 33cm in front of the animal. Craniotomy and durotomy was performed that reveals the area of V1 that corresponds to the foveal representation of the visual field. A cranial titanium chamber was then attached with dental cement and the inner margin sealed with wax. The chamber was then filled with silicone oil and carefully sealed with a glass cover slip. A slight pressure was applied to flatten the cortical surface and to reduce artefacts from respiratory and blood pulsations.

No chamber is required in tree shrews, merely bone thinning, agar application and careful cover slip placement, producing a clear cortical surface representing the major portion of V1. Relatively large blood concentrations of drugs are required to anaesthetise and paralyse these animals due to their higher metabolic rate (ketamine (200mg/kg) and xylazine (5mg/kg)).

After completion of surgery, muscle paralysis was induced with an i.m. injection of Gallamine triethiodide (10mg/kg) and maintained through i.v. infusion (10mg/kg/h). The animal was terminated with a barbiturate overdose administered i.v. once the experiment had reached its conclusion.

2. Optical Imaging Specifics

The following OI methods have been adapted from Bonhoeffer and Grinvald (1996). The optical imaging set-up used in experiments is shown in figure 3.1 below. A 25hz video rate digital CCD camera was positioned above the illuminated cortical surface and focused using a tandem lens macroscope (2 x 50mm, 1.2f). A 100W halogen lamp and filters, with two adjustable guides were used to provide an even illumination of the cortex. 540nm-wavelength light was used to obtain the surface blood vessel pattern for use as a reference image. The low depth of field and high numerical aperture produced with this set-up allows the sharp focusing on a plane 500μm below the cortical surface. Another band pass filter was then added to obtain an accurate wavelength of 700nm, a region of interest selected and the camera focused down by 500 μm for imaging of the intrinsic activity. The reflected photons striking the pixels on the CCD chip liberate electrons, which accumulate in "wells", and create a charge proportional to the number of photons, which is digitised at 8-bit. After amplification of the signal, the imager 2001 box converts this image back into analogue for subtraction of the stimulus-related frames from the reference frames. The result is converted back into digital once again to produce 16-bit floating point data, ready for further manipulation.

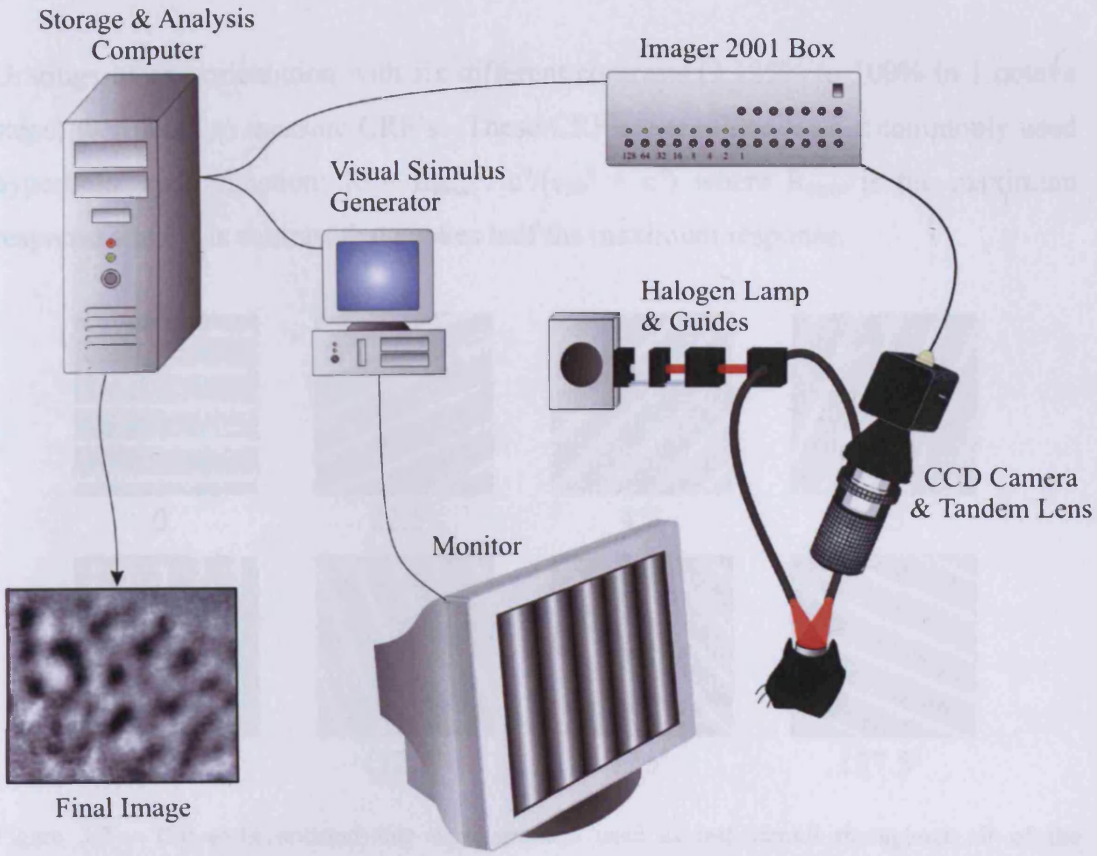

Figure 3.1 - Shows the typical set-up used during an imaging experiment

3. Optical Imaging Stimulus Protocols

A Visual Stimulus Generator (VSG Three, Cambridge Research Systems, Rochester, UK) was used in all protocols to present oriented moving sine wave gratings in the case of cats, or square wave gratings in the case of tree shrews on a 21" monitor with mean luminance of ~40cm/m^2. Test stimuli consisted of eight orientations from 0° to 135° separated by 22.5°, drifting at a temporal frequency of 2Hz with a 100% contrast, shown in figure 3.2.

Initial tree shrew experiments included exploratory retinotopic and contrast response function (CRF) stimulus protocols. Either horizontal or vertical stimulus stripes (each 5.15° wide) alternated with blank stripes that shift across the screen were used to map out the precise extent of the imaging area. Each stripe consisted a chequer board (each check 1.65°*3 = 5.15° per stripe) that flickers black and white to intensely stimulate the cortex.

Gratings of one orientation with six different contrasts (3.125% to 100% in 1 octave steps) were used to measure CRF's. These CRF's were fitted with a commonly used hyperbolic ratio function; $R = R_{max} \cdot c^n/(c_{50}^n + c^n)$ where R_{max} is the maximum response and c_{50} is contrast that evokes half the maximum response.

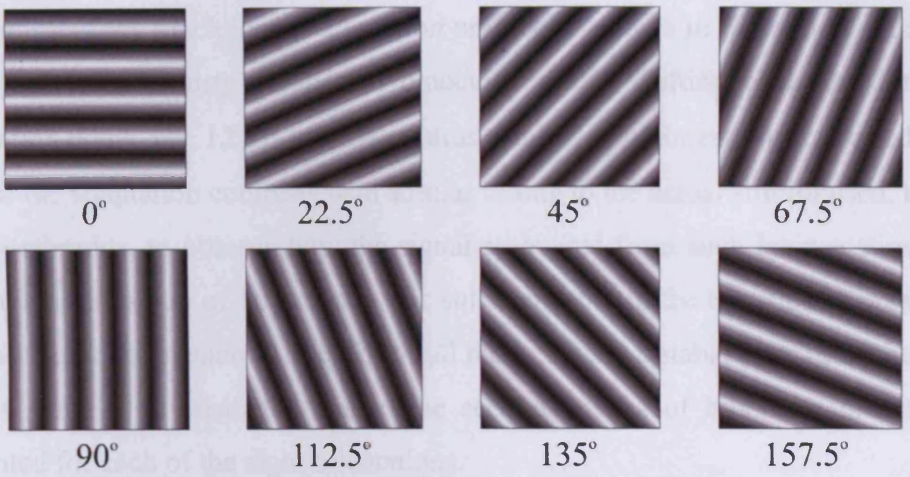

Figure 3.2 - The eight oriented sine wave gratings used as test stimuli throughout all of the experiments.

The stimulus protocol used to produce orientation and OD maps for one trial includes 20 stimuli in total; eight oriented stimuli shown once to each eye and four equiluminant grey blanks. A spatial frequency of 0.1-0.6cyc/deg was chosen, depending on what was optimal for the animal's age and each particular experiment. Reference frames are recorded at the beginning of each trial, producing the overall light modulation image used in the analogue subtraction, mentioned above. The timing of an individual stimulus is shown in figure 3.3.

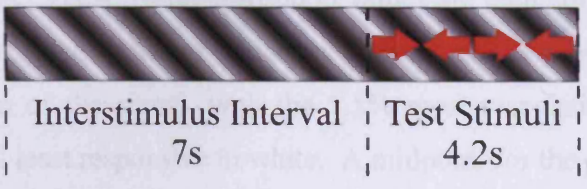

Figure 3.3 - Shows the timing of one trial in the standard imaging protocol. Red arrows indicate drifting grating. The camera records a signal during the test and reference periods using a 600ms frame length, seven frames for the test, and three for the reference. A stationary grating is presented during the interstimulus interval, in order to reduce any 'on' signal in the images, produced when the stimulus appears on screen. The response itself is a change in the reflectance, or absorption, which is averaged over the maximal response period during presentation of the stimulus.

A 7s period is required in between each test stimulus presentation for the intrinsic signal to recover. Recording is separated into blocks of four trials each, after which the data is stored on computer. A full recording consists of 8 or 10 blocks with each trial repeated 32 or 40 times, to reduce artefacts.

The timing of the much longer adaptation protocol is shown in figure 3.4. Adaptation was induced with thirty seconds of binocular grating drifting back and forth with orientation θ and 3%, 12.5% or 50% contrast. Initial experiments were carried out for each of the adaptation contrasts with similar timing to the actual stimuli used, but with no test stimulus, to observe how the signal recovered from such intense stimulation. An interstimulus gap of 10 seconds was sufficient (6.7 in the tree shrew, presumably due to its quicker metabolic rate) for a full recovery and a stable plateau of the signal. A test stimulus consisting of three one second epochs of binocular grating were presented for each of the eight orientations.

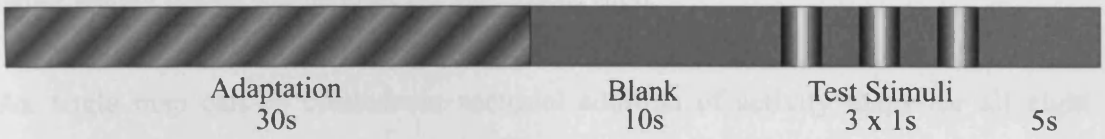

Figure 3.4 - Shows the timing for one trial in the adaptation protocol (all gratings drift). The camera records a signal during all except the adaptation period, using a shorter frame length of 480ms.

4. OI Data Analysis

The trials for one orientation are summed together and then divided by either the blank trial responses or the mean response to all stimuli (cocktail blank) to produce iso-orientation maps. These 16-bit absorption values are then compressed onto an 8-bit 256-point range, each value of which is assigned to an 8-bit grey scale. This allows visualisation of the signal, with the 1.5% most responsive pixels shown in black, and the 1.5% least responsive in white. A midpoint for the division was chosen so that an even spread of pixels across the entire range was achieved. The images were high pass filtered at above 2.2 mm to remove the global DC component that is superimposed on the spatially restricted stimulus specific "mapping" signal (Zepeda *et al* 2004). A preliminary study was carried out to ensure that this high pass cut-off point did not interfere with the mapping signal. The image was also gaussian

smoothed to remove any high frequency noise occurring through stochastic fluctuations in photons and thermal noise. Care was taken to filter all images from one experiment in a similar manner, to allow direct comparison.

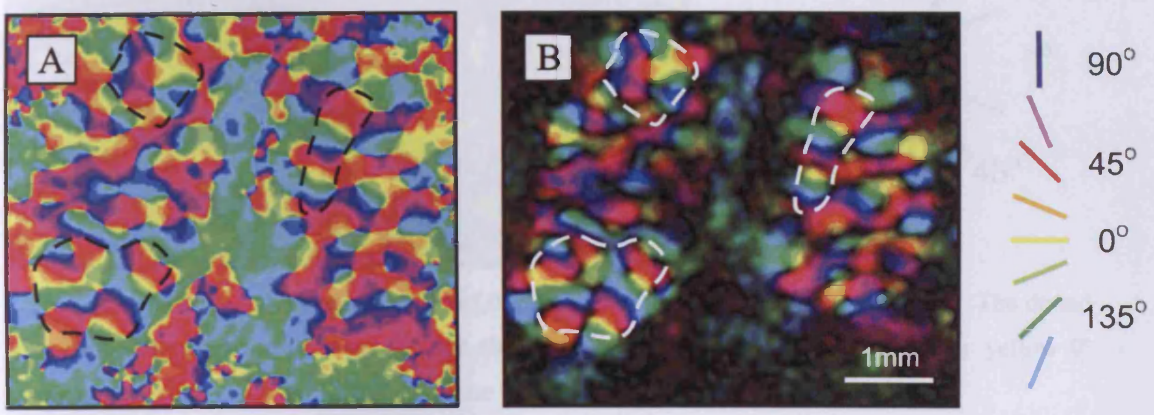

Figure 3.5 - Shows angle (A) and polar map (B) recorded from cat 11-12-01 along with colour coded pixel key. The strongly responding reliable areas of the image were included in the ROI selected for further analysis (shown with the black and white dashed lines).

An angle map can be created via vectorial addition of activity maps for all eight orientations. The angle of the vector for each pixel gives its orientation preference by which it is assigned a colour according to the scale shown in figure 3.5a.

The initial image of the cortex each pixel has a size of 11μm x 11μm, which are rebinned into 22 μm x 22μm pixels, from which a region of interest (ROI) is selected. A careful comparison of the blood vessel pattern, polar & iso-orientation maps was undertaken to ensure that the ROI contained the areas where the strongest, most reliable signal occurred. First, any large blood vessels or other obstructive artefacts which can be seen in the blood vessel map are excluded from the ROI. From the remaining pixels, only those areas where clear columns are observable in the iso-orientation maps are included. Finally, the polar map is checked to ensure that any chosen regions match up with the brightest or most strongly responding pixels (see figure 3.5a&b). Eight selections of pixels are made using the angle map and a 22.55° range of orientation preference. Thus, those pixels that lie between 32.5° and 57.5° are binned together as the 45° preferring domains, see figure 3.6.

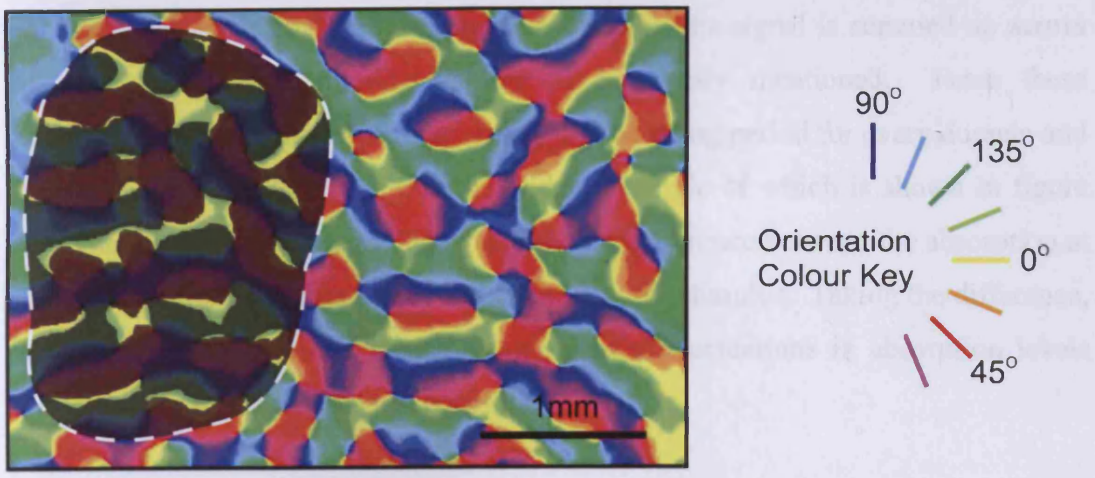

Fig 3.6 - Shows a typical domain selection of 0° pixels taken from a tree shrew angle map. The dotted white line delineates the ROI and the non-shaded areas within it are the predominantly yellow 0° domains, the activity of which is used to create the tuning curves.

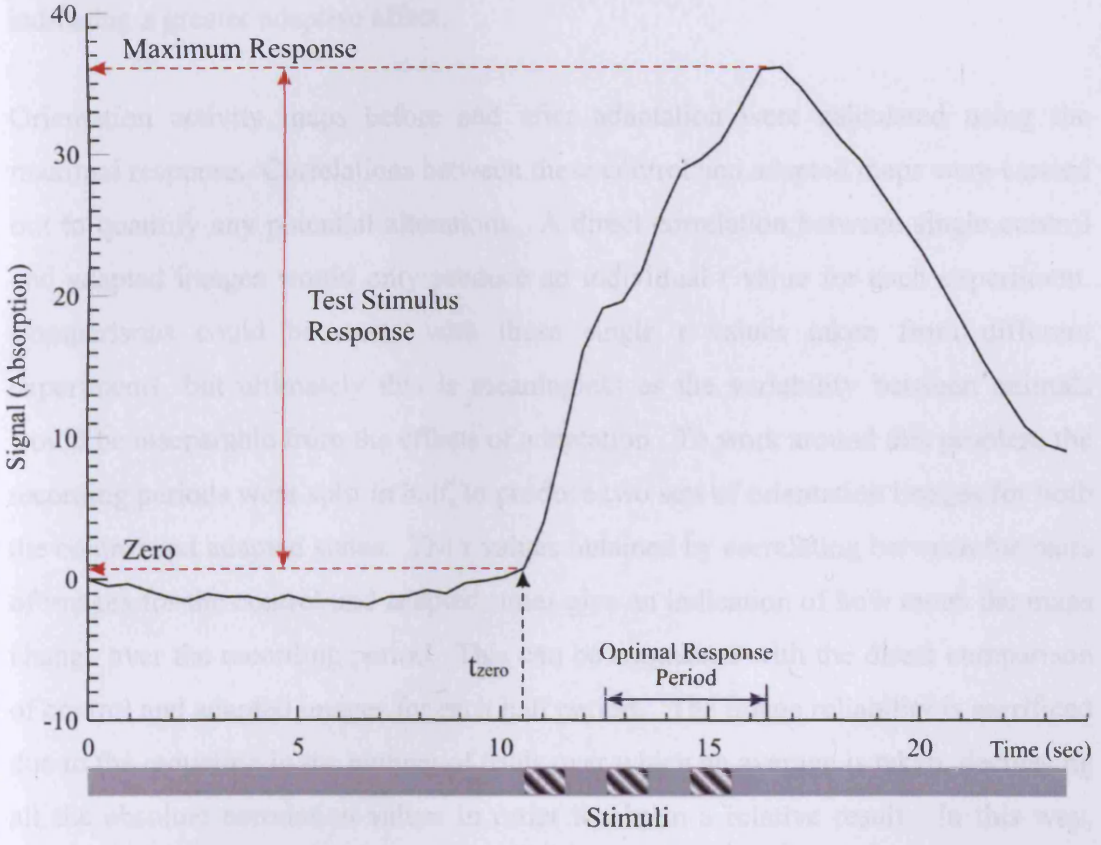

Figure 3.7 - An example absorption time course showing the mean response to 135° in one domain, without any adaptation. Three distinct rises of decreasing magnitude are obvious, shortly after presentation of each 1s test flash. The optimal response period is that over which the frames are summed to produce activity maps. The frame immediately preceding the test stimulus is at t_{zero} from which the base level of absorption for each response is taken.

For each contrast adaptation level and test stimulus, the signal is summed up across all similar trials and filtering applied as previously mentioned. From these summations, a mean absorption signal over the recording period for every domain and all test conditions is calculated, an individual example of which is shown in figure 3.7. The response to a test grating is taken as the difference between the absorption at time t_{zero} and the maximum absorption elicited by the stimulus. Taking the difference, rather than absolute values avoids the problem of fluctuations in absorption levels between control and adapted test conditions.

From these responses, orientation tuning curves can be plotted for all domains and levels of contrast adaptation. An adaptation index was calculated for each domain and adaptation state by dividing the area under the adapted orientation tuning curve by the area under the control curve. This gives values from 0-1, with lower values indicating a greater adaptive affect.

Orientation activity maps before and after adaptation were calculated using the maximal response. Correlations between these control and adapted maps were carried out to quantify any potential alterations. A direct correlation between single control and adapted images would only produce an individual r value for each experiment. Comparisons could be made with these single r values taken from different experiments, but ultimately this is meaningless as the variability between animals would be inseparable from the effects of adaptation. To work around this problem the recording periods were split in half, to produce two sets of orientation images for both the control and adapted states. The r values obtained by correlating between the pairs of images for the control and adapted states give an indication of how much the maps change over the recording period. This can be contrasted with the direct comparison of control and adapted images for each half period. The image reliability is sacrificed due to the reduction in the number of trials over which an average is taken, decreasing all the absolute correlation values in order to obtain a relative result. In this way, comparison between adapted and non-adapted cortical states across the whole of V1 can be investigated.

RESULTS

1. Preliminary Adaptation Experiments

To determine the efficacy of using OI for study of adaptation, and to ascertain the correct stimulus parameters to use in order to obtain the clearest result, numerous preliminary experiments were performed. After activation with a stimulus the cortex requires about seven seconds to recover to baseline, which is the typical interval before the next stimulus response is recorded (Bonhoeffer and Grinvald 1996). Unfortunately, the greater the period allowed for signal recovery, the weaker the post-adaptation after-effect becomes. This means that the length of the recovery period between the adapting and test stimuli needs a compromise, assessed in pilot experiments, resulting in the timecourses shown in figure 3.8 and 3.9.

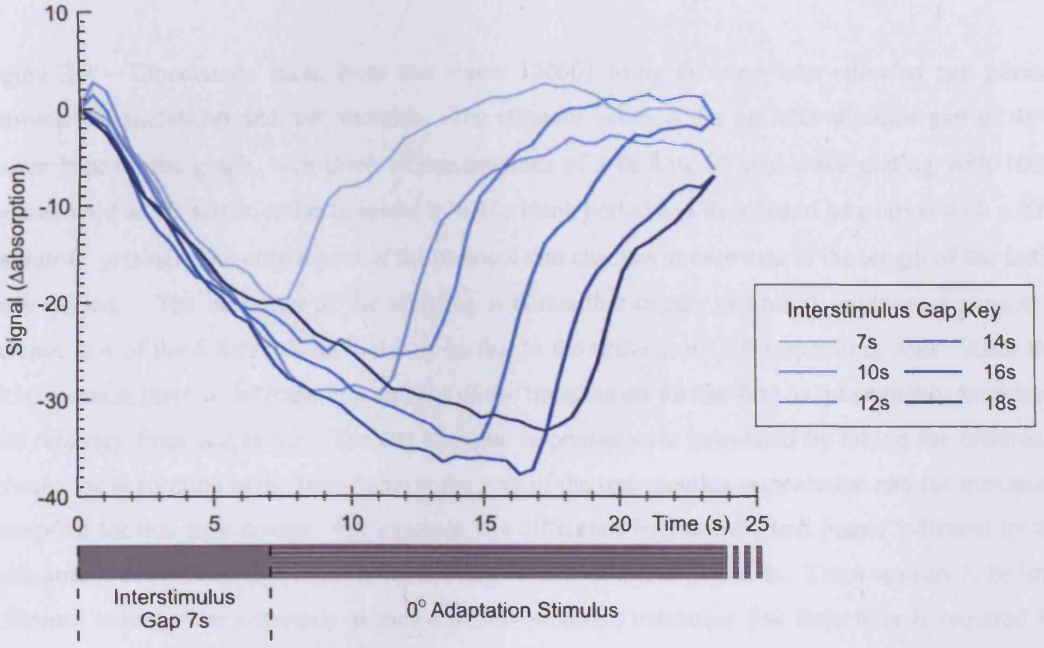

Figure 3.8 - Shows timecourses of the absorption signal recovery when using an adapting, but no test stimulus in cat 111201. A 50% contrast 0° grating was shown for 25s to induce adaptation with different inter-stimulus gaps between each adapting period. The stimulus protocol for an inter-stimulus gap of 7s is shown beneath the graph, matching the lightest blue timecourse above. The other timecourses are colour coded according to the inter-stimulus gap key, bearing in mind that the adaptation continues for longer than the recording period. In general, there appears to be a sharp decrease in the signal for 8-10s that then turns into a much gentler slope. Thus, a base response level taken after 10s of recovery provides a stable measure from which reliable responses can be determined.

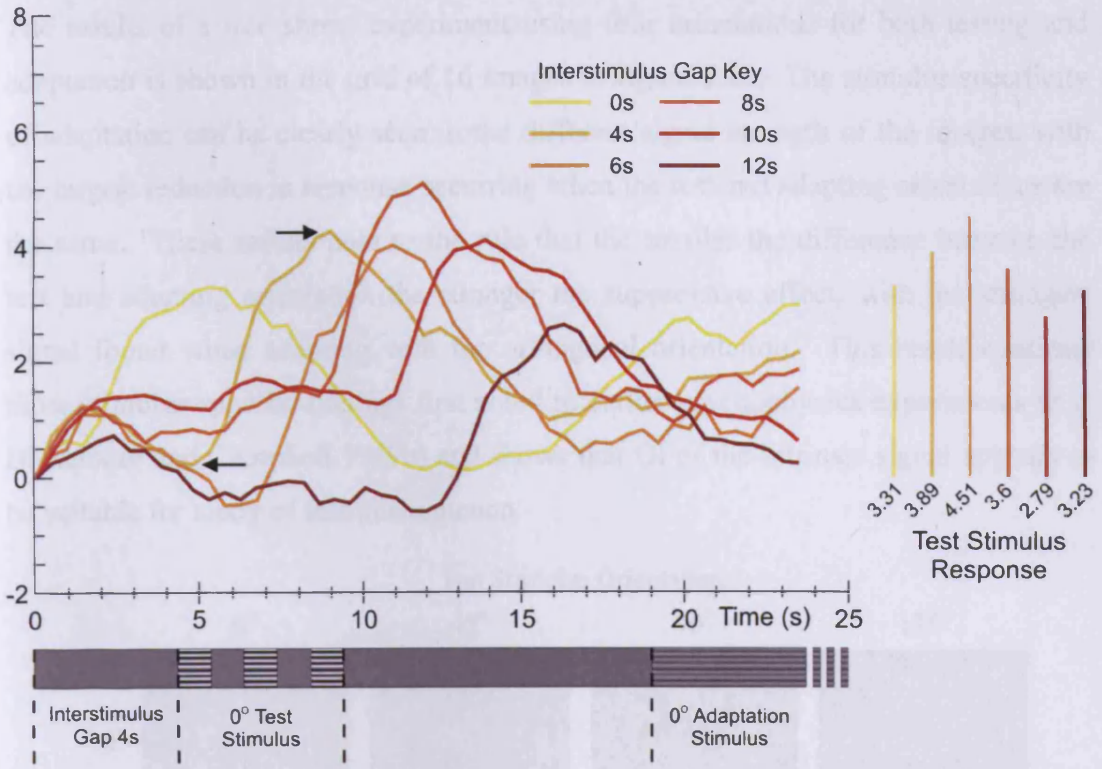

Figure 3.9 - Timecourses taken from tree shrew 120601 using different inter-stimulus gap periods between the adaptation and test stimulus. The stimulus protocol for an inter-stimulus gap of 4s is shown beneath the graph, with three 1s presentations of a drifting 0° sine wave grating with 100% contrast used as the test stimulus followed by a 10s blank period and then 30s of adaptation with a 50% contrast 0° grating. The only aspect of the protocol that changes in each case is the length of the initial blank period. The cessation of the adapting stimulus that occurs at time 0 produces a consistent increase in 4 of the 6 timecourses and may be due to the activity of OFF responding cells. After this initial increase there is decrease in a number of the timecourses for the first 5s, presumably associated with recovery from adaptation. The test stimulus responses were calculated by taking the difference between the absorption in the time frame at the start of the test stimulus presentation and the maximum absorption for that time course. For example, the difference between the two points indicated by the black arrows determined the response when using an inter-stimulus gap of 4s. There appears to be little difference between the responses in each stimulus protocol, indicating that little time is required for recovery.

Running the protocol without a test stimulus in cats showed that the signal tends towards a plateau at around eight seconds (see figure 3.8), giving a dependable test signal with an inter-stimulus gap of 10 seconds. As can be seen in figure 3.9, a shorter recovery period of only 6s is required when imaging in tree shrews, presumably due to their much higher metabolic rate.

The results of a tree shrew experiment using four orientations for both testing and adaptation is shown in the grid of 16 images in figure 3.10. The stimulus specificity of adaptation can be clearly seen in the different signal strength of the images, with the largest reduction in response occurring when the test and adapting orientations are the same. These results hold to the rule that the smaller the difference between the test and adapting orientation the stronger the suppressive effect, with the strongest signal found when adapting with the orthogonal orientation. This result confirms those stimulus specific findings first noted in earlier psychophysics experiments (e.g. Blakemore and Campbell 1969b) and shows that OI of the intrinsic signal appears to be suitable for study of this phenomenon.

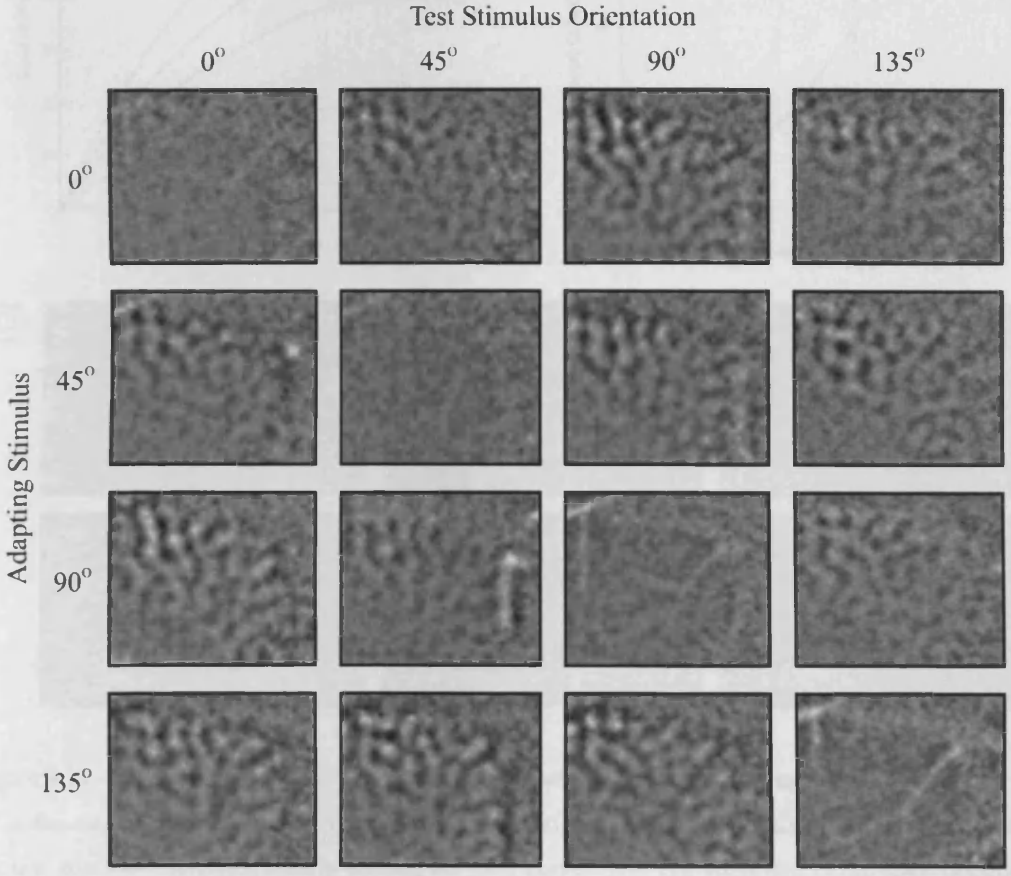

Figure 3.10 - Shows the orientation specific adaptive effect using OI in the tree shrew 011101. Adaptation was induced using 17s of 100% contrast drifting square-wave grating. The almost non-existent signal left after adapting and testing with the same orientation indicates that such high contrast adaptation is unsuitable for long term imaging. Although this is a striking result, the small number of orientations used and strong affect also mean that any subtle changes in this stimulus specific response cannot be quantified.

2. OI of Contrast Response Functions

To determine the optimal contrast to use for adaptation and test stimuli both normal and adapted CRFs were recorded using OI of intrinsic signals. A typical example of a sigmoidally shaped CRF is shown in figure 3.11, directly comparable to those found with single cell recordings (Ohzawa *et al* 1985).

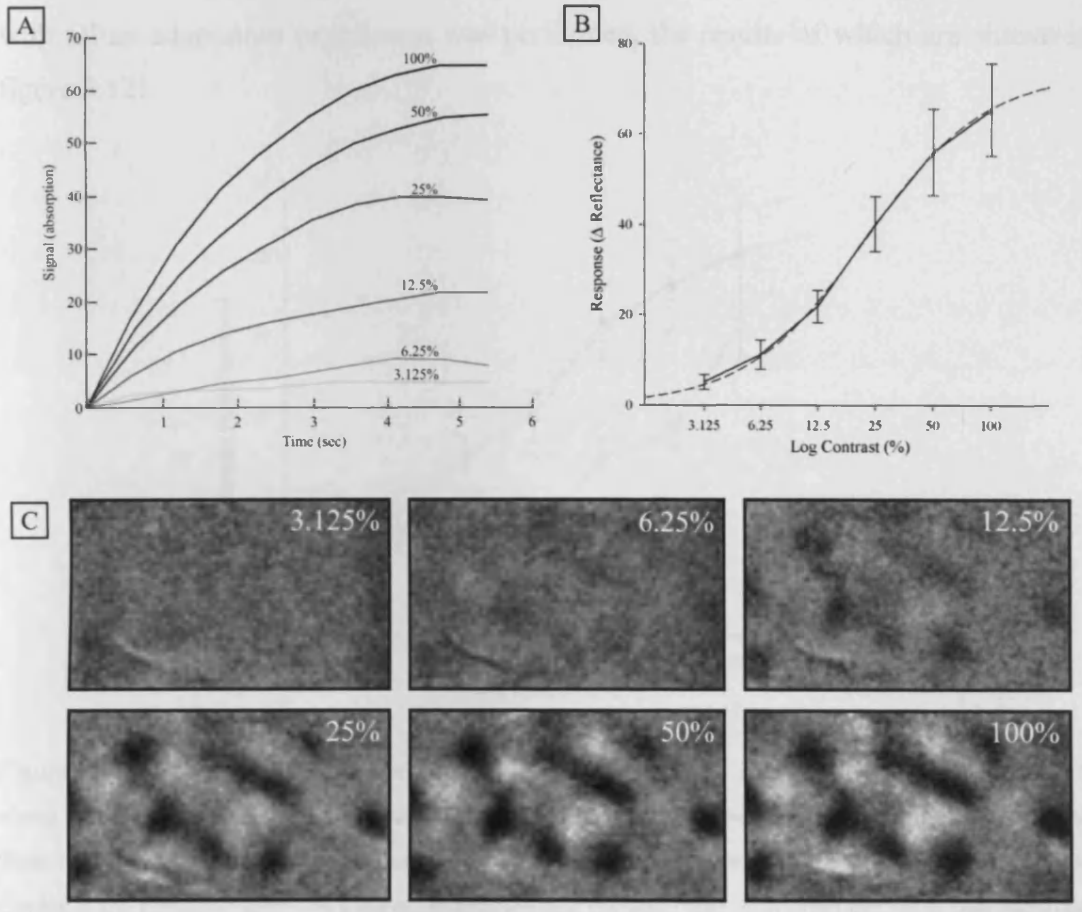

Figure 3.11 - Shows a typical CRF using six contrasts of a 45° oriented grating stimulus, obtained using OI in the cat (532-300701). A - Averaged absorption signal timecourses in the 45° domains for each of the test stimulus contrasts, clearly marked on each curve. B - The solid line is the CRF obtained by taking the maximum response of each timecourse in A. The dashed line indicates the best fit obtained using a hyperbolic ratio as outlined in the methods (R_{max} = 73.83, c_{50} = 22.35, n = 1.39 & Standard Error of fit = 0.76). C - Shows the activity maps from which the results in A & B were taken, with contrast in each case marked in white, in the top right hand corner.

This affirms that responses reflecting the underlying neuronal activity can be obtained by selecting pixels from the appropriate orientation domain (45° in this case) and

averaging the timecourses across many test stimuli repetitions. Significant adaptation tends to be elicited by adapting contrasts that lie to the right of the turning point of the sigmoidal curve, the c_{50} value. Thus, in this case a c_{50} of 22.35% indicates that a 25% contrast grating would be suitable for moderate adaptation and 50% contrast adaptation would produce a much stronger shift and response reduction.

To corroborate this result and clarify whether such a change in the CRF is observable with OI an adaptation experiment was performed, the results of which are shown in figure 3.12.

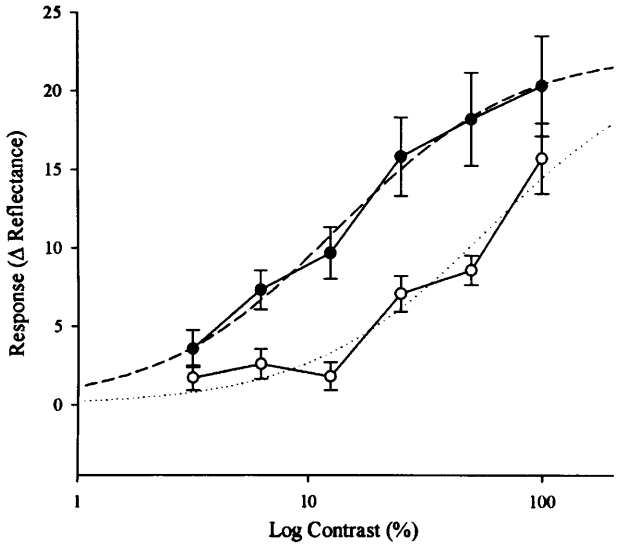

Figure 3.12 - OI in cat 040702 shows the affect of adaptation on the CRF producing a rightward shift along the log contrast axis. The test stimulus contrasts used and method of extracting the response from the timecourses was the same as that used for the data in figure 3.11. The solid line with filled circles is the response after 3% contrast adaptation and the solid line with open circles is that recorded after adapting with a 50% contrast grating. The dashed line indicates the best fit for the 3% adapted data, calculated using a hyperbolic ratio function (R_{max} = 22.51, c_{50} = 13.58, n = 1.22 & Standard Error of fit = 0.88). The dotted line is a best fit for the 50% adapted data that uses the same values for R_{max} & n obtained from the 3% fitting but with c_{50} allowed to vary (c_{50} = 60.17, SE of fit = 1.33).

As predicted, a clear rightward shift occurs after adapting with 50% contrast, raising the c_{50} by 4.43 times or 0.65 log units, from 13.58% to 60.17%. No CRF was recorded using a blank stimulus during the adapting period, instead the responses at 3% adapting contrast (which barely elicits any response itself) were used for comparison. A similar partial fitting of the 50% adapted CRF was carried out only

allowing R_{max} or n to vary which produced a much larger SE for fitting of 2.89 and 6.84 respectively. This indicates that a change in c_{50} or pure contrast gain control is the most adequate explanation for this shift (Albrecht *et al* 1984, Sengpiel *et al* 1998a).

3. Long Term Adaptation Effects on Orientation Maps

It has been previously observed that a shift in the representation of preferred orientations away from the adapting orientation can be seen in angle maps after long-term adaptation in cats (Dragoi *et al* 2000). A similar experiment was performed in tree shrews, to ascertain the stability of cortical responses after such intensive adaptation for extended periods. A comparison between both single-orientation maps and angle maps recorded before and after 1 hour adaptation with a horizontal grating was made using both cross-correlation analysis and average orientation change across orientation domains.

Orientation Map	01/11/01	06/11/01
0°	0.927	0.883
45°	0.842	0.9
90°	0.91	0.889
135°	0.877	0.885

Table 3.1 - Shows the r values when performing 2-dimensional cross-correlations between iso-orientation maps recorded before and after 1 hour of adaptation with a 0° grating from two tree shrews.

Orientation Map	A1 v A2	B1 v A1	B1 v A2	B2 v A1	B2 v A2
0°	0.918	0.847	0.777	0.908	0.866
45°	0.89	0.868	0.805	0.886	0.877
90°	0.831	0.823	0.763	0.896	0.86
135°	0.874	0.825	0.772	0.915	0.84

Table 3.2 – For tree shrew 061103, the blocks recorded before (B) and after (A) adaptation were split into two former & latter periods (B1, B2, A1 & A2 respectively) producing four orientation maps for each of the four groupings. The r values for correlations performed between the different periods for each orientation are shown in the table. In this way, a comparison between spontaneous changes in activity maps occurring over the recording period and those induced by the adaptation can be made. The number of blocks recorded was not sufficient to perform a similar analysis for 01/11/01.

One would expect any significant alterations in the maps to be stimulus specific, with the greatest change occurring in the activity map when testing with the adapting orientation. As can be seen in table 3.1, in both cases all four orientation maps show similarly high *r* values, indicating little overall change. In addition, for 01/11/01 the 0° orientation map (the test which matches the adapting orientation) has the highest *r* value, suggesting that such periods of adaptation do not produce long-term orientation specific changes in the functional layout of the cortical map.

To ascertain whether any changes occurring in the signal can be accounted for by the natural variation over the recording period a more detailed correlation of the 06/11/01 data was performed, the results of which are shown in table 3.2. This confirms the simple correlation result, as regardless of which time periods are compared there is no orientation specific difference between the maps. The sequential correlation of the blocks recorded after adaptation (A1 v A2) produces high *r* values, indicating little change occurring during the recording period. Although overall *r* values are lower for those comparisons between images recorded before and after this does not necessarily mean they are caused by the adaptation. A more likely explanation is that with a greater length of time between each recording period, there is a lower r value. This means that the A1 v A2 & B2 v A1 correlations both have high *r* values even though the adaptive period lay between the latter two acquisitions. B1 v A1 & B2 v A2 have slightly lower *r* values and the lowest values occur when comparing B1 v A2, which also had the largest time separation between them.

Both a qualitative and quantitative comparison of any adaptation dependent changes in the angle map can be seen in figure 3.13. The shape of the orientation domains, and overall character of the functional layout does not appear to change after 1 full hour of adaptation (see figure 3.13b). Even on close inspection any differences are negligible, with a very slight movement of the pinwheels towards the rostral part of the cortex. The stability in the layout of the angle map is reflected quantitatively by the orientation change (before vs. after adaptation) in each pixel (solid line in figure 3.13c). The magnitude of the mean orientation change across all domains is 3.92°, which is similar to the figure of 1.47° taken from a comparison of two sequential maps, both recorded after 1 hour of adaptation. These figures can easily be

accounted for by the natural variation in the signal that occurs throughout the recording period.

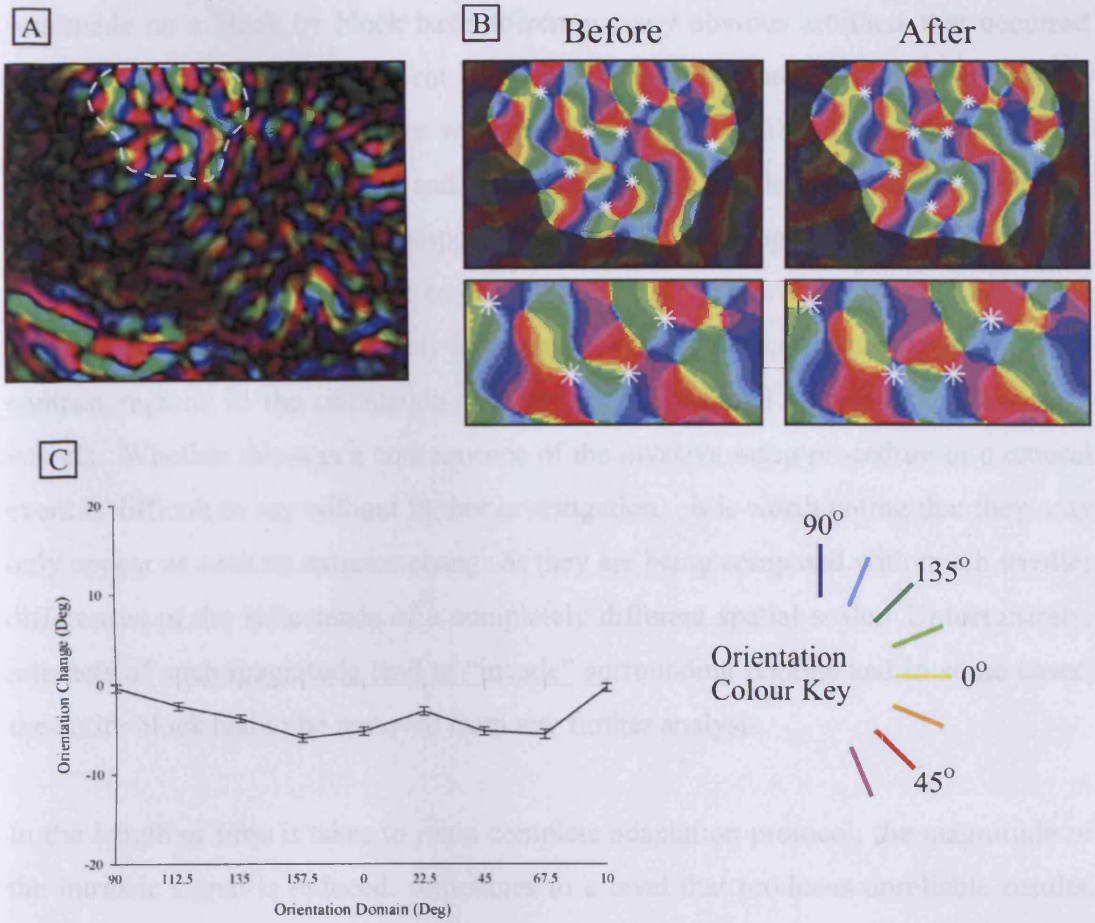

Figure 3.13 - Shows the comparison between angle maps recorded before and after 1 hour 0° adaptation (0° pixels are designated yellow in the maps) in tree shrew 06/11/01. A - Polar map calculated from images recorded after the adaptation period, with the ROI chosen for quantitative analysis delineated by a dotted white line. This area was chosen due to its strong signal and reliability throughout the whole of the recording period. B - Shows two close ups of the angle map before and after adaptation, with the entire ROI displayed above, and a region within this ROI in greater detail below. The white stars in all the images indicate the position of selected pinwheels within the angle map designated before adaptation. C - Shows the mean adaptation dependent change in orientation occurring across all the pixels in eight orientation domains within the ROI. This was calculated in two different ways, with (solid line) and without (dotted line) accounting for the circular nature of orientation values (see main text).

4. Reliability of Long Term Imaging

In each experiment involving long-term imaging of adaptation an initial assessment was made on a block by block basis to remove any obvious artefacts that occurred during the course of an experiment. These were most commonly associated with the largest blood vessels, as if there were periodic surges in blood pressure and flow. Such artefacts were temporary and occurred within a single trial, usually affecting only one or two test stimulus responses. Any slow biological noise as the signal fluctuates over time is removed by subtraction of a reference frame recorded at the start of each trial. These relatively large changes in the intrinsic signal appear as high contrast regions in the orientation activity maps along and surrounding the largest vessels. Whether this was a consequence of the invasive setup procedure or a natural event is difficult to say without further investigation. It is worth noting that they may only appear as such an extreme change as they are being compared with much smaller differences in the reflectance of a completely different spatial scale. Unfortunately, artefacts of such magnitude tend to "invade" surrounding regions and in some cases, the entire block had to be removed from any further analysis.

In the length of time it takes to run a complete adaptation protocol, the magnitude of the intrinsic signal is reduced, sometimes to a level that produces unreliable results. The period between the initial setup and this degradation varies between experiments and is dependent on many factors such as weight, age and general physiological state of the animal. This was taken into consideration when choosing the stimulus protocol, and thus interleaved rather than sequential control and adaptation blocks were used to ensure that any reductions in the signal were related to adaptation rather than a slow decrease in signal. If the signal was too weak in blocks recorded towards the end of the experiment, they were not included in the final analysis. Even if this was the case, orientation maps could usually still be obtained after completion of the adaptation protocol for comparison with those recorded beforehand, as a stronger signal is associated with the shorter period of stimulation required for ordinary orientation maps.

An initial region of interest (ROI) was then selected, based upon a combination of blood vessel and polar maps calculated from the best quality blocks. Thus, only those

areas of the cortex without physical artefacts and from which the strongest signal was obtained throughout control and adapted conditions were included in the ROI.

5. Adaptation Effects On Absorption Time-series Curves

Orientation domains selected from within the ROI provided the groups of pixels from which time-course responses to test stimuli were extracted. Figure 3.14a shows a good example of the range of control responses to different orientations found in the domains responding best to the adapting orientation (θ).

As expected, the test stimulus that elicits the greatest response is the preferred orientation for these domains. As the test stimuli orientation moves away from θ, the strength of response declines until the weakest signal is found at the orthogonal orientation. One might expect no response at all to be elicited by the orthogonal test stimulus, whereas a clearly negative response is present, perhaps indicating some kind of suppressive effect. There are also less obvious reductions occurring in the 67.5° and 112.5° test stimulus responses, the two orientations closest to the orthogonal. Interestingly, this negativity is not as prominent in the responses of domains responding best to the orthogonal orientation (see 22.5° curve in figure 3.15a).

After adaptation (figure 3.14b), the absorption signals undergo various changes. There is a rapid decline of the signal for all test stimuli immediately following the cessation of the adaptation stimulus as the cortex recovers from the previous intense activity. This decline is already starting to plateau after 8s in some of the responses, supporting the preliminary experiments and adding credence to the chosen paradigm of stimulation. Although this has reduced the overall level of the signal in all cases, the responses generated by the test stimuli undergo more specific reductions. The response elicited by the θ stimulus is affected most post adaptation and is reduced to a level similar to that seen for the test stimulus of 22.5°.

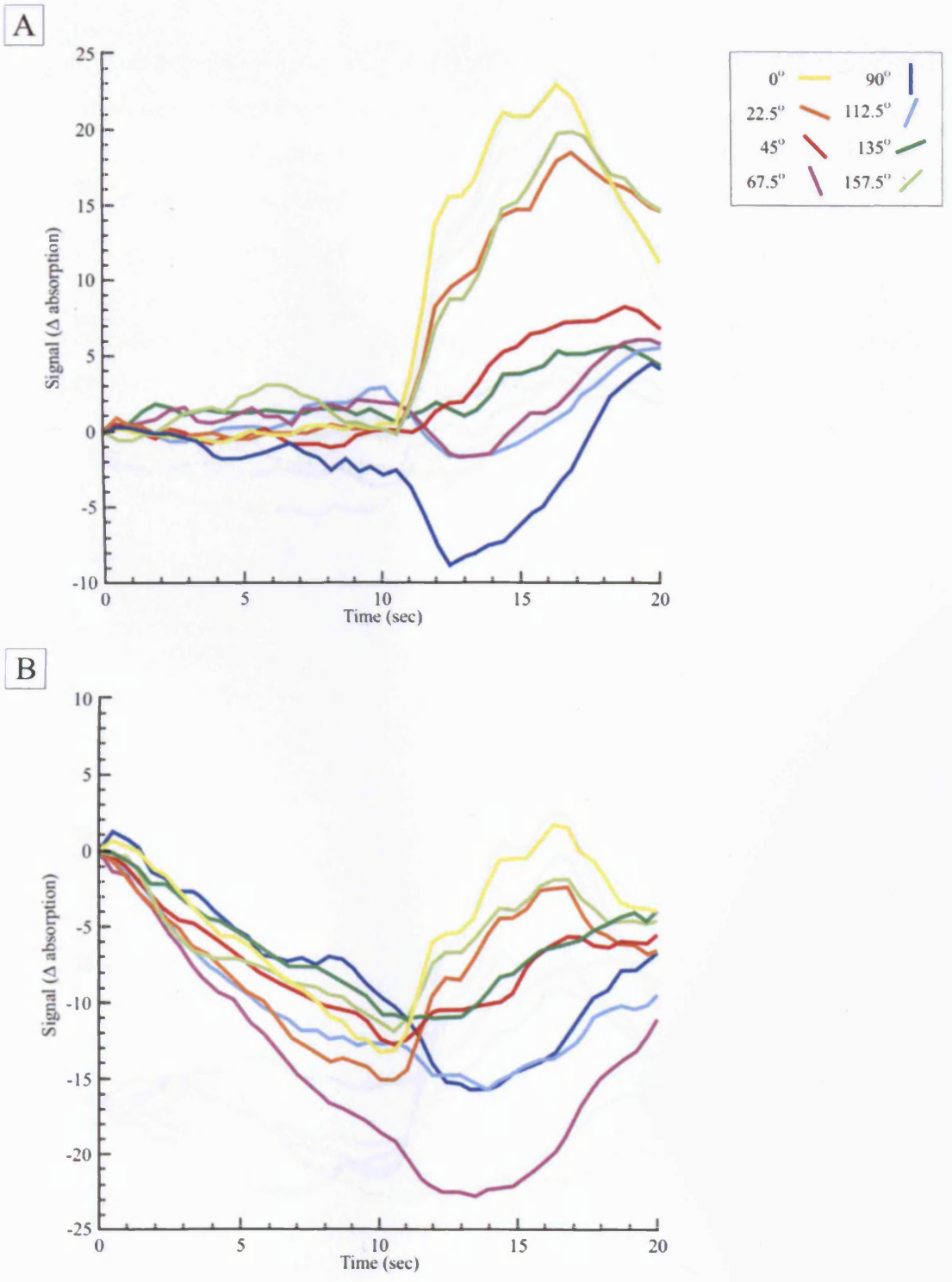

Figure 3.14 - Shows absorption signal time-courses recorded from the domain responding best to the adapting orientation in cat 11-12-01. Adaptation was induced with either a 3% (A) or 50% (B) contrast 0° oriented grating. Responses to all eight test stimuli are shown, the colour of which is designated by the orientation key in the top right hand corner. Although the 67.5° lilac timecourse in B appears to be an anomaly it must be remembered that the actual response to the test stimulus only begins after 10.5s. Thus, the small reduction in absorption is comparable to the response evoked with the other test stimulus orientations.

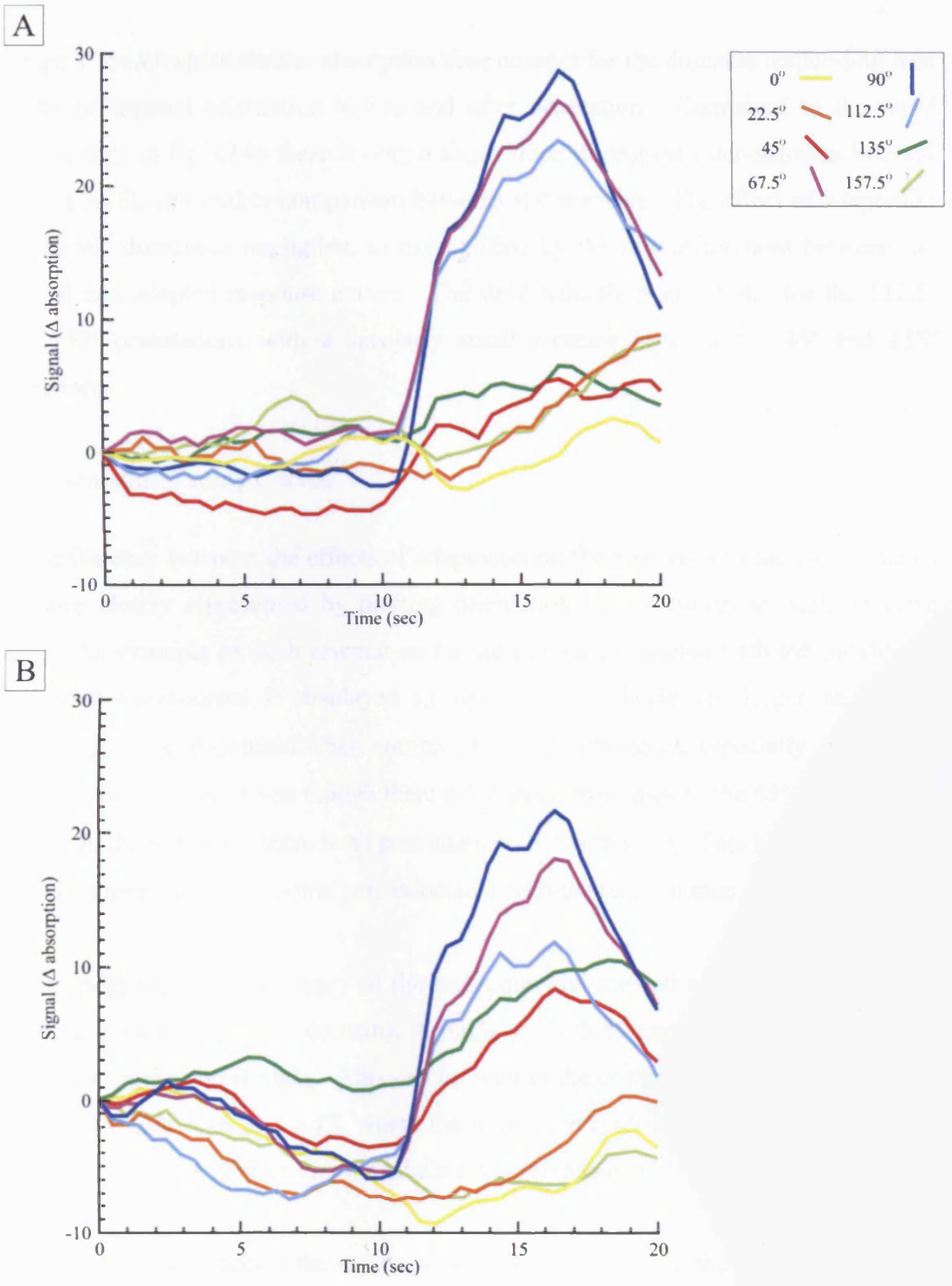

Figure 3.15 - Shows absorption signal time-courses recorded from the domain responding best to the orientation orthogonal to the adapting orientation in cat 11-12-01. Adaptation was induced with either a 3% (A) or 50% (B) contrast 0° oriented grating. Responses to all eight test stimuli are shown, the colour of which is designated by the orientation key in the top right hand corner.

Figure 3.15a&b show similar absorption time courses for the domains responding best to the orthogonal orientation before and after adaptation. Compared to the rapid decline seen in fig 3.14b there is only a slight slope during the inter-stimulus interval seen in 3.15b and makes comparison between states easier. The effect of adaptation on the 90° domain is negligible, as exemplified by the few differences between the control and adapted response curves. The only reductions are slight, for the 112.5° and 157° orientations with a similarly small increase seen in the 45° and 135° responses.

6. Orientation Tuning Curves

The difference between the effects of adaptation on the responses to the two domains is more clearly represented by plotting orientation tuning curves in each adaptive state. An example of such orientation tuning curves, associated with the previously described timecourses is displayed in figure 3.16. There are larger reductions occurring in the θ domain when compared to the orthogonal, especially around the adapting orientation. Even though there are distinct responses to the 45° and 135° test stimuli in the θ domain there is no post adaptation suppression. This indicates that the level of suppression is in some part associated with the test stimulus displayed.

As an indicator of the accuracy of the technique and method of analysis, all control tuning curves for the eight domains, throughout all three experiments are well tuned with clear peaks and troughs. This can be seen in the control curves of the examples shown in figure 3.16 and 3.17, where the maximum response matches the preferred orientation for that domain and the minimum corresponds to its orthogonal.

A feature seen throughout the results was a clear link between the overall strength of the adaptive effect and the orientation domain. The smaller the difference between the orientation used to adapt and the preferred orientation for a domain, the greater the overall adaptive effect. The strength of the adaptive effect can be described using adaptation indices (see methods) with a smaller number indicating a greater level of adaptation. These are shown in the corner of the graphs displayed in figures 3.16 and 3.17. The aforementioned rule holds true in all cases, with lower indices for the 45° domain than the 67.5° after both 25% and 50% contrast adaptation with a 90° grating.

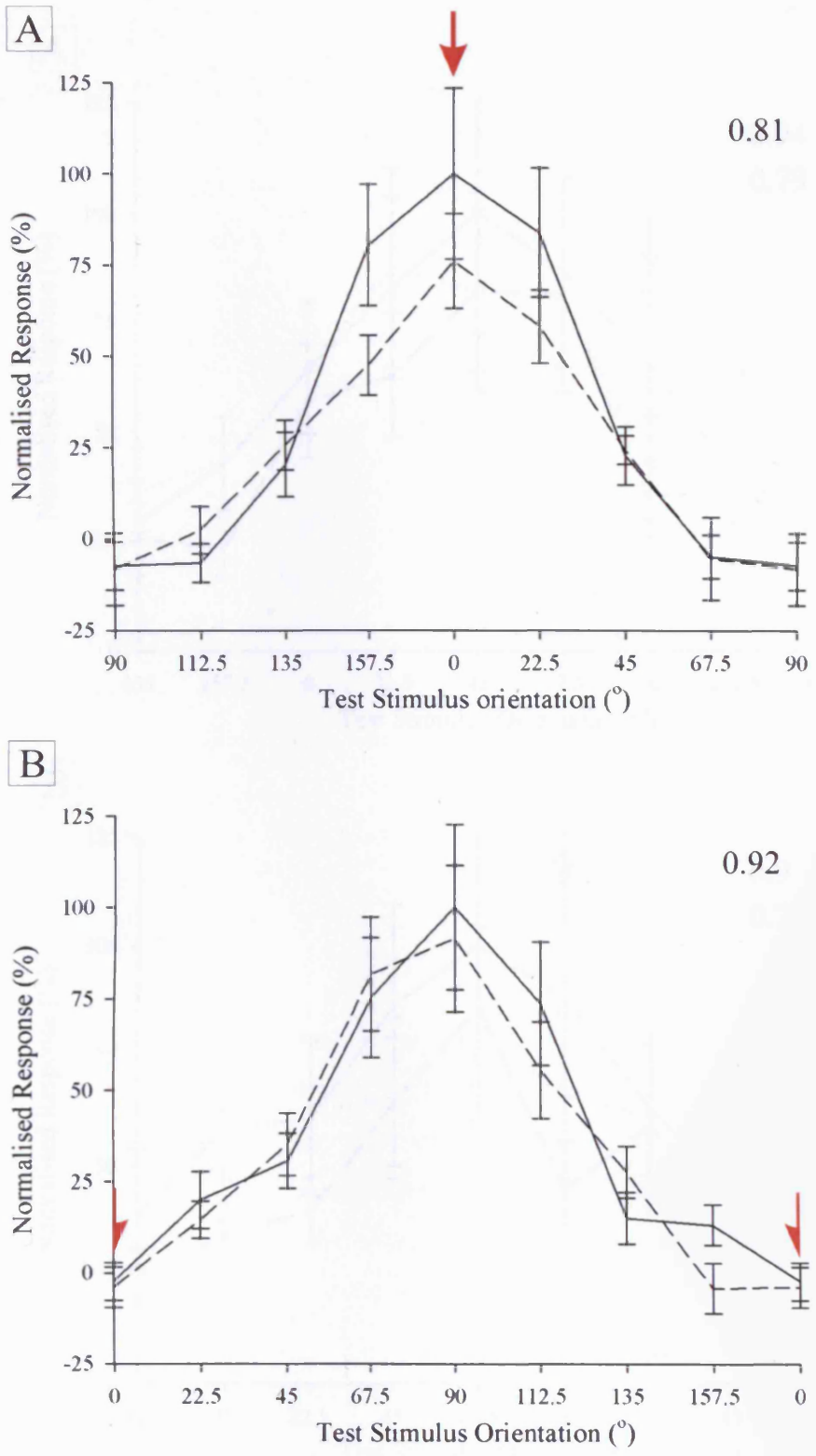

Figure 3.16 - Shows the orientation tuning curves recorded from the 0° (A) and 90° (B) domains in the cat 11-12-01. These curves were calculated by taking the change in response occurring in the timecourses displayed in figures 3.14 & 3.15. A 0° oriented grating with either 3% (solid black lines) or 50% (dotted black lines) was displayed during the adaptation period. Red arrows mark the adapting orientation and the number in the top right corner of each graph is the adaptation index. Note that the abscissa is different for the two domains, with the curves centred on the preferred orientation in each case. Standard error bars are based on the repeated measurements of a test stimulus response across the course of one experiment.

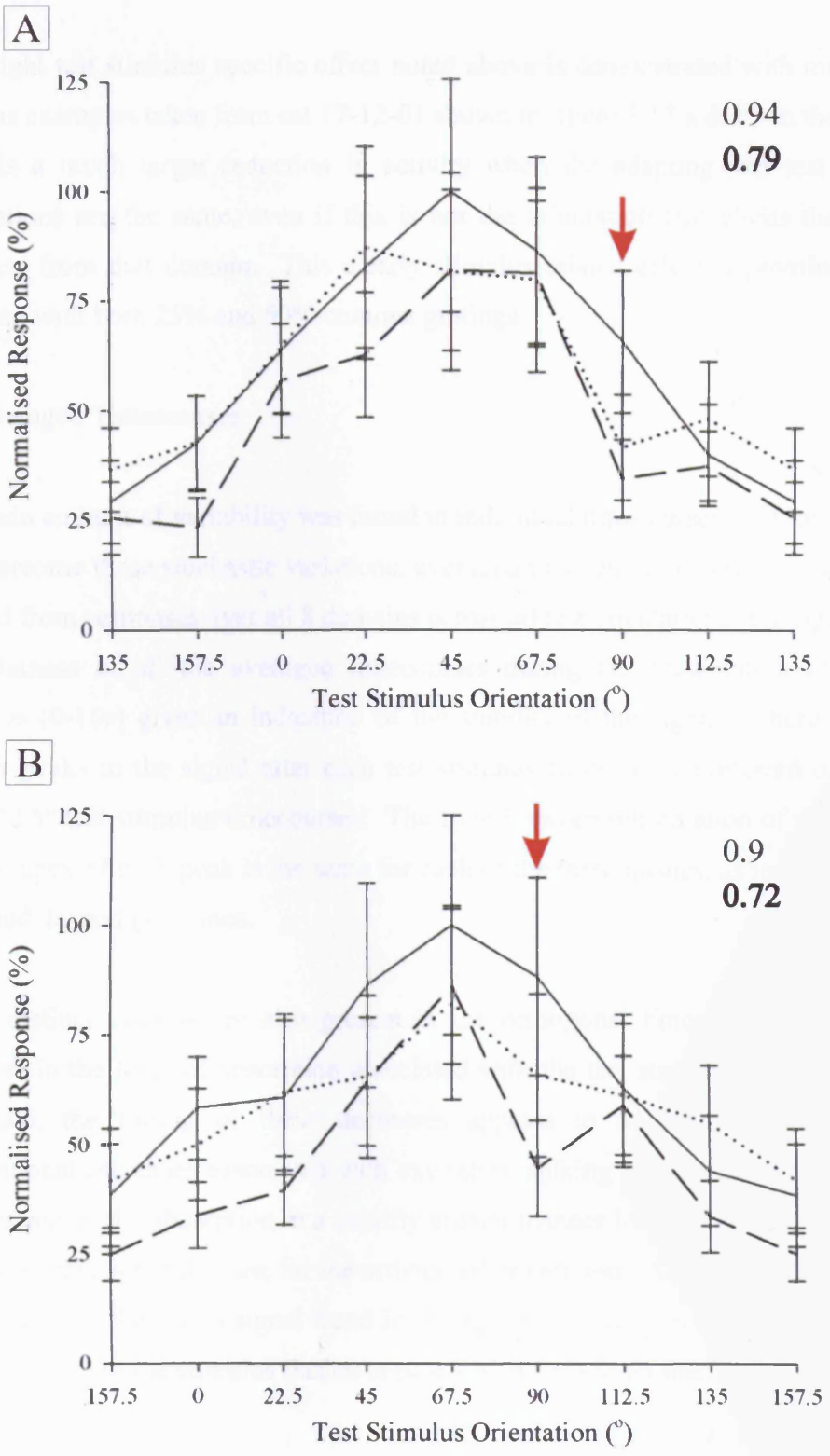

Figure 3.17 - Shows the orientation tuning curves recorded from the 45° (A) and 67.5° (B) domains in the cat 17-12-01. A 90° oriented grating with 0% (solid lines), 25% (dotted lines) or 50% (dashed lines) contrast was displayed during the adaptation period. In the top right corner is shown the 25% (above) and 50% (below in bold) contrast adaptation indices. The adapting orientation is marked with a red arrow and the abscissas are shifted in order to align the preferred orientation in the centre of the graph.

The slight test stimulus specific effect noted above is demonstrated with much more obvious examples taken from cat 17-12-01 shown in figure 3.17 a & b. In these cases, there is a much larger reduction in activity when the adapting and test stimulus orientations are the same, even if this is not the orientation that elicits the greatest response from that domain. This clearly stimulus related effect is prominent when adapting with both 25% and 50% contrast gratings.

7. Averaged Timecourses

A certain amount of variability was found in individual timecourses from one domain. To overcome these stochastic variations, averaged timecourses of greater clarity were created from responses over all 8 domains across all test orientations (see figure 3.18). The flatness of all the averaged timecourses during the presentation of a blank stimulus (0-10s) gives an indication of the stability of the signal. There are three precise peaks in the signal after each test stimulus flash in the preferred orientation and ±22.5° test stimulus timecourses. The time between presentation of the stimulus and the apex of each peak is the same for each of the three flashes, as indicated by the solid and dashed grey lines.

Three distinct troughs are also present in the orthogonal timecourses indicating a decrease in the level of absorption associated with the test stimulus. At least at this timescale, the timing of these decreases appears to be identical to the more conventional increases associated with excitatory spiking responses. Although each flash increases the absorption in a steadily greater manner for the PO, ±22.5° and ±45° responses, this is not the case for the orthogonal orientation. After the initial decrease, it appears that there is a signal trend in the opposing direction and that the troughs corresponding to the stimulus flashes appear superimposed on this.

Thus, it appears that decreases in the level of absorption can occur in response to oriented test stimuli as well as increases. In other words, both the magnitude of any changes in the absorption signal and the direction is dependent on the orientation of the test stimulus.

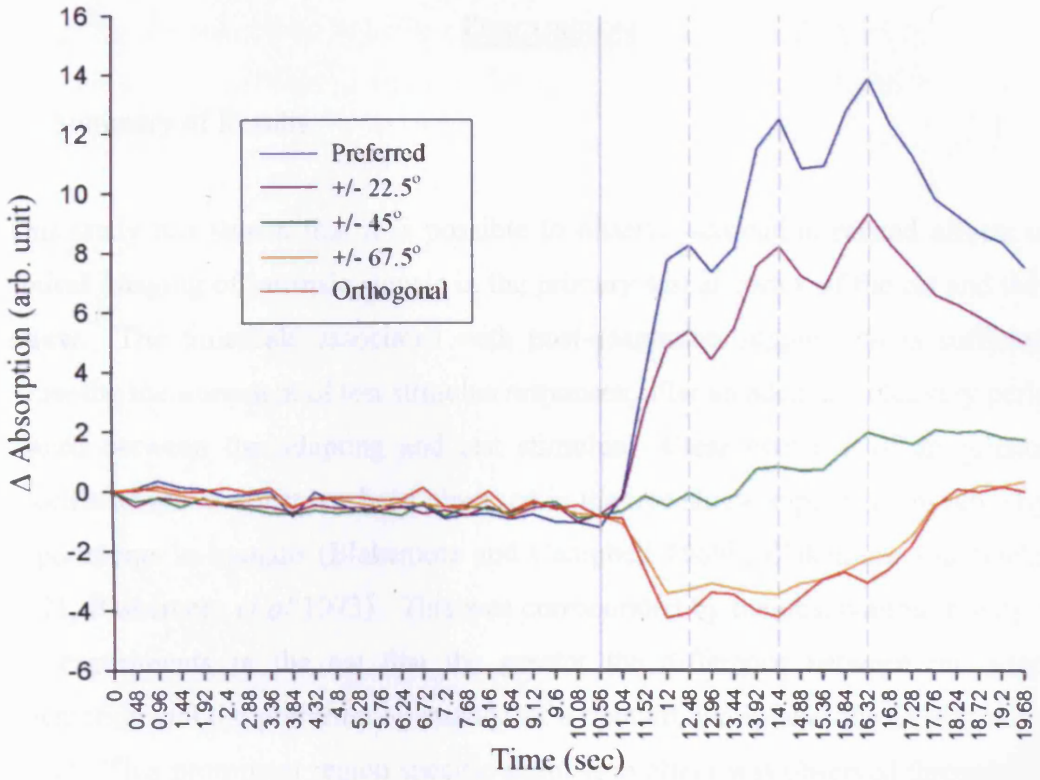

Figure 3.18 - All timecourses were taken from the experiment performed in the cat on 15-04-02. The mean timecourses are calculated on the assumption that the control responses to the preferred orientation (PO) and those relative to this are comparable i.e. the 0° response in the 0° domain is equivalent to the 22.5° response in the 22.5° domain etc. The rest of the timecourses are calculated relative to this PO and coloured according to the key. Because the three pairs of stimuli that are an equal number of degrees away from the PO are also equivalent (i.e. ±22.5°, ±45° & ±67.5°), they are actually an average of 16 timecourses (2 from each domain) rather than only 8 for the PO and its orthogonal. The solid grey horizontal line indicates the start of the test stimulus and the dashed grey lines allow comparison between the peaks in each of the orientation responses.

DISCUSSION

1. Summary of Results

This study has shown that it is possible to observe adaptation related effects using optical imaging of intrinsic signals in the primary visual cortex of the cat and the tree shrew. The timescale associated with post-adaptation suppression is sufficient to allow the measurement of test stimulus responses, after an adequate recovery period is placed between the adapting and test stimulus. Clear evidence of an orientation specific adaptive effect has been observed in the tree shrew supporting psychophysics experiments in humans (Blakemore and Campbell 1969b, Blakemore and Nachmias 1971, Blakemore *et al* 1973). This was corroborated by the observation in long-term OI experiments in the cat that the greater the difference between the adapting orientation and the preferred orientation of a domain, the weaker the overall adaptive effect. This prominent region specific adaptation effect was observed throughout the orientation tuning curve results. Further, specific reductions were observed in the test stimulus responses to the orientation used to adapt in domains where this didn't evoke the strongest response. The many factors that need to be taken into consideration in order to obtain such reliable recordings over long periods of time are explained in greater detail below. An unexpected observation was made after averaging the absorption timecourses across orientation domains in the cat. This revealed a reduction in the absorption signal when stimulating with an orientation orthogonal to that preferred for a domain.

As expected from the hypothesis outlined in the introduction, the functional layout of orientation activity maps in the tree shrew was preserved after extended periods of adaptation. This is in direct contrast to a similar experiment performed in the cat (Dragoi *et al* 2000).

2. Event Related Optical Imaging and Adaptation

By plotting responses of pixel domains to different sets of grating test stimuli I have obtained both orientation tuning curves and contrast response functions similar to those recorded from single cells before and after adaptation. A similar method

involving the extraction of tuning curves from individual pixels has been used to reveal a spatial relationship between the layout of orientation and directional maps in area 18 (Swindale *et al* 2003). Contrast responses have previously been successfully recorded using optical imaging and fitted using a hyperbolic ratio function to show contrast invariance of functional maps in cat primary visual cortex (Carandini and Sengpiel 2004). Such investigation of functional characteristics and layout of cortical maps use pixel-by-pixel analysis of the OI signal to create highly detailed "snapshot" images over a relatively short period of time. One of the main differences with this study is the attempt to capture accurate images of cortical activity in two different states. The time period required to induce the adapted state and allow for recovery of the OI signal necessitates a greater number of stimulus repetitions and a much longer acquisition time to obtain a reliable result. The unique problems associated with these factors and the methods of data analysis required to overcome these difficulties are discussed below.

The first factor to be taken into consideration is the choice of frame from which to take the maximum response and those frames to include in the optimal response period in order to obtain the most accurate images. Measurements of deoxygenated haemoglobin (HbR) using a phosphorescence quenching method have shown that there is a peak in HbR levels at 1.5s from the stimulus onset (Vanzetta *et al* 2002). Increased consumption of oxygen is thought to underlie this change in HbR and is highly co-localised with electrical activity. After this point the activity related signal is masked by more global blood flow changes resulting in images with greater blood vessel artefacts and poorer co-localisation of signal and neuronal activity. In the time courses recorded during my adaptation protocol, the three peaks in the intrinsic signal usually corresponded to the frame recorded between 1.44s and 1.92s after initial presentation of each 1s test stimulus flash (see figure 3.23). This fits neatly with the observations on HbR levels, although in many cases further increases were observed beyond the 1.5s point. At first sight, they appeared to be caused by the test stimulus, sometimes producing misleading results when they were included to define the maximum response. When a narrower time window with respect to the test stimulus flashes was introduced, the consistency of both orientation tuning curves and orientation maps was improved.

To obtain a reliable selection of pixels, the region of interest was refined after a detailed comparison of angle maps in control conditions whilst bearing in mind the following considerations. Orientation maps in developing kittens have been shown to be stable in chronic experiments over a period of weeks (Kim and Bonhoeffer 1994, Godecke and Bonhoeffer 1996). It has been observed by Dragoi *et al* (2000) that reliable angle maps with little change in mean pixel orientation can be recorded 7 hours apart. This indicates the high stability of orientation maps over long periods of time, far greater than that taken to perform a full adaptation experiment. Thus, it is fair to assume that any large changes in orientation preference are not associated with changes in neuronal activity or the underlying network, but more likely represent artefacts. This allows a more precise selection of stable pixels after careful comparison between control angle maps taken from the former and latter half of an experiment. Only after these analysis steps had been followed did a recognisable pattern emerge between experiments performed in different animals.

3. Stability of Orientation Activity Maps

There is only one other study that used optical imaging to directly record the effects of adaptation (Dragoi *et al* 2000). Instead of replicating the stimulus protocol used in single cell recordings (the approach chosen here), they attempted to quantify changes in the orientation maps before and after an hour of adaptation. They observed large post adaptation changes of up to 20° in the preferred orientation of pixels in the angle map. The results of a replication of this experiment in tree shrews were in complete contrast to their observations, with relatively little change in the orientation preference of pixels after such extended adaptation (see figure 3.18). Coincidentally, the mean difference in orientation of 3.92° over all the pixels included in my analysis is virtually identical to the 3.8° mean they quote for the reliability of maps recorded 7 hours apart, in the absence of adaptation (see methods Dragoi *et al* 2000).

The most obvious difference between the two experiments is the choice of species, which may at least partly explain why I could not find similar alterations. As I have observed in the simple recovery protocols, the intrinsic signal recovers at a quicker rate in the tree shrew than in the cat. The much faster metabolic rate may also contribute to a quicker cortical recovery from extended adaptation. However, use of

the tree shrew also confers several advantages. There is a much larger area of cortex available for imaging, which allows recording from the entire primary visual cortex of one hemisphere (see figure 2.5). This results in a greater area of visual space being represented in the images and a higher number of pixels for the analysis, lending more statistical validity to any calculations. Selection of pixels was based upon the polar map to ensure that the area included in the analysis had a strong, reliable response both before and after adaptation. Without such comparison, it is difficult to ascertain whether any changes arise from weakly responding, inherently unreliable pixels or if they are adaptation related. This doubt is raised when considering that the variability between the control and recovery maps in the analysis of Dragoi *et al* (2000) is greater than their own measure of reliability. Another discrepancy is shown in figure 4c, where a shift of over 10° occurs in the 90° domains of the angle map and yet no corresponding shift is observed in the following histograms based upon a smaller selection of pixels (figure 4d). All of the above considerations and methodological differences may account for the discrepancies between the analyses of the Dragoi study and my own.

4. Reductions in the Intrinsic Signal

An interesting result after averaging the absorption timecourses over equivalent orientation responses is an increase in the amount of absorption after orthogonal stimulation (see figure 3.23). The timing of the three troughs following each test stimulus flash match the corresponding peaks seen in the PO and PO±22.5° timecourses. It is puzzling as to why both the peaks and troughs have such similar timing, considering that a large portion of the signal is based upon increased metabolic consumption as a result of neuronal spiking. As mentioned above, the increase in HbR peaks at around 1.5s (Vanzetta *et al* 2002), but a corresponding reduction in neuronal and/or metabolic activity would not cause a release of oxygen and a reduction in HbR levels in such a precisely timed opposing manner. Influx of fresh oxygenated blood could alter the signal in the correct manner, but this is associated with a slower timecourse than the one observed here (Bonheoffer and Grinvald 1996). However, at the wavelength of light used to perform these optical imaging experiments, the light scattering component of the signal predominates. Factors that affect this signal are not only associated with neuronal spiking and

changes in the HbR levels. For instance, the largest energy demands in the rat cortex during excitatory transmission are split fairly evenly between action potential propagation and synaptic transmission (Attwell and Laughlin 2001). Therefore changes in ionic gradients and synaptic activity unrelated to action potentials also alter the intrinsic signal. The size of the reduction was only 14.71% of the increase when stimulating with the preferred orientation for that domain. This means that the observed reductions could be the result of sub-threshold suppression of the orthogonal responses that are revealed using the optical imaging technique. Extracellular recording in V1 shows that in the majority of cases, presentation of an orthogonally oriented stimulus on its own does not reduce the spiking rate of a neurone below its spontaneous level of activity (see orientation tuning curves in chapter 4 for examples). However, orthogonal gratings can produce a suppressive effect when combined with a stimulus of preferred orientation (Bonds 1989, DeAngelis 1992). Thus, the postulated subthreshold changes that have been observed in this study could well underlie the suppressive effect produced by the orthogonal orientation.

5. Domain Specific Adaptation Effects

When the adapting stimulus evokes a strong response from a domain there is also a correspondingly large amount of adaptation. Conversely, when the adapting stimulus evokes little response from a domain the adaptive effect is also small. In other words, the level of adaptation is proportional to the evoked response from a particular domain. This link between the strength of adaptation and the preferred orientation for a domain is clear and stronger than the test stimulus orientation specific effects observed in the orientation tuning curves (discussed below). Due to the strength of this effect, it follows that the mechanism underlying this link contributes towards a large portion of the adaptive effect. However, it fails to account for observations from single cell recording studies where a strong adaptation effect is in induced by stimuli that only themselves elicit a weak response (Maffei *et al* 1986).

The majority of contrast adaptation can be explained by mechanisms intrinsic to the cell as a form of self-regulating mechanism. One such mechanism has been proposed by Carandini and Ferster (1997) and Sanchez-Vives *et al* (2000a,b), which has received a great deal of support in recent years. According to this theory, after intense

stimulation, an increase of the intracellular concentration of sodium (Na^+) and calcium (Ca^{2+}) causes activation of potassium currents out of the cell and this hyperpolarisation results in a reduced likelihood of cell firing. The domain specific adaptive effects observed in the imaging results are neatly explained with such an intrinsic mechanism of adaptation.

6. Stimulus Specific Adaptation Effects

A quantifiable, stimulus specific reduction of the post-adaptation suppression effect was observed across large areas of cat V1. This finding is displayed in the orientation specific reductions in the tuning curves shown in figure 3.22. The dips in the test stimulus responses of the same orientation as that used to adapt, even though this is not the orientation that evokes the largest response from the domain provide a clear example of an adaptation mechanism that may require network interactions. This effect is relatively weak when compared to the domain specific effect (explained above), which is in agreement with the figure of ~25% of the adaptive effect suggested to have a pattern selective component (Albrecht *et al* 1984, Sanchez-Vives 2000a). There have been a number of studies that have observed such pattern selective effects when performing extracellular or voltage evoked potential recordings from the cat primary visual cortex (Movshon *et al* 1979, Albrecht *et al* 1984, Bonds 1984). The original suggestion by these studies was that some kind of inhibitory mechanism could explain this phenomenon. However, this explanation must now be considered highly unlikely, since studies involving the removal of GABAergic inhibition did not affect the level of adaptation (DeBruyn and Bonds 1986, Vidyasagar 1990, McLean and Palmer 1996).

Intrinsic cell mechanisms cannot explain such reductions either, because membrane hyperpolarisation does not contain any information about the nature of the stimulus that caused it. This mechanism would therefore affect the responses to all the oriented stimuli, rather than specifically alter the response to the adapting stimulus orientation.

A possible explanation for this phenomenon is some form of slow depression of those synapses that receive specific thalamocortical input from the adapting stimulus.

Short term synaptic depression has been shown to occur in cat thalamocortical synapses (Stratford *et al* 1996). A model of synaptic depression in V1 has provided evidence that contrast adaptation is possible via this route and produces the gain control effects measured in the shift of contrast response functions (Chance *et al*, 1998). However, this model cannot account for intracellular measurements of membrane potential modulations in simple cells before and after adaptation (Carandini and Ferster 1997). A drifting sinusoidal grating induces corresponding sinusoidal modulation in the membrane potential, the magnitude of which is related to the level of contrast. However, contrast adaptation does not affect the size of this modulation. If synaptic depression did underlie the adaptive effect this would cause a reduction in the amplitude of such modulations.

So it follows that test stimulus specific adaptation of the type observed here is mainly a network effect and most likely involves the intracortical neurones of V1. It must be remembered that the time scale involved requires some form of relatively long-lasting alteration in the properties of the cell. This may come about due to a reduction in the efficacy of excitatory connections due to a temporary depression of synaptic transmission (McLean and Palmer 1996). The majority of intracortical connections between neurones in V1 are excitatory, and over half of these are from cells with similar response properties (Mitchison and Crick 1982, Rockland and Lund 1982, Gilbert and Wiesel 1989, Kisvárday *et al* 1997). When a particular orientation is adapted all the cells in this network which respond preferentially to this orientation undergo hyperpolarisation through intrinsic mechanisms. Thus, there is a large population of interconnected cells that undergo this post adaptation suppression. A temporary depression of the intracortical excitatory synapses between these neurones may well be the mechanism that produces the test stimulus specific aftereffects.

7. Future Directions

The main part of this investigation was an exploration of the potential for using optical imaging of intrinsic signals in the study of adaptation, the success of which provides a firm basis for future work. Further investigations should address the limitations inherent in the different timescales involved in the suppressive effect of adaptation and the recovery period required to obtain a reliable optical imaging signal.

Such difficulties could be overcome by using voltage-sensitive dye imaging (VSDI), which has a much greater temporal resolution. A similar event related methodology as that used above could be carried out in order to obtain orientation tuning curves from individual pixels in functional maps recorded with this technique. The changes in fluorescence recorded with VSDI that correspond to underlying neuronal activity are not adversely affected by the global changes in blood flow that produce difficulties with OI of adaptation. This allows recording of fluorescence changes throughout any adaptation and testing periods, without a gap for recovery. This means that imaging could be instigated immediately following the adaptation period, when the suppression effect is strongest. More importantly however, VSDI allows the recording of activity over a succession of time frames with a temporal resolution of only 5ms (Slovin *et al* 2002). Thus, a VSDI recording of neuronal activity during a stimulus protocol like that shown in figure 1.14 would be possible. This protocol involved stimulation with an oriented grating first with low contrast, followed by a longer period of high contrast adaptation and then finishing with a return to the original lower contrast. This approach clearly demonstrated in simple cells the reduction of the response during adaptation and subsequent post-adaptation suppression (Albrecht *et al* 1984). The high spatial and temporal resolution of VSDI would answer numerous questions associated with the mechanism of pattern adaptation in the primary visual cortex. For instance, does the region of activated cortex change size during the adaptation period? Do different areas of the cortex adapt at the same speed, or is there some kind of spreading of the effect out from the domains most affected by the adapting orientation? A range of orientations could be presented in the low contrast periods to obtain orientation tuning curves before and after the adaptation period. Thus, the progression of the effects of adaptation on the shape and character of orientation tuning curves recorded from different regions in the cortex could be assessed. This would reveal any shifts in orientation preference that occur on a short time scale. Although this technique conveys many advantages, there are time limits associated with prolonged exposure to illumination that have to be taken into account when considering the long periods required for study of adaptation. However, the proposed stimulus protocol would be a great deal shorter than that used with OI due to the lack of a need for recovery periods.

As regards future work concerning long-term adaptation, a developmental study appears promising. The experiments performed by Dragoi *et al* (2000) were carried out in adult cats whose cortical responses are more stable than those found in younger animals. A single-cell study into the effect of adaptation on contrast response functions has shown that the responses of individual neurones recorded from kittens show a greater susceptibility to adaptation than those from adults (Sclar *et al* 1985). Investigations into cortical development have shown that manipulation of the visual environment in young animals, especially during a critical period of plasticity can cause long term changes in the functional layout the cortex (Sengpiel *et al* 1998b, 1999). This means that in theory, long-term adaptation should result in greater alterations in the cortical functional architecture in younger animals. Therefore I propose a future experiment comparing any changes in cortical map of the primary visual cortex during the critical period, in young kittens and in adults.

CHAPTER FOUR

INTRODUCTION

1. Inter-Ocular Transfer Definition and Discovery

When an aftereffect is induced in one eye and a corresponding effect is found when the test stimulus is presented to the other eye, this is termed Inter-Ocular Transfer (IOT). Many aftereffects, including motion, tilt and contrast adaptation show IOT (Georgeson 1980, Bjørklund *et al* 1981, Campbell and Maffei 1971). It is generally assumed that this relies on some kind of binocular process and that the neural locus of IOT is downstream from the point of binocular integration. IOT was first described in various psychophysics investigations, with by far the most work performed using the motion aftereffect (MAE). Numerous early studies, involving spirals and the MAE mention the presence of IOT and some even noted its smaller magnitude than that elicited monocularly, without any quantification (Wohlgemuth 1911, Hunter 1914). A common mechanism underlying both the monocular and IOT effects is suggested by the fact that both display similar characteristics. For instance, a concurrent change for both ipsilateral and interocular affects on spatial frequency tuning curve and magnitude of effect with increasing adaptation time was found for contrast adaptation (Bjørklund *et al* 1981).

Putting a value to the magnitude of IOT occurring in the MAE has since been achieved with many different psychophysics methods and measures, but with surprisingly similar results. Whether moving sine or square wave gratings, spirals or checks were used, a figure of 50-75% IOT is found regularly throughout more than 20 studies (see table 4.1 and similar table dealing solely with the various MAE's in Wade *et al* 1993). In one case, 100% transfer of the tilt AE was found (Campbell and Maffei 1971) although only a single subject was observed, with manual, subjective curve fitting of the data. However, when this result is considered in context and including many more test subjects, a more convincing figure of 50% is found to dominate the literature, as shown in table 4.1. The virtually identical 70% IOT value found in all papers considering the Contrast Threshold Elevation (CTE) effect comes in part from the ease in making subjective judgments about stimulus visibility. This inherent reliability makes it an ideal candidate for use in a clinical environment

(Anderson *et al* 1980). Although a little more variable, a fairly constant IOT magnitude has been reported throughout the MAE papers producing a figure of 60-80% for effects involving moving oriented gratings. The consistency in results found throughout the years indicates a similar underlying mechanism and clearly demonstrates the partial nature of IOT in these three AE's.

Authors	Aftereffect	Mean IOT
Campbell & Maffei (1971)	TAE	100%
Movshon *et al* (1972)	TAE	70%
Mitchell & Ware (1974)	TAE	50%
Mohn & van Hof-van Duin (1983)	TAE	71%
Parasido *et al* (1989)	TAE	46%
Wilcox *et al* (1990)	TAE	54%
Timney *et al* (1995)	TAE	50%
Gilinsky & Doherty (1969)	CTE	70%
Blakemore & Campbell (1969b)	CTE	70%
Anderson *et al* (1980)	CTE	66%
Bjørklund & Magnessen (1981)	CTE	74%
Blake *et al* (1981)	CTE	65%
Timney *et al* (1995)	CTE	75%
Smith & Over (1975)	MAE	58%
Lehmkuhle & Fox (1976)	MAE	76%
O'Shea & Crassini (1981)	MAE	65%
Keck & Price (1982)	MAE	78%
Smith & Hammond (1985)	MAE	58%
Burke & Wenderoth (1993)	MAE	37%
Timney *et al* (1996)	MAE	60%

Table 4.1 - Shows a summary of IOT found in three different AE's commonly used in many studies over the years. All MAE involve translational movement of sine or square wave gratings with equiluminant occlusion of the non-adapted eye during inducement and testing. TAE = Tilt Aftereffect, CTE = Contrast Threshold Elevation, MAE = Motion Aftereffect.

2. The Common Psychophysics Model

The classic model that is used to explain IOT, explicitly stated or otherwise, is outlined in the Venn diagram in figure 4.1. The sets show three pools of neurones,

two monocular pools that can only be activated through the left or right eye and a binocular pool that can be activated through either eye. Adapting the LE affects both the LE monocular cells and binocular neurones. Testing with the RE only stimulates the adapted binocular and non-adapted monocular RE neurones. The main implicit assumption in many of the psychophysics papers is that the strength of the measured aftereffect is dependent on the proportion of adapted neurones out of the total tested. In the above example, the proportion of adapted cells is lower when testing with the RE rather than the LE, and the resulting IOT is smaller than the direct monocular effect. Thus, any aftereffect is reduced according to the number of non-adapted neurones included in the summation that creates the conscious percept (Blake *et al* 1981).

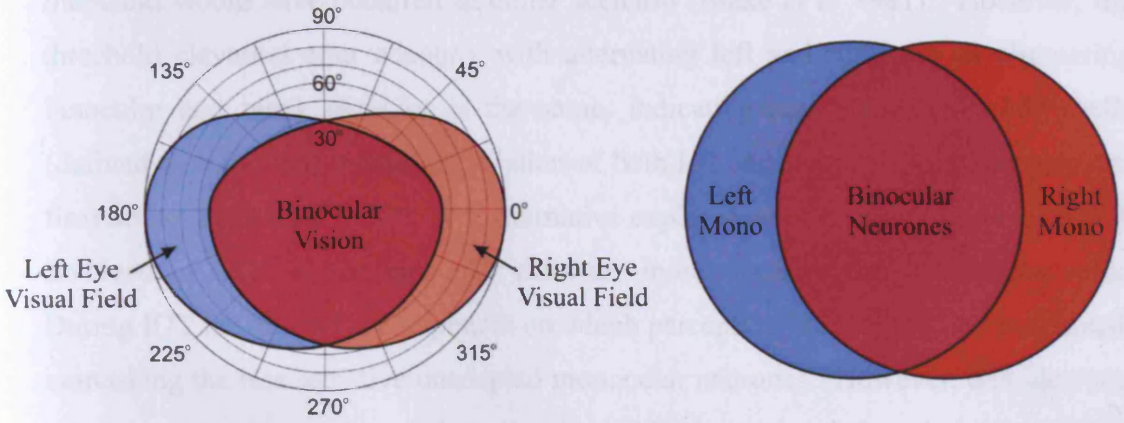

Figure 4.1 - Shows the human visual fields for each eye on the left with the overlapping portion indicating binocular vision. The model implicitly assumed by virtually all psychophysics experiments is shown on the right, a description of which is included in the text (adapted from Blake *et al* 1981). The intuitive logic that led from the way visual space is seen by each eye, to pools of neurones that process this segregated information becomes obvious when both ideas are considered together. However, it must be noted that such pools of neurones do not exist in the primary visual cortex, where there is a spectrum of neurones with varying levels of binocularity. This psychophysics model is concerned purely with monocular or binocular percepts and the associated theoretical pools, rather than representing actual processing streams in the visual system.

When taking the fact that IOT is a binocular process and the assumption just mentioned above, it follows on that the amount of IOT that occurs in a particular AE can be used as an indicator of the magnitude of binocularity involved in the underlying system. This idea is used as a diagnostic tool to measure the binocularity

and stereopsis in patients with visual disorders such as strabismus (Mitchell and Ware 1974, Mohn and van Hof-van Duin, 1983, McColl and Mitchell 1998). IOT has also been used as a measure of interhemispheric transfer after discovery of an enlarged corpus callosum in schizophrenic patients (Tress and Kugler 1979).

The underlying assumptions of this model have been thoroughly tested using the CTE of oriented, stationary gratings and various combinations of monocular and binocular adaptation and testing paradigms (Blake *et al* 1981, Sloane and Blake 1984). The involvement of monocular neurones was confirmed by comparing the effect of adapting continuously with one eye or alternating left and right eyes on a monocular test stimulus. A greater effect was found for the continuous adaptation paradigm, whereas if only binocular neurone responses were responsible, a similar increase in threshold would have occurred in either scenario (Blake *et al* 1981). However, the threshold elevation after adapting with alternating left and right eye or alternating binocular and blank stimulus is the same, indicating that binocular 'AND' cells (defined as those that require stimulation of both left and right eye simultaneously to fire) do not contribute to IOT. An alternative explanation of the partial aspect of IOT involved in CTE is that binocular cells are more sensitive than monocular cells. During IOT the binocular component on which perception is usually based is adapted, unmasking the less sensitive unadapted monocular neurones. However, this idea was ruled out after it was found that adapting with alternating left and right eye time periods of different ratios produces a similar magnitude of IOT (Sloane and Blake 1984). The level of response to any particular stimulus is therefore dependent upon the pooled activity of monocular and binocular neurones, rather than just on the most sensitive neurones for that particular stimulus.

3. Different Aftereffects Provide Evidence for the Site of IOT

Since the first experiments investigating AE's, the methods used to produce and record them have undergone a great deal of refinement. Many AE's that were initially considered to result from similar processes have now been separated into distinct categories, with the degree of IOT sometimes used as the distinguishing factor.

For instance, aftereffects using stimuli which are optimal for geniculate neurones but have little affect on V1 do not display IOT (Green *et al* 1983, Ibbotson and Maddess 1994). A comparison of the effects of motion and flickering adaptation showed that the former displayed significant IOT whereas the latter did not transfer at all (Ibbotson and Maddess 1994). A similar effect was noted using low spatial frequency, high contrast moving gratings and homogenous flickering as a test (Green *et al* 1983). This effect is specific for stimuli with rapid motion, which indicates the LGN as the neural locus, whose cells are able to respond to much higher temporal frequencies (Hawken *et al* 1996). The preference of LGN cells for such low spatial frequency adaptation stimuli (Guido *et al* 1989) also supports this idea. Moving stimuli with higher spatial frequencies and clear orientations presented during adaptation, elicit responses in V1 and the subsequent inclusion of the binocular neurones thought to mediate IOT. This provides evidence that IOT does not occur before V1 in the visual hierarchy, although it doesn't rule out the possibility of transfer via cortico-thalamic feedback connections.

Another example of an aftereffect that shows a link between its physiological substrate location and the level of IOT is the stochastic MAE. This requires the use of random dot kinetograms (RDKs) to produce the overall perception of coherent motion without involving oriented lines *per se*. Such stochastic MAE's show 100% IOT and utilise dynamic, moving stimuli in the both the adapting and test periods (Raymond 1993). Another study involving stereodeficient subjects found that even though no IOT of the classic MAE was observed, there was still almost total transfer of the stochastic MAE (McColl and Mitchell 1998). This suggests not only that the classic and stochastic MAE have different underlying mechanisms but also that they occur in different cortical locations. Extrastriate regions of the cortex further along the visual hierarchy have been shown to almost completely binocular (Baizer *et al* 1977, Zeki 1978, Livingstone and Hubel 1987) and as such provide the most likely location for the stochastic MAE. Interocular testing of the TAE using subjective contours also produces almost complete transfer (Paradiso *et al* 1989) and physiological correlates for such contours have been located in area V2 (Von der Heydt *et al* 1984). Interestingly, if a static rather than dynamic test pattern is displayed in the stochastic MAE only partial IOT is observed as extrastriate areas are unresponsive to such stimuli (Albright 1984). This provides yet more evidence that physiological location

of an AE determines its level of IOT and that those with partial transfer occur in the primary visual cortex.

As mentioned above, a great deal of the simpler AE involving motion, tilt and contrast of oriented lines, sine/square wave gratings or spirals produce some level of incomplete IOT. The most obvious location for such transfer to take place is V1, where the neuronal responses of cells represent a range of binocularity. The mixture of mainly binocular and monocular neurones found in V1 supports the idea that a summation of their responses would produce the partial transfer observed. This leads to the conclusion that such IOT occurs in the primary visual cortex, the first location of binocular neurones in the visual processing stream.

If two moving gratings are placed above and below a stationary grating fixated by the observer with no background reference point, it appears that the fixed grating is the moving one, in the opposite direction to the other two. The resulting monocular & interocularly transferred MAE from such stimulation is based upon the observed relative motion, rather than the actually moving stimuli. This is relevant to many of the MAE studies, because many of the stimuli used move relative to the background, be that a dimly lit laboratory or edge of the display apparatus. Two studies address the question of where relative motion is processed, each reaching very different conclusions. If the relative motion is extracted before binocular summation then no IOT should take place but as in the scenario described above, this is not the case (Wade *et al* 1993). They also noted however, that a lower level of IOT was induced if the background was blacked out, removing the relative portion of the AE. Thus, many MAE studies may well have over estimated the level of IOT that occurs, because they did not take account of this relative affect. However, Symons *et al* (1996) used combinations of random dot moving central stimuli with or without stationary surround to statistically separate the contribution of relative motion to the monocular and interocular affect. Even though relative motion enhances the MAE, this only occurs monocularly and such processing is deemed to occur before binocular summation. It can then be argued that the common MAE is binocular in some part and uses absolute motion sensors, and that the addition of monocular relative motion sensors causes the additional affect.

4. The Function of IOT

A possible function of IOT could be to provide a binocular gain control mechanism. If the main function of adaptation is as a gain mechanism to maintain a sensitive neuronal response in different visual environments, it makes intuitive sense that any changes would be transferred from one eye to the other. This stops any imbalance occurring between the two eyes and ensures accurate binocular vision in changing circumstances. However, decomposition of monocular and binocular gain components using dichoptic static and varying contrast stimuli have shown that major contrast gain reductions occur at the monocular level, before convergence of binocular information (Truchard *et al* 2000). It must be noted that the Truchard study was concerned with rapid gain mechanisms of less than 5sec and that adaptation times associated with IOT are usually between 15-30sec. There is obviously a great deal of overlap, but there is still the possibility of interocular interaction occurring over moderate time periods influencing contrast gain mechanisms. Although it is worth remembering that the adapting stimulus protocol is an artificially created scenario that is unlikely to occur in nature. This means that the adaptation mechanism may not have a specific function under normal viewing circumstances.

It is clear that depth perception and a fused single perception of visual space are vital benefits of binocular vision. Such advantages require some level of interocular interaction, and perhaps the involvement of similar pathways or physiological substrates as those utilised during IOT. Comparing and contrasting the images from both eyes underlies binocular disparity, the main mechanism underlying positioning of objects in a 3D environment. The small distance separating the two eyes means that each eye has a slightly different view of an object. This difference is what forms the basis of depth discrimination and stereovision in species with two forward facing eyes. In order to explain further, consider the situation in a human whose two eyes are fixating precisely at some point in space. If an object is positioned such that two lines drawn from it through the anterior nodal point of each eye hit corresponding retinal points there is zero disparity. Corresponding retinal points have exactly the same position relative to the fovea in each eye, and the angles subtended between the aforementioned lines from the object and similar ones from the fixation point to the fovea are equal. This situation is represented diagrammatically in figure 4.2 which

also shows the Vieth-Müller circle, a theoretical ring of positions that produce zero horizontal disparity.

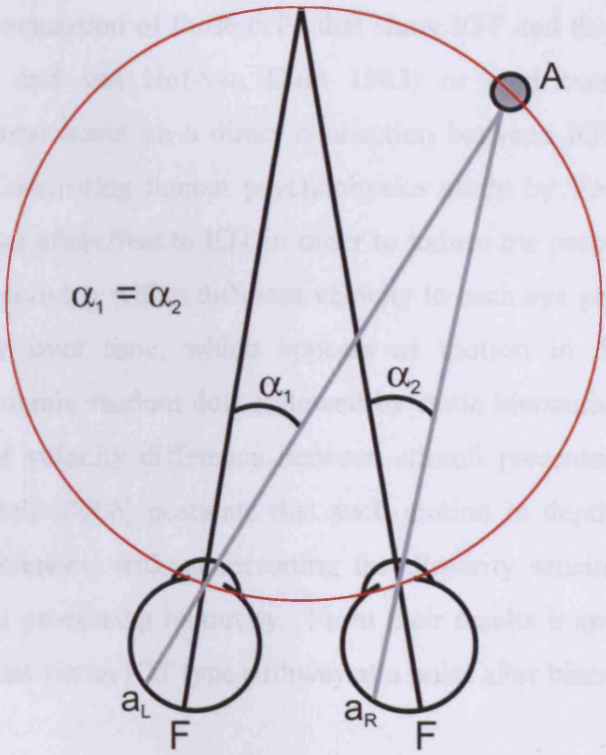

Figure 4.2 – The red ring in this diagram is the Vieth-Müller circle, which represents those points that have zero horizontal disparity when fixating on a point straight ahead. The two lines drawn from an object A, placed upon the circle hit corresponding retinal points a_L and a_R. The horizontal disparity can be calculated by taking the difference between the two angles α_1 and α_2. Any points within this ring have convergent disparity and any without have divergent disparity. F designates the fovea in each eye.

Both simple and complex binocular cells in V1 show disparity sensitivity and are thought to be directly involved in stereopsis (Hubel and Wiesel 1962, Ohzawa and Freeman 1986 a,b). These are the same cell types from which IOT aftereffects have been recorded, which suggests a similar underlying physiological substrate (Maffei *et al* 1986, Marlin *et al* 1991). Further evidence for this is found in studies that show a correspondence between reduction in IOT and deficient stereovision in observers (Mitchell *et al* 1975, Mohn and van Hof-van Duin 1983, McColl and Mitchell 1998).

However, the link between IOT and stereopsis is not as straightforward as such studies appear to indicate. The presence of IOT in stereoblind observers (Mohn and

van Hof-van Duin 1983) and the lack of binocular 'AND' cells involvement in IOT, which have been shown to be sensitive to depth (Poggio and Fischer 1977, Blake *et al* 1981, Anstis and Duncan 1983) show that this relationship is not as clear as would first appear. This separation of those cells that show IOT and those that show depth perception (Mohn and van Hof-van Duin 1983) or contribute to its conscious perception casts some doubt on a direct connection between IOT, binocularity and stereo vision. An interesting human psychophysics study by Fernandez and Farell (2006) uses a similar aftereffect to IOT in order to induce the perception of motion in depth. A stimulus moving with a different velocity in each eye produces a change in binocular disparity over time, which appears as motion in depth. Monocular adaptation with dynamic random dots followed by static binocular testing can create such an interocular velocity difference between stimuli presented to the two eyes. Fernandez and Farell (2006) postulate that such motion in depth can occur purely from velocity differences, without recruiting the disparity sensitive cells which lie earlier in the visual processing hierarchy. From their results it appears that dynamic stereovision can exist via an IOT type pathway at a point after binocular combination.

It is worth mentioning that binocular rivalry and IOT are entirely independent of each other, even though it has been postulated that they both occur in V1 binocular cells (O'Shea and Crassini 1981, Logothetis and Schall 1989, Leopold and Logothetis 1996, Sheinberg and Logothetis 1997, Fries *et al* 1997). When viewing two rival stimuli, one of which produces an AE, the magnitude of such an affect is dependent on the entire length of time the stimulus is presented, not the period of conscious perception (O'Shea and Crassini 1981). Thus, it appears that the MAE and IOT occur in cells that do not contribute directly to perception. Another study using a combination of adaptation and binocular rivalry stimuli places the rivalrous suppression at a location after that involving adaptation (Blake and Overton 1979). Although this is tempered by a later paper that found the strength of contrast adaptation was reduced in a rivalrous situation where the adapting stimulus was only perceived for 10% of the time (Lehky and Blake 1991).

5. Limitations of Psychophysics Experiments

The main problem with eking out the precise mechanism underlying IOT with psychophysics experiments is that there is no precise way of stimulating or testing purely monocular or binocular channels. Any stimulus shown to one eye will always activate binocular neurones as well and the contribution of the individual channels to IOT is lost. There are relatively few purely monocular neurones found in V1 and the pool of binocular neurones contains a full spectrum of cells with varying degrees of ocular dominance (Hubel and Wiesel 1962 [cat], 1969 [macaque]). However, the perception of the aftereffect is based upon the entire pool of responding cells rather than those that are most sensitive. The binocular 'AND' cells, although not directly responsible for IOT, may still influence those 'OR' cells that are, although the physiological evidence for 'AND' cells is sparse. Therefore, it is very difficult to ascertain how much IOT occurs within each channel, and know which neurones contribute to the transfer and which do not. Nor is it possible to ascertain the relative sensitivities of monocular and binocular channels (Blake *et al* 1981). Subjective experience gives little indication as to what is occurring in those neurones that do not contribute to the conscious perception even though it is precisely in these cells that IOT may well take place. All these discrepancies contribute to the difficulty of making assumptions about the IOT process based upon psychophysics evidence.

6. Physiological Studies of IOT

Considering the limitations mentioned above, it is surprising how little physiological work involving IOT has been carried out to address these issues. Physiological correlates for IOT of contrast adaptation have been found in V1 (Sclar *et al* 1985, Maffei *et al* 1986, Hammond and Mouat 1988, Marlin *et al* 1991) confirming the aforementioned psychophysics evidence. Hammond and Mouat (1988) found direction selective, partial IOT in binocular cells of the striate cortex. The direction selective aspect and the high SF of the square wave gratings used, rule out pre-cortical mechanisms for IOT in this type of AE. They found no IOT in the singular monocular cell from which they recorded, which provides a weak argument either for, or against such a possibility. They also found no IOT for randomly textured fields, which concurs with an extrastriate role in the perception of such stimuli.

Maffei *et al* (1986) attempted to narrow down the precise location of transfer by recording the level of direct and interocular contrast adaptation in split chiasm cats. When the chiasm is sectioned, those retinal ganglion cells that usually send their afferents across to the other hemisphere go through a process of degeneration, resulting in large scale reduction of cells in the nasal region of both retinas. This can be clearly seen histologically, leaving the binocular temporal retinal regions relatively intact. As such, even though there is only monocular input of the adjacent contralateral visual hemi-fields one would expect a large amount of callosal interconnections, especially around the vertical meridian. Both the direct and callosal pathway produced comparable levels of adaptation, indicating that IOT occurs in cats with a split chiasm. Additional evidence to rule out a pre-cortical transfer is provided with the complete lack of IOT in one cat that had both chiasm and corpus callosum sectioned (Maffei *et al* 1986). Similar recordings of adaptation and IOT were also undertaken in animals with sectioned corpus callosum and intact chiasm. From these results, one can definitively state that either the callosal or the binocular chiasmic route is sufficient to allow IOT to occur although it is difficult to ascertain how much each pathway contributes to IOT, possibly in equal measure. In contrast to Hammond and Mouat (1988), in cells where there appears to be little or no initial response to contralateral stimulation, IOT still occurred via the callosal pathway.

7. Aims and Objectives

The main aim of this study is to elucidate the precise mechanisms and pathways of IOT in the primary visual cortex by using a combination of optical imaging and single cell recording. The orientation and ocular dominance maps provide a means to accurately select regions with binocular or monocular characteristics in which to obtain extracellular recordings. The single cell recording investigations will be used to corroborate and contribute to the small body of work already existing. This will be achieved through *a priori* characterisation of control cell responses and a precise quantification of any IOT in normal cats.

There is a relation between the partial transfer of adaptation and the binocularity of the primary visual cortex. The LGN is largely monocular, and correspondingly no

IOT is found when adapting with stimuli that specifically stimulate geniculate but not cortical neurones (Green *et al* 1983, Ibbotson and Maddess 1994). On the other end of the scale, cortical areas beyond V1 in the visual processing hierarchy are thought to be totally binocular, and have corresponding aftereffects that display complete transfer (Paradiso *et al* 1989). The majority of cells in V1 are binocular and most of the adaptive effect is transferred. Thus, there is a link between the binocularity and the level of IOT found in psychophysics studies of those AE's thought to occur in V1. Although making statements about perception based upon the responses of individual cells is fraught with difficulties, one would expect the single cell results to reflect the link observed in the psychophysics experiments. In other words, the ocular dominance of an individual cell will in some way relate to the level of IOT displayed by that cell. An *a priori* classification of cells into ocular dominance groups and assessment of the level of IOT will be carried out in order to find any such link.

Differences between the presence of IOT in simple and complex cells have been noted in a previous study on split chiasm cats (Maffei *et al* 1986). Virtually all the simple cells recorded displayed IOT, compared with only 20% of the complex cells. However, the ocular dominance distribution of area 17 in split chiasm cats is shifted towards the ipsilateral eye. Could a more monocular cortex account for the low number of complex cells that display IOT? As the cells recorded in this work are from normal cats that have not undergone any kind of developmental interference they will offer an answer to this question. Thus, a similar classification of neurones into simple and complex cells and subsequent comparison with the level of IOT will be undertaken.

Optical imaging maps captured prior to the single cell recording allows the accurate positioning of the electrodes with regard to the functional layout of the cortex. This makes it possible to observe whether the characteristics of the cortical region immediately surrounding a penetration site affect the level of transfer of cells recorded from that position. For instance, there could be greater levels of transfer occurring in the binocular regions of the cortex, in-between the ocular dominance columns. The information provided by the ocular dominance maps allows the binocularity of pixels surrounding recording sites to be quantified and the testing of such a theory. Thus, comparison of the level of IOT in cells recorded from binocular

or monocular cortical regions will clarify whether any such localised effect on IOT is apparent. Considering the fact that no correlation between orientation map location and stimulus specific contrast adaptation has been found in a previous study (Sengpiel and Bonhoeffer 2002) it seems unlikely that the local layout of the orientation map will affect IOT.

METHODS

1. Animal Preparation and Optical Imaging

All drugs were administered and animal preparation was carried out as mentioned previously for the 19 cats that were used in all the IOT experiment. A preliminary optical imaging session was performed using the methods outlined previously in order to obtain angle, polar and ocular dominance maps before commencing any single cell recording procedures.

2. Extracellular Recording Specifics

Glass insulated, sharpened tungsten electrodes were used to record activity, precisely advanced into the cortex using an EPS system (alpha-omega, Nazareth, Israel) and pre -amplified with a bioamp headstage (TDT technologies, Alachua, US). The analogue signal was then amplified (x20k) and high & low pass filtered (300 & 3000Hz cut off points respectively) with brainware system II equipment (TDT technologies, Alachua, US). Humbug (Quest scientific, Vancouver, Canada) eliminated 50Hz noise in real time, before the signal was converted from analogue into digital. This effectively removed possible interference from the 50hz alternating current supply, improving the signal to noise ratio. A cathode ray oscilloscope (CRO) and speakers were used to subjectively isolate cell responses from noise whilst advancing the electrode in a direction perpendicular to the cortical surface. Precise locations of each penetration site were chosen from the intrinsic activity and blood vessel maps obtained in the preceding imaging session. Penetration sites were primarily chosen where the optical imaging signal was strongest and in grey regions of the OD map where predominantly binocular cells were present, as these were considered the most likely sites where IOT might take place, typically three or four penetrations for each experiment. Brainware software (J Schnupp, Oxford, UK) was used for online analysis to select a suitable voltage threshold for spike recognition and isolation of individual cell responses through spike shape analysis based on various timing and voltage magnitude parameters. The typical setup used in all IOT single cell recording experiments is shown in figure 4.3. A Wheatstone stereoscope made of four front-silvered mirrors

allowed stimulation of left or right eye only when displaying stimuli on one half of the monitor screen or the other, as shown in figure 4.4.

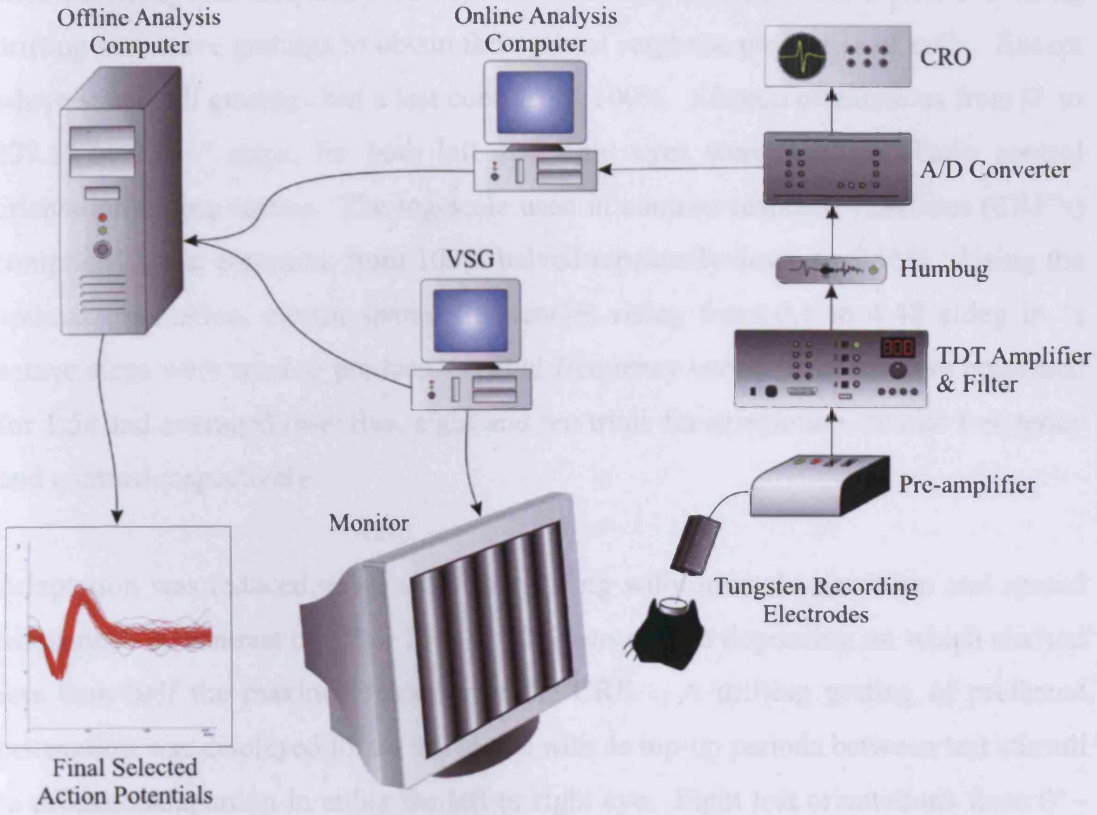

Figure 4.3 - Typical setup used for single cell unit recording, for categorising cells response properties and simple adaptation procedures.

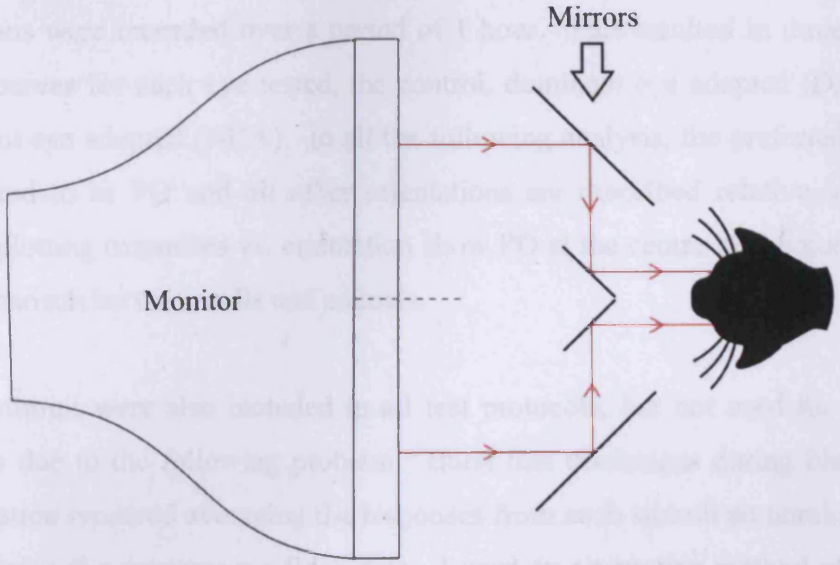

Figure 4.4 - By using four mirrors set at 45° the right and left hand sides of the monitor stimulate either the right or the left eye respectively. Red lines shows path taken by light.

3. Single Cell Stimulus Protocols

Orientation, spatial frequency and contrast response functions were recorded using drifting sine wave gratings to obtain the optimal response properties of cells. Except where stated, all gratings had a test contrast of 100%. Sixteen orientations from 0° to 337.5° in 22.5 ° steps, for both left and right eyes were used to obtain control orientation tuning curves. The log-scale used in contrast response functions (CRF's) comprised 7 test contrasts, from 100% halved repeatedly down to 1.56%. Using the optimal orientation, eleven spatial frequencies rising from 0.1 to 4.48 c/deg in ½ octave steps were used to produce a spatial frequency curve. Stimuli were presented for 1.5s and averaged over five, eight and ten trials for orientation, spatial frequency and contrast respectively.

Adaptation was induced using a drifting grating with optimal orientation and spatial frequency. A contrast of either 25% or 50% was chosen depending on which elicited less than half the maximal response in the CRF. A drifting grating of preferred orientation was displayed for an initial 60s with 4s top-up periods between test stimuli to produce adaptation in either the left or right eye. Eight test orientations from 0° - 315° in 45° increments were shown to the left and right eye for both adapting conditions. Each stimulus was again presented for 1.5s, and responses were averaged over eight trials. The control orientation tuning protocol and two adaptation conditions were recorded over a period of 1 hour. This resulted in three orientation tuning curves for each eye tested, the control, dominant eye adapted (DA) and non-dominant eye adapted (NDA). In all the following analysis, the preferred orientation is referred to as PO and all other orientations are described relative to PO. Any graphs plotting responses vs. orientation show PO at the centre of the x-axis, for ease of comparison between cells and animals.

Blank stimuli were also included in all test protocols, but not used for quantitative analysis due to the following problem. Burst like discharges during blank stimulus presentation rendered averaging the responses from such stimuli an unreliable method of obtaining the spontaneous firing rate. I used an alternative method of calculating the spontaneous level of activity in any of the adapted or control states. Even though the test stimulus was only presented for 1.5s, actual recording of activity also took

place over the preceding 500ms period. . A reliable approximation of spontaneous activity was therefore reached by taking the mean activity occurring in the aforementioned 500ms blank period across all stimuli in each protocol.

4. Offline Analysis of Signal Spikes

A more precise isolation of individual cell responses was carried out offline using Brainware software (Jan Schnupp, Oxford, UK). By forming clusters of spikes with similar spike shapes, two or even three cells recorded at the same location can be separated from each other. Principal parameters for distinguishing between different spike shapes included magnitude of the first (negative) and second (positive) peaks, peak-to-peak time, trigger-to-peak time and the peaks area. Spikes with abnormal delay times between stimulus trigger and peak were removed to ensure that only those responses that were a direct result of the stimulus were included. In many cases, only those spike clusters which contained the largest number of control responses were included in the analysis, for sake of clarity. Auto-correlation histograms of the time interval between one spike and any other were sometimes used for further clarification that all responses were from only one cell. If a spike cluster only includes the responses from one cell then the histogram should show a lack of <=1ms spike intervals, equating to the absolute refractory period of neurones.

Cells were classified as either simple or complex based upon the relative modulation of the post stimulus time histogram (PSTH) responses. A discrete fourier transform was performed on the PSTH and the ratio between the F1 component (response modulation) and F0 component (mean) was calculated. If the F1:F0 ratio was greater than one then the cell was classified as simple and if less than one, as complex (Skottun *et al* 1988).

Ocular dominance ratios were calculated by dividing the total response to all orientations in the left eye by the sum of responses to the right eye. Cells could then be placed into 7 OD categories (Hubel and Wiesel 1962) according to the values in table 4.2, below. A directionality index was calculated by the taking the area under the orientation tuning curve responses to the five orientations that made up the non-

preferred direction (i.e. +90°, +135°, +180°, +225° & +270°) and dividing this by the area under the preferred orientations (i.e. PO + 45°, +90°, +270° & +315°).

OD Category	OD Index Range	Description
1	>10	Left Monocular
2	4-10	
3	1.5-4	
4	0.66-1.5	Binocular
5	0.25-0.66	
6	0.1-0.25	
7	<0.1	Right Monocular

Table 4.2 – Shows the criteria for splitting the cells into seven OD categories based upon the OD index. This 7 category system was first introduced by Hubel and Wiesel (1962) and has since become a standard method of classifying binocularity.

The orientation tuning curves were fitted to a gaussian function in order to obtain quantitative measures of their characteristics. The Gaussian fitting uses the formula, (taken from Carandini and Sengpiel 2004):

$$f(o) = R_{max} \exp(-[o-o_p]^2/2o_w^2)$$

the parameters for which can be seen in the idealised curve in figure 4.5.

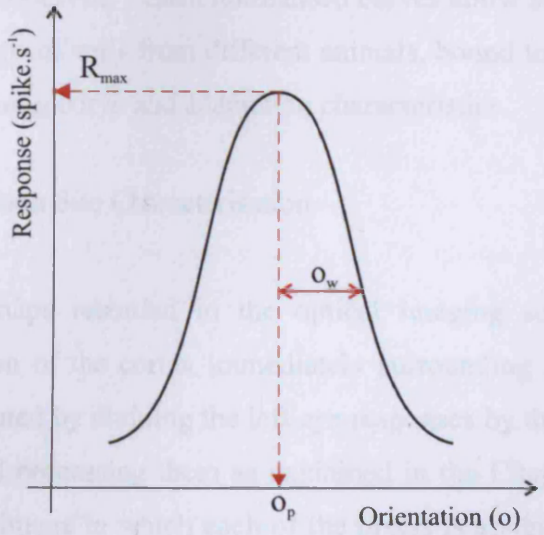

Figure 4.5 - Shows an idealised smooth gaussian curve and its fitting parameters where R_{max} is the maximum response, o_w is the ½height at ½width (hhhw) and o_p the preferred orientation.

Numerous calculations were performed on the control and adapted orientation tuning curves in order to quantify the effects of adaptation and IOT. Any of the following quantifications that rely on NDE responses were omitted for monocular cells The percentage change in the control response after presentation of the adapting stimuli was used as the main indicator of adaptive effect. The absolute transfer of DE adaptation was calculated by dividing the NDE response change by that occurring in the DE. The NDE adaptation transfer was arrived at by a similar but reversed calculation. This sum requires an observable and reliable response change in both eyes and as such, the absolute IOT cannot be calculated for monocular cells. Also of interest was the transfer taking place beyond that expected from the OD of a cell. This was quantified by taking the difference between the ratio of the NDE:DE adaptation effect in each eye, and the ratio of the original NDE:DE control responses. All these calculations were performed for each eyes response to the PO and all the stimuli orientations combined.

Cells with similar control responses and IOT results were grouped together into various categories, the reasons for which are outlined in the results. Orientation tuning curves normalised to the maximal control response were created in order to compare responses between different cells. The adaptive change in the control responses were normalised to the maximal adaptive effect. These values were then plotted to produce an adaptive change tuning curve from which stimulus specific alterations are easily observed. Such normalised curves allow summation and means to be taken over groups of cells from different animals, bound together due to similar control orientation tuning curve and adaptation characteristics.

5. Electrode Penetration Site Characterisation

Ocular dominance maps recorded in the optical imaging session were used to characterise the region of the cortex immediately surrounding a recording location. These maps were created by dividing the left eye responses by the right eye responses and then filtering and processing them as explained in the Chapter 3 methods. The end result is an 8-bit image in which each of the pixels is assigned a greyscale value from 0 (black) to 255 (white), spread across the entire range. Thus, a pixel that responds more readily to the LE would have a greyscale value closer to 0, a binocular

pixel would be around 127 and RE pixels closer to 255. The 256 greyscale values were then split into 7 groups equating to the Hubel and Wiesel classification system so that each pixel, or groups of pixels can be assigned an ocular dominance category. Using this method, the mean greyscale value of the 49 pixels in a 7x7 square surrounding each penetration site was calculated and its ocular dominance quantified. The images shown in figure 4.6 below show the pixel selection process more clearly.

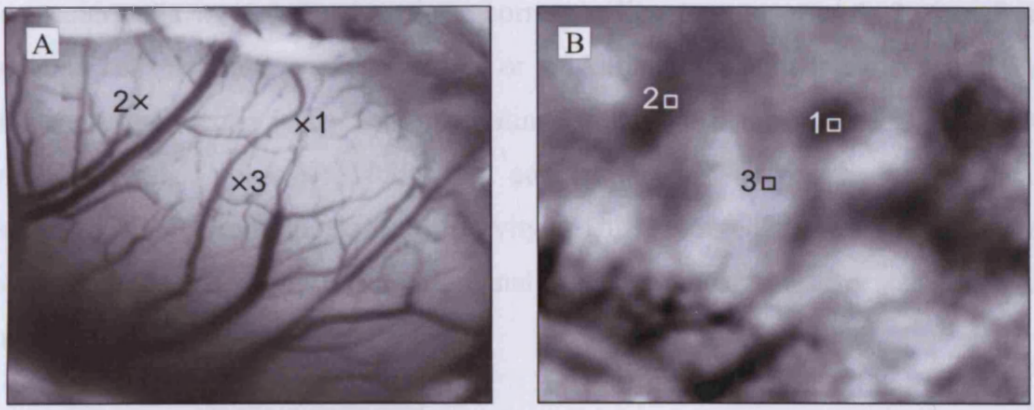

C

82	83	84	85	86	87	89
81	82	83	85	86	87	90
80	81	83	84	86	87	89
79	80	82	83	85	86	89
78	79	80	82	84	85	88
76	78	79	81	83	85	88
75	77	79	81	82	84	88

Figure 4.6 – A – Shows the positions of three recording sites on the cortical blood vessel map taken from an extracellular recording experiment in cat 171203. These locations correspond to areas in the optical imaging maps that respond with a strong intrinsic signal. B – The same three penetration sites are shown in relation to the ocular dominance activity map. The squares delineate the 7x7 pixel area immediately surrounding a site over which the mean greyscale value is calculated in order to characterise its binocularity. The mean greyscale value for each site is 54.69, 83.18 and 161.88 for sites 1, 2 and 3 respectively. These values correspond to the Hubel and Wiesel ocular dominance categories 2, 3 and 5 respectively. C – Shows the expanded 7x7 pixel square surrounding site 2 with the greyscale value associated with each pixel numbered in white. There is a gradual change from the lowest figure in the bottom left corner to higher values in the top right. A similar mean greyscale value is obtained when using different sized surround squares due to the subtle gradation that is found throughout OD maps.

RESULTS

1. Single Cell Results

A total of 59 cells were included in the analysis of interocular transfer (IOT) in the cat primary visual cortex. These cells were split into monocular and binocular groups based upon the Hubel and Wiesel (1962) seven OD category classification system. Monocular cells were defined as those corresponding to categories 1, 2, 6 or 7 and binocular cells as those in categories 3, 4 or 5. Although cells in category 2 and 6 are not strictly monocular in the sense that stimulation of the non-dominant eye (NDE) evokes a weak response, following adaptation this response was typically indistinguishable from spontaneous activity. This rendered these cells effectively monocular and made any quantitative analysis of the adaptive effects in the NDE impossible.

2. Monocular Cells

There were 17 cells, which fit the monocular categorisation as defined above, the majority of which (12 out of 17) are considered together and contribute to the main findings concerning monocular cells and IOT. When the normalised change in response after NDE adaptation is considered for all 17 cells, an unexpected result was noticed in the orthogonal orientation test stimuli activity. Increases in the responses to orthogonal orientations after adaptation with the NDE were seen in five cells. As this finding does not relate directly to the link between OD and IOT these cells will be considered separately and outlined in detail below. The remaining twelve cells typically show reductions or no change in their responses after presentation of the adapting stimuli. They have a group OD index mean of 7.04, which gives an indication of the low level of activity evoked by stimulation of the NDE. Two typical examples of cells in this group are shown in figures 4.7 and 4.8.

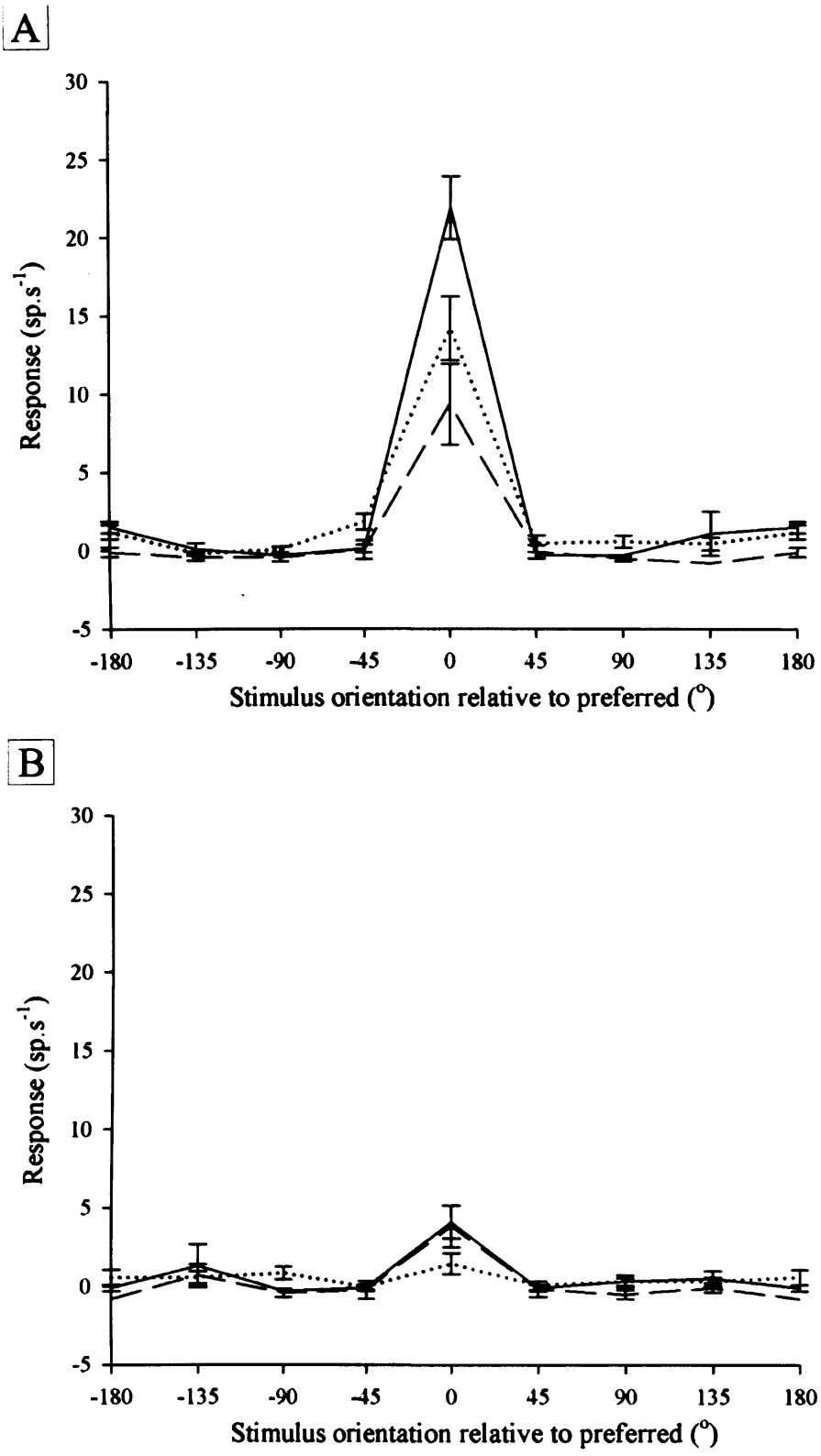

Figure 4.7 - Shows the control (solid lines), LE adapted (dashed lines) and RE adapted (dotted lines) orientation tuning curves for cell 15/07 9b, which displays the typical characteristics of a monocular, directional cell. A - The dominant left eye responses are sharply tuned (O_w = 12.62) and highly directional (Dir^{ind} = 8.96). Adapting with both the left eye and right eye produces large decreases in activity. B - The non-dominant right eye responses, although tuned to the preferred orientation are too low for any changes to be reliably quantified. Adaptation with the right eye lowers the response to a level that is inseparable from stochastic fluctuations in the signal, whereas left eye adaptation results in no significant change at all.

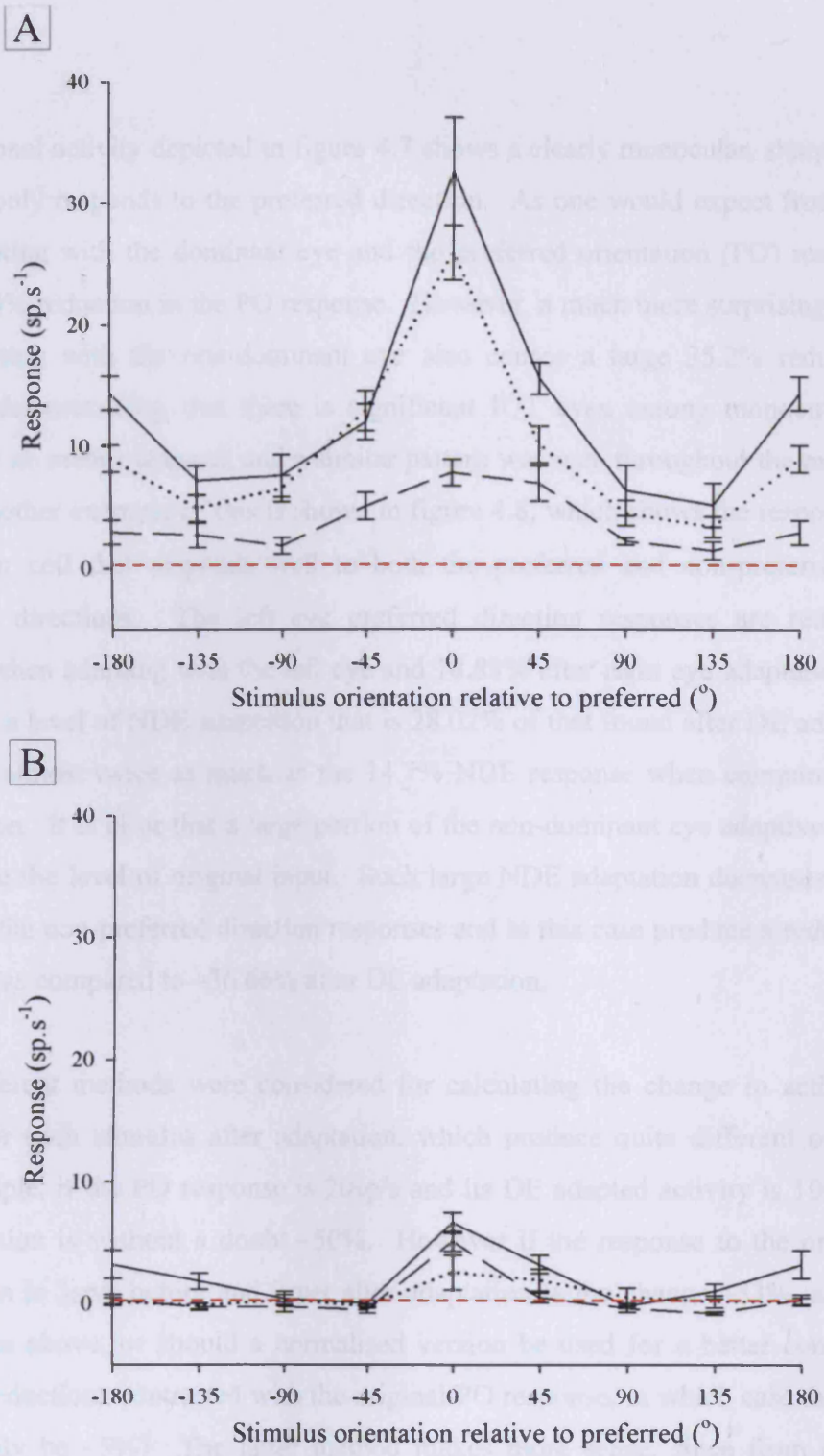

Figure 4.8 – Shows the orientation tuning curves for cell 23/07 3, another example of a monocular cell that in this case responds well to the non-preferred direction. All key attributes of these graphs are the same as that shown in figure 4.7. A - The dominant left eye responses are well tuned (O_w = 42.12), with a directional index of 1.99. Adapting with either eye produces a decrease in activity, although the NDE adaptation reductions are not as prominent as those seen in the example in figure 4.6. B - The non-dominant right eye control responses, although tuned to the preferred orientation are too low for any changes to be reliably quantified. This is apparent by comparing the level of error associated with the spontaneous activity (red dashed lines) with the responses after adaptation with either eye.

The neuronal activity depicted in figure 4.7 shows a clearly monocular, sharply tuned cell that only responds to the preferred direction. As one would expect from such a cell, adapting with the dominant eye and the preferred orientation (PO) results in a large 57.4% reduction in the PO response. However, a much more surprising result is that adapting with the non-dominant eye also causes a large 35.2% reduction in activity, demonstrating that there is significant IOT even among monocular cells. This is by no means unusual, and a similar pattern was seen throughout the monocular cells. Another example of this is shown in figure 4.8, which shows the responses of a monocular cell that responds well to both the preferred and non-preferred (180° stimulus) directions. The left eye preferred direction responses are reduced by 67.37% when adapting with the left eye and 18.88% after right eye adaptation. This produces a level of NDE adaptation that is 28.02% of that found after DE adaptation, which is almost twice as much as the 14.7% NDE response when compared to DE stimulation. It is clear that a large portion of the non-dominant eye adaptive effect is not due to the level of original input. Such large NDE adaptation decreases are also found in the non-preferred direction responses and in this case produce a reduction of –16.24% as compared to –36.66% after DE adaptation.

Two different methods were considered for calculating the change in activity that occurs for each stimulus after adaptation, which produce quite different outcomes. For example, if the PO response is 20sp/s and its DE adapted activity is 10sp/s then the reduction is without a doubt –50%. However if the response to the orthogonal orientation is 3sp/s before and 2sp/s after adaptation is the change –33%, as per the calculation above, or should a normalised version be used for a better comparison, with all reductions contrasted with the original PO response, in which case the change would only be –5%? The latter method makes more sense, since from an ideal-observer point of view a change in response by 1 sp/s for a cell that responds at up to 20sp/s is unlikely to be discernible. These normalised differences accentuate any subtle changes, and allow a more accurate comparison of adaptation effects between cells that have different levels of absolute response. The summarised results of the monocular cells using this calculation are shown diagrammatically in figure 4.9b.

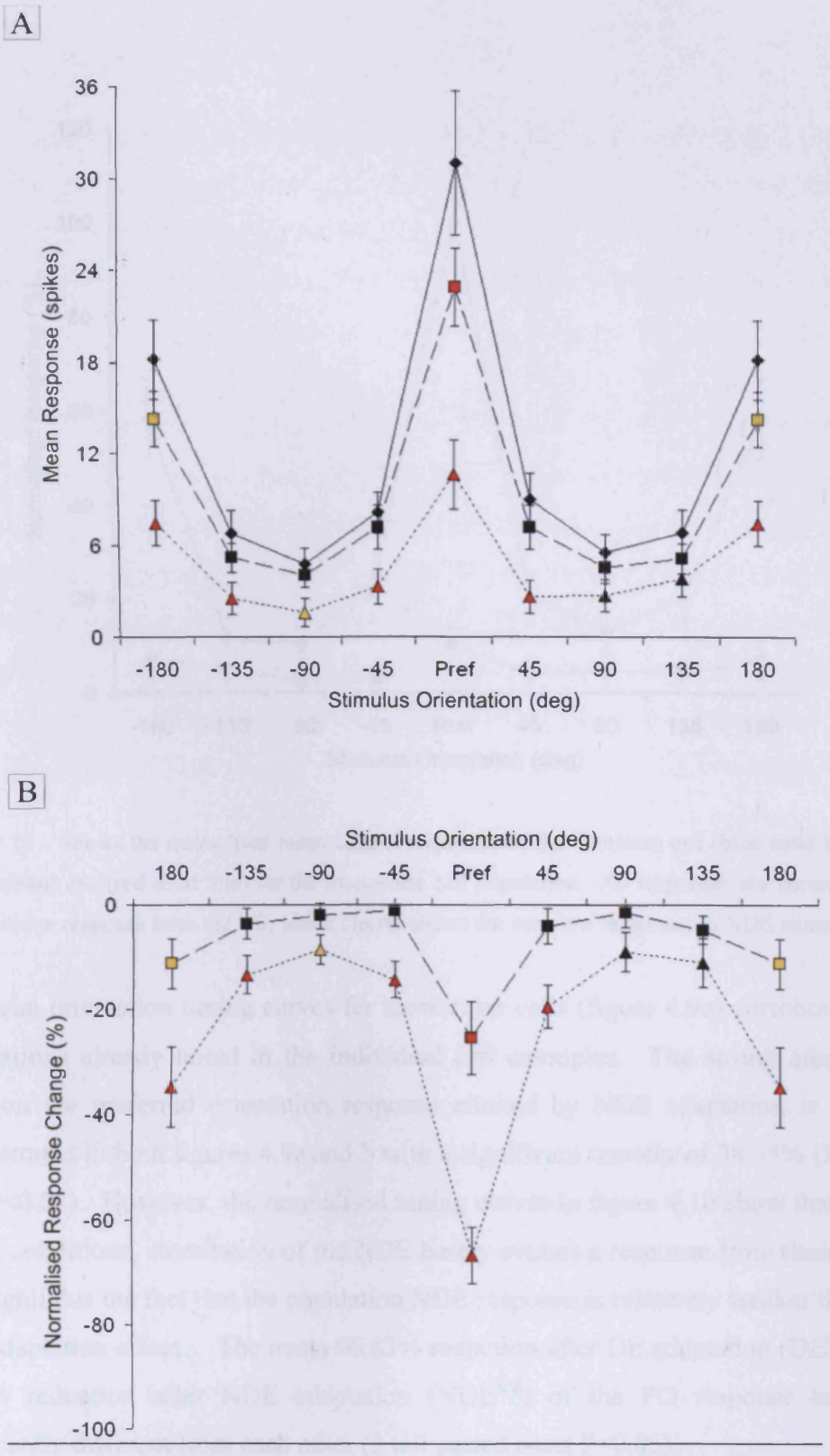

Figure 4.9 - Shows the summarised charts for the dominant eye responses of the twelve monocular cells. A – Mean orientation tuning curve for the control state (solid line) and after adaptation with the non-dominant eye (long dashed line) or the dominant eye (short dashed line). Coloured symbols designate significant differences between the control and adapted responses (2-tailed paired t-test, red and yellow colours indicate $P<0.01$ & $P<0.05$, respectively) B - Comparison of the normalised reduction after adapting with the non-dominant eye (long dashed line) and dominant eye (short dashed line) across all orientation responses.

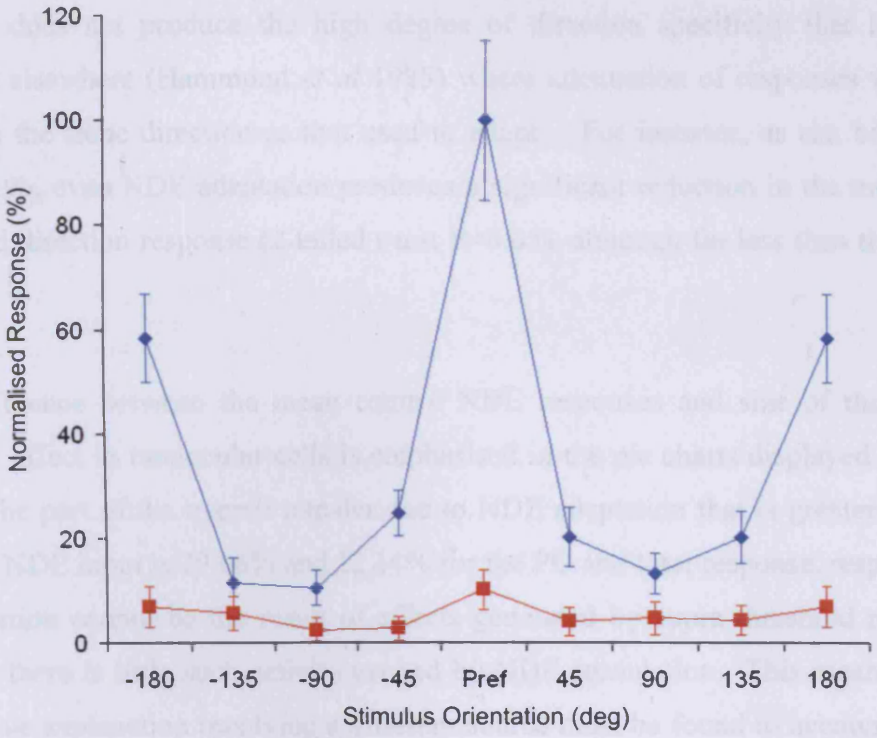

Figure 4.10 - Shows the normalised mean control responses of the dominant eye (blue solid line) and non-dominant eye (red solid line) for the monocular cell population. All responses are normalised to the maximum response from the DE, which clearly shows the very low responses to NDE stimulation.

The mean orientation tuning curves for monocular cells (figure 4.9a) corroborate the observations already noted in the individual cell examples. The strong adaptation effect on the preferred orientation response elicited by NDE adaptation is clearly demonstrated in both figures 4.9a and b with a significant transfer of 38.35% (2-tailed t-test $P<0.01$). However, the normalised tuning curves in figure 4.10 show that under control conditions, stimulation of the NDE barely evokes a response from these cells. This highlights the fact that the population NDE response is relatively weaker than the NDE adaptation effect. The mean 66.83% reduction after DE adaptation (DE^{red}) and 25.63% reduction after NDE adaptation (NDE^{red}) of the PO response are also significantly different from each other (2 tail paired t-test $P<0.05$).

Test stimulus orientation specificity can be seen in the level of adaptation for both DE and NDE adaptation, with the greatest reduction occurring when the adapting and test stimulus are the same. As the difference between the adapting and test orientation increases, the adaptation effect decreases up to the orthogonal orientations and then increases again up to the non-preferred direction. This stimulus specificity, although

marked, does not produce the high degree of direction specificity that has been reported elsewhere (Hammond *et al* 1985) where attenuation of responses was only found in the same direction as that used to adapt. For instance, as can be seen in figure 4.9b, even NDE adaptation produces a significant reduction in the mean non-preferred direction response (2-tailed t-test $P<0.05$), although far less than that in the PO.

The difference between the mean control NDE responses and size of the elicited adaptive effect in monocular cells is emphasised in the pie charts displayed in figure 4.11. The part of the overall transfer due to NDE adaptation that is greater than the original NDE input is 29.06% and 12.14% for the PO and total response, respectively. This portion cannot be the result of effects generated by supra threshold responses because there is little such activity evoked by NDE stimulation. This means that an alternative explanation involving a different source must be found to account for this result.

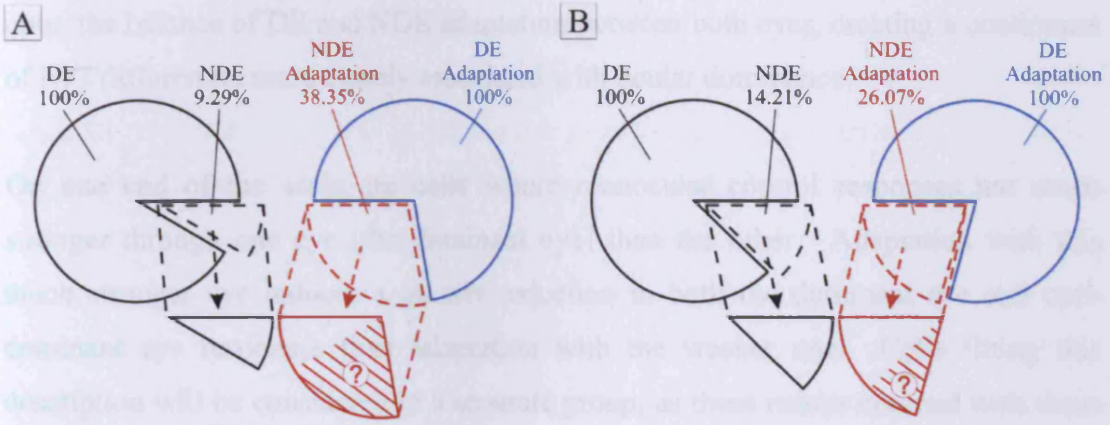

Figure 4.11 - Pie charts that display the discrepancy between the responses evoked by stimulating the non-dominant eye and the level of NDE adaptation. A - Shows the ratio of DE:NDE response for the preferred orientation in the pie chart on the left and the ratio of adaptive effect on the PO response in the red and blue pie chart on the right. There is a large portion of the NDE adaptation that cannot be explained with intrinsic mechanisms of adaptation (shaded region with question mark). B - Shows similar ratios as A, except they are for all the stimulus responses combined rather than just the PO orientation. The unexplained portion is still of significant size, although the effect is diluted by the test stimulus orientation specific nature of adaptation, making it much smaller than when considering the PO alone.

3. Binocular Cells

There were 42 cells included in the binocular group according to the Hubel and Wiesel ocular dominance categories 3, 4 and 5. Five of these cells displayed similar increases in the orthogonal orientation responses to those noted in some monocular cells and will be considered separately. The rest of the cells were organised according to their response characteristics as explained below.

Simplified graphs, clearly showing the OD and adaptation induced reductions of each cell's responses were used to visualise the activity of many cells quickly and efficiently. This type of overview was useful for three reasons. Any erratic or inconsistent results are more easily spotted and discarded, smaller groups of cells with similar adaptive response properties can be recognised and overall patterns emerge that would otherwise go unnoticed. One of the key factors determining IOT is the balance between the inputs of each eye to a cell, and dominance of one over the other. The overview mentioned above was required to achieve a finer categorisation based upon the balance of DE and NDE adaptation between both eyes, creating a continuum of IOT differences more closely associated with ocular dominance.

On one end of the scale are cells where monocular control responses are much stronger through one eye (the dominant eye) than the other. Adaptation with this much stronger eye induces a greater reduction in both the dominant eye and non-dominant eye responses than adaptation with the weaker one. Cells fitting this description will be considered in a separate group, as these results contrast with those findings in the monocular cell section. Also considered in their own right are those cells at the other end of the scale, with perfectly balanced inputs and almost identical control responses for both eyes. This means that regardless of which eye is considered, adapting and testing with the same eye produces a similar reduction in response. When the adapting and test eyes are different in those cells, the resulting effect is also comparable in size between the eyes. The responses from those cells that fall between these two categories were grouped together in order make the link in a sequence of IOT results changing from one to the other. This sequence forms the basis of the trend linking the binocularity of a cell and the IOT displayed by that cell.

The actual boundaries between the groups were chosen fairly subjectively, the more precise aspects of which are outlined below.

4. Binocular Cells Dominated by One Eye

This category contains a total of 13 cells, all of which show much stronger control responses and a greater adaptive affect after stimulation of the dominant eye than after non-dominant eye stimulation. This is reflected quantitatively in the group OD^{ind} with values of 2.37 & 3.48 for area and PO respectively. A good example of a cell that demonstrates the characteristics of this group can be seen in figure 4.12. Adaptation with the DE causes large reductions in the responses to both eyes whereas adapting with the non-dominant left eye only reduces responses in the left eye.

The mean dominant eye responses of cells for this group are shown in figure 4.13a, where it can be clearly seen that the effect of adapting with the DE is larger than that for the NDE. There are no significant changes caused by NDE adaptation in the dominant eye. This lack of NDE adaptation effect in the dominant eye directly contrasts with the monocular cell results and suggests the link between IOT and OD is complex and indirect. The DE adaptation reductions are significant (2-tailed t-test, $P<0.01$) for the total area, and all orientations except -135°.

The summary graph for the non-dominant eye results can be seen in figure 4.13b. The most important point to note is that the level of reduction induced with dominant eye adaptation is greater than that found after adapting with the non-dominant eye. Statistically speaking, the reductions in responses to all orientations after DE adaptation are significant, whereas only the PO and 180° orientations show significant changes after NDE adaptation. However, only the responses to the orthogonal orientations show a significant difference between NDE and DE reductions (2-tailed t-test. $P<0.01$). As expected with such domination of one eye, the level of transfer occurring for DE adaptation is very high, with 78.49% & 98.15% IOT for the PO and total NDE responses, respectively.

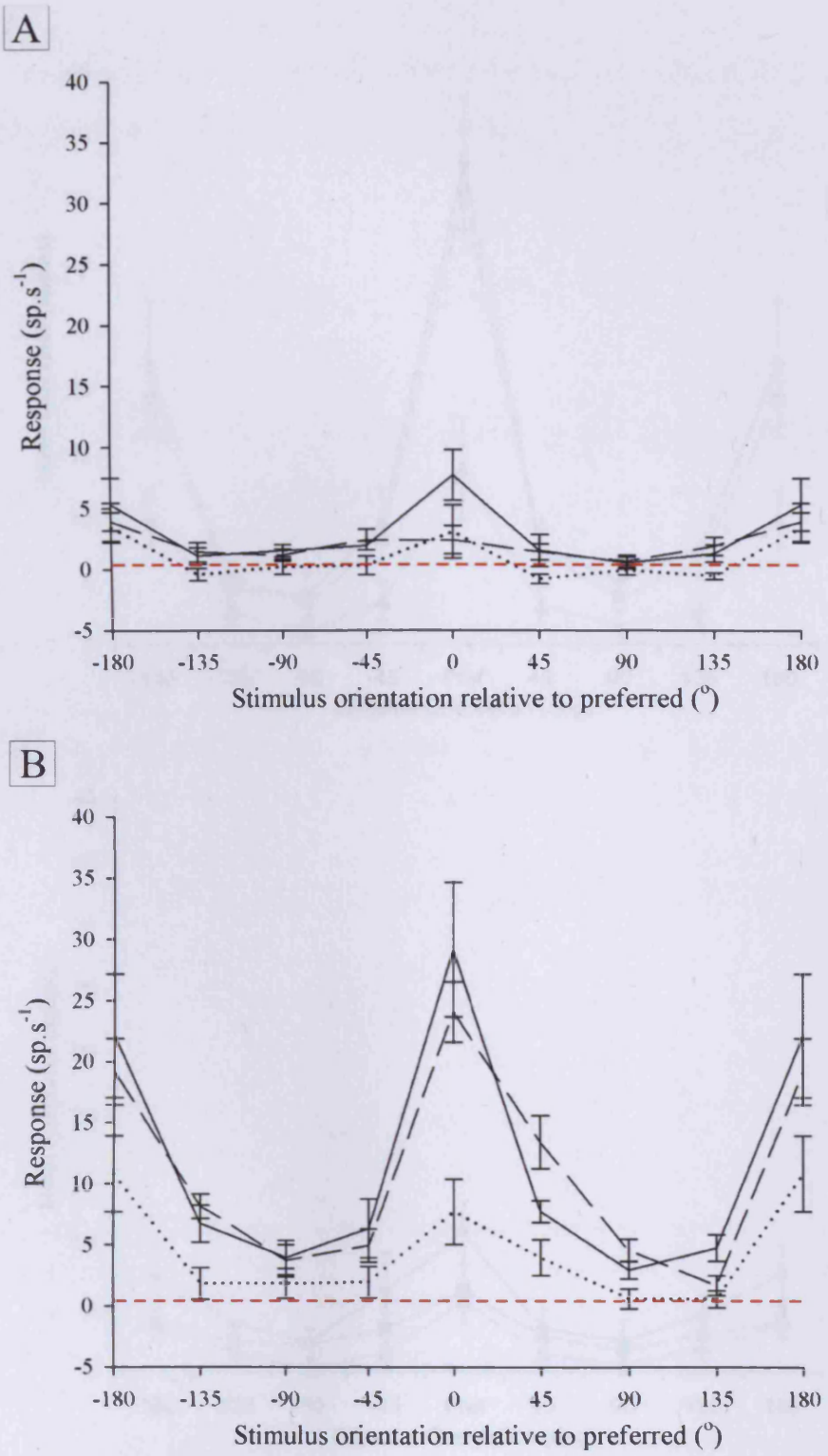

Figure 4.12 - Shows the control (solid lines), LE adapted (dashed lines) and RE adapted (dotted lines) orientation tuning curves for cell 17/12 3'3, which displays the typical characteristics of a binocular cell dominated by one eye. The left eye responses (A) are much lower than the right eye (B) which corresponds with the fact that the NDE adaptive effect in the left eye responses is less than that caused by DE adaptation. Adapting with the dominant eye causes large reductions in both eyes responses (dotted line in both figures). However, adapting with the left eye causes little change in any of the orientation responses to the right eye.

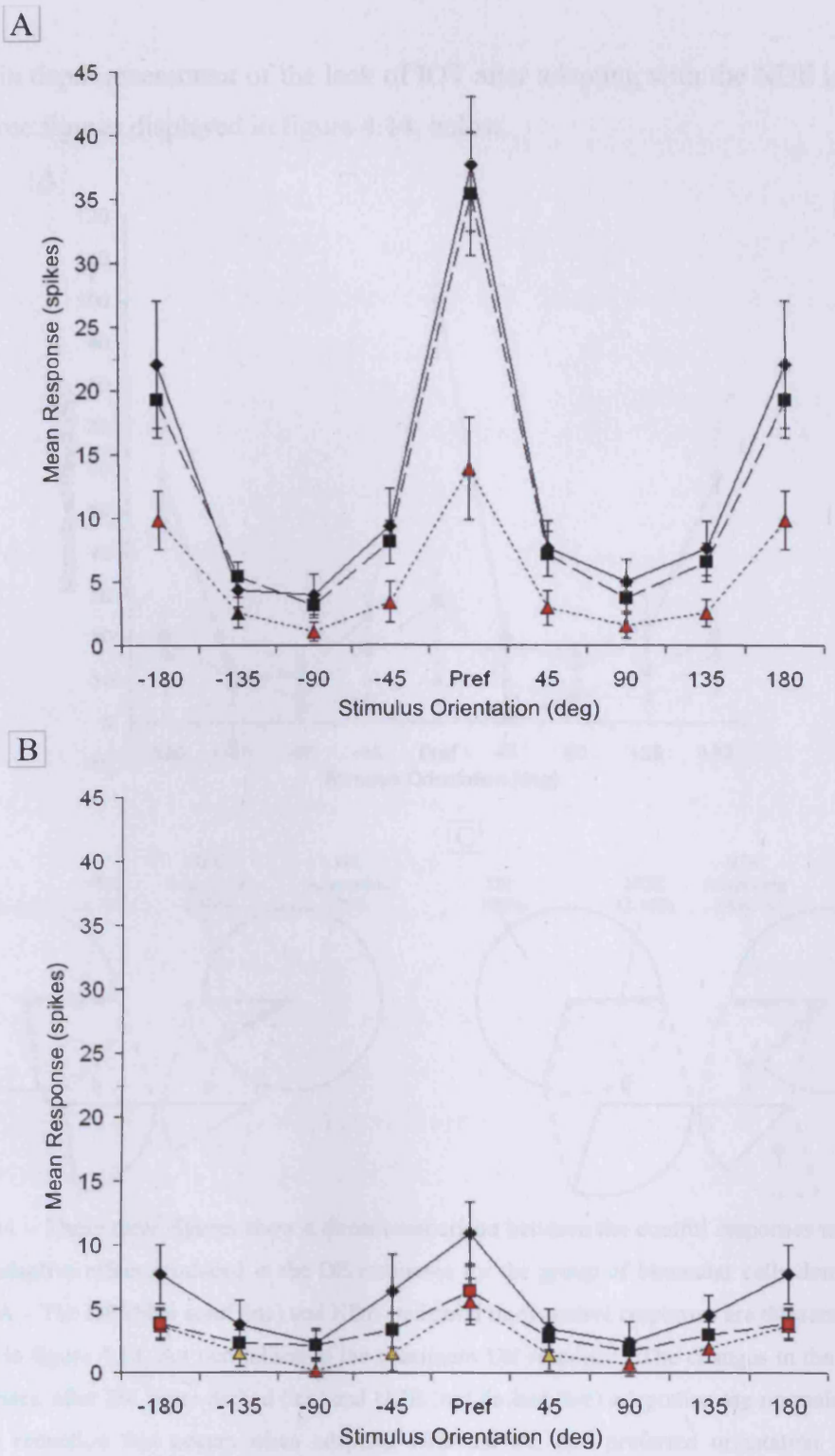

Figure 4.13 - Shows the mean orientation tuning curves for the 13 binocular cells dominated by one eye. The layout is similar to individual cell examples with responses for control (solid lines), dominant eye adapted (short dashed lines) and NDE adapted (long dashed lines) displayed. Coloured symbols designate significant differences between the control and adapted responses (2-tailed paired t-test, red and orange colours indicate $P<0.01$ & $P<0.05$, respectively). A – The dominant eye tuning curves show that after DE adaptation a similar effect is produced on the responses as was noted in the monocular cells. However, adapting with the NDE results in no significant changes. B – The NDE tuning curves show that the effect produced by adapting with the DE is greater than that after NDE, but this difference is only significant for the orthogonally oriented stimuli (2-tailed paired t-test, $P<0.01$).

A more in depth assessment of the lack of IOT after adapting with the NDE is shown in the three figures displayed in figure 4.14, below.

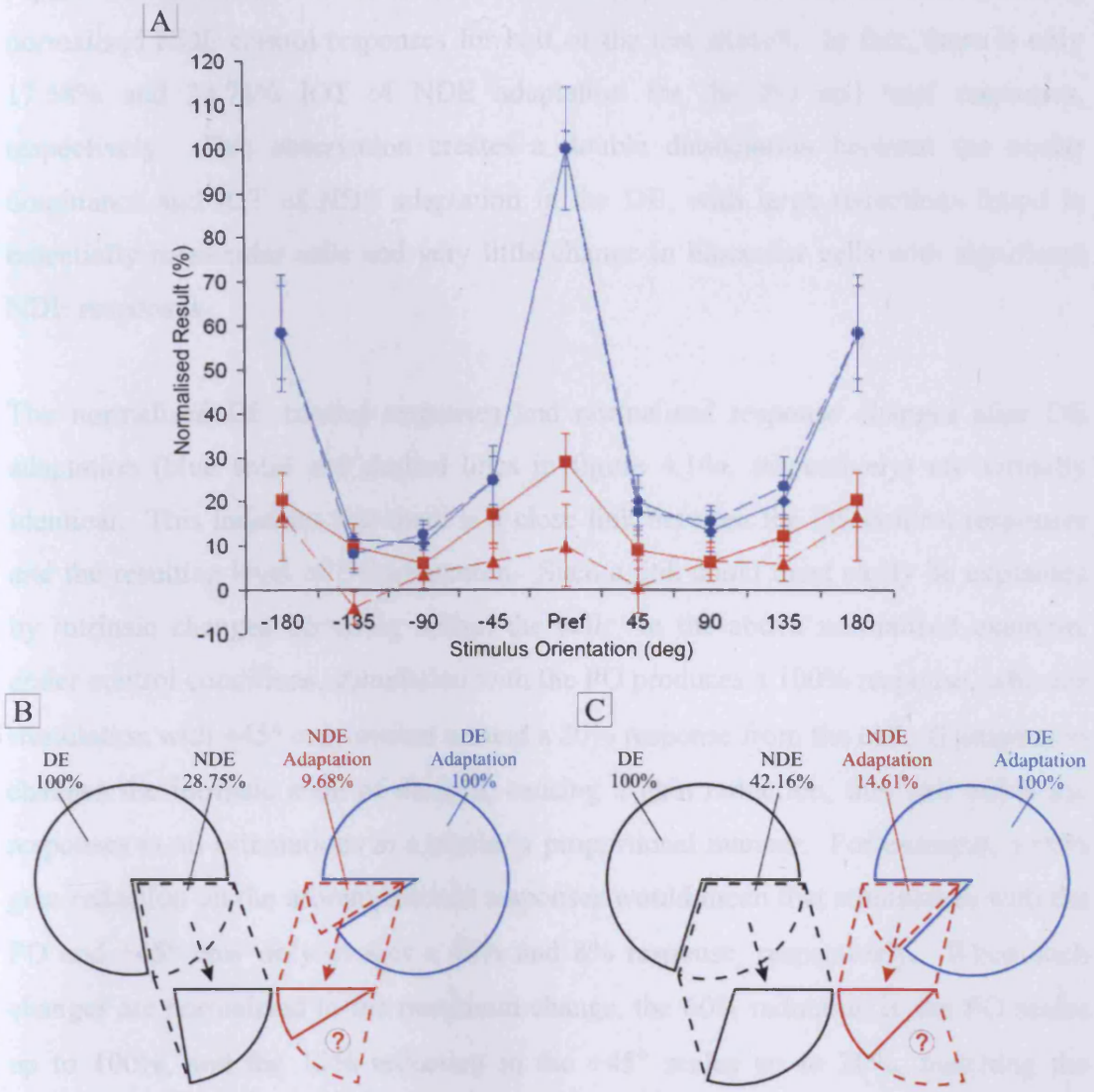

Figure 4.14 – These three figures show a direct comparison between the control responses to each eye with the adaptive effect produced in the DE responses for the group of binocular cells dominated by one eye. A – The DE (blue solid line) and NDE (red solid line) control responses are the same as those displayed in figure 4.13, but normalised to the maximum DE response. The changes in the dominant eye responses, after DE (blue dashed line) and NDE (red dashed line) adaptation are normalised to the maximum reduction that occurs when adapting with the DE and preferred orientation. The DE adaptation effect appears to be directly proportional to the control response elicited by each test stimulus orientation. This is not the case after NDE adaptation, as for half the test stimulus orientations less adaptive effect is produced, when compared with the original NDE responses. B & C – The discrepancy between the NDE control response and adaptive effect is emphasised in these pie charts. The layout and colour scheme is identical to those shown for the monocular results in figure 4.11, with figure B and C relating to the PO and all orientation responses, respectively. A large portion of the control NDE activity in both cases does not produce an equivalent adaptation response, as indicated by the question marked areas bounded by dashed red lines. This creates an opposite scenario to the result observed in monocular cells.

Figure 4.14 shows that the normalised NDE adaptation is less than the corresponding normalised NDE control responses for half of the test stimuli. In fact, there is only 17.58% and 34.74% IOT of NDE adaptation for the PO and total responses, respectively. This observation creates a double dissociation between the ocular dominance and IOT of NDE adaptation in the DE, with large reductions found in essentially monocular cells and very little change in binocular cells with significant NDE responses.

The normalised DE control responses and normalised response changes after DE adaptation (blue solid and dashed lines in figure 4.14a, respectively) are virtually identical. This indicates that there is a close link between the DE control responses and the resulting level of DE adaptation. Such a link could most easily be explained by intrinsic changes occurring within the cell. In the above normalised example, under control conditions, stimulation with the PO produces a 100% response, whereas stimulation with +45° only evokes around a 20% response from the cell. If adaptation changes the intrinsic state of the cell, causing a gain reduction, this will affect the responses to all orientations in a similarly proportional manner. For example, a 60% gain reduction on the aforementioned responses would mean that stimulation with the PO and +45° now only evokes a 40% and 8% response, respectively. When such changes are normalised to the maximum change, the 60% reduction in the PO scales up to 100%, and the 12% reduction in the +45° scales up to 20%, matching the original normalised control responses. And this is what is finally observed in figure 4.14a.

5. Balanced Binocular Cells

A number of cells showed a balance between the left and right eye responses and adaptive effects. The large majority of these cells (10 out of 13) responded equally well to stimulation of either eye and are in ocular dominance category 4. This is reflected in the group mean OD indices of 1.22 and 1.2 for PO and area respectively. An ideal version of this type of binocular cell displays the characteristics required to explain the level of IOT found in the psychophysics investigations.

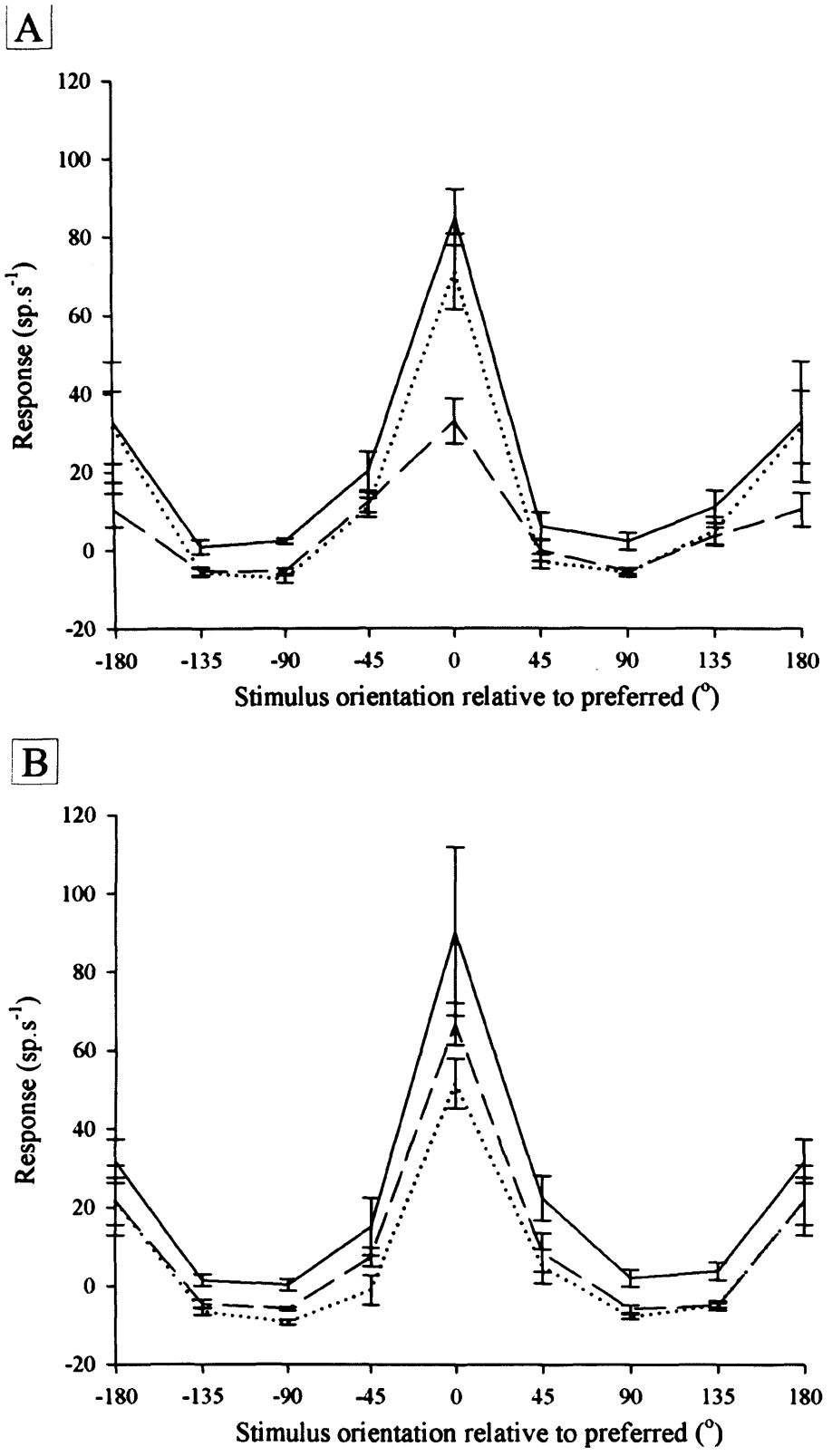

Figure 4.15 - Shows the orientation tuning curves for cell 03/02 4'6, which displays the typical characteristics of a balanced binocular cell. It is immediately obvious that the responses in the different adaptive states are very similar between the two eyes. The area OD^{ind} of 1.04 in favour of the right eye shows how little difference there is between the control responses for left and right eyes. There are only slight differences in the change of individual orientations, with is a large reduction of the NDE, PO after NDE adaptation and little change in the NDE, 180° responses after DE adaptation.

Such a cell receives perfectly balanced inputs from each eye and the resultant level of IOT is identical between the eyes, no matter whether adapting with the DE and testing with the NDE, or vice versa. This similarity between the eyes is also true when adapting with the DE in the dominant eye & the NDE in the non-dominant eye. Consequently, more often than not, in the non-dominant eye the effect of NDE adaptation is greater than that caused by the DE. However, those cells where the DE adaptive effect equals that of the NDE in both eyes are also included in this group.

A typical example of such a cell showing these characteristics is shown in figure 4.15. The OD^{ind} for this cell is 1.04, as the control responses for each eye are virtually identical. Adapting and testing with the same eye produces a similar reduction of 70.92% and 73.48% in the total response for the DE and NDE respectively. When the testing and adapting eyes are different, the total response is reduced by 50.25% in the DE and 39.97% for the NDE. Thus, these quantitative values correspond well with the ideal balanced cell described above. The level of transfer also matches that found in the psychophysics, with 56.36% and 68.38% IOT for DE and NDE adaptation, respectively.

The mean response tuning curves shown in figure 4.16 display the main characteristics already described for the ideal and individual examples of a balanced binocular cell. The only differences between the adaptation effects of the two eyes seem to arise from the closer proximity of the weaker NDE control responses to the spontaneous level of activity. For instance, there is little difference in the NDE responses to all the orientations except the preferred and its opposite direction when adapting with either eye. However, there is a significant difference between adapting with different eyes for half the DE responses (2-tail paired t-test, $P<0.05$). Because the weaker NDE responses are already so low, adapting with the NDE cannot reduce them much further, limiting its effect. Another such subtle difference is that all the DE changes after adapting with the dominant eye are significant (2-tail paired t-test, $P<0.05$) whereas the changes in the NDE orthogonal responses after NDE adaptation are not. This slight threshold effect helps to explain the difference in IOT of the total response with a larger value of 70.46% for NDE adaptation, when compared with only 53.85% for DE adaptation. However, both values correspond well with those recorded in psychophysics investigations (see table 4.1 in this chapters introduction).

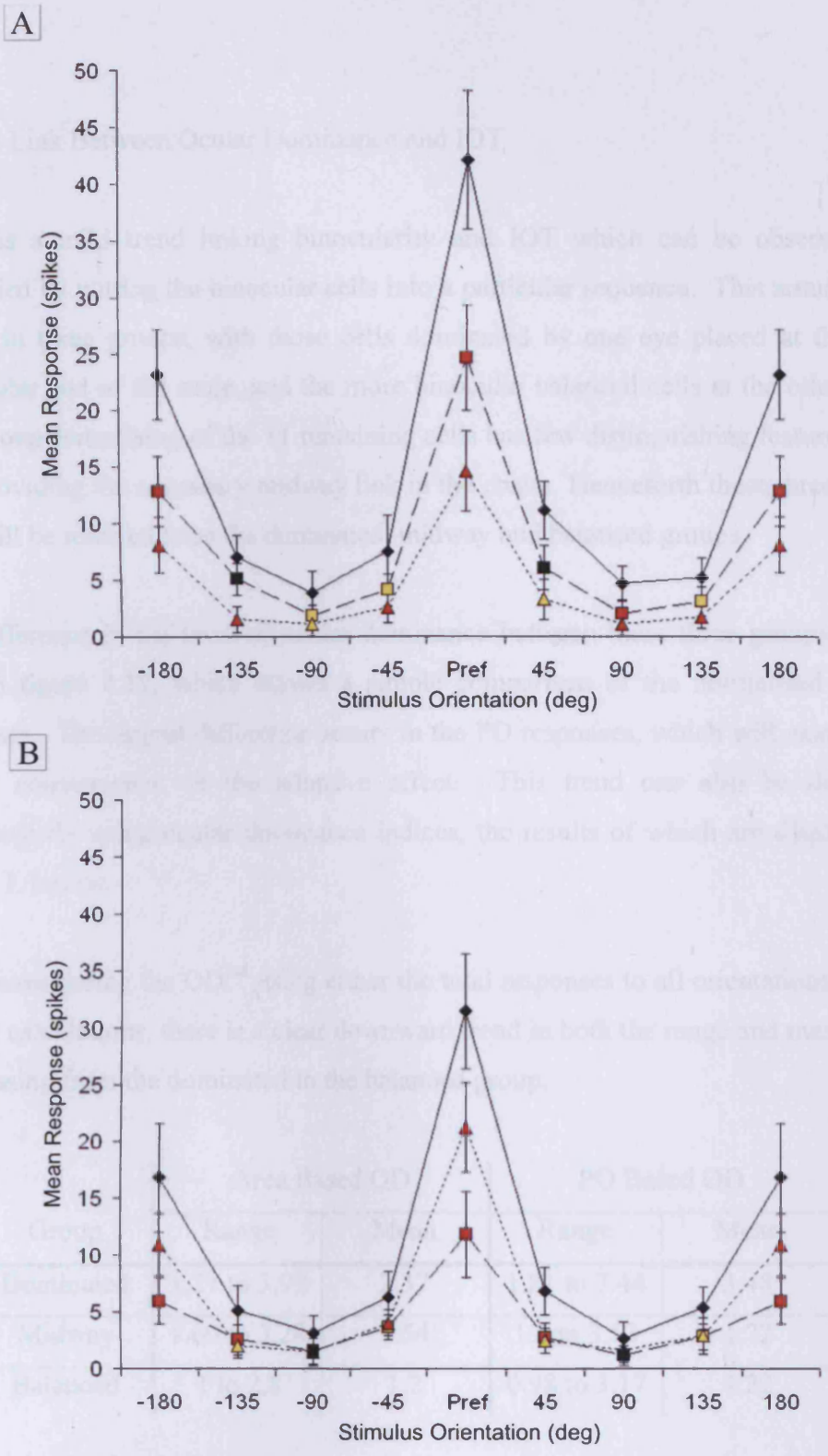

Figure 4.16 - Shows the mean orientation tuning curves for the 13 binocular cells that had balanced responses and adaptation between the eyes. The layout and key is identical to the diagrams shown in figure 4.13. Apart from slightly greater responses to the dominant eye, the control and adapted tuning curves from the two eyes are very similar. A – All test stimulus orientations of the dominant eye show a larger reduction in response after adapting with the DE as compared with the NDE. B – The NDE tuning curves show that there is only a significant difference between the PO and 180° NDE and DE adapted responses (2 tail paired t-test, $P<0.05$).

6. The Link Between Ocular Dominance and IOT

There is a mild trend linking binocularity and IOT which can be observed and quantified by putting the binocular cells into a particular sequence. This arrangement results in three groups, with those cells dominated by one eye placed at the most monocular end of the scale, and the more binocular balanced cells at the other. The final group comprising of the 11 remaining cells has few distinguishing features other than providing the necessary midway link in the chain. Henceforth these three sets of cells will be referred to as the dominated, midway and balanced groups.

The difference in the level of ocular dominance between these three groups can be seen in figure 4.17, which allows a simple comparison of the normalised control responses. The largest difference occurs in the PO responses, which will also have a greater consequence on the adaptive effect. This trend can also be described quantitatively using ocular dominance indices, the results of which are displayed in table 4.1, below.

When considering the OD^{ind} using either the total responses to all orientations, or just the PO calculations, there is a clear downward trend in both the range and mean when progressing from the dominated to the balanced group.

	Area Based OD		PO Based OD	
Group	Range	Mean	Range	Mean
Dominated	1.21 to 3.99	2.37	1.81 to 7.44	3.48
Midway	1.09 to 3.28	1.54	1.2 to 3.53	1.72
Balanced	1 to 2.8	1.2	0.98 to 3.17	1.22

Table 4.1 – Shows the ocular dominance indices for the three groups of cell that form a sequence of increasing binocularity. The area referred to is the total under the control orientation tuning curve for each eye and PO stands for preferred orientation. The greater range and larger OD indices for the PO merely indicate the greater variability of an individual orientation's responses when compared to many.

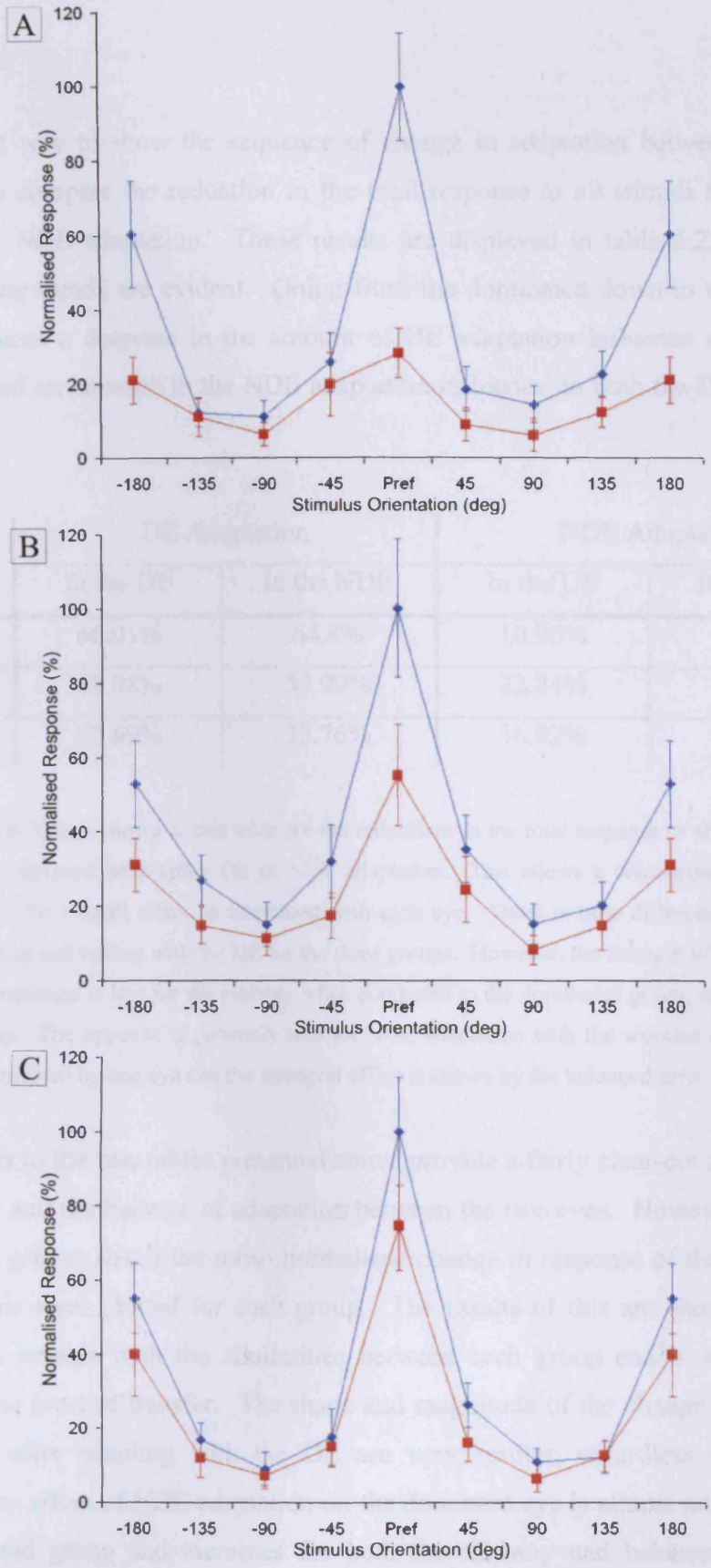

Figure 4.17 - Shows the normalised mean control responses for the dominant eye (blue lines) and non-dominant eye (red lines) for the dominated, midway and balanced groups (A, B and C respectively). The control responses for the dominant eye are very similar between the three groups. However, it can be plainly seen that the non-dominant eye responses are lowest in figure A, larger in B and greatest in figure C in a relatively smooth sequence.

The clearest way to show the sequence of change in adaptation between the three groups is to compare the reduction in the total response to all stimuli for each eye after DE or NDE adaptation. These results are displayed in table 4.2, where two corresponding trends are evident. Going from the dominated down to the balanced group produces a decrease in the amount of DE adaptation influence on the NDE responses and an increase in the NDE adaptation influence on both the DE and NDE responses.

	DE Adaptation		NDE Adaptation	
Group	In the DE	In the NDE	In the DE	In the NDE
Dominated	66.01%	64.8%	10.96%	31.55%
Midway	61.08%	53.99%	22.84%	49.08%
Balanced	62.69%	33.76%	36.92%	52.39%

Table 4.2 – The figures shown in this table are the reductions in the total response to all stimuli of the particular eye indicated after either DE or NDE adaptation. This allows a comparison between the three groups of the overall effect of adaptation with each eye. There is little difference between the effect of adapting and testing with the DE for the three groups. However, the strength of DE adaptation on the NDE responses is less for the midway when compared to the dominated group, and least for the balanced group. The opposite is generally true for NDE adaptation with the weakest effect found in those cells dominated by one eye and the strongest effect is shown by the balanced cells.

The numbers in the two tables presented above provide a fairly clear-cut link between binocularity and the balance of adaptation between the two eyes. However, to assess the trend in greater detail the mean normalised change in response of the orientation tuning curves were plotted for each group. The results of this are shown in figure 4.18, which reveals both the similarities between each group and a more gradual change in the level of transfer. The shape and magnitude of the change in dominant eye curves after adapting with the DE are very similar, regardless of category. However, the affect of NDE adaptation on the dominant eye is almost non-existent in the dominated group and increases for both the midway and balanced groups in similar fashion to the strength of NDE input.

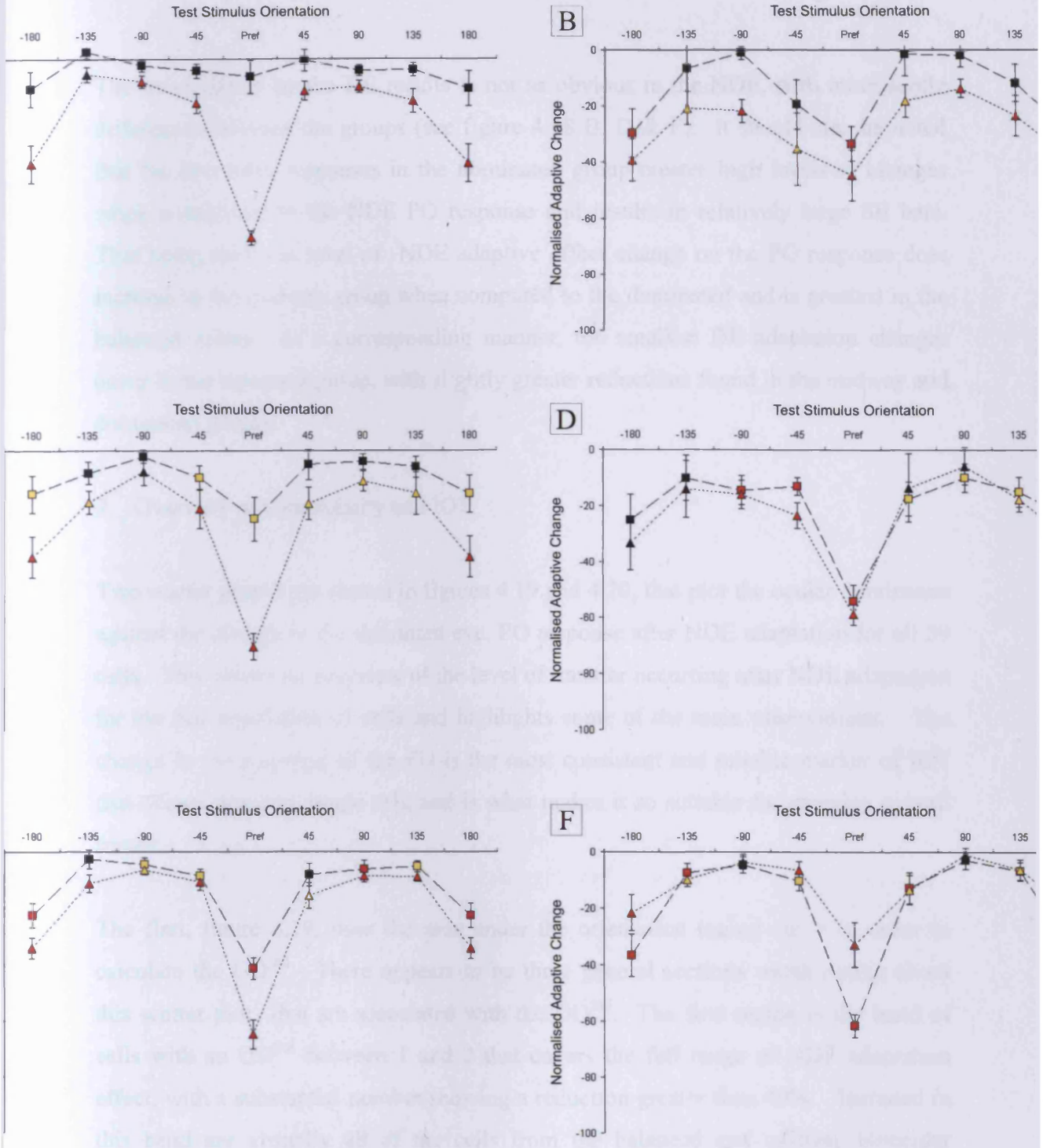

Figure 4.18 - Shows the summary of mean normalised adaptive changes in the dominant eye for the three main binocular cell groups. The graphs in the left column (A, C & E) represent the dominant eye and those in the right column (B, D & F), the non-dominant eye. The three groups are displayed according to the three rows with the dominated pair at the top (A&B), the midway pair in the middle (C&D) and the balanced pair at the bottom (E & F). All short dashed lines show the DE adaptive effect and all the long dashed lines show the NDE adaptive effect. In a similar fashion to the previous summary tuning curves, coloured symbols designate significant differences between the control and adapted response (2-tailed paired t-test, red and orange colours indicate $P<0.01$ & $P<0.05$, respectively).

The trend shown by the DE results is not as obvious in the NDE, with more subtle differences between the groups (see figure 4.18 B, D & F). It should also be noted that the low NDE responses in the dominated group creates high levels of changes when normalised to the NDE PO response and results in relatively large SE bars. That being said, the level of NDE adaptive effect change on the PO response does increase in the midway group when compared to the dominated and is greatest in the balanced group. In a corresponding manner, the smallest DE adaptation changes occur in the balanced group, with slightly greater reductions found in the midway and dominated groups.

7. Overview of Binocularity and IOT

Two scatter graphs are shown in figures 4.19 and 4.20, that plot the ocular dominance against the change in the dominant eye, PO response after NDE adaptation for all 59 cells. This allows an overview of the level of transfer occurring after NDE adaptation for the full population of cells and highlights some of the main observations. The change in the response of the PO is the most consistent and reliable marker of IOT that occurs in every single cell, and is what makes it so suitable for showing overall trends.

The first, figure 4.19, uses the area under the orientation tuning curve in order to calculate the OD^{ind}. There appears to be three general sections worth noting about this scatter plot that are associated with the OD^{ind}. The first region is the band of cells with an OD^{ind} between 1 and 2 that covers the full range of NDE adaptation effect, with a substantial number showing a reduction greater than 40%. Included in this band are virtually all of the cells from the balanced and midway binocular groupings. The second area is for those cells with an OD^{ind} between 2 and 4, which has a reduced range of NDE adaptation effect and virtually no reductions greater than 40%. This region contains the majority of the cells found within the dominated binocular category. Clearly, there are a number of highly binocular cells that do not undergo any change in the PO response after NDE adaptation. The third section is for those more monocular cells with an OD^{ind} of around 4 and over. The level of NDE adaptation in these cells appears to bear little relation to their OD.

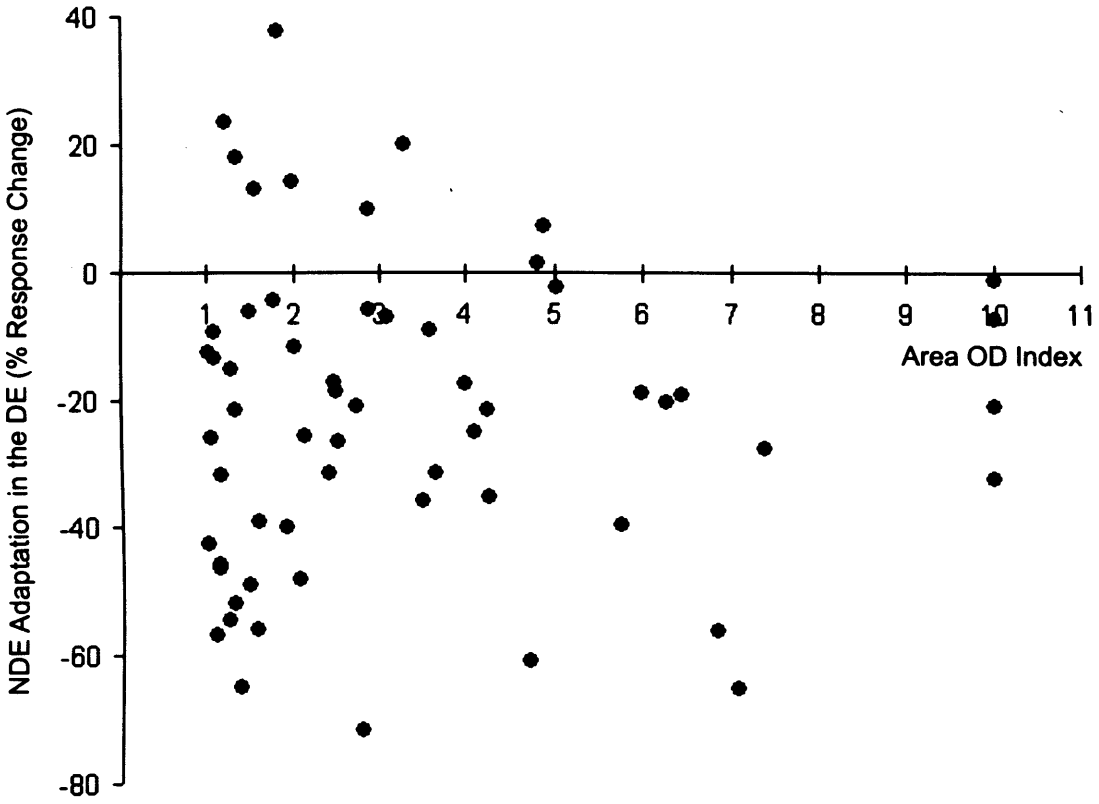

Figure 4.19 – Shows the link between ocular dominance and the transfer of NDE adaptation over to the dominant eye. The normalised change in the PO responses is used to represent the NDE adaptation effect. The OD^{ind} was calculated by dividing the total area under the control orientation tuning curve for the DE by the that for the NDE. Using the DE and NDE rather than the LE and RE allows a direct comparison between the cells to be made. As the ocular dominance increases, and therefore the DE response becomes larger relative to the NDE the likelihood of a large level of NDE adaptation transfer decreases. This is only a mild trend that appears to hold true as the OD^{ind} increases from 1 up to 5. However, at one end of the OD scale there are binocular cells that don't display any change after NDE adaptation and at the other end are those monocular cells that do show significant reductions. Both these factors dilute the strength of the aforementioned trend linking OD and IOT.

The second scatter plot (figure 4.20), utilises the responses to the PO to calculate the OD rather than the full area. Although this may not yield an accurate quantitative description of the full binocularity of a cell it could arguably be more relevant as it is the PO stimuli that are used to induce adaptation. Whatever the case, ocular dominance indices calculated this way are an the whole larger, and result in a greater range of cell binocularity. There aren't three particular regions to this plot as seen in figure 4.19, but more of a gradual reduction in the NDE adaptation effect in the DE as the OD^{ind} increases from 1 up to around 6. There also appears to be a separate group

of monocular cells, with an OD^{ind} greater than 7, many of which show large changes in the dominant eye PO response after adaptation with the NDE.

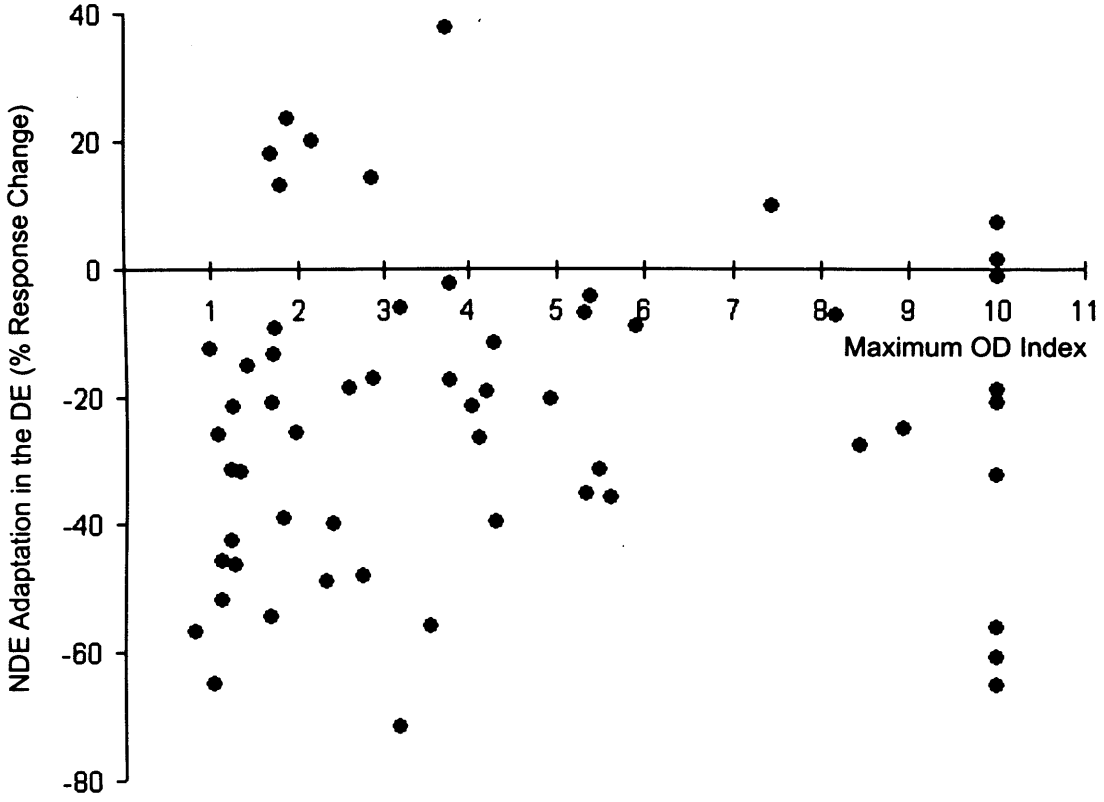

Figure 4.20 – Shows a similar scatter plot to that shown in figure 4.19, except that the OD^{ind} was calculated by dividing the control PO response for the DE by that for the NDE. Due to the nature of the calculation, some of the monocular cells that have very low NDE responses end up with unrealistically large OD indices. To compensate for this, the OD^{ind} range was curtailed and overly large indices renumbered with a maximum figure of 10. The trend linking an increase in OD with a decrease in NDE adaptation in the DE is actually more prominent in this figure, showing a more gradual change that extends over the full OD range. This plot also highlights eight monocular cells that have an OD^{ind} greater than 8 and distinct reductions after NDE adaptation.

8. Cells Displaying Orthogonal Increases

Approximately 17% of the cells (10 of 59) show an increase in dominant eye responses to orthogonal orientations after adapting with the non-dominant eye. This was noticed after attempting to do an *a priori* categorisation in order to separate cells based upon a comparison of the original control responses ocular dominance index.

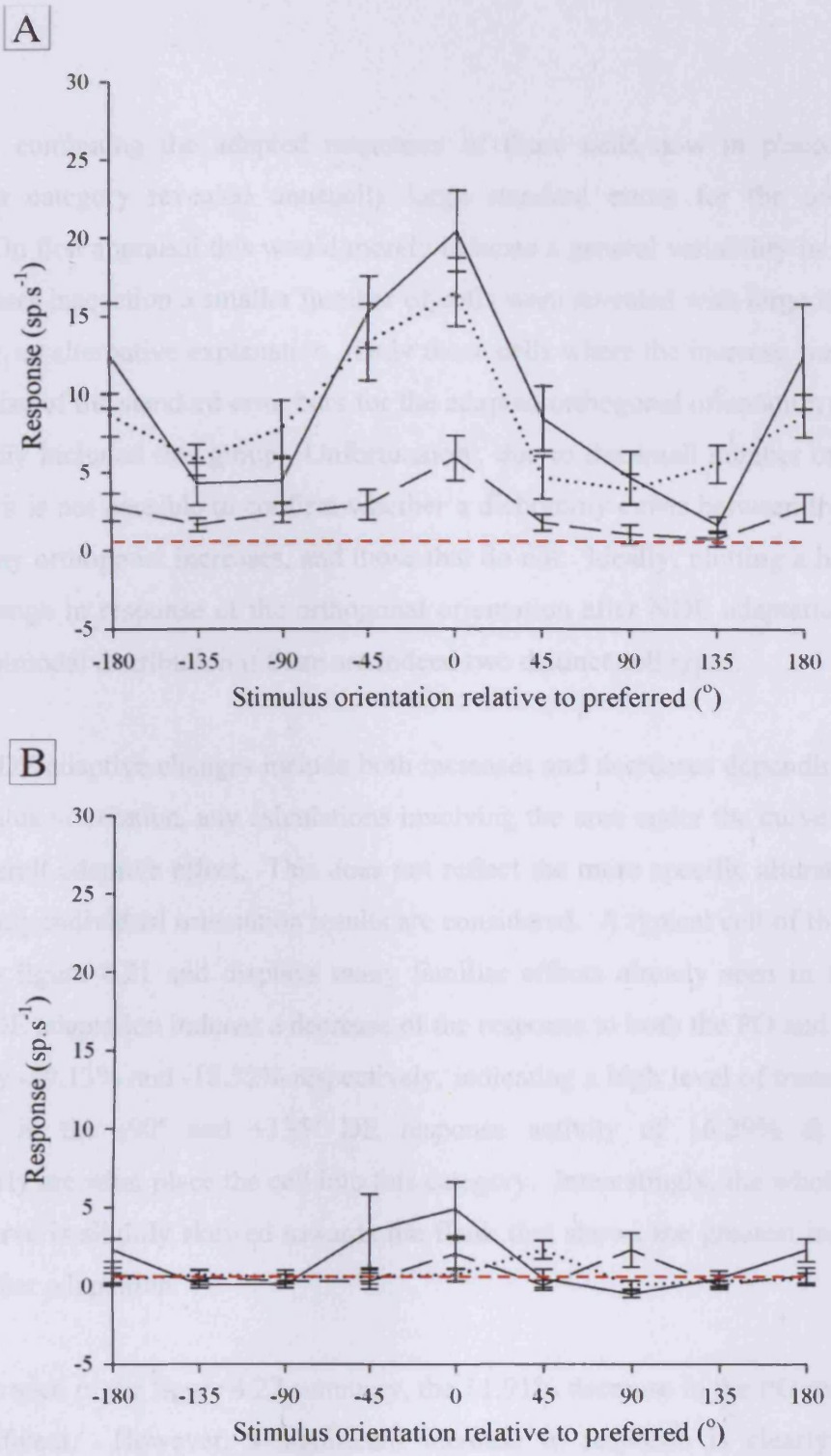

Figure 4.21 - Shows the control (solid lines), LE adapted (dashed lines) and RE adapted (dotted lines) orientation tuning curves for the monocular cell 23/07 2a, a typical example of response increases after NDE adaptation. The red dashed lines indicate the standard error associated with spontaneous activity. A - Adapting with both the left and right eye produces decreases in activity for the PO and 180°, although this effect is less prominent than that seen in other monocular cells. The important factor is that increases are observed in the responses to orientations near to and/or for the orthogonal, after adapting through the right eye (the NDE). B - For the sake of completeness, the non-preferred right eye responses are shown, although after adapting with either eye there is virtually no response evoked for any orientation.

However, combining the adapted responses of those cells now in placed in the monocular category revealed unusually large standard errors for the orthogonal stimuli. On first appraisal this would merely indicate a general variability in the data, but on closer inspection a smaller number of cells were revealed with large increases, providing an alternative explanation. Only those cells where the increase was greater than the size of the standard error bars for the adapted orthogonal orientation response were finally included this group. Unfortunately, due to the small number of cells in question, it is not possible to confirm whether a dichotomy exists between those cells that display orthogonal increases, and those that do not. Ideally, plotting a histogram of the change in response of the orthogonal orientation after NDE adaptation would reveal a bimodal distribution if there are indeed two distinct cell types.

As the NDE adaptive changes include both increases and decreases depending on the test stimulus orientation, any calculations involving the area under the curve result in a low overall adaptive effect. This does not reflect the more specific alterations and as such only individual orientation results are considered. A typical cell of this type is shown in figure 4.21 and displays many familiar effects already seen in the other cells. NDE adaptation induces a decrease of the response to both the PO and 180° DE stimuli by -19.13% and -18.52% respectively, indicating a high level of transfer. The increases in the -90° and +135° DE response activity of 16.29% & 18.98% respectively are what place the cell into this category. Interestingly, the whole control tuning curve is slightly skewed towards the flank that shows the greatest increase in activity after adaptation.

As can be seen in the figure 4.22 summary, the 11.91% decrease in the PO response is not significant. However, a significant increase in response is clearly seen at orthogonal orientations after NDE adaptation, producing changes of +13.55% & +10.05% for -90° and +90° respectively (2-tail paired t-test $P<0.05$). These increases appear to bear no relation to the original control NDE response to the orthogonal orientation. Although there are clear responses to NDE stimulation under control conditions (see red curve in figure 4.22b), the inclusion of so many monocular cells in this group resulted in unreliable adapted NDE responses with large standard errors.

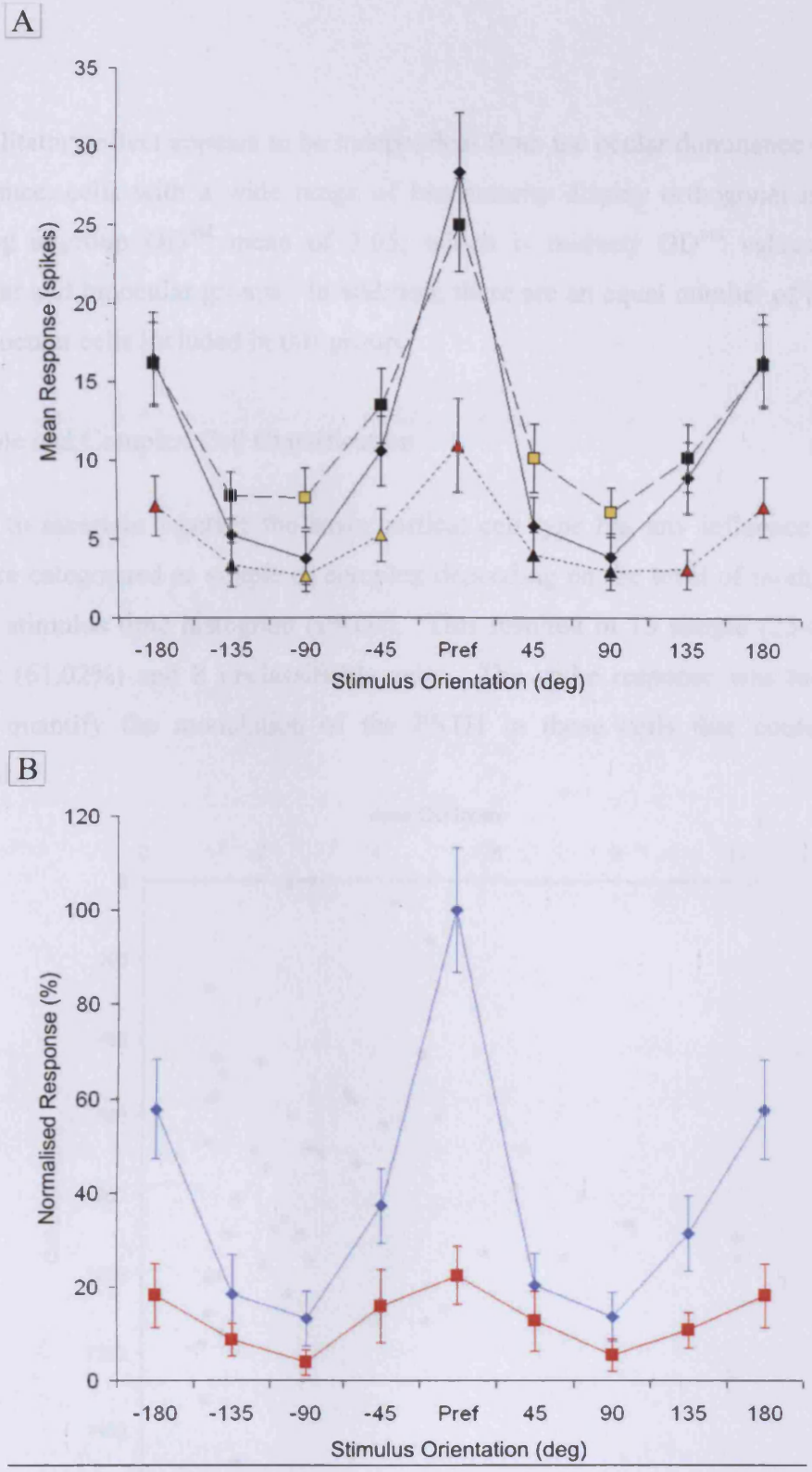

Figure 4.22 – Shows summary orientation tuning curves for the group of cells that displayed increases in orthogonally oriented stimulus responses after adaptation with the NDE. A - Mean orientation tuning curve for the control (solid line), NDE adapted (long dashed line) and the DE adapted (short dashed line) states. Coloured symbols designate significant differences between the control and adapted responses (2-tailed paired t-test, red and yellow colours indicate $P<0.01$ & $P<0.05$, respectively). B - Shows the mean control responses for the dominant eye (blue lines) and non-dominant eye (red lines) normalised to the maximal DE control response.

This facilitatory effect appears to be independent from the ocular dominance of a cell. For instance, cells with a wide range of binocularity display orthogonal increases, producing a group OD^{ind} mean of 3.05, which is midway OD^{ind} values for the monocular and binocular groups. In addition, there are an equal number of binocular and monocular cells included in this group.

9. Simple and Complex Cell Classification

In order to ascertain whether the basic cortical cell type has any influence on IOT, cells were categorised as simple or complex depending on the level of modulation in the post stimulus time histogram (PSTH). This resulted in 15 simple (25.42%), 36 complex (61.02%) and 8 unclassifiable cells. The spike response was too low to reliably quantify the modulation of the PSTH in those cells that could not be classified.

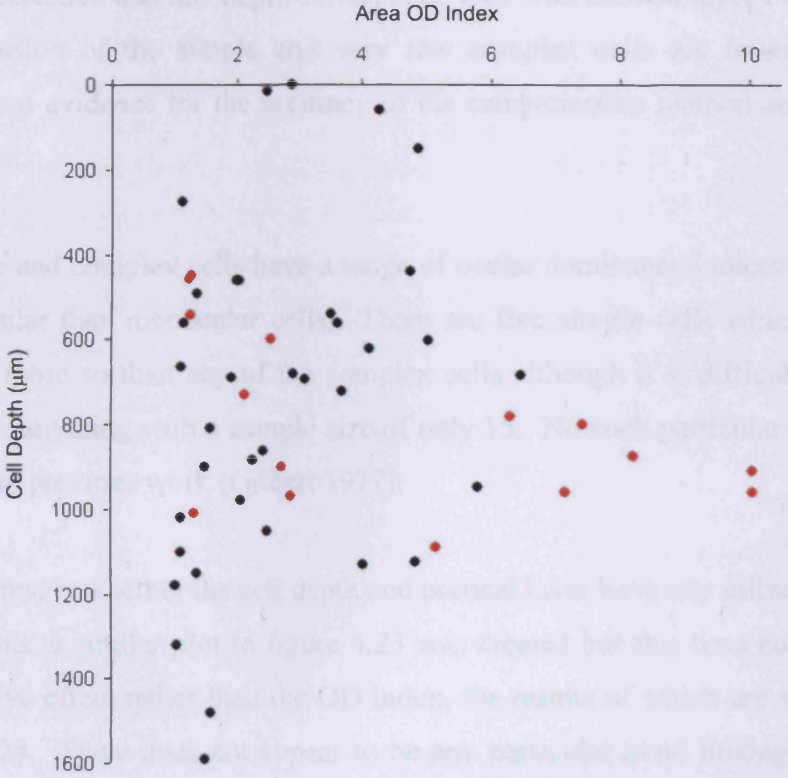

Figure 4.23 – Shows the depth from the cortical surface from which simple cells (red dots) and complex cells (black dots) were recorded, and their associated ocular dominance index. Around half the simple cells are monocular (7 out of 15), and the majority were recorded from a depth between 800µm and 1000µm. On the other hand, complex cells are mainly found in a greater range between a depth of 400µm and 1200µm. There is also a narrow strip around 800µm where fewer complex cells are located, that could correspond to the upper potion of cortical layer IV.

The scatter plot in figure 4.23 shows the distribution of simple and complex cells throughout the cortex. A quick qualification of the cell depth measurement is worth noting. The positioning system used for these experiments can only provide a precise measurement of the distance between the cortical surface and the tip of the electrode. Histological preparations to show the path of the electrode advancement are required to directly ascertain in which cortical layer a cell is situated. That being said, the positions of simple and complex cells recorded in this work are in general agreement with those noted in previous studies. Simple cells are found in layer VI and predominate in layer IV of the cortex whereas complex cells are located throughout cortical layers II, III, V and VI, with a general scarcity in layer IV (Hubel and Wiesel 1962, Gilbert 1977). It can be seen in figure 4.23 that the majority of simple cells are found in a fairly narrow band that covers depths from 800μm to 1000μm and that there is also a lack of complex cells at a depth of around 800μm. From this, it can be indirectly presumed that this depth corresponds well with cortical layer IV, in which a large proportion of the simple and very few complex cells are found. This also provides good evidence for the accuracy of the categorisation method and cell depth measurement.

Both simple and complex cells have a range of ocular dominance indices with overall more binocular than monocular cells. There are five simple cells which are highly monocular, more so than any of the complex cells although it is difficult to know if this signifies anything with a sample size of only 15. No such particular OD bias has been noted in previous work (Gilbert 1977).

Also of interest is whether the cell depth and cortical layer have any influence on IOT. To assess this, a similar plot to figure 4.23 was created but this time concerning the NDE adaptive effect rather than the OD index, the results of which are shown below in figure 4.24. There does not appear to be any particular trend linking the level of NDE adaptation in the DE with the recording depth or by implication, a particular cortical layer. In other words, no matter how deep a cell is located the likelihood of adaptation with the NDE having a strong or weak effect is similar. There is no difference between simple and complex cells in this particular criterion.

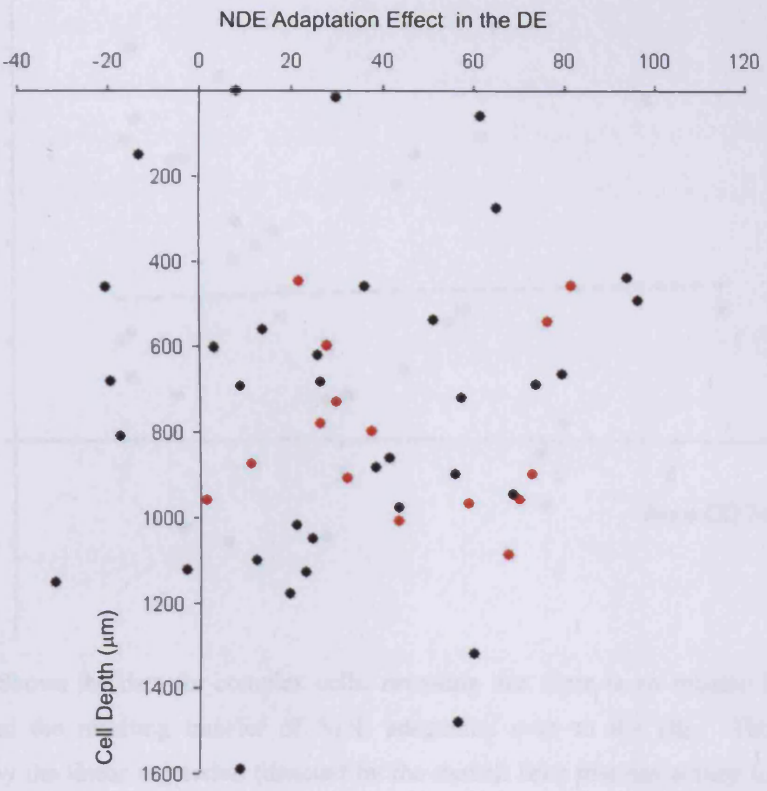

Figure 4.24 – This figure shows the same cells and depth information as that found in figure 4.23, but this time plotted against the NDE adaptation effect. The NDE adaptation effect is calculated by dividing the NDE adapted response change to the PO with that recorded after DE adaptation. As the change in the dominant eye PO response after DE adaptation is one of the most consistent measurements of adaptation, this calculation provides a good comparative measure of NDE adaptation between cells. For the range of depths where the majority of the cells are found (between 400µm and 1200µm), there is no discerning difference in the range of NDE adaptive effects. This holds true for both simple (red dots) and complex (black dots) cell types.

A mild trend linking the ocular dominance for a cell with the resulting level of IOT has already been observed for the full population of cells. The question of whether or not this trend is specific to simple or complex cells is addressed in figures 4.25 and 4.26. It turns out that there is indeed a difference between the two cell types concerning this relation, with no connection found in the complex cell group and clear link observed with the simple cells. As can be seen in figure 4.25, the trend line associated with the complex cell scatter plot is essentially flat, and a Pearson r value of 0.02 indicates that the OD and NDE adaptation effect have no influence on each other.

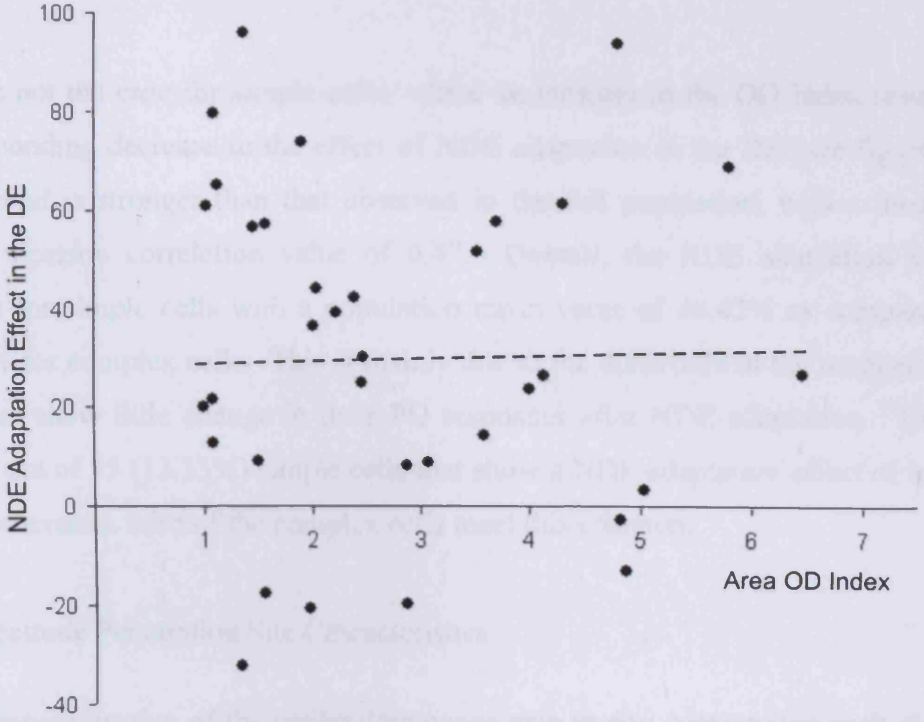

Figure 4.25 – Shows the data for complex cells, revealing that there is no relation between a cells binocularity and the resulting transfer of NDE adaptation over to the DE. This is confirmed quantitatively by the linear regression (denoted by the dashed line) that has a very low gradient and Pearson correlation value of 0.54 and 0.02, respectively. There are also a number of cells, both binocular and monocular, that show a NDE adaptation effect of less than 20%. The NDE adaptation effect is identical to that used in figure 4.24, and calculated in the same manner.

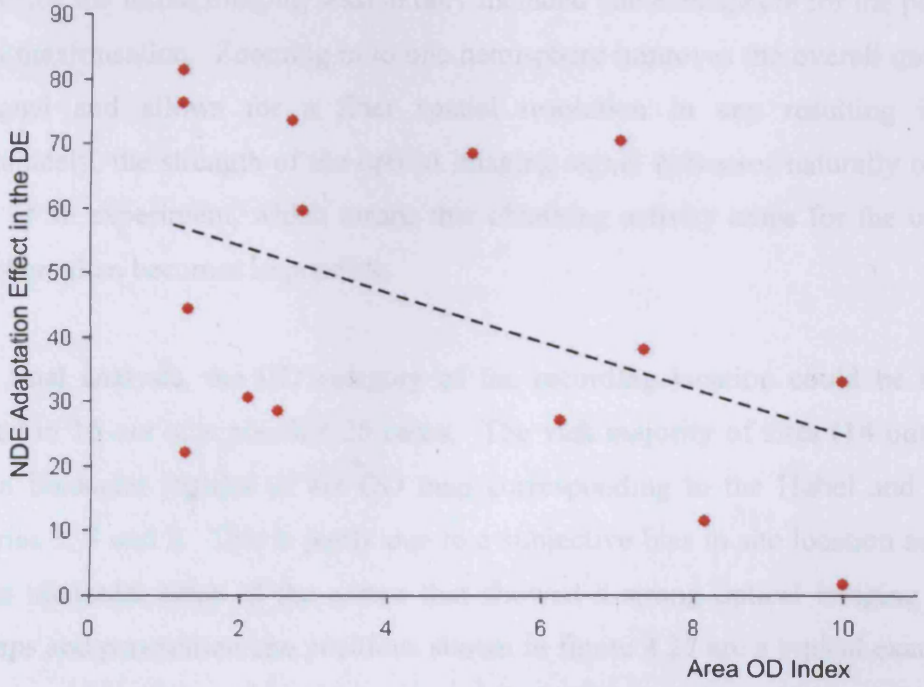

Figure 4.26 - In contrast to the complex cells, the data for simple cells shows a negative relation between a cells binocularity and the resulting transfer of NDE adaptation over to the DE. The linear regression of this trend produces gradient and Pearson correlation values of –3.66 and 0.47, respectively. The NDE adaptation effect is identical to that used in figure 4.24 and 4.25, and calculated in the same manner.

This is not the case for simple cells, where an increase in the OD index results in a corresponding decrease in the effect of NDE adaptation in the DE (see figure 4.26). This trend is stronger than that observed in the full population, with a moderately strong Pearson correlation value of 0.47. Overall, the NDE adaptation effect is greater for simple cells with a population mean value of 45.42% as compared with 29.64% for complex cells. This is mainly due to the difference in the number of cells that that show little change in their PO responses after NDE adaptation. There are only 2 out of 15 (13.33%) simple cells that show a NDE adaptation effect of less than 20%, whereas a third of the complex cells meet this criterion.

10. Electrode Penetration Site Characteristics

The characterisation of the ocular dominance map region surrounding each electrode penetration site yielded rather inconclusive results. Not all the electrode sites from which cells were recorded could be included in the analysis because sometimes the optical imaging signal strength was too weak for accurate quantification. Additionally, certain recordings were performed from the opposite hemisphere to that which was imaged, and as such no OD maps were available to analyse. This would occur when the initial imaging session only included one hemisphere for the purposes of data maximisation. Zooming in to one hemisphere improves the overall quality of the signal and allows for a finer spatial resolution in any resulting images. Unfortunately, the strength of the optical imaging signal decreases naturally over the course of an experiment, which means that obtaining activity maps for the opposite hemisphere then becomes impossible.

In the final analysis, the OD category of the recording location could be reliably assigned in 16 out of a possible 25 cases. The vast majority of sites (14 out of 16) were in binocular regions of the OD map corresponding to the Hubel and Wiesel categories 3, 4 and 5. This is partly due to a subjective bias in site location selection towards binocular areas of the cortex that showed a strong optical imaging signal. The maps and penetration site positions shown in figure 4.27 are a typical example of this, and a good representation of those used throughout this investigation. However, even without any such site location bias a smaller number of monocular sites would be expected due to the largely binocular nature of the adult cat primary visual cortex.

In order to obtain a more 'balanced' selection of sites covering the full range of binocularity, an active selection of monocular regions would have to be implemented.

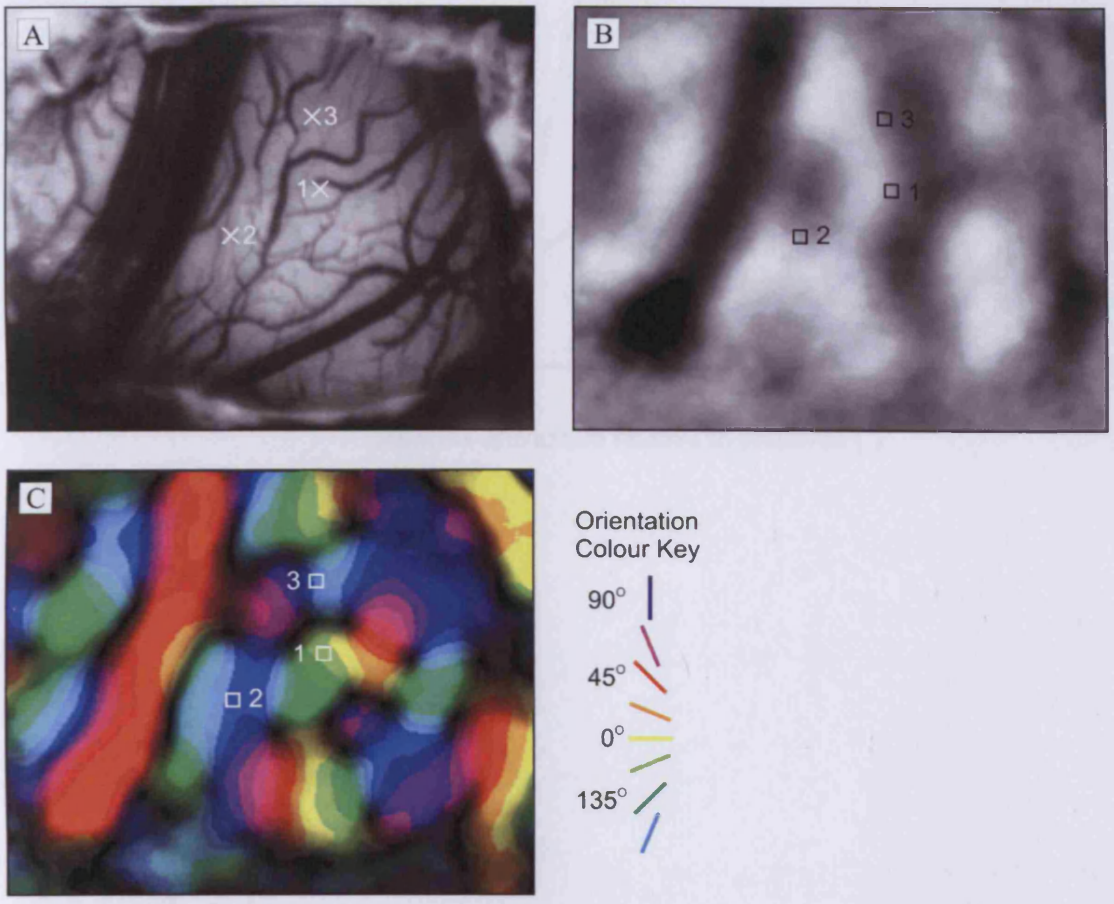

Figure 4.27 – Shows the blood vessel image (A), OD map (B) and angle map (C) recorded during an optical imaging session in cat 011904. The positions of the three recording sites chosen for the subsequent extracellular recording of IOT are shown on each of the three images. As was typical for most of the experiments, binocular regions in the centre of iso-orientation domains with a strong optical imaging signal were selected as optimal positions for penetrations. The chosen locations were then overlaid onto the blood vessel map, which could then be used to position the electrode whilst viewing the cortical surface through a binocular microscope. The square outlines in the OD map in figure B denote the region over which the greyscale values were averaged in order to obtain an OD category of the area surrounding each penetration site. The mean greyscale value for each site is 134.53, 160.82 and 113.49 for sites 1, 2 and 3 respectively. These values correspond to the Hubel and Wiesel ocular dominance categories 4, 5 and 4 respectively.

In order to complement the images shown above for the experiment performed on cat 011904 the tuning curves of a cell recorded from the third penetration site is shown in figure 4.28.

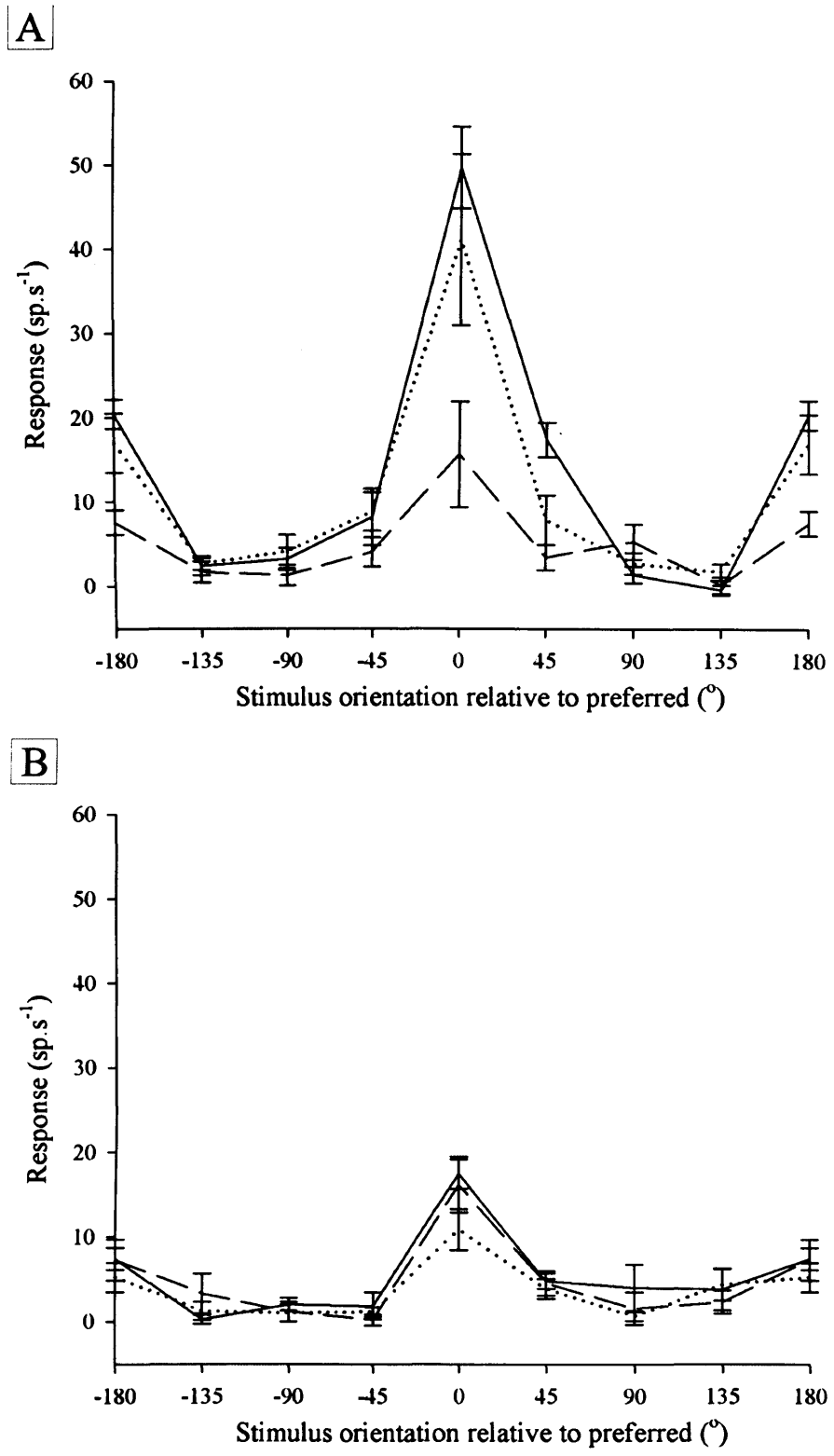

Figure 4.28 – Shows the left eye (A) and right eye (B) orientation tuning curves for a cell recorded from the third penetration in cat 011904. The dashed lines denote left eye adapted responses and the dotted lines show responses after right eye adaptation. This cell has an area OD index of 2.47 and was thus placed in the binocular group of cells dominated by one eye. The left eye dominance of this cell matches the slight bias towards the left eye of the penetration site with its mean OD greyscale value of 113.49. The level of IOT occurring in the PO response was 10% and 45% for DE and NDE adaptation, respectively. This relatively low level of transfer was typical of the complex cells dominated by one eye.

There is a good correspondence between the OD category of a penetration site and the binocularity of the cells recorded from within it. This is shown in figure 4.29, where it can be seen that cells recorded from the monocular sites of category 1 and 2 tend to have a higher OD index than those recorded from the binocular sites of category 3, 4 and 5. This shows that the position of a cell in the cortical map does have a bearing on its control response characteristics, as one would expect.

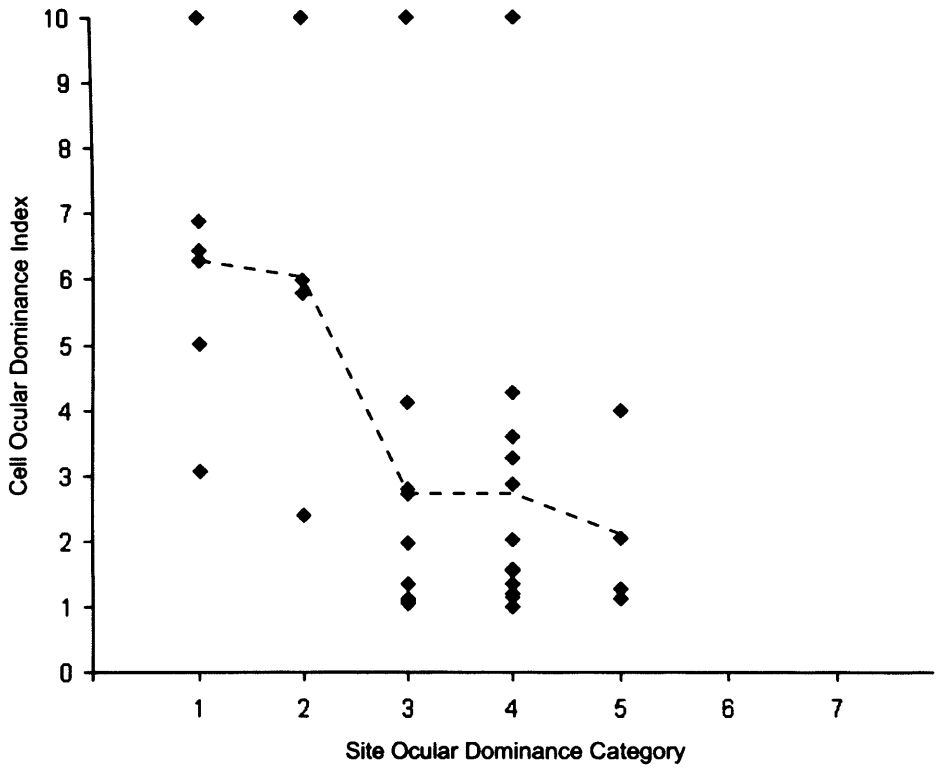

Figure 4.29 – Shows that there is a fairly good correspondence between the ocular dominance of cells recorded from a penetration site and its OD category. The dashed line links the mean ocular dominance for the group of cells recorded from the site/s in each particular OD category. Due to the bias towards binocular recording sites, there was only one recording location to represent each of the OD categories 1 and 2, with none to represent categories 6 and 7. Presumably, if the full range of site binocularity were represented then the shape of the dashed line would be a U shape as the OD index rises again for the right eye monocular categories 6 and 7.

However, it is difficult to state definitively whether the position of a cell in the OD map influences the level of IOT. Figure 4.30 shows the same layout of penetration site ocular dominance categories as figure 4.29, but shows the level of NDE adaptation in the DE of a cell instead of the OD index. A low level of NDE adaptive effect is found for those cells recorded from the site placed in the most monocular

category. This NDE adaptive effect increases for those cells taken from the site with OD category 2, as the strength of the NDE influence increases. However, this trend does not continue for the sites from more binocular regions of the cortex. Instead, a greater range of NDE adaptive effect is found for those cells taken from sites with the ocular dominance categories 3 and 4. It is difficult to know if this is related to the location within the OD map or if it is merely because there were a lot more binocular sites. A larger number of sites and associated cells will naturally have a larger range even if pulled randomly from the total population. Thus, the final result is rather inconclusive, with more data required to make any definitive statements.

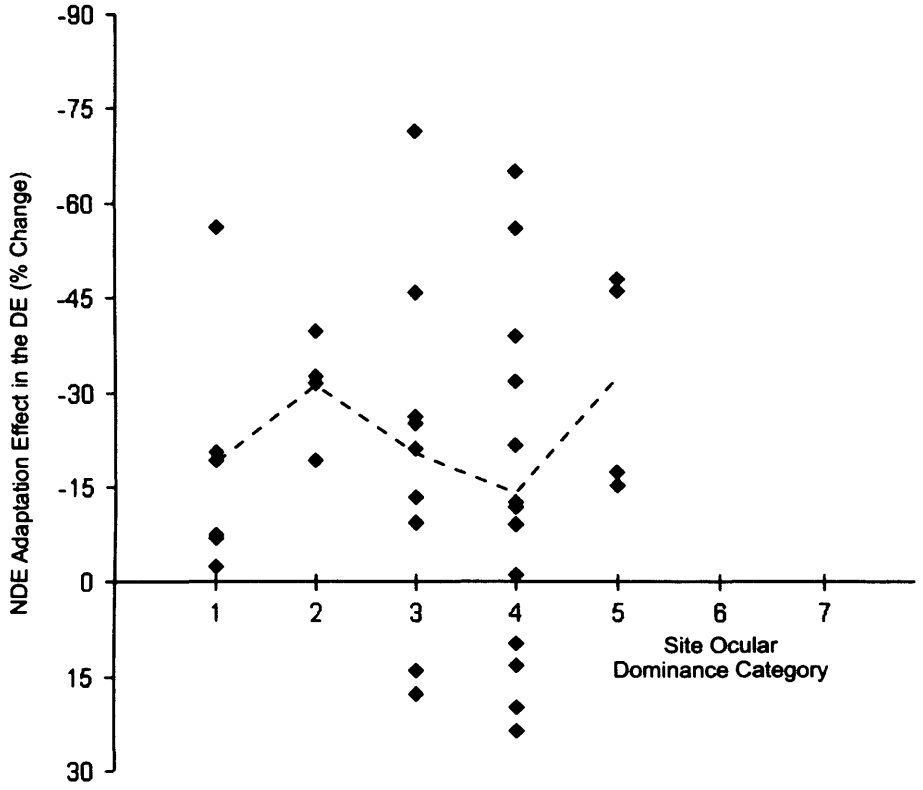

Figure 4.30 – Shows the relationship between the ocular dominance of a penetration site and the level of NDE adaptation in the DE. The range of response change after adaptation appears to increase with more binocular recording locations, but this may also be due to the greater number of sites for OD categories 3 and 4. There also appears to be an increase in the maximum effect of NDE adaptation as you go from monocular to binocular regions, but this is not reflected in the mean adaptation levels for each OD category (denoted by the dashed line).

DISCUSSION

1. Summary of Results

Observations from both the monocular and binocular groups lead to the conclusion that there is only a weak link between the ocular dominance and level of inter ocular transfer exhibited by a cell. Although this is contrary to my hypothesis, the results point towards a potential substrate for IOT which is worthy of further investigation. There is clear evidence that large magnitudes of interocular transfer occur in monocular cells, despite the absence of an evoked response when using a non-dominant eye adapting stimulus. In other words, even though presentation of a NDE grating with preferred orientation elicited little or no response from a cell, using this same stimulus to adapt still induces significant reduction in activity in response to stimulation of the dominant eye. The link between OD and IOT is further weakened by the fact that a subset of binocular cells which do respond to NDE stimulation, do not display any significant level of transfer. Finally, a thorough attempt to find a correlation between the ocular dominance in binocular cells and the level of adaptation in each eye or the transfer between them resulted in only mild trends.

The strength of the adaptive effect is stimulus specific, no matter which eye is adapted and tested. However, adaptation through the NDE with a stimulus of the preferred direction still significantly alters the response to the non-preferred direction through the dominant eye in the large majority of cases. In general terms, as the difference between the adapting and test orientation increases the level of both direct and transferred adaptation decreases, but this specificity is rarely completely directional. A related observation in the binocular cell group dominated by one eye is that the normalised adaptation effect precisely matches the normalised test stimulus response across the range of stimulus orientations, when both the adapting and test stimulus are presented to the dominant eye. This matching of the normalised adaptation and test responses is in itself stimulus specific, but the close similarity suggests that they are directly related to one another. A potentially more controversial observation was that a subset of cells displayed clear increases in the orthogonal-to-optimum responses

after adapting with the NDE. The presence of this effect on both monocular and binocular neurons suggests that it is independent from the ocular dominance of a cell.

There was a tendency for more complex cells to show a lack of IOT than simple cells, although with such a small sample size this was not significant (chi-squared test, $p<0.1$). This tendency is in agreement with a similar observation made by Maffei *et al* (1986) in split chiasm cats. An inverse relationship was found between the OD of a cell and the NDE adaptation effect in simple cells. No such link was found for complex cells, which partly explains why this same trend is weaker when considering the full population of cells.

The following further observations about how the position of a neurone in the cortex affects IOT were made. First, no link was found between IOT and the depth of cell below the cortical surface. This indicates that the strength of IOT is not dependent on the cortical layer in which a neurone is located. Second, the binocularity of the local region surrounding a recording site corresponded fairly well with the recorded cells' OD, but did not appear to correlate with the strength of IOT. However, more data from monocular regions of the visual cortex are required to reach definite conclusions in this matter.

2. IOT in Monocular Cells

As is highlighted in the pie charts of figure 4.11 that accompany the monocular group results, the interocular transfer of adaptation from the NDE to the DE is greater than the NDE:DE response ratio. This larger-than-expected reduction induced after adapting with the NDE indicates a source of adaptation that does not depend on a supra-threshold spiking response to the adapting stimulus, and is therefore certainly not some kind of fatigue. So what is the mechanism underlying this IOT in the monocular cells? Two potential answers to this question will be explored in the following discussion. The first involves subthreshold binocular interactions that occur when adapting with the NDE. The second involves a disinhibitory pathway that indirectly influences the tested neurone.

3. Sub-threshold Binocular Interactions

Although there is no obvious link between ocular dominance and IOT, there are other alternatives to classifying binocular cells that could be more revealing. The method of ocular dominance classification used in this investigation was based upon a comparison of monocular supra-threshold spiked responses. However, many cells in V1 show high levels of binocular summation when presented with binocular stimuli, including those sensitive to disparity (Hubel and Wiesel 1962, Bishop *et al* 1971). Such changes were investigated in greater detail in a study on binocular interaction, using dichoptic sinusoidal gratings of optimal spatial frequency and orientation but different relative phase (which translates into relative disparity). It was found that changing the relative spatial phase can result in phase specific binocular interactions of both simple and complex cells of the primary visual cortex (Ohzawa and Freeman 1986a,b). In those cells that are phase specific, an optimal spatial phase difference produces a facilitatory effect when compared with the response to monocular stimulation of the DE. Conversely, a phase difference of 180° away from the optimal produces a suppression effect that can reduce responses to zero. A similar test to IOT was also performed with dichoptic stimuli by showing low contrast to one eye and high contrast to the other and again changing the relative spatial phase (Ohzawa and Freeman 1986a). Strong modulations still occurred even though the gain of the cell was altered according to the higher contrast, resulting in no response when using the lower contrast. Thus, it is possible for these modulating effects to occur when the stimulation through one eye is sub-threshold and does not evoke a response from the cell. This means that a subset of the cells that were classified as monocular in my study could still be influenced to a large degree by NDE stimuli. Subthreshold stimuli can also influence the responses of otherwise monocular neurones during interocular suppression (Sengpiel *et al* 1994). This suppression is induced by first presenting a conditioning sinusoidal grating stimulus of optimal parameters to the DE and then introducing a second grating to the NDE. In contrast to IOT and relative spatial phase, this interocular suppression appears to be independent of the orientation of the second grating (Sengpiel *et al* 1994). Thus, it is possible for subthreshold activity produced by using NDE stimuli to influence the responses of an otherwise monocular cell. This activity can be revealed under certain specific conditions, such as the IOT

observed in this study or changes in the relative spatial phase of dichoptic stimuli. However, without further investigation it is not possible to say whether there is any direct link between these binocular interactions, and the monocular stimuli conditions that result in IOT.

Further support for the contribution of subthreshold activity to IOT in monocular cells is provided from an intracellular recording of adaptation from neurones in the cat primary visual cortex. Sanchez-Vives *et al* (2000a) showed that it is possible for excitatory activity in the neurone to produce post-adaptation hyperpolarisation even if it is below the threshold required to induce a spiked response. This tonic hyperpolarisation is intrinsic to the neurone and is significantly correlated with the strength of post-adaptation suppression. The above observation was made by keeping a cell in a hyperpolarised state with an injection of DC current and then using a high contrast sinusoidal grating stimulus of optimal orientation and spatial phase to induce adaptation. This meant that the adapting stimulus could still induce a large depolarisation and modulations in the DC membrane potential of the cell without the occurrence of action potentials. Large modulations in the membrane potential of the neurone are required to induce the necessary hyperpolarisation that results in post-adaptation suppression. This principle causes problems when trying to explain the large difference between the DE and NDE responses and the level of transfer in some cases. For instance, in one example a reduction of 65% was observed in the DE response to the preferred orientation even though stimulation with the NDE only evoked a response of $0.5sp.s^{-1}$. Is it possible for the NDE adapting stimulus to produce modulations in the subthreshold activity that are large enough to induce a level of hyperpolarisation sufficient to explain this level of IOT? An intracellular recording of IOT from monocular cells is required to provide an answer to this question. Without the information provided from such a study, there are still doubts as to whether the proposed subthreshold mechanisms are sufficient to provide a satisfactory explanation for IOT in monocular cells. Whilst certainly not impossible, it is worthwhile considering alternatives, one such explanation involving disinhibitory pathways is explained below.

4. Inhibition and Interocular Transfer

The postulation that inhibition is involved in both adaptation and IOT is not a new one. Although inhibitory theories once used to explain adaptation have been ruled out after experiments involving pharmacological application of N-methyl bicuculline (DeBruyn and Bonds 1986, Vidyasagar 1990), this does not exclude its involvement in IOT.

The increases in the orthogonal to optimal orientation responses of the DE after adaptation with the NDE may well be due to a release from inhibitory influence. This inhibition appears to be connected with orientation selectivity, considering that its removal during NDE adaptation results in a less sharply tuned orientation tuning curve (see figure 4.22a). Ferster (1986) has shown that in many cells of cat V1 there are inhibitory post-synaptic potentials (IPSPs) that are well tuned to the preferred orientation of a cell. Considering that the NDE adaptation stimulus also uses the preferred orientation then similar IPSPs could well be invoked during NDE stimulation. However, if this inhibition had a similar tuning width as any excitatory post-synaptic potentials it would produce a subtractive scaling of the responses to all orientations and actually decrease orientation selectivity. Therefore, for this inhibition to cause an enhancement in orientation selectivity it must be more broadly tuned than the excitatory input. There is evidence for the existence of broad orientation tuning of inhibitory inputs of cells in ferret V1 (Roerig and Chen 2002). The broadly tuned nature of local inhibitory inputs has also been incorporated into a model that shows how they can cause a sharpening of orientation tuning (by amplifying the response to the preferred orientation, Somers *et al* 1995).

It must be noted that such broadly tuned inhibition would have the strongest effect on the flanks of the orientation tuning curve, around 20-40° away from the preferred orientation. This does not correspond with my results, where the largest increases were found in the orthogonal-to-optimum orientation responses. A limitation of the extracellular single cell recording technique is that it does not allow the separation of inhibitory and excitatory influences. This means that the final shape of the adapted orientation tuning curve can be governed by changes in either or both influences. Thus, any increases due to the release from inhibition are combined with the more

prevalent adaptive reductions around the PO seen in other cells to produce the final result. This means that the largest increases in response are found in the orthogonal-to-optimum orientation responses because that is where the adaptation related changes in excitatory influence are weakest, allowing changes in inhibition to be revealed.

Dealy and Tolhurst (1974) suggested that inhibition can be transferred between channels to explain how an individual channel can be adapted by a stimulus that may not cause any excitation. The term channels mentioned here is now largely obsolete but was used in past psychophysics experiments and theories to describe potential pathways (or populations of cells) with specific response characteristics. Reductions in activity can also occur without the firing of a cell, perhaps via intracortical inhibition invoked by cells that receive direct geniculate input during adaptation (Ohzawa *et al* 1985). This could produce a divisive scaling of the responses which underlies the cortical gain mechanism. In the model of IOT suggested by Maffei *et al* (1986) recurrent inhibition is harnessed to transfer callosal adaptation. Levels of recurrent inhibition (or excitation) usually rely on the response of the cell to activate feedback loops. The postulation is that these same recurrent loops can be activated by callosal connections and/or direct activation of the cell. Although in some monocular cells there is very little response to activate such loops, a similar pathway could be involved. The possibility of intracortical inhibitory connections contributing towards the mechanisms underlying IOT is outlined in a model, described below.

5. A Possible Model of IOT in Monocular Cells

The pathway outlined in the model below (figure 4.31) offers an alternative explanation for the surprising behaviour observed in the monocular neurons. It is entirely feasible that at least a part of the physiological substrate of IOT is inhibitory interneurones of V1. The adaptive effect may be transferred by horizontal connections from neurones dominated by the NDE and thereby respond strongly during NDE adaptation, but which have no direct connection with DE cells.

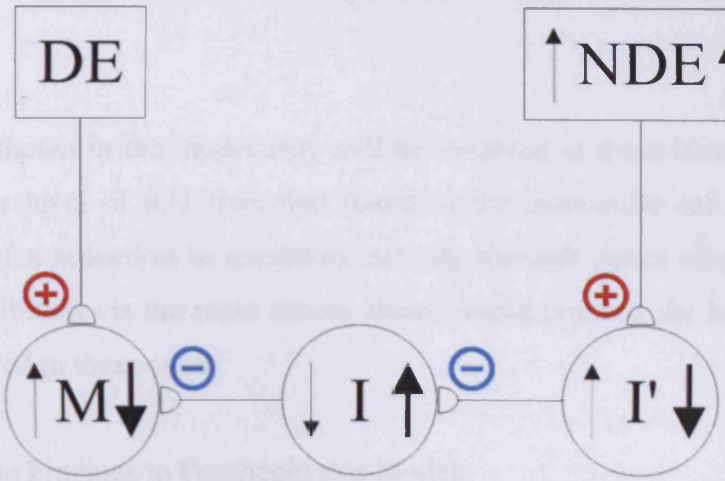

Figure 4.31 - Shows the hypothesised disinhibitory model that may partly underlie the large transfer of the aftereffect observed in monocular cells. The monocular cell from which recording takes place is labelled M, and the two inhibitory interneurones required for the process labelled I and I'. The arrows indicate the decrease or increase in neuronal activity associated with NDE test (thin arrows on left of letters) and adapted (thick arrows on right) stimulus conditions.

For this model to make sense it must work when either testing or adapting with the NDE. During NDE test stimulation an increase in NDE input results in raised inhibition of I', a lowered inhibitory contribution of I and a resulting increase in the possibility of cell firing of the monocular cell. However it must be noted that no excitatory influence is present in this pathway, and as such this could subliminally influence cell M, without eliciting an actual response. Conversely, adapting with the NDE reduces the inhibitory influence of I' on I, resulting in an increased activity of I, reducing the response when stimulating with the DE. The NDE input can be considered to come directly from the LGN or from the opposite hemisphere via the corpus callosum.

The lack of response to NDE stimulation in monocular cells means that the combined input from the LGN and binocular portion of the network does not produce a suprathreshold response to a NDE test stimulus. A reduction in firing of binocular cells that inhibit inhibitory interneurones would have the desired effect. A decrease in activity of both these disinhibitory neurones and those associated with the callosal pathway would cause an increase in inhibition onto the monocular cells in question.

This means that large reductions in response can occur, without the need for any direct NDE.

The pathway shown in the model may still be involved in those binocular cells that show a greater level of IOT than that found in the monocular cell categories. A combination of a reduction in excitatory activity through direct adaptation and the transfer of inhibition via the route shown above would produce the larger reductions that are observed in these cases.

6. Relating the Findings to Psychophysics Models

There are a number of reasons why the classic psychophysics model (Blake *et al* 1981) described in the introduction and assumed by many psychophysics papers does not fit with the single cell data. On the surface this model is satisfactory and conceptually may still be accurate, depending on the definition of monocular and binocular. The only way to align this model with our results is to do away with numbers of neurones and talk more about monocular and binocular components and relative levels of OD, adaptive affect and IOT. The main assumption of many previous theories is that there is a group of monocular cells that remains unadapted when using a NDE stimulus to adapt (Blake *et al* 1981, Hammond and Mouat 1988, McColl and Mitchell 1998). However, as shown by my results, almost all the cells seem to show some form of adaptation, regardless of how monocular they are (in the conventional sense), or which eye is adapted. So accordingly, the entire concept of a pool of non-adapted cells in V1 appears to be incorrect. The transfer of adaptation may well be reliant on a pooling of responses and network connections, even at this early stage. Perhaps the following would be a better model of IOT in V1.

The strength of the measured aftereffect is proportional to the total amount of neuronal adaptation in the contributing network. Adapting the LE only produces full adaptation in the more monocular LE cells and partial adaptation in binocular neurones. Testing the RE stimulates the partially adapted binocular and weakly adapted RE neurones. Thus, the aftereffect is reduced according to the level of summed adaptation in those neurones that contribute to the conscious percept.

For example, consider a monocular cell that receives the majority of its LGN input from cells that respond to the DE and that the network contains both a monocular and binocular component. One would expect the entire network pool for this cell to be affected by the DE adaptation whereas only the binocular component of the network would be affected by the NDE adaptation. When adapting and testing with the DE there is both an intrinsic and a network-based adaptive effect. When adapting with the NDE there is only a change in the network-based transfer effect.

This description is in agreement with the normalisation model first proposed by Heeger (1991) to explain non-linear properties of simple cells, including gain control and saturation of response to high contrast stimulation. This model involves a divisive scaling of a cell's response by the total activity in the network of cells that influence it, known as the normalisation pool. Any adapting stimulus that affects part or all of this normalisation pool will raise the total conductance; producing a division of the linear LGN input and contrast gain control (Carandini *et al* 1997). When IOT occurs in monocular cells, the binocular component of the network influences the normalisation pool, which then affects the response to subsequent DE stimulation.

7. A Comparison of IOT in Normal and Split Chiasm Cats

Previous work involving extracellular recording from the primary visual cortex of the cat has shown interocular transfer in monocular cells, although in this case the recordings were from animals which had undergone a splitting of the optic chiasm (Maffei *et al* 1986). This cutting of the chiasm leaves only monocular input (representing the temporal hemiretina) from the LGN, removing the convergence of left and right thalamic fibres onto binocular cortical cells. Nevertheless, a similar aftereffect was still observed when either the ipsilateral or the contralateral eye was used to adapt. This clearly shows that no geniculate input is required for IOT to occur when adapting through the contralateral eye.

Only 20% of the complex cells recorded from split chiasm cats showed IOT of adaptation (Maffei *et al* 1986). Whether this was due to a sampling bias in their population of 16 complex cells recorded from area 17 or due to underlying differences between normal and split chiasm cats is difficult to say. The ocular dominance of the

primary visual cortex in split chiasm cats is skewed towards the ipsilateral eye, which could affect IOT in complex cells. However, this does not appear to affect the occurrence of IOT in simple cells (Maffei *et al* 1986). There was a tendency for more complex cells to show a lack of IOT than simple cells in my data, although this was not significant (chi-squared test, $p<0.1$). A shift towards a more monocular cortex would reduce the binocular portion of the network, and change the characteristics of the 'normalisation pool' as described in the Heeger model, above. In theory, this would reduce the amount of IOT in all cells and provide an explanation for the lack of IOT in complex cells of split chiasm cats. However, the monocularity of the cortex induced by splitting the optic chiasm is rather artificial, resulting from removal of half of the retinal input rather than a natural developmental process. A better model of a monocular cortex that could be used in future studies is found in strabismic cats. Strabismus involves the deviation of the visual axis of one eye with respect to the other. Due to the misalignment of the visual axes the afferent input from the left and right eyes tends to make connections with separate cortical cells. This results in a reduction the number binocularly driven cells, and shifts the ocular dominance of the cortex towards a U-shaped distribution (Hubel and Wiesel 1965). The characteristics of strabismic cats would therefore be very useful for assessing IOT in a cortex dominated by monocular neurones. One would expect a reduction in both the number of cells that display IOT and the overall magnitude of any observed transfer. Of particular interest, is whether IOT can be found in any of the monocular cells (as defined in my study).

IOT was also found in all the neurones recorded from cats whose corpus callosum was sectioned, but with an intact chiasm (Maffei *et al* 1986). This clearly demonstrates that IOT is possible by depression of geniculocortical inputs (explained below) or a within-hemisphere network effect only, without participation of between-hemispheres interactions. Although the method used in their study produces a clear qualitative result, it doesn't provide a quantitative description of the magnitude of IOT. Without undertaking a more detailed investigation, it is not possible to quantify the relative contributions of the geniculate and callosal pathways to IOT. Thus, in a cat with either its split chiasm or corpus callosum sectioned the inputs required to produce IOT in simple cells are preserved.

8. Depression at Excitatory Synapses

A slow form of synaptic depression has been proposed as a mechanism by which contrast adaptation can occur in neurones of the primary visual cortex (Chance *et al* 1998). The most likely location of this depression would be at excitatory metabotropic glutamate receptors, which have been shown to be involved in the adaptation process (McLean and Palmer 1998). For the depression of excitatory synapses to play a role in the IOT of contrast adaptation, there must be a network of binocular connections that can be activated during the stimulation of either eye. It has been postulated that there is a recurrent excitatory network of lateral connections between cells in the superficial layers of V1 that tend to share similar response properties, such as orientation preference (Kisvárday and Eysel 1992). However, this network of like-with-like connections between neurones is not as strict as was once thought (Yoshioka 1996, Kisvárday *et al* 1997). An investigation into the connectivity of pyramidal neurones in the superficial layers of Macaque V1 found only a moderate tendency for links between cells in columns with the same ocular dominance preference (Yoshioka 1996). In this study, almost 30% of these connections were made between OD columns of opposite eye preference. Considering that there is a more distinct segregation of OD columns in the macaque than in the cat one would presume that the predominance of like-with-like connectivity found here represents an upper limit. This shows the existence of a network of excitatory connections in the superficial cortical layers of area V1 that can propagate information along binocular-to-binocular and binocular-to-monocular pathways.

Thus, a typical binocular cell located in the superficial layers of the cortex receives excitatory binocular input from various different sources, including the lateral connections mentioned above. In addition to this network, there are also callosal projections from the opposite hemisphere and vertical projections from cells located in layer IV. The role of callosal input in IOT was highlighted by Maffei *et al* (1986) who showed that it is capable of mediating IOT on its own, without any geniculate input. There are excitatory cells in layer IV that relay information to neurones in the superficial layers II/III above (Thomson *et al* 2002). This inter-laminar pathway has been shown to have highly specific fine scale connections in the rat (Yoshimura 2005)

which presumably underlie the ocular dominance columns that traverse the 6 cortical layers in the cat (Lowel and Singer 1993). This provides evidence for another potential route for binocular input. Thus, when using a monocular NDE stimulus, a portion of these binocular pathways can be activated along with their associated excitatory synapses. If these binocular excitatory synapses are depressed during NDE adaptation then they will affect the responses when subsequently testing with DE stimuli that recruit the same pathways, resulting in IOT.

9. The Lack of IOT in a Subset of Complex Cells

All of the neurones placed in the binocular group of cells dominated by one eye (taken from OD group 3 or 5) are of the complex type. Surprisingly, they did not show any change in DE activity after adapting with the NDE, even though there was a clear NDE response. Unfortunately, it is difficult to ascertain other attributes of these complex cells which may explain this lack of IOT. For instance, there was no correlation between the cortical layer and the level of IOT in complex cells. This matter is further complicated by the observation from previous studies that on the whole complex cells are actually more susceptible to adaptation than simple cells (Albrecht *et al* 1984, Sanchez-Vives 2000a). There are complex cells that do not display a post-adaptation hyperpolarisation, even after large responses to an adapting stimulus (Sanchez-Vives 2000a). This is certainly the case after NDE adaptation in these cells, as any changes in the intrinsic state of the neurone would affect the responses to DE stimuli too. Although these cells do show their susceptibility to DE adaptation, there is only a change in the NDE test stimulus responses when adapting with the NDE. This is more fitting with a selective depression of monocular excitatory synapses associated with geniculocortical input. It has been shown that a selective depression of excitatory synapses can allow a single neurone to reduce its responses to a stimulus with specific parameters, whilst maintaining its sensitivity to other stimuli (Abbott *et al* 1997). In this case, specific reductions to test stimuli in the same eye could occur, whilst maintaining a normal response to test stimuli in the other eye.

10. Potential Future Directions

Unfortunately, the attempt to find an association between the location of a recording site in the OD map and the level of IOT proved inconclusive. This was partly to do with the subjective selection of recording sites in binocular, iso-oriented regions of the activity map and the fact that the adult cat primary visual cortex is predominantly binocular. This subsequently led to a scarcity in the number of penetration sites in monocular or pinwheel regions. The binocular regions were thought to be more promising in terms of exhibiting IOT, and a high level of NDE adaptation was not expected in monocular cells. A similar study combining imaging and extracellular recordings but with a selection of penetration sites that cover the full range of OD and angle map characteristics would address this issue.

The classification of ocular dominance used in this study was based upon monocular supra-threshold spike responses and does not reveal more subtle binocular interactions. A more detailed assessment of binocular interaction under control conditions is required to identify those cells classified as monocular which can be influenced by NDE stimulation. For instance, otherwise monocular cells can display much larger responses if stimulated with binocular stimuli of optimal relative interocular phase (Ohzawa and Freeman 1986a,b). It would be interesting to see if there is any link between the depth of such relative phase tuning and IOT. Those monocular cells in this study that displayed large changes in activity after NDE adaptation could potentially have high levels of binocular interaction. Thus, I propose a comparison of the phase specific tuning of cells under both control and adapted conditions in order to reveal the interplay between these two phenomena as a worthwhile direction for future investigations.

Understanding the role that inhibition plays in IOT is crucial to uncovering the precise nature of the underlying mechanism. A possible way of achieving this is through the use of iontophoretic application of N-methyl bicuculline (NMB), a potent γ-aminobutyric acid (GABA) antagonist. Iontophoresis is a technique that allows the controlled application of drugs to highly localised regions via groups of micropipettes, one of which can contain a recording electrode. This allows the extracellular

recording from neurones without the influence of GABA, the main inhibitory neurotransmitter in the primary visual cortex. This method has already been used to investigate contrast adaptation, and it was found that GABAergic inhibition is not directly involved (DeBruyn and Bonds 1986, Vidyasagar 1990, Mclean & Palmer 1996). Thus, the null effect of NMB application on contrast adaptation when adapting and testing with the same eye can be compared with its effect on IOT. It is also known that the removal of GABA based inhibition can alter the overall response level, directionality and the sharpness of orientation tuning (Sillito *et al* 1980, Crook *et al* 1997). These factors allow a quantification of the effectiveness of the NMB application and subsequent recovery from orientation tuning curve recordings. Such an approach will help to give a definitive answer as to how GABAergic inhibition influences the transfer of adaptation. For instance, if the level of IOT is unaffected by the application of NMB, then the model suggested to explain the monocular results is called in to question.

REFERENCES

Abbott LF, Varela JA, Sen K, Nelson SB. Synaptic depression and cortical gain control. *Science.* 1997 Jan 10;275(5297):220-4.

Albrecht DG, Farrar SB & Hamilton DB. Spatial contrast adaptation characteristics of neurones recorded in the cat's visual cortex. *J.Physiol* 1984; **347**, 713-739.

Albright TD. Direction and orientation selectivity of neurons in visual area MT of the macaque. *J Neurophysiol.* 1984 Dec;52(6):1106-30.

Anderson P, Mitchell DE, Timney B. Residual binocular interaction in stereoblind humans. *Vision Res.* 1980;20(7):603-11.

Anstis S, Duncan K. Separate motion aftereffects from each eye and from both eyes. *Vision Res.* 1983;23(2):161-9.

Arieli A, Shoham D, Hildesheim R, Grinvald A. Coherent spatiotemporal patterns of ongoing activity revealed by real-time optical imaging coupled with single-unit recording in the cat visual cortex. *J Neurophysiol.* 1995 May;73(5):2072-93.

Attwell D, Laughlin SB. An energy budget for signaling in the grey matter of the brain. *J Cereb Blood Flow Metab.* 2001 Oct;21(10):1133-45. Review.

Baizer JS, Robinson DL, Dow BM. Visual responses of area 18 neurons in awake, behaving monkey. *J Neurophysiol.* 1977 Sep;40(5):1024-37.

Barlow HB & Hill RM. Evidence for a physiological explanation for the waterfall phenomenon and figural after-effects. *Nature, Lond.* 1963; **200**, 1345-1347.

Bienenstock EL, Cooper LN, Munro PW. Theory for the development of neuron selectivity: orientation specificity and binocular interaction in visual cortex. *J Neurosci.* 1982 Jan;2(1):32-48.

Berkley MA. Behavioral determination of the spatial selectivity of contrast adaptation in cats: some evidence for a common plan in the mammalian visual system. *Vis.Neurosci.* 1990; **4**, 413-426.

Bickford ME, Guido W, Godwin DW. Neurofilament Proteins in Y-Cells of the Cat Lateral Geniculate Nucleus: Normal Expression and Alteration with Visual Deprivation. *J Neurosci.* 1998; 18(16):6549-6557

Bishop PO, Henry GH, Smith CJ. Binocular interaction fields of single units in the cat striate cortex. *J Physiol.* 1971 Jul;216(1):39-68.

Bjørklund RA, Magnussen S. A study of interocular transfer of spatial adaptation. *Perception.* 1981;10(5):511-8.

Blake R, Fox R. Interocular transfer of adaptation to spatial frequency during retinal ischaemia. *Nat New Biol.* 1972 Nov 15;240(98):76-7.

Blake R, Overton R. The site of binocular rivalry suppression. *Perception.* 1979;8(2):143-52.

Blake R, Overton R, Lema-Stern S. Interocular transfer of visual aftereffects. *J Exp Psychol Hum Percept Perform.* 1981 Apr;7(2):367-81.

Blakemore C & Campbell FW. Adaptation to spatial stimuli. *J Physiol.* 1969a;**200**, 11-13.

Blakemore C & Campbell FW. On the existence of neurones in the human visual system selectively sensitive to the orientation and size of retinal images. *J.Physiol.* 1969b; **203**, 237-260.

Blakemore C, Nachmias J, Sutton P. The perceived spatial frequency shift: evidence for frequency-selective neurones in the human brain. *J Physiol.* 1970 Oct;210(3):727-50.

Blakemore C & Nachmias J. The orientation specificity of two visual after-effects. *J.Physiol.* 1971;**213**, 157-174.

Blakemore C, Muncey JP & Ridley RM. Stimulus specificity in the human visual system. *Vision Res.* 1973;**13**, 1915-1931.

Blasdel GG, Salama G. Voltage-sensitive dyes reveal a modular organization in monkey striate cortex. *Nature.* 1986 Jun 5-11;321(6070):579-85.

Blasdel G, Campbell D. Functional retinotopy of monkey visual cortex. *J Neurosci.* 2001 Oct 15;21(20):8286-301.

Bonds AB. Spatial adaptation of the cortical visual evoked potential of the cat. *Invest Ophthalmol Vis* Sci. 1984 Jun;25(6):640-6.

Bonds AB. Role of inhibition in the specification of orientation selectivity of cells in the cat striate cortex. *Vis.Neurosci.* 1989;**2**, 41-55.

Bonhoeffer T, Grinvald A. Iso-orientation domains in cat visual cortex are arranged in pinwheel-like patterns. *Nature.* 1991 Oct 3;353(6343):429-31.

Bonhoeffer T & Grinvald A. Optical imaging based on intrinsic signals. The methodology. Toga AW & Mazziotta JC (eds) 1996; *Brain Mapping: The Methods.* Academic Press, London, pp. 55-97.

Bosking WH, Zhang Y, Schofield B, Fitzpatrick D. Orientation selectivity and the arrangement of horizontal connections in tree shrew striate cortex. *J Neurosci.* 1997 Mar 15;17(6):2112-27.

Bowling DB, Michael CR. Terminal patterns of single, physiologically characterized optic tract fibbers in the cat's lateral geniculate nucleus. *J Neurosci.* 1984 Jan;4(1):198-216.

Boyd JD, Matsubara JA. Laminar and columnar patterns of geniculocortical projections in the cat: relationship to cytochrome oxidase. *J Comp Neurol.* 1996 Feb 19;365(4):659-82.

Burke D, Wenderoth P. Determinants of two-dimensional motion aftereffects induced by simultaneously- and alternately-presented plaid components. *Vision Res.* 1993 Feb;33(3):351-9.

Cai D, DeAngelis GC, Freeman RD. Spatiotemporal receptive field organization in the lateral geniculate nucleus of cats and kittens. *J Neurophysiol.* 1997 Aug;78(2):1045-61.

Campbell FW, Maffei L. The tilt after-effect: a fresh look. *Vision Res.* 1971 Aug;11(8):833-40.

Carandini M, Ferster D. A tonic hyperpolarization underlying contrast adaptation in cat visual cortex. *Science.* 1997 May 9;276(5314):949-52.

Carandini M, Heeger DJ, Movshon JA. Linearity and normalization in simple cells of the macaque primary visual cortex. *J Neurosci.* 1997 Nov 1;17(21):8621-44.

Carandini M, Sengpiel F. Contrast invariance of functional maps in cat primary visual cortex. *J Vision.* 2004;4:130–43.

Chance B, Cohen P, Jobsis F, Schoener B. Intracellular oxidation-reduction states in vivo. *Science.* 1962 Aug 17;137:499-508.

Chance FS, Nelson SB, Abbott LF. Synaptic depression and the temporal response characteristics of V1 cells. *J Neurosci.* 1998 Jun 15;18(12):4785-99.

Chen-Bee CH, Kwon MC, Masino SA, Frostig RD. Areal extent quantification of functional representations using intrinsic signal optical imaging. *Journal of Neuroscience Methods.* 1996; 68: 27-37.

Chen-Bee CH, Polley DB, Brett-Green B, Prakash N, Kwon MC, Frostig RD. (2000) Visualizing and quantifying evoked cortical activity assessed with intrinsic signal imaging. *Journal of Neuroscience Methods.* 2000; 97: 157-173.

Cleland BG, Levick WR, Morstyn R, Wagner HG. Lateral geniculate relay of slowly conducting retinal afferents to cat visual cortex. *J Physiol.* 1976 Feb;255(1):299-320.

Cohen MS, Bookheimer SY. Localization of brain function using magnetic resonance imaging. *Trends Neurosci.* 1994 Jul;17(7):268-77. Review.

Condo GJ, Lachica EA, Casagrande VA. Postnatal development of retinogeniculate axonal arbors in the tree shrew. *Soc Neurosci Abstr.* 1986; 12:440

Conley M, Fitzpatrick D, Diamond IT. The laminar organization of the lateral geniculate body and the striate cortex in the tree shrew (Tupaia glis). *J Neurosci.* 1984 Jan;4(1):171-97.

Conway JL, Schiller PH. Laminar organization of tree shrew dorsal lateral geniculate nucleus. *J Neurophysiol.* 1983 Dec;50(6):1330-42.

Crook JM, Kisvárday ZF & Eysel UT. Evidence for a contribution of lateral inhibition to orientation tuning and direction selectivity in cat visual cortex: reversible inactivation of functionally characterized sites combined with neuroanatomical tracing techniques. *Eur.J.Neurosci.* 1998;**10**, 2056-2075.

Cynader M, Timney BN, Mitchell DE. Period of susceptibility of kitten visual cortex to the effects of monocular deprivation extends beyond six months of age. *Brain Res.* 1980 Jun 9;191(2):545-50.

Daniel PM, Whitteridge D. The representation of the visual field on the cerebral cortex in monkeys. *J Physiol (Paris).* 1961 Dec;159:203-21.

Dartnall HJ, Bowmaker JK, Mollon JD. Human visual pigments: microspectrophotometric results from the eyes of seven persons. *Proc R Soc Lond B Biol Sci.* 1983 Nov 22;220(1218):115-30. Review.

Dealy RS & Tolhurst DJ. Is spatial adaptation an after-effect of prolonged inhibition? *J. Physiol. (Lond).* 1974;**241**, 261-270.

DeAngelis GC, Robson JG, Ohzawa I, Freeman RD. Organization of suppression in receptive fields of neurons in cat visual cortex. *J Neurophysiol.* 1992 Jul;68(1):144-63.

DeBruyn EJ & Bonds AB. Contrast adaptation in cat visual cortex is not mediated by GABA. *Brain Res.* 1986;**383**, 339-342.

Douglas RJ, Koch C, Mahowald M, Martin KAC & Suarez H. Recurrent Excitation in Neocortical Circuits. *Science.* 1995;**269**, 981-984.

Dragoi V, Sharma J, Sur M. Adaptation-induced plasticity of orientation tuning in adult visual cortex. *Neuron.* 2000 Oct;28(1):287-98.

Duong TQ, Kim DS, Ugurbil K, Kim SG. Localized cerebral blood flow response at submillimeter columnar resolution. *Proc Natl Acad Sci U S A.* 2001 Sep 11;98(19):10904-9.

Enroth-Cugell C & Robson JG. The contrast sensitivity of retinal ganglion cells of the cat. *J Physiol.* 1966; 187:517-522

Erisir A, Van Horn SC, Sherman SM. Distribution of synapses in the lateral geniculate nucleus of the cat: differences between laminae A and A1 and between relay cells and interneurons. *J Comp Neurol.* 1998 Jan 12;390(2):247-55.

Eysel UT, Shevelev IA, Lazareva NA, Sharaev GA. Orientation tuning and receptive field structure in cat striate neurons during local blockade of intracortical inhibition. *Neuroscience.* 1998 May;84(1):25-36.

Feldmeyer D, Lubke J, Silver RA, Sakmann B. Synaptic connections between layer 4 spiny neuron-layer 2/3 pyramidal cell pairs in juvenile rat barrel cortex: physiology and anatomy of interlaminar signalling within a cortical column. *J Physiol.* 2002; 538: 803–822.

Fernandez JM, Farell B. Motion in depth from interocular velocity differences revealed by differential motion aftereffect. *Vision Res.* 2006 Apr;46(8-9):1307-17

Ferster D. Orientation selectivity of synaptic potentials in neurons of cat primary visual cortex. *J Neurosci.* 1986 May;6(5):1284-301.

Ferster D, Koch C. Neuronal connections underlying orientation selectivity in cat visual cortex. *TINS.* 1987;10(12):487-492

Fitzpatrick D. The functional organization of local circuits in visual cortex: insights from the study of tree shrew striate cortex. *Cereb Cortex.* 1996 May-Jun;6(3):329-41. Review.

Frascella J, Lehmkuhle S. A comparison between Y-cells in A-laminae and lamina C of cat dorsal lateral geniculate nucleus. *J Neurophysiol.* 1984 Nov;52(5):911-20.

Fries P, Roelfsema PR, Engel AK, Konig P, Singer W. Synchronization of oscillatory responses in visual cortex correlates with perception in interocular rivalry. *Proc Natl Acad Sci U S A.* 1997 Nov 11;94(23):12699-704.

Frostig RD, Lieke EE, Ts'o DY, Grinvald A. Cortical functional architecture and local coupling between neuronal activity and the microcirculation revealed by in vivo high-resolution optical imaging of intrinsic signals. *Proc Natl Acad Sci U S A.* 1990 Aug;87(16):6082-6.

Georgeson MA. The perceived spatial frequency, contrast, and orientation of illusory gratings. *Perception.* 1980;9(6):695-712.

Gilbert CD. Laminar differences in receptive field properties of cells in cat primary visual cortex. *J Physiol.* 1977 Jun;268(2):391-421.

Gilbert CD, Wiesel TN. Columnar specificity of intrinsic horizontal and corticocortical connections in cat visual cortex. *J Neurosci.* 1989 Jul;9(7):2432-42.

Gilbert CD. Circuitry, architecture, and functional dynamics of visual cortex. *Cereb Cortex.* 1993 Sep-Oct;3(5):373-86.

Gilinsky AS. Orientation-specific effects of patterns of adapting light on visual acuity. *J Opt Soc Am.* 1968 Jan;58(1):13-8.

Gilinsky AS, Doherty RS. Interocular transfer of orientational effects. *Science.* 1969 Apr 25;164(878):454-5.

Ginovart N, Wilson AA, Meyer JH, Hussey D, Houle S. [11C]-DASB, a tool for in vivo measurement of SSRI-induced occupancy of the serotonin transporter: PET characterization and evaluation in cats. *Synapse.* 2003 Feb;47(2):123-33.

Godecke I, Bonhoeffer T. Development of identical orientation maps for two eyes without common visual experience. *Nature.* 1996 Jan 18;379(6562):251-4.

Goldstein AG. Judgments of visual velocity as a function of length of observation time. *J Exp Psychol.* 1957 Dec;54(6):457-61.

Green M, Chilcoat M, Stromeyer CF 3rd. Rapid motion aftereffect seen within uniform flickering test fields. *Nature.* 1983 Jul 7-13;304(5921):61-2.

Grinvald A, Lieke E, Frostig RD, Gilbert CD, Wiesel TN. Functional architecture of cortex revealed by optical imaging of intrinsic signals. *Nature.* 1986 Nov 27-Dec 3;324(6095):361-4.

Grinvald A, Arieli A, Tsodyks M, Kenet T. Neuronal assemblies: single cortical neurons are obedient members of a huge orchestra. *Biopolymers.* 2003 Mar;68(3):422-36.

Guido W, Tumosa N, Spear PD. Binocular interactions in the cat's dorsal lateral geniculate nucleus. I. Spatial-frequency analysis of responses of X, Y, and W cells to nondominant-eye stimulation. *J Neurophysiol.* 1989 Aug;62(2):526-43.

Hammond P, Mouat GS, Smith AT. Motion after-effects in cat striate cortex elicited by moving gratings. *Exp Brain Res.* 1985;60(2):411-6.

Hammond P, Mouat GS. Neural correlates of motion after-effects in cat striate cortical neurones: interocular transfer. *Exp Brain Res.* 1988;72(1):21-8.

Harting JK, Diamond IT, Hall WC. Anterograde degeneration study of the cortical projections of the lateral geniculate and pulvinar nuclei in the tree shrew (*Tupaia glis*). *J Compar. Neurol.* 1973 Aug; 150(4):393-440.

Hassoun W, Le Cavorsin M, Ginovart N, Zimmer L, Gualda V, Bonnefoi F, Leviel V. PET study of the [11C]raclopride binding in the striatum of the awake cat: effects of anaesthetics and role of cerebral blood flow. *Eur J Nucl Med Mol Imaging.* 2003 Jan;30(1):141-8.

Hawken MJ, Shapley RM, Grosof DH. Temporal-frequency selectivity in monkey visual cortex. *Vis Neurosci.* 1996 May-Jun;13(3):477-92.

Heeger DJ. Normalization of cell responses in cat striate cortex. *Vis Neurosci.* 1992; 9:181–198.

Heller D, Ziefle M. Motion aftereffect in analysis of the visual system. *Z Psychol Z Angew Psychol.* 1993;201(3):317-47. German.

Hendry SH, Jones EG. GABA neuronal subpopulations in cat primary auditory cortex: co-localization with calcium binding proteins. *Brain Res.* 1991 Mar 8;543(1):45-55.

Hirsch JA, Gallagher CA, Alonso JM, Martinez LM. Ascending projections of simple and complex cells in layer 6 of the cat striate cortex. *J Neurosci.* 1998 Oct 1;18(19):8086-94.

Hirsch JA. Synaptic physiology and receptive field structure in the early visual pathway of the cat. *Cereb Cortex.* 2003 Jan;13(1):63-9. Review. Erratum in: *Cereb Cortex.* 2003 Apr;13(4):434.

Hirsch JA, Martinez LM, Pillai C, Alonso JM, Wang Q, Sommer FT. Functionally distinct inhibitory neurons at the first stage of visual cortical processing. *Nat Neurosci.* 2003 Dec;6(12):1300-8.

Holdefer RN, Norton TT. Laminar organization of receptive field properties in the dorsal lateral geniculate nucleus of the tree shrew (Tupaiaglis belangeri). *J Comp Neurol.* 1995 Jul 31;358(3):401-13.

Horecker BL. The absorption spectra of hemoglobin and its derivatives in the visible and near infra-red regions. *J. Biol. Chem.* 1943 148: 173-183.

Hubel DH, Wiesel TN. Receptive fields, binocular interaction and functional architecture in the cat's visual cortex. *J Physiol.* 1962 Jan;160:106-54.

Hubel DH, Wiesel TN. Anatomical demonstration of columns in the monkey striate cortex. *Nature.* 1969 Feb 22;221(182):747-50.

Hubel DH, Wiesel TN, Stryker MP. Orientation columns in macaque monkey visual cortex demonstrated by the 2-deoxyglucose autoradiographic technique. *Nature.* 1977 Sep 22;269(5626):328-30.

Hubel DH, Wiesel TN, Stryker MP. Anatomical demonstration of orientation columns in macaque monkey. *J Comp Neurol.* 1978 Feb 1;177(3):361-80.

Hubener M, Shoham D, Grinvald A, Bonhoeffer T. Spatial relationships among three columnar systems in cat area 17. *J Neurosci.* 1997 Dec 1;17(23):9270-84.

Hunter WS. The after-effect of visual motion. *Psychological Review.* 1914; 21:245-277

Ibbotson MR, Maddess T. The effects of adaptation to visual stimuli on the velocity of subsequent ocular following responses. Exp Brain Res. 1994;99(1):148-54.

Issa NP, Trepel C, Stryker MP. Spatial frequency maps in cat visual cortex. *J Neurosci.* 2000 Nov 15;20(22):8504-14.

Jacobs GH, Neitz J. Spectral mechanisms and color vision in the tree shrew (Tupaia belangeri). *Vision Res.* 1986;26(2):291-8.

Jasdzewski G, Strangman G, Wagner J, Kwong KK, Poldrack RA, Boas DA. Differences in the hemodynamic response to event-related motor and visual paradigms as measured by near-infrared spectroscopy. *Neuroimage.* 2003 Sep;20(1):479-88.

Jobsis FF, Keizer JH, LaManna JC, Rosenthal M. Reflectance spectrophotometry of cytochrome aa3 in vivo. *J Appl Physiol.* 1977 Nov;43(5):858-72.

Justo MS, Bermudez MA, Perez R, Gonzalez F. Binocular interaction and performance of visual tasks. *Ophthalmic Physiol Opt.* 2004 Mar;24(2):82-90.

Keck MJ, Price RL. Interocular transfer. An assessment of binocularity in strabismus. *Cleve Clin Q.* 1982 Winter;53(4):325-33.

Kenet T, Bibitchkov D, Tsodyks M, Grinvald A, Arieli A. Spontaneously emerging cortical representations of visual attributes. *Nature.* 2003 Oct 30;425(6961):954-6.

Kim DS & Bonhoeffer T. Reverse occlusion leads to a precise restoration of orientation preference maps in visual cortex. *Nature.* 1994 Aug 4;370(6488):370-2. Erratum in: *Nature* 1994 Nov 10;372(6502):196.

Kim DS, Duong TQ, Kim SG. High-resolution mapping of iso-orientation columns by fMRI. *Nat Neurosci.* 2000 Feb;3(2):164-9.

Kisvárday ZF, Eysel UT. Cellular organization of reciprocal patchy networks in layer III of cat visual cortex (area 17). *Neuroscience.* 1992;46(2):275-86.

Kisvárday ZF, Toth E, Rausch M, Eysel UT. Orientation-specific relationship between populations of excitatory and inhibitory lateral connections in the visual cortex of the cat. *Cereb Cortex.* 1997 Oct-Nov;7(7):605-18.

Kwong KK, Belliveau JW, Chesler DA, Goldberg IE, Weisskoff RM, Poncelet BP, Kennedy DN, Hoppel BE, Cohen MS, Turner R, et al. Dynamic magnetic resonance imaging of human brain activity during primary sensory stimulation. *Proc Natl Acad Sci U S A.* 1992 Jun 15;89(12):5675-9.

Landowne D. Measuring nerve excitation with polarized light. *Jpn J Physiol.* 1993;43 Suppl 1:S7-11. Review.

Lehky SR, Blake R. Organization of Binocular Pathways: Modeling and Data Related to Rivalry. *Neural Comp.* 1991; 3: 44-53

Lehmkuhle SW, Fox R. On measuring interocular transfer. *Vision Res.* 1976;16(4):428-30.

Leopold DA, Logothetis NK. Activity changes in early visual cortex reflect monkeys' percepts during binocular rivalry. *Nature.* 1996 Feb 8;379(6565):549-53.

LeVay S, Ferster D. Relay cell classes in the lateral geniculate nucleus of the cat and the effects of visual deprivation. *J Comp Neurol.* 1977;172:563–584.

LeVay S, Gilbert CD. Laminar patterns of geniculocortical projection in the cat. *Brain Res.* 1976 Aug 20;113(1):1-19.

LeVay S, Stryker MP, Shatz CJ. Ocular dominance columns and their development in layer IV of the cat's visual cortex: a quantitative study. *J Comp Neurol.* 1978 May 1;179(1):223-44.

Leventhal AG. Evidence that the different classes of relay cells of the cat's lateral geniculate nucleus terminate in different layers of the striate cortex. *Exp Brain Res.* 1979 Oct;37(2):349-72.

Lipton P. Effects of membrane depolarization on light scattering by cerebral cortical slices. *J Physiol.* 1973 Jun;231(2):365-83.

Livingstone MS, Hubel DH. Psychophysical evidence for separate channels for the perception of form, color, movement, and depth. *J Neurosci.* 1987 Nov;7(11):3416-68. Review.

Logothetis NK, Schall JD. Neuronal correlates of subjective visual perception. *Science.* 1989 Aug 18;245(4919):761-3.

Logothetis NK, Guggenberger H, Peled S, Pauls J. Functional imaging of the monkey brain. *Nat Neurosci.* 1999 Jun;2(6):555-62.

Lowel S, Singer W. Monocularly induced 2-deoxyglucose patterns in the visual cortex and lateral geniculate nucleus of the cat: II. Awake animals and strabismic animals. *Eur J Neurosci.* 1993 Jul 1;5(7):857-69.

Loop MS, Millican CL, Thomas SR. Photopic spectral sensitivity of the cat. *J Physiol.* 1987 Jan;382:537-53.

Maffei L, Fiorentini A, Bisti S. Neural correlate of perceptual adaptation to gratings. *Science.* 1973 Dec 7;182(116):1036-8.

Maffei L, Berardi N, Bisti S. Interocular transfer of adaptation after effect in neurons of area 17 and 18 of split chiasm cats. *J Neurophysiol.* 1986 May;55(5):966-76.

Maldonado PE, Godecke I, Gray CM, Bonhoeffer T. Orientation selectivity in pinwheel centers in cat striate cortex. *Science.* 1997 Jun 6;276(5318):1551-5.

Malonek D, Dirnagl U, Lindauer U, Yamada K, Kanno I, Grinvald A. Vascular imprints of neuronal activity: relationships between the dynamics of cortical blood flow, oxygenation, and volume changes following sensory stimulation. *Proc Natl Acad Sci U S A.* 1997 Dec 23;94(26):14826-31.

Markram H, Toledo-Rodriguez M, Wang Y, Gupta A, Silberberg G, Wu C. Interneurons of the neocortical inhibitory system. *Nat Rev Neurosci.* 2004 Oct;5(10):793-807. Review.

Marlin SG, Douglas RM, Cynader MS. Position-specific adaptation in simple cell receptive fields of the cat striate cortex. *J Neurophysiol.* 1991 Nov;66(5):1769-84.

McColl SL, Mitchell DE. Stereodeficient subjects show substantial differences in interocular transfer of two motion adaptation aftereffects. *Vision Res.* 1998 Jun;38(12):1889-900.

McLean J & Palmer LA. Contrast adaptation and excitatory amino acid receptors in cat striate cortex. *Vis.Neurosci.* 1996;**13**, 1069-1087.

McLoughlin NP, Blasdel GG. Wavelength-dependent differences between optically determined functional maps from macaque striate cortex. *Neuroimage.* 1998 May;7(4 Pt 1):326-36.

Mitchell DE, Ware C. Interocular transfer of a visual after-effect in normal and stereoblind humans. *J Physiol.* 1974 Feb;236(3):707-21.

Mitchell DE, Reardon J, Muir DW. Interocular transfer of the motion after-effect in normal and stereoblind observers. *Exp Brain Res.* 1975;22(2):163-73.

Mitchison G & Crick F. Long axons within the striate cortex: Their distribution, orientation, and patterns of connection. 1982. *Proc.Natl.Acad.Sci.USA.* **79**, 3661-3665.

Mohn G, van Hof-van Duin J. On the relation of stereoacuity to interocular transfer of the motion and the tilt aftereffects. *Vision Res.* 1983;23(10):1087-96.

Montero VM. A quantitative study of synaptic contacts on interneurons and relay cells of the cat lateral geniculate nucleus. 1991. *Exp Brain Res.* 86:257–270.

Movshon JA, Chambers BE, Blakemore C. Interocular transfer in normal humans, and those who lack stereopsis. *Perception.* 1972;1(4):483-90.

Movshon JA & Lennie P. Pattern-selective adaptation in visual cortical neurones. *Nature*,1979; **278**, 850-852.

Muller B, Peichl L. Topography of cones and rods in the tree shrew retina. *J Comp Neurol.* 1989 Apr 22;282(4):581-94.

Muly EC, Fitzpatrick D. The morphological basis for binocular and ON/OFF convergence in tree shrew striate cortex. *J Neurosci.* 1992 Apr;12(4):1319-34.

Murphy PC, Sillito AM. Continuity of orientation columns between superficial and deep laminae of the cat primary visual cortex. *J Physiol.* 1986 Dec;381:95-110.

Murphy PC, Sillito AM. Corticofugal feedback influences the generation of length tuning in the visual pathway. *Nature.* 1987 Oct 22-28;329(6141):727-9.

Murphy, K.M. Jones, D.G. Van sluyters, R.C. Cytochrome oxidase blobs in the cat primary visual cortex. *J. Neurosci* 1995 **15**: 4196-4208

Murphy PC, Duckett SG, Sillito AM. Feedback connections to the lateral geniculate nucleus and cortical response properties. *Science.* 1999 Nov 19;286(5444):1552-4.

Ogawa S, Tank DW, Menon R, Ellermann JM, Kim SG, Merkle H, Ugurbil K. Intrinsic signal changes accompanying sensory stimulation: functional brain mapping with magnetic resonance imaging. *Proc Natl Acad Sci U S A.* 1992 Jul 1;89(13):5951-5.

Ohzawa I, Sclar G & Freeman RD. Contrast gain control in the cat visual cortex. *Nature*, 1982; **298**, 266-268.

Ohzawa I, Sclar G & Freeman RD. Contrast gain control in the cat's visual system. *J.Neurophysiol.*1985; **54**, 651-667.

Ohzawa I, Freeman RD. The binocular organization of simple cells in the cat's visual cortex. *J Neurophysiol.* 1986a Jul;56(1):221-42.

Ohzawa I, Freeman RD. The binocular organization of complex cells in the cat's visual cortex. *J Neurophysiol.* 1986b Jul;56(1):243-59.

Ollivier FJ, Samuelson DA, Brooks DE, Lewis PA, Kallberg ME, Komaromy AM. Comparative morphology of the tapetum lucidum (among selected species). *Vet Ophthalmol.* 2004 Jan-Feb;7(1):11-22.

Olson CR, Freeman RD. Profile of the sensitive period for monocular deprivation in kittens. *Exp Brain Res.* 1980;39(1):17-21.

Orbach HS, Cohen LB, Grinvald A. Optical mapping of electrical activity in rat somatosensory and visual cortex. *J Neurosci.* 1985 Jul;5(7):1886-95.

O'Shea RP, Crassini B. Interocular transfer of the motion after-effect is not reduced by binocular rivalry. *Vision Res.* 1981;21(6):801-4.

Paradiso MA, Shimojo S, Nakayama K. Subjective contours, tilt aftereffects, and visual cortical organization. *Vision Res.* 1989;29(9):1205-13.

Peters A, Yilmaz E. Neuronal organization in area 17 of cat visual cortex. *Cereb Cortex.* 1993 Jan-Feb;3(1):49-68.

Petry HM, Fox R, Casagrande VA. Spatial contrast sensitivity of the tree shrew. *Vision Res.* 1984;24(9):1037-42.

Petry HM, Harosi FI. Visual pigments of the tree shrew (Tupaia belangeri) and greater galago (Galago crassicaudatus): a microspectrophotometric investigation. *Vision Res.* 1990; 30(6):839-51.

Poggio GF, Fischer B. Binocular interaction and depth sensitivity in striate and prestriate cortex of behaving rhesus monkey. *J Neurophysiol.* 1977 Nov;40(6):1392-405.

Raymond JE. Complete interocular transfer of motion adaptation effects on motion coherence thresholds. *Vision Res.* 1993 Sep;33(13):1865-70

Rector DM, Poe GR, Kristensen MP, Harper RM. Light scattering changes follow evoked potentials from hippocampal Schaeffer collateral stimulation. *J Neurophysiol.* 1997 Sep;78(3):1707-13.

Reid RC, Alonso JM. Specificity of monosynaptic connections from thalamus to visual cortex. *Nature.* 1995 Nov 16;378(6554):281-4.

Ringo JL, Wolbarsht ML. Spectral coding in cat retinal ganglion cell receptive fields. *J Neurophysiol.* 1986 Feb;55(2):320-30.

Rockland KS & Lund JS. Widespread periodic intrinsic connections in the tree shrew visual cortex. 1982 *Science*, **215**, 1532-1534.

Rodieck RW Quantitative analysis of cat retinal ganglion cell response to visual stimuli. *Vision Research.* 1965 Dec; 5(12) : 583-601

Roerig B, Chen B. Relationships of local inhibitory and excitatory circuits to orientation preference maps in ferret visual cortex. *Cereb Cortex.* 2002 Feb;12(2):187-98.

Ross J & Speed HD. Perceived contrast following adaptation to gratings of different orientations. *Vision Res.* 1996; **36**, 1811-1818.

Saito HA. Morphology of physiologically identified X-, Y-, and W-type retinal ganglion cells of the cat. *J Comp Neurol.* 1983 Dec 10;221(3):279-88.

Sanchez-Vives MV, Nowak LG & McCormick DA. Membrane mechanisms underlying contrast adaptation in cat area 17 in vivo. *J. Neurosci.* 2000a; **20**, 4267-4285.

Sanchez-Vives MV, Nowak LG & McCormick DA. Cellular mechanisms of long-lasting adaptation in visual cortical neurons in vitro. *J. Neurosci.* 2000b;**20**, 4286-4299.

Schaller B, Graf R, Sanada Y, Wienhard K, Heiss WD. Decompressive hemicraniectomy in a new cat model. Methodological description of the PET study protocol. *Brain Res Brain Res Protoc.* 2004 Feb;12(3):125-31.

Schummers J, Marino J, Sur M. Synaptic integration by V1 neurons depends on location within the orientation map. *Neuron.* 2002 Dec 5;36(5):969-78.

Sclar G, Ohzawa I, Freeman RD. Contrast gain control in the kitten's visual system. *J Neurophysiol.* 1985 Sep;54(3):668-75.

Sekuler RW and Ganz L. After-effect of seen motion with a stabilized retinal image. *Science, N.Y.* 1963;**139**, 419-420.

Sekuler R & Pantle A. A model for after-effects of seen movement. *Vision Res.* 1967;**7**, 427-439.

Sengpiel F, Blakemore C, Kind PC, Harrad R. Interocular suppression in the visual cortex of strabismic cats. *J Neurosci.* 1994 Nov;14(11 Pt 2):6855-71.

Sengpiel F, Baddeley RJ, Freeman TC, Harrad R, Blakemore C. Different mechanisms underlie three inhibitory phenomena in cat area 17. *Vision Res.* 1998 Jul;38(14):2067-80.

Sengpiel F, Bonhoeffer T. Orientation specificity of contrast adaptation in visual cortical pinwheel centres and iso-orientation domains. *Eur J Neurosci.* 2002 Mar;15(5):876-86.

Sheinberg DL, Logothetis NK. The role of temporal cortical areas in perceptual organization. *Proc Natl Acad Sci USA.* 1997 Apr 1;94(7):3408-13.

Sherman SM, Norton TT, Casagrande VA. X- and Y-cells in the dorsal lateral geniculate nucleus of the tree shrew (Tupaia glis). *Brain Res.* 1975 Jul 25;93(1):152-7.

Shimada Y, Uemura K, Ardekani BA, Nagaoka T, Ishiwata K, Toyama H, Ono K, Senda M. Application of PET-MRI registration techniques to cat brain imaging. *J Neurosci Methods.* 2000 Aug 15;101(1):1-7.

Shoham D, Hubener M, Schulze S, Grinvald A, Bonhoeffer T. Spatio-temporal frequency domains and their relation to cytochrome oxidase staining in cat visual cortex. *Nature.* 1997 Feb 6;385(6616):529-33.

Shoham D, Glaser DE, Arieli A, Kenet T, Wijnbergen C, Toledo Y, Hildesheim R, Grinvald A. Imaging cortical dynamics at high spatial and temporal resolution with novel blue voltage-sensitive dyes. *Neuron.* 1999 Dec;24(4):791-802.

Shtoyerman E, Arieli A, Slovin H, Vanzetta I, Grinvald A. Long-term optical imaging and spectroscopy reveal mechanisms underlying the intrinsic signal and stability of cortical maps in V1 of behaving monkeys. *J Neurosci.* 2000 Nov 1;20(21):8111-21.

Sillito AM, Kemp JA, Milson JA, Berardi N. A re-evaluation of the mechanisms underlying simple cell orientation selectivity. *Brain Res.* 1980 Aug 4;194(2):517-20.

Sillito AM, Jones HE, Gerstein GL, West DC. Feature-linked synchronization of thalamic relay cell firing induced by feedback from the visual cortex. *Nature.* 1994 Jun 9;369(6480):479-82.

Skottun BC, Grosof DH, De Valois RL. Responses of simple and complex cells to random dot patterns: a quantitative comparison. *J Neurophysiol.* 1988 Jun;59(6):1719-35.

Skottun BC, De Valois RL, Grosof DH, Movshon JA, Albrecht DG, Bonds AB. Classifying simple and complex cells on the basis of response modulation. *Vision Res.* 1991;31(7-8):1079-86. Review.

Sloane M, Blake R. Selective adaptation of monocular and binocular neurons in human vision. *J Exp Psychol Hum Percept Perform.* 1984 Jun;10(3):406-12.

Slovin H, Arieli A, Hildesheim R, Grinvald A. Long-Term Voltage-Sensitive Dye Imaging Reveals Cortical Dynamics in Behaving Monkeys. *J Neurophysiol.* 2002 Dec;88(6):3421-38.

Smith A, Over R. Tilt aftereffects with subjective contours. *Nature.* 1975 Oct 16;257(5527):581-2.

Smith AT, Hammond P. The pattern specificity of velocity aftereffects. *Exp Brain Res.* 1985;60(1):71-8.

Snowden RJ & Hammett ST. Spatial frequency adaptation: threshold elevation and perceived contrast. *Vision Res.* 1996;**36**, 1797-1809.

Somers DC, Nelson SB, Sur M. An emergent model of orientation selectivity in cat visual cortical simple cells. *J Neurosci.* 1995 Aug;15(8):5448-65.

Steinberg, R.H., Reid, M. and Lacy, P.L. The distribution of rods and cones in the retina of the cat. *Journal of Comparative Neurology* 1973;148 :229–248.

Stepnoski RA, LaPorta A, Raccuia-Behling F, Blonder GE, Slusher RE, Kleinfeld D. Noninvasive detection of changes in membrane potential in cultured neurons by light scattering. *Proc Natl Acad Sci U S A.* 1991 Nov 1;88(21):9382-6.

Stratford KJ, Tarczy-Hornoch K, Martin KA, Bannister NJ, Jack JJ. Excitatory synaptic inputs to spiny stellate cells in cat visual cortex. *Nature.* 1996 Jul 18;382(6588):258-61.

Sur M, Sherman SM. Linear and nonlinear W-cells in C-laminae of the cat's lateral geniculate nucleus. *J Neurophysiol.* 1982 May;47(5):869-84.

Sutherland NS. Figural after-effects and apparent size. *Q.J.exp.Psychol.* 1961;**17**, 29-39

Swindale NV, Grinvald A, Shmuel A. The spatial pattern of response magnitude and selectivity for orientation and direction in cat visual cortex. *Cereb Cortex.* 2003 Mar;13(3):225-38.

Symons LA, Pearson PM, Timney B. The aftereffect to relative motion does not show interocular transfer. *Perception.* 1996;25(6):651-60.

Tao R, Lankheet MJ, van de Grind WA, van Wezel RJ. Velocity dependence of the interocular transfer of dynamic motion aftereffects.Perception. 2003;32(7):855-66

Thomson AM, West DC, Wang Y, Bannister AP. Synaptic connections and small circuits involving excitatory and inhibitory neurons in layers 2-5 of adult rat and cat neocortex: triple intracellular recordings and biocytin labelling in vitro. *Cereb Cortex.* 2002 Sep;12(9):936-53.

Thompson JK, Peterson MR, Freeman RD. Single-neuron activity and tissue oxygenation in the cerebral cortex. *Science.* 2003 Feb 14;299(5609):1070-2.

Timney B, Symons LA, Wilcox LM, O'Shea RP. The effect of dark and equiluminant occlusion on the interocular transfer of visual aftereffects. *Vision Res.* 1996 Mar;36(5):707-15.

Toth LJ, Rao SC, Kim DS, Somers D & Sur M. Subthreshold facilitation and suppression in primary visual cortex revealed by intrinsic signal imaging. *Proc. Natl. Acad. Sci.* 1996; **93**, 9869-9874.

Tress KH, Kugler BT. Interocular transfer of movement after-effects in schizophrenia. *Br J Psychol.* 1979 Aug;70(3):389-92.

Truchard AM, Ohzawa I, Freeman RD. Contrast gain control in the visual cortex: monocular versus binocular mechanisms. *J Neurosci.* 2000 Apr 15;20(8):3017-32.

Tsodyks M, Kenet T, Grinvald A, Arieli A. Linking spontaneous activity of single cortical neurons and the underlying functional architecture. *Science.* 1999 Dec 3;286(5446):1943-6.

Turner R, Le Bihan D, Moonen CT, Despres D, Frank J. Echo-planar time course MRI of cat brain oxygenation changes. *Magn Reson Med.* 1991 Nov;22(1):159-66.

Tusa RJ, Palmer LA, Rosenquist AC. The retinotopic organization of area 17 (striate cortex) in the cat. *J Comp Neurol.* 1978 Jan 15;177(2):213-35.

van Dongen PA, ter Laak HJ, Thijssen JM, Vendrik AJ. Functional classification of cells in the optic tract of a tree shrew (Tupaia chinensis). *Exp Brain Res.* 1976 Feb 26;24(4):441-6.

Vanzetta I, Slovin H, Grinvald A. Spatio-temporal characteristics of neurovascular coupling in the anesthetized cat and the awake monkey. *International Congress Series.* 2002;1235:145-153.

Vautin RG & Berkley MA. Responses of single cells in cat visual cortex to prolonged stimulus movement: neural correlates of visual aftereffects. *J.Neurophysiol.* 1977; **40**, 1051-1065.

Vidyasagar TR. Pattern adaptation in cat visual cortex is a co-operative phenomenon. *Neuroscience.* 1990;**36**, 175-179.

Von der Heydt R, Peterhans E, Baumgartner G. Illusory contours and cortical neuron responses. *Science.* 1984 Jun 15;224(4654):1260-2.

Wade NJ, de Weert CM. Aftereffects in binocular rivalry. *Perception.* 1986;15(4):419-34.

Wade NJ, Swanston MT, de Weert CM. On interocular transfer of motion aftereffects. *Perception.* 1993;22(11):1365-80.

Wang Y, Gupta A, Toledo-Rodriguez M, Wu CZ, Markram H. Anatomical, physiological, molecular and circuit properties of nest basket cells in the developing somatosensory cortex. *Cereb Cortex.* 2002 Apr;12(4):395-410.

Wang Y, Toledo-Rodriguez M, Gupta A, Wu C, Silberberg G, Luo J, Markram H. Anatomical, physiological and molecular properties of Martinotti cells in the somatosensory cortex of the juvenile rat. *J Physiol.* 2004 Nov 15;561(Pt 1):65-90.

Wienrich M, Zrenner E. Cone mechanisms and their colour-opponent interaction in monkeys and cat. *Ophthalmic Res.* 1984;16(1-2):40-7

Wilcox LM, Timney B, St John R. Measurement of visual aftereffects and inferences about binocular mechanisms in human vision. *Perception.* 1990;19(1):43-55.

Wilson PD, Rowe MH, Stone J. Properties of relay cells in cat's lateral geniculate nucleus: a comparison of W-cells with X- and Y-cells. *J Neurophysiol.* 1976 Nov;39(6):1193-209.

Wohlgemuth A On the after-effect of seen movement. *British Journal of Psycholog, Monograph Supplement.* 1911; 1:1-117.

Yoshimura Y, Dantzker JL, Callaway EM. Excitatory cortical neurons form fine-scale functional networks. *Nature.* 2005 Feb 24;433(7028):868-73.

Yoshioka T, Blasdel GG, Levitt JB, Lund JS. Relation between patterns of intrinsic lateral connectivity, ocular dominance, and cytochrome oxidase-reactive regions in macaque monkey striate cortex. *Cereb Cortex.* 1996 Mar-Apr;6(2):297-310.

Zeki SM. Uniformity and diversity of structure and function in rhesus monkey prestriate visual cortex. *J Physiol.* 1978 Apr;277:273-90.

Zepeda A, Arias C, Sengpiel F. Optical imaging of intrinsic signals: recent developments in the methodology and its applications. *J Neurosci Methods.* 2004 Jun 15;136(1):1-21. Review.